EFFECT OF VEHICULAR AND SEISMIC LOADS ON THE PERFORMANCE OF INTEGRAL BRIDGES

A THESIS SUBMITTED TO
THE GRADUATE SCHOOL OF NATURAL AND APPLIED SCIENCES
OF
MIDDLE EAST TECHNICAL UNIVERSITY

BY

SEMİH ERHAN

IN PARTIAL FULFILLMENT OF THE REQUIREMENTS
FOR
THE DEGREE OF DOCTOR OF PHILOSOPHY
IN
ENGINEERING SCIENCES

SEPTEMBER 2011

Approval of the thesis

EFFECT OF VEHICULAR AND SEISMIC LOADS ON THE PERFORMANCE OF INTEGRAL BRIDGES

submitted by **SEMİH ERHAN** in partial fulfillment of the requirements for the degree of **Doctor of Philosophy in Engineering Sciences Department, Middle East Technical University** by,

Prof. Dr. Canan ÖZGEN ________________
Dean, Graduate School of **Natural and Applied Sciences**

Prof. Dr. Turgut TOKDEMİR ________________
Head of Department, **Engineering Sciences**

Prof. Dr. Murat DİCLELİ ________________
Supervisor, Engineering Sciences Dept., METU

Examining Committee Members:

Prof. Dr. Çetin YILMAZ ________________
Civil Engineering Dept., METU

Prof. Dr. Murat DİCLELİ ________________
Engineering Sciences Dept., METU

Prof. Dr. Ayşe Gülin BİRLİK ________________
Engineering Sciences Dept., METU

Assist. Prof. Dr. Fatih YALÇIN ________________
Civil Engineering Dept., Dumlupınar University

Assist. Prof. Dr. Ferhat AKGÜL ________________
Engineering Sciences Dept., METU

Date : ______________

I hereby declare that all information in this document has been obtained and presented in accordance with academic rules and ethical conduct. I also declare that, as required by these rules and conduct, I have fully cited and referenced all material and results that are not original to this work.

Name, Surname : Semih ERHAN

Signature :

ABSTRACT

EFFECT OF VEHICULAR AND SEISMIC LOADS ON THE PERFORMANCE OF INTEGRAL BRIDGES

Erhan, Semih
Ph.D., Department of Engineering Sciences
Supervisor: Prof. Dr. Murat Dicleli

September 2011, 423 Pages

Integral bridges (IBs) are defined as a class of rigid frame bridges with a single row of piles at the abutments cast monolithically with the superstructure. In the last decade, IBs have become very popular in North America and Europe as they provide many economical and functional advantages. However, standard design methods for IBs have not been established yet. Therefore, most bridge engineers depend on the knowledge acquired from performance of previously constructed IBs and the design codes developed for conventional jointed bridges to design these types of bridges. This include the live load distribution factors used to account for the effect of truck loads on bridge components in the design as well as issues related to the seismic design of such bridges. Accordingly in this study issues related to live load effects as well as seismic effects on IB components are addressed in two separate parts.

In the first part of this study, live load distribution formulae for IB components are developed and verified. For this purpose, numerous there dimensional and corresponding two dimensional finite element models (FEMs) of IBs are built and analyzed under live load. The results from the analyses of two and three dimensional FEMs are then used to calculate the live load distribution factors (LLDFs) for the components of IBs (girders, abutments and piles) as a function of some substructure, superstructure and soil properties. Then, live load distribution formulae for the determination of LLDFs are developed to estimate to the live load moments and shears in the girders, abutments and piles of IBs. It is observed that the developed formulae yield a reasonably good estimate of live load effects in IB girders, abutments and piles.

In the second part of this study, seismic performance of IBs in comparison to that of conventional bridges is studied. In addition, the effect of several structural and geotechnical parameters on the performance of IBs is assessed. For this purpose, three existing IBs and conventional bridges with similar properties are considered. FEMs of these IBs are built to perform nonlinear time history analyses of these bridges. The analyses results revealed that IBs have a better overall seismic performance compared to that of conventional bridges. Moreover, IBs with thick, stub abutments supported by steel H piles oriented to bend about their strong axis driven in loose to medium dense sand are observed to have better seismic performance. The level of backfill compaction is found to have no influence on the seismic performance of IBs.

Keywords: Live load distribution, seismic, soil-bridge interaction, integral bridge.

ÖZ

HAREKETLİ YÜKLERİN VE SİSMİK YÜKLERİN İNTEGRAL KÖPRÜLERİN PERFORMANSINA ETKİLERİ

Erhan, Semih

Ph.D., Mühendislik Bilimleri Bölümü

Tez Yöneticisi: Prof. Dr. Murat Dicleli

Eylül 2011, 423 Sayfa

İntegral köprüler, uç ayakları tek sıra çelik kazıklarla desteklenen, rijit çerçeveli köprüler olarak tanımlanabilir. Bu köprüler, inşaat, bakım ve onarım masrafları yönünden ekonomik olmaları sebebiyle, pek çok ülkede son yıllarda yaygın bir şekilde inşa edilerek geleneksel genleşme derzli köprülerin yerini almaktadırlar. Fakat bu köprülerin tasarımları için henüz kapsamlı bir teknik standart mevcut değildir. Bu yüzden bu ülkeler de inşa edilen integral köprüler genelde geçmişte inşa edilmiş bu tür köprülerin performansları dikkate alınarak ve genleşme derzli köprülere ait standartlar kullanılarak tasarlanmaktadır. İntegral köprülerin tasarımları sırasında kullanılan hareketli yük dağılım katsayılarının hesabında ve sismik tasarımları esnasında yapılan kabullerde geleneksel genleşme derzli köprüler için hazırlanmış olan tasarım standartları kullanılmaktadır.

Bu tez çalışmasının ilk bölümünde, integral köprü elemanları için hareketli yük dağılım formülleri geliştirilmiştir. Bu amaçla, çok sayıda integral köprünün iki ve üç boyutlu yapısal modelleri kurularak AASHTO hareketli yükleri etkisi altında analiz edilmiştir. Bu analiz sonuçları kullanılarak, integral köprülerin alt yapı, üst yapı ve temel zeminine ait çeşitli özelliklerinin bir fonksiyonu olacak şekilde hareketli yük dağılım katsayıları hesaplanmıştır. Bu katsayılar vasıtasıyla, integral köprü uç ayak, kazık ve kirişleri için hareketli yük dağılım formülleri geliştirilmiştir.

Bu tez çalışmasının ilk bölümünde, intgeral köprülerin ve genleşme derzli köprülerin sismik performansları karşılaştırılmıştır. Buna ilaveten, çeşitli yapısal ve geoteknik parametrelerin, integral köprülerin sismik performansına etkileri araştırılmıştır. Bu amaçla, üç farklı integral ve bu integral köprülere benzer yapısal özelliklere sahip üç farklı genleşme derzli köprü ele alınmıştır. Bu köprülerin yapısal modelleri kurularak, doğrusal olmayan zaman tanım analizleri yapılmıştır. Analiz sonuçları değerlendirildiğinde, integral köprülerin genleşme derzli köprülere oranla daha iyi sismik performans gösterdiği anlaşılmıştır. Buna ilaveten, gevşek ve orta kum zeminlere inşa edilmiş, kısa ve kalın uç ayakları kuvvetli dönme ekseni yönünde yerleştirilmiş çelik kazıklarla desteklenen integral köprülerin daha iyi sismik performans verdiği anlaşılmıştır.

Anahtar Kelimeler: Hareketli yük dağılımı, sismik, köprü zemin etkileşimi, integral köprü

To my family

ACKNOWLEDGEMENTS

I would like to express my deepest gratitude to my thesis supervisor Prof. Dr. Murat DİCLELİ for his guidance, understanding, kind support, encouraging advices, criticism, and valuable discussions throughout my thesis.

I would sincerely thank to Cömert BALCIOĞLU, Uğur DEMİRBAŞ, Özgür SAĞLAM, Fatih DEMİREZEN, Bora BAYRİ, Fatih ÖZARSLAN and Metin ÖZARSLAN for their endless friendship.

I would also like to thank to my friends Gözde ÖZERKAN, Yasemin KAYA, Ebru DURAL, Serap GERİDÖNMEZ, Pınar DEMİRCİOĞLU, Buket BEZGİN ÇARBAŞ, Renata VAZQUEZ SANTAMARIA, Fuat KORKUT, Alper AKIN, Serdar ÇARBAŞ, Ferhat ERDAL, Shahin Nayyeri AMIRI, Kaveh HASSANZEHTAB, Refik Burak TAYMUŞ, İbrahim AYDOĞDU, Memduh KARALAR, Erkan DOĞAN, Hakan BAYRAK, Ali SALEM MILANI, Cengizhan DURUCAN, Mehmet Ali EROL for cooperation and friendship, and helping me in all the possible ways.

My greatest thanks go to my parents, Hanife ERHAN and Nafiz ERHAN and my sisters Sıdıka ERTEM, Serpil ALTUNAY, Sevil ACARA and their husbands, and my brother Sinan ERHAN and of course, my nephew Batu and my niece Ceylin for their support, guidance and inspiration all through my life.

TABLE OF CONTENTS

LIST OF FIGURES

FIGURES

LIST OF TABLES

TABLES

LIST OF ABBREVIATIONS

A	: Cross-sectional area of the girder
AASHTO	: Association of State Highway and Transportation Officials, 2007
C_u	: Undrained shear strength
d_p	: Pile width
E_s	: Secant soil modulus (Secant Young's moduls of soil)
ε_{50}	: Soil strain at 50% of ultimate soil resistance (shear stength)
FEA	: Finite Element Analysis
FEM	: Finite Element Model
GT	: Girder type
H	: Height of abutment
H_c	: The abutment height measured from deck soffit
I_c	: Moment of inertia of the composite slab-on-girder section
I_g	: Moment of inertia of girder
I_s	: Moment of inertia of the slab tributary to each girder
IB	: Integral Bridge
k	: Backfill pressure coefficient
K_g	: The parameter representing the longitudinal stiffness of the composite slab-on-girder section of the bridge
k_{sh}	: Coefficient of sub-grade reaction modulus for the granular backfill
L	: Span length
LLDE	: Live load Distribution Equation
LLDF	: Live load Distribution Factor
M_a	: Abutment moment

M_g Girder moment

M_p : Pile moment

n : The ratio of the modulus of elasticity of the girder material to that of the slab material

N_b : Number of beams

P : Lateral soil resistance per unit length of pile

Q_u : Ultimate Soil resistance per unit length of pile

S : Girder spacing

SSB : Simple Supported Bridges

t_s : Slab thickness

V_a : Abutment shear

V_g : Girder shear

V_p : Pile Shear

CHAPTER 1

INTRODUCTION

An IB is one in which the continuous deck and the abutments are cast monolithically to form a rigid frame structure as shown in Fig 1.1. The main difference between a conventional jointed bridge (bridges with expansion joints) and an IB is at the abutments. In IB s, the abutments are generally thinner than those of conventional jointed bridges and are supported on a single row of steel H-piles to provide the required lateral flexibility for accommodating the longitudinal bridge movements due to daily and seasonal temperature variations. IBs have many advantages when compared to conventional jointed bridges. The main advantages of IBs are:

i. Deck joints and expansion bearings are expensive to buy and install. The use of integral abutments eliminates the need for deck joints and expansion bearings. This significantly reduces construction cost of the bridges.

ii. In conventional jointed bridges, generally the abutments are supported by multiple rows of piles. The single row of piles used at IB abutments results in significant cost savings.

iii. Deck joints allow water to leak through and accelerate deterioration to the bearings and the substructures. Thus, maintenance costs are significantly expensive in conventional jointed bridges (Wolde et al. 1988a, b; Burke 1988, 1990a; Steiger 1993). The absence of expansion joints reduces maintenance costs in IBs.

iv. Widening or bridge replacement in IB s becomes easier, since simple design of such bridges lends itself to simple structural modification.

v. Elimination of joints increases the stability and durability of the bridges. This enhances the life expectancy of the bridges.

As mentioned above, IBs have so many economical and functional advantages that they are becoming very popular and considered as alternative to conventional jointed bridges in most parts of USA, Canada and Europe (Wolde et al. 1988a, b; Burke 1990a, b, 1994; Soltani and Kukreti 1992; Dicleli, 2000). However, standard design methods for IBs have not been established yet. Most practicing engineers use the provisions for regular jointed bridges in Bridge Design Specifications such as AASHTO (American Association State Highway Transportation Officials, 2004) to design IBs. This also includes the live load distribution factors used to calculate the effect of the truck loading on the girders of slab-on-girder bridges. Furthermore, no design specifications currently exist to determine live load effects via using live load distribution factors for the abutments and the piles in IBs. As a result, the design engineers generally use arbitrary methods to include the effect of the live load in the design of the abutments and the piles. Accordingly, live load distribution factors for the abutments and piles of IBs are presently needed.

In addition, although modern IBs are known to have performed well in recent earthquakes, a comprehensive research study has not yet been conducted to assess and quantify their seismic performance. Particularly, the assessment of the seismic performance of IBs in relation to that of jointed bridges is scarce in the literature. Moreover, the effects of backfill-abutment and soil-pile interactions on the seismic performance of IBs are not known. Accordingly, in addition to the issues related to live load effects on IBs, the second aim of the proposed research study is to enlighten issues related to the seismic behavior and performance of IBs and provide recommendations to bridge engineers for the seismic design of IBs.

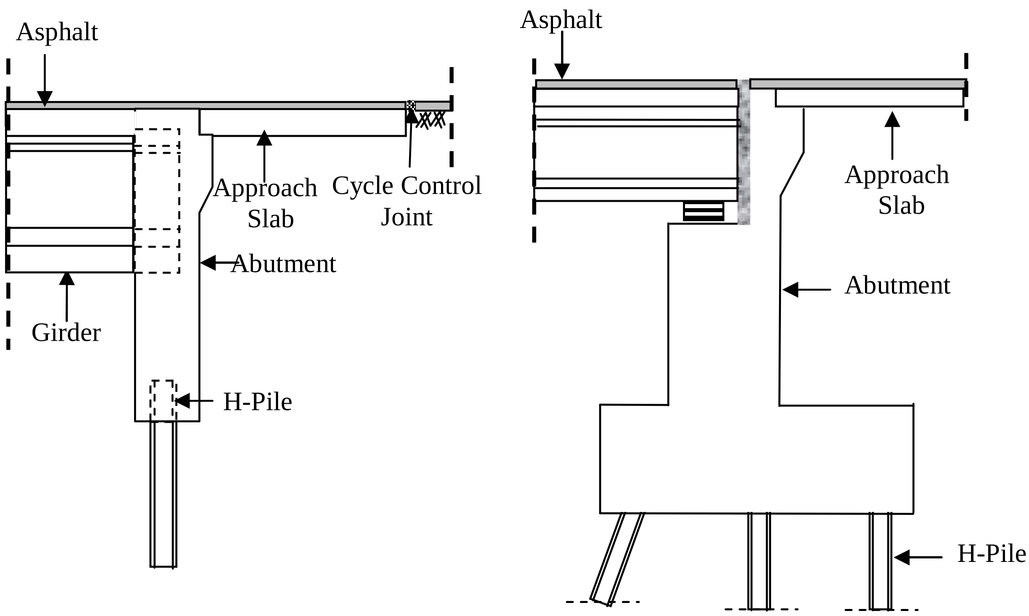

Figure 1.1 Integral and Conventional Bridges Components

1.1. RESEARCH OBJECTIVES AND SCOPE

This research study is composed of two parts. In the first part, the objectives of the present research study are;

i. To test the applicability of AASHTO's live load distribution factors for girders, which are developed for jointed bridges, to IBs.

ii. To develop live load distribution formulae for IB abutments, piles and girders.

In the second part, the objectives of the present research study are;

iii. To investigate the seismic performance of IBs.

The IBs considered in the present research study are assumed to have either prestressed or steel girders. The abutments at both ends of the bridge are assumed to be identical. Typical granular backfill used in IB construction is assumed behind the abutments. The research study is also limited to straight IBs with end-bearing steel H piles driven in sand. Furthermore, the IBs considered in this study are assumed to have no skew.

1.2. RESEARCH OUTLINE

The first part of the research study, which is related to live load effects on IBs, is composed of the following seven main phases:

i. In the first phase of the research study, an extensive literature review is conducted on the development of the live load distribution factors for jointed bridges. Next, a literature review is conducted on finite element modeling techniques for bridges. The information acquired from this literature review will be used to built an accurate finite element model (FEM) of IBs to determine the live load effects on their components as precisely as possible. Furthermore, literature review on soil-pile and backfill-abutment interaction is also conducted to determine the effect of the backfill and foundation soil on the distribution of live load effects to the girders, abutments and piles.

ii. In the second phase of the research, the effect of soil-bridge interaction on the magnitude of the internal forces in IB components due to live load effects is studied. For this purpose, structural models of typical IBs are built by including and excluding the effect of backfill and foundation soil. The analyses of the models are then conducted under AASHTO live load. In the analyses, the effects of the backfill and foundation soil on the magnitude of the internal forces in IB components are studied for various structural, geometric and geotechnical parameters such as bridge size, abutment height and thickness, pile size and orientation, number of spans and foundation soil stiffness.

iii. This phase of the research includes the determination of geometric, structural and geotechnical parameters to be included in FEM analysis of IBs to obtain live load distribution formulae. Based on the determined parameters, a set of IBs will be configured for finite element analyses.

iv. In the fourth phase of the research, three dimensional (3-D) finite element models are developed for the bridges which have different geometric, structural and geotechnical parameters and analyzed under AASHTO live load using the finite-element-based software SAP2000 (Computers and Structures inc. 2000). From the finite element analyses (FEA) maximum live load moments and shears at girders, abutments and piles are determined for each one of the IB models considered.

v. In this phase of the research, two-dimensional (2D) frame models are built for the set of IBs considered for analyses. Then the maximum moments and shears at the girders, abutments and piles are obtained from the analyses of the frames subjected to AASHTO live load and the maximum moments and shear forces found in the fourth step are divided these values to calculate live load distribution factors.

vi. This phase of the research includes the assessment of the effect of the deck-abutment continuity in IBs on the distribution of live load to the girders. For this purpose, the live load distribution factors obtained from FEA of models including and excluding the monolithic abutment-pile system will be compared. Furthermore, AASHTO live load distribution factors for girders will be compared with the analyses results to assess their applicability to IBs.

vii. In this phase of the research, live load distribution formulae will be developed for the abutments, piles and if necessary for the interior and exterior girders of IBs.

In the second part of this thesis study, seismic performance of IBs are investigated. The main phases of this part of thesis study can be summarized as follows.

i. In the first phase of this part, a literature review is conducted to determine the present state of knowledge on the seismic performance of IBs. Additionally a comprehensive literature review is conducted to determine the most recent and realistic techniques for modeling soil-bridge interaction effects.

ii. In the second phase, several existing IBs with various properties are selected and then designed as conventional jointed bridges in compliance with AASHTO LRFD Bridge Design Specifications.

iii. In this phase of the research project first, moment-curvature relationships of the steel and reinforced concrete members of the bridges are determined. Next, using these moment-curvature relationships, pushover analyses of the bridges are conducted to determine their lateral displacement / rotation capacity.

iv. In the fourth phase of this research study, seven ground motions recorded on rock are selected for the nonlinear time history analyses. In the selection of these ground motions, the fault rupture mechanism is assumed to be one of the most commonly found rupture mechanisms namely; strike-slip, reverse normal or reverse oblique. The moment magnitude of the earthquakes used in the analyses is assumed to be larger than 6.0. Furthermore, the distance of the recording station from the fault is assumed to be between 25 and 50 km so as to exclude those ground motions with negligible shaking level (distance larger than 50 km) and those ground motions within the near-fault category (distance less than 20 km). However, the ground motions are also scaled to have various peak ground accelerations to study the performance of IBs at various intensity levels.

v. Next, for the soil types considered in this study, the equivalent dynamic properties, namely the stiffness and damping ratio of the soil profile are determined using the PROSHAKE software for each ground motion as well as ground shaking intensity (peak ground acceleration) considered. These properties are used for modeling the dynamic soil pile interaction effects via a soil column.

vi. Subsequently, for the foundation soil types considered in this study, appropriate p-y curves are established to incorporate local soil-pile interaction effects into the structural model. These p-y curves are modeled as nonlinear springs connected between the soil column and the pile. In addition, to model radiation damping due to the interaction between the piles and site soil, dashpots are connected between the pile and the soil column. The dashpot properties for each soil type are determined using the available empirical data in the literature.

vii. In this phase of the research study, a soil column will be modeled independently without the bridge in SAP2000 and time history analyses of the model are conducted using the selected ground motions and the range of intensities considered in this study. The displacement and acceleration time histories at the top of the soil columns obtained from SAP2000 analyses are then compared with those obtained from PROSHAKE. This is basically done to verify the accuracy of the soil column model that is used to simulate dynamic soil-pile interaction effects in the time history analyses.

viii. In the eighth phase of the research study, the integral and conventional bridges will be modeled together with the soil column using the finite element based software SAP2000. This modeling also includes a detailed static or if possible dynamic abutment-backfill interaction simulation.

ix. Next, time history analyses of the bridge models are conducted using the selected ground motions with various intensities representing small, medium and large intensity ground motions.

x. In this phase of the research study, the seismic performance of integral and conventional bridges are compared and the performance of IBs will be quantified in relation to that of conventional jointed bridges. The comparison will first be done by assessing the displacement ductilities of the bridge components and displacement capacity over demand ratios. In the case of IBs, potential damage due to low cycle fatigue of steel H piles are also assessed.

xi. Finally, the seismic performance of IBs will be assessed as a function of various structural and geotechnical parameters and design recommendations will be provided.

1.3. REVIEW OF PREVIOUS STUDIES

1.3.1 PART I: LIVE LOAD EFFECTS ON IBS

1.3.1.1. INTEGRAL BRIDGES

IBs are defined as a class of rigid frame bridges without deck joints. Arch bridges, rigid-frame bridges and culverts can be classified as IBs (Dicleli 2000). IBs were first considered after observing the successful performance of older bridges with inoperative joints (Mourad and Tabsh 1999). Subsequently, bridge engineers started to eliminate the deck joints at piers and abutments after the moment distribution method (cross method) was first developed by Cross in early 1930s since this method allowed for the analysis of statically indeterminate structures such as rigid frame bridges. Therefore, concrete rigid frame bridges became very popular and a standard type of construction for many transportation departments by the mid of 20^{th} century. Currently a number of state departments of transportation provide limited in-house design guidelines for IBs based on past experience and performance of older IBs. However, the design of IBs has not been addressed in formal bridge design specifications such as AASHTO (2007).

Most recent research publications on IBs are related to the effect of thermal loadings (Dicleli and Albhaisi, 2003, 2004, Dicleli, 2005) on the performance of IBs. Only few studies on live load analysis of IBs have been found in the literature (Mourad and Tabsh 1998, 1999).

1.3.1.2 LIVE LOAD DISTRIBUTION FACTOR

Structural analysis of highway bridges using complicated 3-D FEM to determine live load effects in bridge components is possible due to the readily available computational tools in design offices. However, building such complicated 3-D FEM is tedious and time consuming. Accordingly, most design engineers prefer using simplified 2-D structural models of the bridge and live load distribution factors available in current design codes to determine live load effects in bridge components. Using the live load distribution factor, the maximum moment and shear of an individual bridge member is determined by multiplying the maximum moment and shear obtained from 2-D frame analysis of the bridge under truck load by the live load distribution factor. Currently, live load distribution factors for moment and shear for highway bridge girders are determined by using the AASHTO Standard Specifications (AASHTO 2002), AASHTO Load and Resistance Factor Design (LRFD) Specifications (AASHTO 2007) or methods specified by state departments of transportation.

The AASHTO Standard Specifications for Highway Bridges' simple *S/D* formulas have been used as live load distribution factors in most common cases for calculating the live load bending moment and shear in bridge girder design; where *S* is the girder spacing and *D* is a constant which depends on the type of the bridge superstructure. The AASHTO Standard Specifications for Highway Bridges have contained live load distribution factors since 1931. The earlier versions of live load distribution factors were based on the work done by Westergaard (1930) and Newmark (1948), but the factors were modified as new research results became available (Barr et. al. 2001). The traditional *S/D* formulae are easy to apply, although they can be overly conservative for some ranges of span lengths while unconservative for others (Cai, 2005; Huo et al., 2005). The applicability of these formulae in the AASHTO Standard Specifications is limited by the fact that they were developed considering only non-skewed, simply supported bridges. However, the S/D formulae are also used by some bridge designers even in bridges with complicated geometries such as high skew, curved alignment, as well as continuous and IBs (Mourad and Tabsh 1999) since design guidelines for such bridges do not exist. Therefore, these bridges may either be designed in a conservative way which involves the additional cost or in an unconservative way which leads to unsafe bridge designs (Zokaie et al 1991).

The studies on the development of live load distribution factors before 90's were based on the determination of new *D* values in the AASHTO load distribution formula (*S*/*D*) (Bakth and Moses, 1988; Hays, 1990). Bakth and Moses (1988) presented a procedure to calculate the constant *D* which was expressed as a function of the span length. The span length was found to be an important parameter in calculating the distribution factor.

After 90's, additional geometric and structural parameters such as slab thickness, bridge span, girder stiffness etc., were included in the new AASHTO girder live load distribution formulae to get more accurate results. More precise but complex live load distribution factors were developed under National Cooperative Highway Research Program (NCHRP) Project 12-26 (Zokaie et al 1991). These new equations have been published in the AASHTO LRFD Bridge Design Specifications (1994) then modified in more recent editions of AASHTO LRFD Bridge Design Specifications (1998, 2004). The live load distribution factors in AASHTO LRFD Bridge Design Specifications are more accurate than those provided in AASHTO Standard Specifications (Mabsout et al. 1997, Cai 2005). However, designers are concerned mainly about the complexity of the LRFD ditribution factor equations. The LRFD procedure includes a different set of equations and skew correction factors for moment and shear, different sets of equations for interior and exterior girders, the use of pile analogy method for consideration of the diaphragms as well as limited ranges of applicability due to the bridge structural and geometric properties imposed on the equations. Therefore, simpler and less complex live load distribution factor equations would be welcomed by the bridge design community. As a result, a new study under project NCHRP 12-62 was initiated for this purpose and is on-going (Cai 2005).

The literature review revealed that the discussions about the determination of realistic and applicable live load distribution formulae are still on-going for conventional jointed bridges. Furthermore, the literature review revealed that no study has been conducted to develop live load distribution formulae for the components of IBs. These confirm the necessity of conducting research on live load distribution factors for IB components.

1.3.1.3. MODELLING

The finite element method is a well-accepted method of analysis. However, any method of analysis or modeling technique requires some degree of approximation when applied to a real structure. Therefore, a realistic finite element model is required for an accurate determination of live load distribution factors. For this purpose, many researchers have developed FEM to obtain accurate predictions of live load distribution factors for bridge girders. One of the most simple but accurate FEM to evaluate the lateral load distribution characteristic of simple span bridges in flexure was developed by (Hays et al. 1986) for the Florida Department of Transportation. In the FEM, linear elastic behavior was assumed. The concrete slab was idealized as quadrilateral shell elements with five degrees of freedom at each node and steel girders and diaphragms were modeled as standard frame elements. Several bridges covering a wide range of span lengths and girder spacing were analyzed using the FEM and the results were compared with those from AASHTO Standard specifications. The AASHTO results were found to be slightly unconservative for short spans and quite conservative for longer spans.

A study was performed on deck slab stresses in integral abutment bridges using a finite element program called ALGOR to simulate the bridge features (Mourad and Tabash, 1999). In this program, the deck slab and beam web were modeled with four node rectangular shell elements, flanges and piles were modeled with two node space beams and the abutments were modeled with eigth node brick elements. In this study, the deck stresses determined from the FEA were about 40% less than those calculated using AASHTO LRFD equations.

Mounir and Mabsout (1997) conducted extensive research to compare four finite element modeling techniques reported in the literature used in evaluating the wheel load distribution factors of steel girders bridges. In the first model, the concrete slab was idealized as quadrilateral shell elements with five degree of freedom at each node and steel girders were idealized as space frame members (Hays et. al. 1986). In the second model, the concrete slab and girders were modeled as quadrilateral shell elements and eccentrically connected space frame members respectively (Imbsen and Nutt 1978), In the third one, the concrete slab and steel girder web were modeled as quadrilateral shell elements and girder flanges were modeled as space frame elements (Brockenbrough 1986). In the last one, the concrete slab was modeled using isotropic eight node brick elements with three degrees of freedom at each node and the steel girder flanges and webs were modeled using quadrilateral shell elements. Although the first model is the simplest one, the results from this model were found to be the most realistic compared to those from field tests and AASHTO procedure.

Faraji et. al. (2001) used a 3D finite element model to simulate the behavior of a three-span IB under thermal loading. In this model, the deck slab is modeled using bending and stretching plate elements while the steel stingers and diaphragms are modeled as beam elements. Abutment walls are modeled as plate elements. The piers are modeled as beam elements. The soil response behind the abutment walls is modeled using uncoupled nonlinear springs. HP-Piles are modeled using beam elements. Soil response next to each pile is modeled with 15 nonlinear springs. A similar modeling technique is used to model substructure members of IBs considered in this study.

1.3.1.4. SOIL-BRIDGE INTERACTION

Soil-Bridge interaction is one of the most important factors that affect the IB behavior especially under thermal loading. In the FEM's for the determination of live load distribution factors, these effects seem to be negligible. However, in this study, sensitivity analyses are conducted to determine the effects of backfill and foundation soil response on the distribution of live load. The sensitivity analyses reveal that backfill and foundation soil have an important effect on the live load distribution in the abutments. Accordingly, more complex FEMs of the considered bridges including the effects of the interaction between abutment and backfill soil as well as pile and foundation soil is established.

In the literature, the interaction between the abutment and backfill soil as well as pile and foundation soil are considered only under thermal effects (Duncan, Arsoy 2003; Dicleli and Albhaisi, 2003, 2004, 2005). The backfill pressure distribution behind the abutment is inherently nonlinear and depends on depth, amount and mode of wall displacement (Clough and Duncan 1991, Faraji et al. 2001, Khodair and Hassiotis 2005). Clough and Duncan (1991) obtained the variation of the backfill pressure coefficient (K) as a function of the abutment displacement from the experimental data and finite element analysis. This relationship was used recently by Dicleli, (2000, 2003, 2004, 2005) to model abutment-backfill behavior under thermal-induced displacements of IBs. Such thermal-induced displacements are large and hence require a fully defined pressure-distribution versus abutment displacement relationship over a complete range of active to passive state. However, for live load analysis, since the lateral displacement of the abutment results from the deck-abutment joint rotation, it is anticipated to be very small. As a result a linear approximation of abutment-backfill interaction may be adequate using linear springs under compression and no springs under tension. The linear properties of these springs may be obtained from the initial slope of abutment-backfill interaction relationship provided by (Clough and Duncan 1991, Tseng and England, 2006)

Generally, the soil pile interaction for a particular point along the pile is defined as a nonlinear load (P) – deformation (Y) curve, where P is the lateral soil resistance per unit length of pile and Y is the lateral deflection (Faraji et. al. 2001; Dicleli and Albhaisi 2004) under lateral loading. Several nonlinear models for P-Y curves are available (Clough and Duncan 1991, Husain and Bagnariol 1996, Tseng and England, 2006) in the literature. Load-deformation relationship can be modelled as elostoplastic (Dicleli and Albhaisi 2004) as well as nonlinear (Faraji et. al. 2001). However, under live load, the initial linear portion of the P-Y curve is anticipated to be adequate due to smaller lateral displacement of the piles. Accordingly, an analysis that incorporates the linear response of the soil to pile movement may be adequate when studying the live load distribution in IBs.

1.3.2 PART 2: SEISMIC PERFORMANCE OF INTEGRAL BRIDGES

As stated earlier, the main objective of this research study is to assess and quantify the seismic performance of IBs in relation to that of conventional jointed bridges. Accordingly, first a comprehensive literature review needs to be conducted to obtain the current state of knowledge on the seismic performance of IBs. This research study also requires a detailed non-linear modeling and analysis of the bridges including the effect of soil-structure interaction to accurately calculate the seismic demands on bridge components. The AASHTO specifications make specific recommendations with respect to structural analysis and design of bridges for earthquake loading. However they are less specific regarding the soil-structure interaction modeling procedures for seismic performance assessment of bridges (Spyrakos and Loannidis 2003). Nevertheless, bridge response data obtained from recent earthquakes indicate that soil-pile and abutment-backfill interactions can be an important consideration in evaluating the seismic response of pile-supported bridges (Shamsabadi et al. 2007). Accordingly, a comprehensive literature review is conducted on the following topics:

- Seismic performance of IBs
- Modeling integral and conventional bridges for seismic analysis
- Modeling soil-structure interaction for seismic analysis

1. Abutment- backfill interaction
2. Soil-pile interaction

1.3.2.1 STUDIES ON SEISMIC PERFORMANCE OF INTEGRAL BRIDGES

In the last decade, several studies have been conducted to assess the seismic performance of IBs. These studies reveal that soil-structure interaction has significant effects on the seismic performance of IBs (Wilson 1988; Dehne and Hassiotis 2003, Spyrakos and Loannidis 2003). Wilson (1988) conducted a research study to assess the effects of the stiffness of monolithic bridge abutments on the seismic performance of IBs. In this study, a simple analytical model was developed that describes the stiffness of the abutments with six equivalent discrete springs for three translational and three rotational degrees of freedom. These springs are assigned various stiffnesses to include the effects of the abutment wall, pile foundations and soil. However, inertial effects arising from acceleration of the abutment and backfill mass during the excitations caused by an earthquake was not considered in this model. In addition, an accurate simulation of the three dimensional behavior of the abutment-backfill system including the combination of translational and rotational modes of the abutment under seismic effects is not possible with this model. More recently, Spyrakos and Loannidis (2003) have conducted a research study on the seismic behavior of IBs . In this study, the effect of soil-structure interaction on the seismic performance of IBs was evaluated. Linear elastic half space theory and a two-step approach was utilized to simulate the effect of soil structure interaction. The analytical model was also validated with field measurement. However, the nonlinear effects of soil-structure interaction was neglected and a single direct analysis technique that models the whole system including the superstructure, substructure and soil was not used due to its complexity. In addition, Dehne and Hassiotis (2003) conducted a research study on the seismic analysis of IBs. In the research study, p-y curves were used to simulate soil-pile interaction and equivalent secant stiffness was utilized to simulate abutment-backfill interaction. The inertial effects of the site soil on the piles were neglected in the analyses. Dehne and Hassiotis (2003) found that dense soil behind the abutment and loose sand around the piles reduce stresses in the piles due to the earthquake loading.

1.3.2.2 SEISMIC ANALYSIS AND MODELING TECHNIQUES FOR INTEGRAL AND CONVENTIONAL BRIDGES

The results of previous studies on structural modeling of bridges have been utilized to build an accurate analytical model of the bridges studied in this research so as to capture their actual seismic behavior as closely as possible. Tseng and Penzien (1973) observed that linear seismic analysis provides a reasonable estimate of the maximum displacement response. However, it was found that predicting the internal forces in the substructure members may be highly erroneous if yielding occurs. Kawashima and Penzien (1976) demonstrated that the seismic response of a curved bridge under low intensity excitation could be predicted with fairly good accuracy using linear analytical models. As the bridges considered in this study will be analyzed under various ground motion intensities (small to high), using a simple linear structural model to predict the seismic response of the bridges is not possible. Eberhard and Marsh (1997) had conducted an iterative linear response spectrum analysis of an existing bridge to successfully account for the nonlinear effects as verified by the load tests performed on the same bridge. However this iterative solution becomes complicated when the number of nonlinearities including that of the soil increase. In addition, this type of an iterative linear analysis technique is not suitable for realistically capturing the inertial effects of the site soil and radiation damping. Thus, a regular nonlinear time history analysis procedure is preferred in this study.

For the nonlinear time history analyses of bridges, several choices with varied complexity are available for modeling the bridge deck. The most complicated modeling technique is to model the deck with all of its components, using shell and beam elements. This modeling technique increases the degrees of freedoms in the structural model considerably. Therefore, it is beyond the state of practice (Maleki 2002). Another option is to model the superstructure with a grillage model that eliminates the shell elements and uses beam elements in two directions (Memory et al. 1995). This type of a modeling technique, although more simple than the full shell-beam model, is still computationally demanding. The other alternative deck modeling technique for seismic analysis is the equivalent beam model (Alfawakhiri and Bruneau 2000). In this modeling technique, the deck is modeled with a beam element that has the same mass and stiffness of the whole superstructure. Itani et al. (1999) conducted a research study to compare the dynamic characteristics of five medium span steel bridges that were modeled using beam models and 3-D finite element models. The comparison of the analyses results showed that the beam element models were able to capture the dynamic characteristics of the bridge as well as the 3-D finite element models. Accordingly, the simplified beam model for the deck seems to be more suitable for the nonlinear time history analyses of IBs considering the computational demand associated with high degree of nonlinearity and complexity of soil-structure interaction modeling. Thus, a similar modeling technique for the deck will be used in this study to account for the dynamic behavior of the bridges.

The stiffness of the bearings are also modeled using the information available from the literature (Buckle et al. 2006). Modeling techniques developed to accurately simulate the interaction between the bridge superstructure, bearings and the substructures were used to build a simplified but accurate model of the bridges (Dicleli and Mansour 2003).

Several modeling techniques for the abutments of integral and conventional bridges have been found in the literature. It was found that, while studying thermal and live load effects, modeling of IB abutments using shell elements is more appropriate due to the relatively less computational demand required (Faraji et al. 2001, Dicleli and Erhan 2008). However, because of the high computational demand in nonlinear seismic analyses, more simplistic modeling techniques are generally used for the abutments. Saadeghvaziri (2000) have used three linear springs to model the abutment including its interaction with the soil. However, this type of a modeling technique is not able to capture the three dimensional behavior of the abutment including its translational and rotational movements due to inertial effects. Hindi and Dicleli (2006) used a grid of 3-D beam elements to model the abutments. While this modeling technique is computationally less demanding than a 3-D finite element model using shell elements, it is also able to capture the actual three dimensional behavior of the abutments under seismic inertial forces. Thus, a similar modeling technique will be used in this study to model the abutments of the bridges considered in this study.

In the literature, there are several methods to simulate the inelastic cyclic behavior of reinforced concrete members (Takeda et al. 1970, Dutta and Das 2002, Chao and Loh 2007) under seismic loads. The hysteresis model proposed by Takeda et al. (1970) has been used widely and is available in many commercially available software including SAP2000. Therefore, the hysteresis model proposed by Takeda et al (1970) will be used to simulate the inelastic cyclic behavior of reinforced concrete members of the bridges considered in this study. However, the backbone moment rotation curve used to define the hysteresis model will be obtained using the software COLA developed by Saatcioglu and Yalcin (2003).

Steel H-piles used in IBs are laterally supported by the surrounding soil. Thus, their lateral-torsional or global buckling instability need not be considered. Local buckling is the only instability type that may be considered when determining the lateral displacement capacity of steel H-piles (Dicleli and Albhaisi 2003, Burdette et al. 2004). Therefore, the cyclic behavior of steel H-piles may be modeled using an elasto-plastic hysteretic behavior. Accordingly, the Plastic-Wen model will be used to simulate the nonlinear behavior of the piles until their displacement capacity is reached (Dicleli 2007). The web-flange interaction approach presented by Kato (1989) will be used to calculate the local buckling strength and hence the monotonic lateral displacement capacity of steel HP piles used in this study.

Imbsen and Penzien (1986) compared the nonlinear and linear dynamic analysis results of several multi-span simply supported bridges. It was found that the correlation between elastic and nonlinear analysis results is poor when impacting of the bridge deck occurs. Therefore, for the analyses of conventional bridges conducted in this research, the possibility of impact between the bridge deck and abutments is considered. Several research studies have been conducted on the impact (pounding) effects between the adjacent decks of multi-span bridges (Ruangrassamee and Kawashima 2003, Zanardo et al. 2002, Jankowski et al. 2000, Malhotra 1998). Zanardo et al. (2002) have used non-linear gap elements to simulate the impact effects in the structural models. The nonlinear gap elements consist of spring-dashpot elements with stiffness and damping properties representing pounding effect in a single segment of a multiple span bridge. Jankowski et al. (2000) placed gap-friction elements at the ends of the deck segments of a multiple span bridge to control the pounding effects between the adjacent superstructure parts. However, the energy, which is dissipated as heat during the impact, has not been considered in the aforementioned study. Ruangrassamee and Kawashima (2003) have installed linear viscous dampers in series with gap elements between adjacent decks to simulate the energy dissipation during the impact. Thus, a similar modeling technique will be used in this study to model the impact between adjacent decks of the conventional bridges considered in this study.

1.3.2.3 MODELING OF NONLINEAR SOIL-STRUCTURE INTERACTION

Previous studies reveal that soil-structure interaction has significant effects on the seismic performance of bridges (Wilson 1988; Crouse et al. 1987, Spyrakos and Loannidis 2003, Shamsabadi et al. 2007, Kotsoglou and Pantazopoulou 2007). More recent studies also reveal that abutment-backfill and soil-pile interactions are nonlinear under moderate and strong earthquake loading (Romo and Shelley 1999, Shamsabadi et al. 2007). Accordingly, the effect of non linear soil-bridge interaction is included in the analysis of the bridges considered in this study. For this purpose, an extensive literature review has been conducted on non-linear modeling techniques of abutment-backfill and soil-pile interaction to select an accurate but a simple modeling technique for the numerical simulation of the seismic response of bridges. The details of various modeling techniques available in the literature for abutment-backfill and soil-pile interactions are given in the following subsections.

1.3.2.3.1 Nonlinear Abutment-Backfill Interaction

Results from previous studies have revealed that abutment-backfill interaction may have a significant effect on the seismic response of particularly shorter bridges and need to be considered when analyzing such bridges under earthquake loadings (Dicleli and Mansour 2003, Shamsabadi et al. 2007). The backfill pressure distribution behind the abutment is inherently nonlinear and depends on the depth, amount and mode of wall displacement (Clough and Duncan 1991, Faraji et al. 2001, Khodair and Hassiotis 2005). At rest earth pressure behind the abutment is assumed when there is no movement. However, during a seismic excitation, when the bridge deck moves laterally toward the abutment, the bridge structure applies a lateral compressive force to the abutment. This force mobilizes the passive resistance in the backfill and leads to permanent soil displacements. This results in both hysteretic and radiation damping in the backfill. Then, the bridge moves away from the abutment, where a gap may form between the abutment and the soil. The assumptions made for the nonlinear stiffness as well as the hysteretic and radiation damping of the abutment have been shown to have a profound effect on the global seismic response and performance of the bridge (El-Gamal and Siddhartan 1998, Faraji et al. 2001, Shamsabadi et al. 2007). Accordingly an accurate estimation of these properties is critical to realistically assess the seismic response of bridges. Furthermore, proper modeling of the abutment-backfill system reflecting the behavior described above is critical for an accurate assessment of the seismic performance of the bridges considered in this study.

In the last decades, many studies have been conducted on proper modeling techniques of abutment-backfill interaction. Crouse et al. (1987) conducted a research study to model abutment backfill interaction. In this model, winkler springs are attached to each node of the abutment walls in the lateral direction.

However, the frictional forces between the abutment and backfill were omitted. Wilson (1988) purposed a similar analytical model to describe the stiffness of non-skew monolithic highway bridge abutments for purposes of seismic bridge analysis. In this model, the stiffness of the abutment backfill system is simulated by six equivalent discrete springs for three translational and three rotational degrees of freedom. The spring stiffness for each degree-of-freedom at the abutment are developed by considering the resistance the soil provides to statically applied displacements of the abutment walls. However, inertial effects arising from the acceleration of the abutment and the backfill mass during an earthquake are not considered in this model. In addition, an accurate simulation of the three dimensional behavior of the abutment-backfill system including the combination of translational and rotational displacement modes of the abutment under seismic effects is not possible with this model. Therefore, this modeling technique will not be employed in this study. Similarly, El-Gamal and Siddharthan (1998) presents a relatively simple and realistic methodology to simulate the nonlinear translational (longitudinal and transverse) seismic response of bridge abutments founded on pile foundation. In their model, El-Gamal and Siddharthan (1998) have accounted for many important factors such as the abutment dimensions, nonlinear pile-soil interaction, superstructure loads, and difference in soil behavior under active and passive conditions. However, the modeling technique proposed by El-Gamal and Siddharthan (1998) involves an iterative analysis procedure that is not suitable for simulating the nonlinear abutment-backfill behavior via a single time history analysis. More recently, a nonlinear abutment-backfill interaction modeling technique for seismic analysis of bridges was purposed by Shamsabadi et al. (2007). In this modeling technique, a modified hyperbolic soil stress-strain behavior (LSH model) has been defined to estimate the nonlinear force displacement relationship of the abutment. Although, the hysteretic and radiation damping are not considered in this study, comparison of the developed model and field experiments conducted on various typical structures with backfill show very good agreement. Several research studies have been conducted to evaluate the response of retaining walls and backfill soil under dynamic loading (Jain and Scott, 1989, Veletsos and Younan 1993). In these studies, the backfill is modeled as a shear beam and the interaction between the wall and the backfill is modeled using Winkler springs and appropriate dashpots. In this study, a mixed modeling technique utilizing those proposed by Shamsabadi et al. (2007), Jain and Scott (1989) as well as Veletsos and Younan (1993) will be used for modeling the abutment-backfill interaction.

1.3.2.3.2. Nonlınear Soil-Pile Interaction

Earlier research studies reveal that soil-pile interaction has a significant effect on the seismic response of structures (Boulanger et al. 1999). Design engineers generally use p-y methods (Faraji et al. 2001, Dicleli and Albhaisi 2004, Dicleli and Erhan 2008) or finite element models (Angelides and Roesset 1981, Wu and Finn 1997, Cai et al. 2000, Maheshwari et al. 2004, Khodair and Hassiotis 2005,) to simulate local soil-pile interaction effects in the structural model. Although, the p-y methods are considerably less complex than finite element modeling of piles and surrounding soil, a reasonably good agreement was obtained between the p-y modeling, finite element modeling and the experimental results in previous studies (Ramachandran 2005). Accordingly, in this study, the p-y method will be used to model local soil-pile interaction effects.

The analysis and design of the pile next to the foundation soil is a typical example of soil-structure interaction problem. This interaction is nonlinear in nature so that the magnitudes of the soil and structural deformations and stresses are dependent on each other (Novak and Aboul-Ella 1978; Faraji et al. 2001). This nonlinear relationship is defined by a nonlinear load (p)-deformation (y) curve. The p-y curves represent the nonlinear behavior of the soil by relating the soil reaction and pile deflection at points along the pile length. The initial deflection of soil is almost linear, but at higher load levels the deformation of soil increases rapidly with small increments of the load (Dicleli and Albhaisi 2004). In the literature, many p-y criteria are recommended for different soils. The earlier studies about p-y curves were conducted by Matlock (1970) and Reese et al. (1974) to determine realistic p-y curves for the analysis of laterally loaded piles.

However, these p-y curves were developed under static loading. Therefore, they may not be suitable for use in this study. Seismic soil-pile interaction analyses are generally conducted by using dynamic p-y curves. Dynamic p-y curves are generally obtained by modifying the static p-y curves. Such modifications account for the degradation of soil stiffness and the reduction of strength in some soils due to the effect of repeated loading. In addition, a dashpot is added in parallel to the nonlinear p-y springs in order to account for the radiation damping (Nogami et al. 1992). In addition, In the last decades, numerous research studies are conducted to develop easily applicable dynamic p-y analyses methods to seismic problems (Nogami et al. 1992, Dou and Byrne 1996, Boulanger et al. 1999, Romo and Shelley 1999, El Naggar and Bentley 2000). Wang et al. (1998) compared several dynamic p-y modeling techniques found in the literature and obtained similar results under seismic loading. In these methods, nonlinear p-y springs and dashpots are used to simulate the behavior of soil-pile interaction under seismic excitations (Fig 1.6). Boulanger et al (1999) tested the validity and reliability of the dynamic p-y analysis methods experimentally in the cases of soft clay ground conditions. A reasonably good agreement was obtained between the dynamic p-y analyses and the experimental results. In the study conducted by Boulanger et al (1999), a nonlinear p-y element was developed that can simulate a range of desired p-y behaviors and was implemented into a finite element program. The nonlinear p-y behavior is conceptualized as consisting of elastic (p-y^e), plastic (p-y^p) and gap (p-y^g) components in series. A similar p-y curve modeling technique was applied to cohesionless soil (sand) by Wilson et al. (2000) and Brandenberg et al. (2001). A reasonably good agreement was obtained between the dynamic p-y analyses and the experimental results. Consequently, a modeling technique similar to that used by Wilson et al. (2000) and Brandenberg et al. (2001) will be used to model the soil-pile interaction effects in this research study.

CHAPTER 2

MODELLING OF INTEGRAL BRIDGES UNDER LIVE LOADS

The live load distribution factors are calculated as the ratio of the maximum live load effects obtained from 3-D analyses to those obtained from 2-D analyses. Analytically, the LLDFs for girder moment ($LLDF_M$) and shear ($LLDF_V$) are expressed as follows;

$$LLDF_M = \frac{M_{3D}}{M_{2D}} \tag{2.1}$$

$$LLDF_V = \frac{V_{3D}}{V_{2D}} \tag{2.2}$$

where M_{3D} and V_{3D} are respectively the maximum girder live load moment and shear force obtained from the analyses of the 3-D structural model for the most unfavorable longitudinal and transverse positions of multiple trucks and M_{2D} and V_{2D} are respectively the maximum girder live load moment and shear force obtained from the analysis of the 2-D structural model under a single truck load placed at the same longitudinal position as that of the trucks in the 3-D model. Accordingly, realistic 2-D and 3-D structural models of considered IBs is needed to calculate LLDFs. In this section, the assumptions of 2-D and 3-D structural models of considered bridges are discussed. Details about 2-D and 3-D modeling of the superstructures, substructures, and soil-structure interaction are presented in the following subsections.

2.1. 3-D MODELS

Several computational procedures such as grillage analogy, finite-strip and finite element methods have been used to analyze 3-D slab-on-girder bridges (Hays et al. 1986). In this study, the models subjected to truck loading are analyzed using the finite element method. A realistic finite element model is required for an accurate determination of live load distribution factors. Details about modeling of the superstructure, substructure and soil-structure interaction effects are presented in the following subsections.

2.1.1 SUPERSTRUCTURE MODELLING

2.1.1.1 SELECTION OF THE FINITE ELEMENT MODEL

The results from the comparative study on finite element modeling of slab-on-girder bridges conducted by Mounir et al. (1997) is used to select an accurate and practical FEM appropriate for this study. Mounir et al. (1997) compared four FEMs of slab-on-girder bridges. The first model is based on a study conducted by Hays et al (1986). The concrete slab is idealized as quadrilateral shell elements with five degrees of freedom (DOF) in each node and the steel girders are idealized as space frame member with six degree of freedom system. The center of gravity of the slab coincides with the girders' center of gravity and the girder properties are transformed to the deck center of gravity as shown in Fig.2.1. below.

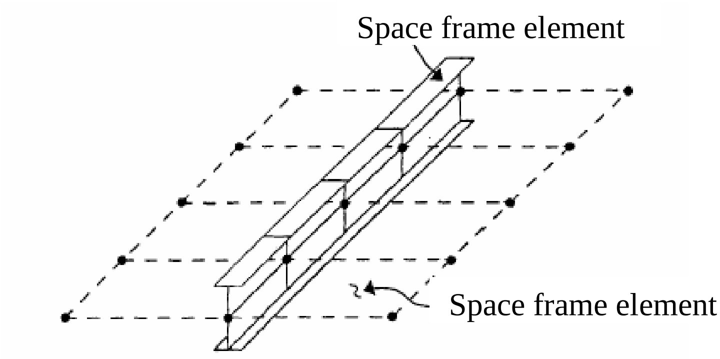

Figure 2.1 Finite element model conducted by Hays et al (1986)

The second FEM is based on the research conducted by Imbsen and Nutt (1978). The concrete slab is idealized as quadrilateral shell elements and the girders are idealized using eccentrically placed space frame members. This model is similar to the first one but, rigid links are imposed to accommodate for the eccentricity of the girders with respect to the slab as illustrated in Fig.2.2.

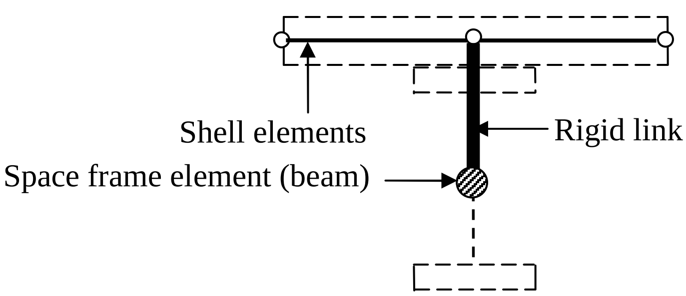

Figure 2.2 Finite element model conducted by Imbsen and Nutt (1978)

The third FEM is based on the research reported by Brockenbrough (1986). The concrete slab and the steel girder web are modeled as quadrilateral shell elements; the girder flanges are modeled as space frame elements while the flange to deck eccentricity is modeled by imposing a rigid link as shown in Fig. 2.3.

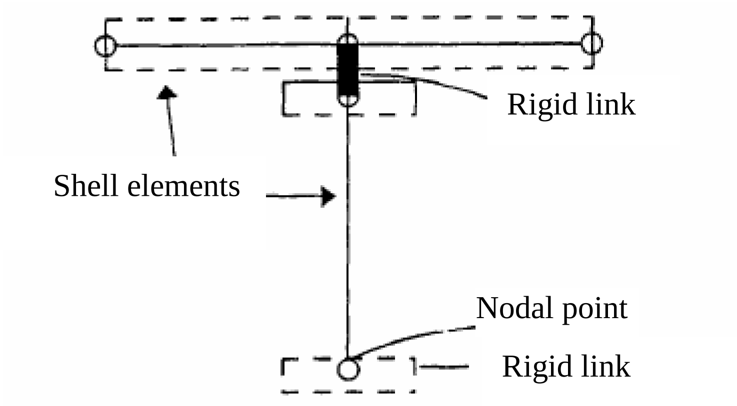

Figure 2.3 Finite element model conducted by Brockenbrough (1986).

The fourth FEM is based on the research study of Tarhini and Frederick (1992). The concrete slab is modeled using isotropic eight node brick (solid) elements with three DOF at each node. The steel girder flanges and webs are modeled using quadrilateral shell elements as demonstrated in Fig.2.4.

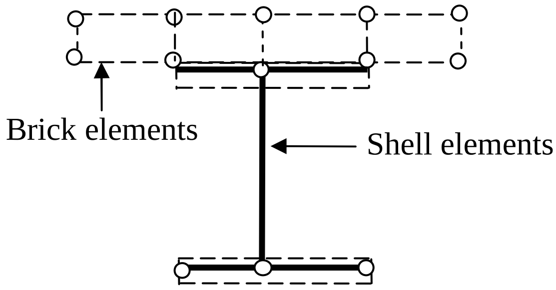

Figure 2.4. Finite element model conducted by Tarhini and Frederick (1992)

A research study similar to that of Monuir et al. (1997) has also been conducted by Hindi and Yousif (2005). The studies conducted by Mabsout et al. (1997) and Yousif and Hindi (2007) have concluded that the model proposed by Hays et al (1986) although simple, gives comparable results to those of the other more complicated three models. For the steel slab on girder bridge analyzed by Mabsout et al. (1997) (bridge length=56 feet., bridge width=30 feet, girder spacing=8 feet, slab thickness=7.5 inches and girder size=W36x160), the maximum girder moments are calculated as 5.396, 5.396, 4.968 and 5.206 kip-in, for the models proposed by Hays et al. (1986), Imbsen and Nutt (1978), Brockenbrough (1986) and Tarhini and Frederick (1992) respectively. To further verify the accuracy of the model used by Hays et al, three integral bridges and SSBs with 20, 30 and 40 m. spans are modeled using the modeling techniques proposed by Hays et al. (1986) and Imbsen and Nutt (1978) (using rigid links connecting the slab to beam). The analyses results for the maximum girder moments are presented in Table 2.1. As observed from the table, there is a reasonably good agreement between the maximum moments obtained from the two different modeling techniques. Thus, a finite element modeling technique similar to that proposed by Hays et al. (1986) is used to model the slab-on-girder deck of the SSBs and IBs used in this study. Accordingly, the bridge slab is modeled using quadrilateral shell elements with six DOF at each node and the girders are modeled as 3-D frame elements with six DOF's at each node as shown in the 3-D structural models presented in Fig. 2.1. Each girder is divided longitudinally into equal 0.6 m long segments. The slab is divided into four equal shell elements with a width of 0.6 m between the girders. The 0.6 m node spacing is chosen to facilitate the placement of the truck wheel loads at the nodes in the transverse direction of the bridge and to obtain square shell elements for better analysis accuracy. A convergency test is also conducted to assess the adequacy of the 0.6x0.6 m. shell element size used in the analyses. For this purpose, two IBs with 20 and 40 m. span length are modeled by using shell element sizes of 0.3x0.3 m., 0.6x0.6 m. and 1.2x1.2 m. The bridge models are then analyzed under AASHTO LRFD truck load. The analyses results are presented in Table 2.2. As observed from the table, there is a reasonably good agreement between the abutment and pile moment LLDFs obtained from the analyses of IBs modeled using different shell element sizes. This is mainly due to the large size of the bridge compared to the size of the shell elements used in the analyses.

Table 2.1. Comparison of the analyses results for the maximum girder moment using the modeling techniques proposed by Hays et al. (1986) and Imbsen and Nutt (1992)

Span Length (m)	**Bridge Type**	**Moment (kN.m) (Hays et al. 1986)**	**Moment (kN.m) (Imbsen and Nutt 1978)**
20	IB	533.08	530.53
	SSB	773.66	770.74
30	IB	1072.16	1070.20
	SSB	1315.58	1313.09
40	IB	1567.18	1565.64
	SSB	1810.36	1808.25

Table 2.2 Comparison of maximum moments and moment LLDFs for girder (M_a) abutment (M_a) and pile (M_p) in the cases of different element sizes for IBs having type IV girders spaced 2.4 m.

	Element Size (m)	20 m		40 m	
		Maximum Moment (kN.m)	LLDF	Maximum Moment (kN.m)	LLDF
	0.3	672.51	0.74	1376.31	0.62
$\mathbf{M_g}$	0.6	674.62	0.75	1377.78	0.62
	1.2	673.96	0.75	1376.96	0.62
	0.3	74.23	0.88	199.25	0.62
$\mathbf{M_a}$	0.6	76.70	0.90	201.42	0.63
	1.2	75.30	0.89	200.53	0.62
	0.3	10.83	0.47	39.25	0.48
$\mathbf{M_p}$	0.6	11.04	0.47	39.50	0.48
	1.2	10.98	0.47	39.35	0.48

Full composite action between the slab and the girders is assumed in the models. For that reason, the moment of inertia, I_g, of the girder used in the FEM is calculated as the moment of inertia, I_c, of the composite slab-on-girder section minus the moment of inertia, I_s, of the slab tributary to each girder (i.e. $I_g = I_c - I_s$.). Furthermore, in order to improve the accuracy of the analysis results for the bridges with the AASHTO type prestressed concrete girders, an exact solution for the torsional constant of the girders is used in the FEM (Yousif and Hindi 2007, Chen and Aswad 1996). In addition, to model the rigidity of the deck-abutment joint in the IBs models, the deck shell elements located within the joint area are assigned a large modulus of elasticity. However, to assess the effect of rigid joint assumption between the superstructure and the abutment on the magnitude of the design moment due to live load, sensitivity analyses are conducted on typical IB models with 20 and 40 m span lengths (The other parameters used are; AASHTO Type IV girders spaced at 2.4 m, slab thickness of 0.20 m, HP 250x85 piles and medium-stiff clay). In the analyses, the rigidities of the girder and the shell elements within the joint are modified between 1-20 times (N) their original rigidities and the analyses results for the girder design live load moment are presented in Table 2.3.

Table 2.3. Effect of slab and girder rigidity within the superstructure-abutment joint (joint rigidity) on girder live load moments

Joint Rigidity Scale Factor (N)	Design Live Load Moment (kN.m)	
	20 (m)	40 (m)
1	689.01	1315.87
2	684.15	1315.26
4	681.56	1315.12
8	680.23	1315.01
16	679.56	1314.96
20	679.33	1314.94

As observed from the table, the rigidity of the joint does not significantly affect the magnitude of the design girder moments. This is basically due to the small stiffness of the abutment-pile system relative to that of the superstructure. For SSBs, the diaphragms at the supports are modeled using 3-D frame elements. The nodes of the diaphragms are connected to the slab and to the girders.

The FEMs of IBs are built and analyzed using the program SAP2000 (2006). To verify the analysis results obtained from SAP2000, a similar FEM is also built using the program ANSYS (2007). The analysis results from both programs for a 20 m and a 40 m long IBs are presented in Table 4. The table shows the maximum girder moment and corresponding vertical girder displacements under AASHTO truck load. As observed from the table, nearly identical results are obtained from the analysis of FEMs using both programs.

Table 2.4. Maximum girder moment and displacements obtained using SAP2000 and ANSYS for IBs having type IV girders spaced 2.4 m.

Span length (m)	FEM Program	Max. Moment (kN.m)	Max. Girder Displacement (m)
20	SAP2000	674.6	0.0033
	ANSYS	675.4	0.0033
40	SAP2000	1377.8	0.020
	ANSYS	1378.7	0.020

2.1.2 SUBSTRUCTURE MODELING FOR INTEGRAL BRIDGES

The literature study on the finite element modeling of abutments and piles has revealed that the piles are modeled using 3-D beam elements (Faraji et al. 2001, Mourad and Tabsh 1999) while the abutments are generally modeled using either 8-node brick elements (Mourad and Tabsh 1999) or shell elements (Faraji et al. 2001). Modeling the abutments using 8-node brick elements requires the integration of stresses to calculate the shears and moments. Accordingly, in this study, the abutments are modeled using Mindlin shell elements (Cook 1995) with six DOF at each node to accurately simulate shear and bending deformations with minimal computational effort and the piles are modeled using 3-D beam elements. In addition, to model the rigidity of the deck-abutment joint, the abutment shell elements located within the joint area are assigned a large modulus of elasticity.

2.1.3 SOIL-BRIDGE INTERACTION

For modeling the soil-structure interaction in IBs, although the behavior of the backfill and foundation soil is nonlinear in nature, a linear elastic behavior is assumed due to the small lateral displacements of the abutments and piles under live load. The linear soil behavior under live load has already been validated in an earlier research study (Dicleli and Erhan 2008). The linear soil-pile and backfill-abutment interaction modeling is summarized below.

2.1.3.1 SOIL-PILE INTERACTION

The analysis and design of the pile next to the foundation soil is a typical example of soil-structure interaction problem. This interaction is nonlinear in nature such that the magnitudes of the soil and structural deformations and stresses are dependent on each other. This nonlinear relationship is defined by a nonlinear load (P)-deformation (Y) curve. The initial deflection of the soil is almost linear. However, at higher load levels, the deformation of soil increases rapidly with small increments of the load. This highly non-linear behavior can be simplified and modeled as elasto-plastic. This model is illustrated in Fig.2.5.

In this study, elastic portion of this elasto-plastic model is used to simulate the force-deformation response of the soil due to small lateral displacement of the piles under live load effects. This portion can be defined with a slope equal to the initial soil modulus E_{s}.

The calculation of the initial soil modulus E_s for clay requires the calculation of the ultimate soil resistance (Q_u) and the soil strain at 50% of the ultimate soil resistance (Δ_{50}).

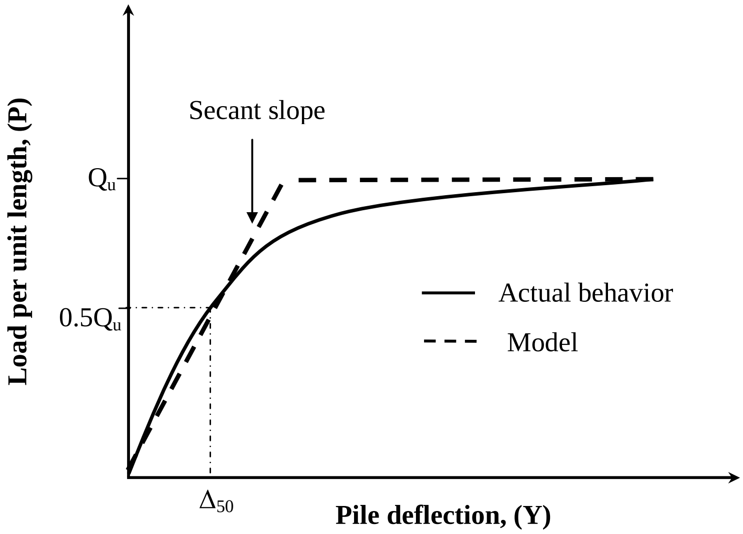

Figure 2.5. A typical P-Y curve and its elasto-plastic idealization

2.1.3.1.1. Estimation of Soil Modulus E_s

Two types of soil behavior are generally considered in estimating the ultimate soil resistance for laterally loaded piles in cohesive soil. The first type of behavior occurs near the ground surface, where the pile may push up a soil wedge by lateral movement, resulting so-called wedge action (Haliburton, 1971). For this type of behavior, the ultimate soil resistance is calculated as follows,

$$Q_u = \gamma \cdot d_p \cdot x_t + 3 \cdot C_u \cdot d_p + 0.5 \cdot C_u \cdot x_t \tag{2.3}$$

$$x_t = \frac{6 \cdot d_p \cdot C_u}{\gamma \cdot d_p + 0.5 \cdot C_u} \tag{2.4}$$

where, γ is unit weight of soil, C_u is the undrained shear strength of soil, d_p is diameter of piles and x_t is the depth from the soil surface where the wedge action occurs.

The second type of behavior occurs at some depth below the ground surface, where the soil attempts to flow around the pile. The ultimate soil resistance, Q_u is assumed as;

$$Q_u = 9 \cdot C_u \cdot d_p \tag{2.5}$$

It is noteworthy that the wedge action is critical for piles driven in soil where the pile top is located at or near the soil surface. In the case of IBs, the backfill soil behind the abutment and the embankment exert a surcharge pressures on the foundation soil and may prevent wedge action. Accordingly, the wedge action is not considered in the determination of Q_u. Thus, in this study, Eq. (2.5) is used to evaluate Q_u at any depth below the ground surface.

Skempton (1951) proposed a method based on laboratory test data, correlated with field test to calculate the initial elastic soil modulus E_s. Skempton (1951) found that about one-half of the ultimate soil resistance for a beam resting on soil is developed at a structure deflection, Δ_{50}, as follows;

$$\Delta_{50} = 2.5 \cdot \varepsilon_{50} \cdot d_p \tag{2.6}$$

where, ε_{50} is the soil strain at 50% of ultimate soil resistance.

Undrained shear strength of the clay, C_u and the corresponding values of ε_{50} used in the analyses to calculate the ultimate soil resistance, Q_u and the deflection at half resistance , Δ_{50} are obtained using a range of suggested values by Evans (1982) in Table 2.5. If the ultimate soil resistance, Q_u and the deflection at half resistance, Δ_{50} is computed, then the soil modulus for clay can be calculated using the following expression:

$$E_s = \frac{Q_u / 2}{\Delta_{50}} = \frac{Q_u}{5 \cdot \varepsilon_{50} \cdot d_p} \tag{2.7}$$

Table 2.5. Clay Properties.

CLAY STIFFNESS	***C_u(KPa)***	**ε_{50}**
SOFT	20	0.02
MEDIUM	40	0.01
MEDIUM-STIFF	80	0.0065
STIFF	120	0.005

2.1.3.1.2. Structural Model for the Analysis of the Piles

Linear springs are attached at each node along to the pile to model the linear force-deformation behavior of the soil, as shown in Fig.2.6 The lateral soil reaction is concentrated along the top 5 to 10 pile diameters of the pile (FHWA, 1986). Accordingly, nearly for the top 2m of pile, the spacing of the nodes is set as 10 cm. to accurately model the behavior of the soil. The spacing of the nodes is then gradually increased in steps along the length of the pile.

The elastic stiffness, k, of the soil surrounding the pile can be obtained by multiplying the initial soil modulus, E_s, by the tributary length, h, between the nodes along the pile. Thus;

$$k = \frac{Q_u \cdot h}{5 \cdot \varepsilon_{50} \cdot d_p} \tag{2.8}$$

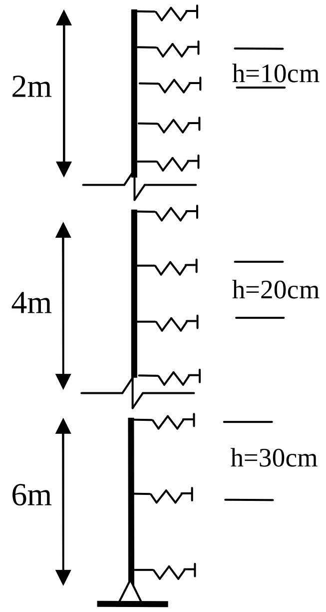

Figure 2.6. Structural Model for Analysis of Piles

2.1.3.2 ABUTMENT-BACKFILL INTERACTION MODELING

For the backfill behind the abutment, at rest earth pressure is assumed when there is no abutment movement. In the case of single span IBs, the abutment always moves towards the backfill under live load effects (Fig. 2.7). To prove this fact, the lateral displacements of the left and right abutments of the small and large single span IBs are plotted along the depth of the abutment in Fig.2.8

for various foundation soil stiffnesses. As observed from the figure, the abutment always moves towards the backfill under live load. Accordingly, only passive earth pressure develops behind the abutment in the case of single span IBs due to live load.

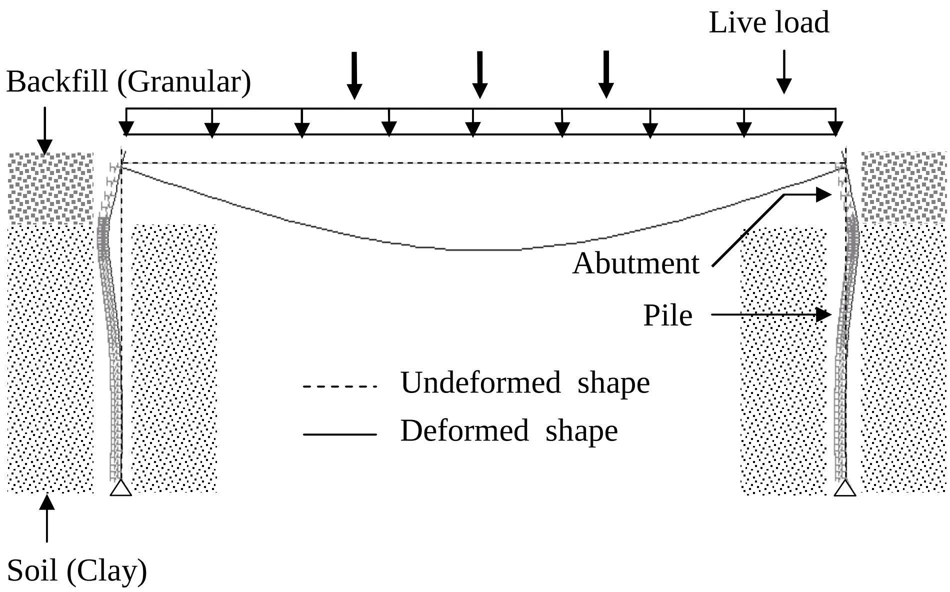

Figure 2.7. Deformed and undeformed shapes of an IB under live load

The active backfill pressure simply becomes a load (pressure) behind the abutment (i.e no stiffness to restrain the movement), which is already taken into consideration (either as active or as at-rest backfill pressure depending on the flexibility of the abutment) regardless of the presence of the live load to incorporate the effect of the backfill pressure at zero temperature condition in the design of the bridge (Dicleli 2000). Furthermore, the active backfill pressure condition behind the abutment does not restrain further movement of the abutment away from the backfill. Thus, it neither affects the lateral and rotational stiffness of the abutment nor creates a true backfill-abutment interaction condition where the resistance created by the soil depends on the movement of the structure. Consequently, the active backfill pressure condition is not considered in this study. However, when the abutment moves towards the backfill as a result of the rotation at the superstructure-abutment joint under live load effects, the restraining effect of the backfill creates a true abutment-backfill interaction condition affecting the lateral and rotational stiffness of the abutment (i.e. it is not simply a load due to backfill pressure as in the case of active condition). In this passive backfill condition, the intensity of the backfill pressure depends on the magnitude of the abutment displacement towards the backfill.

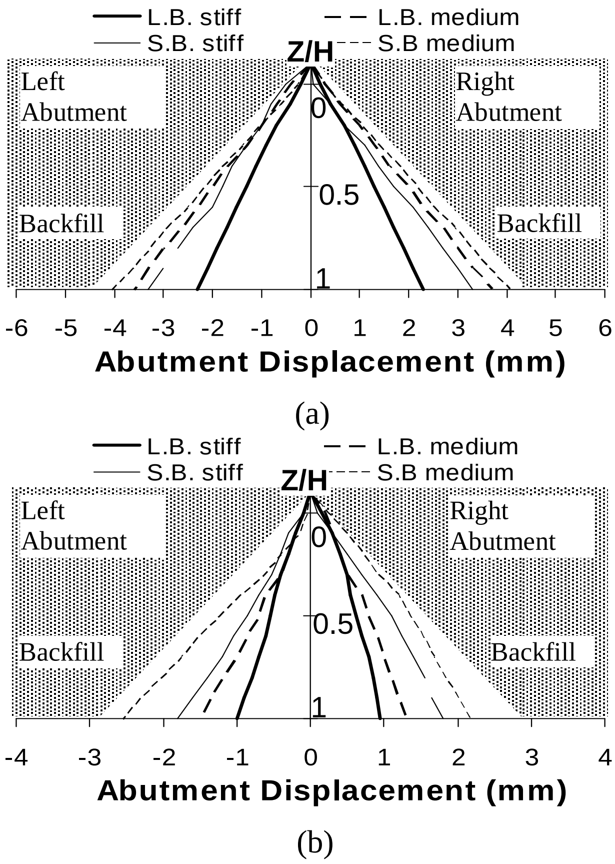

Figure 2.8 Abutment displacements vs. the ratio of abutment depth (Z) to abutment height (H) for (a) Symmetrical loading case (b) Unsymmetrical loading case for small and large bridges for various soil stiffness.

The actual earth pressure coefficient, K, may change between at rest, K_0, and passive, K_p, earth pressure coefficients depending on the amount of displacement. Clough and Duncan (1991) modeled the variation of the lateral earth pressure coefficient, K, as a function of the ratio, Δ/H, of abutment movement to abutment height using experimental data and finite element analyses. This relationship is presented in Fig. 2.9(a) for granular material commonly used behind abutments in bridge construction.

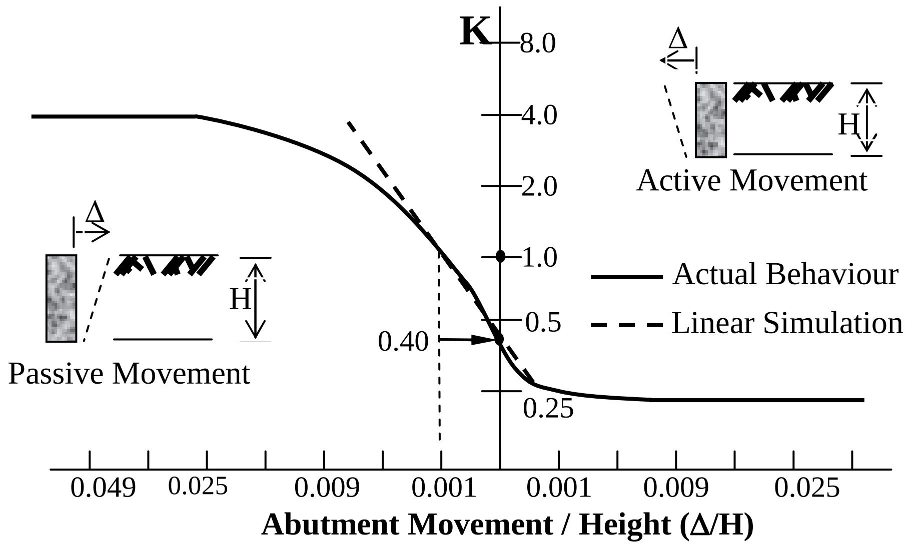

(a)

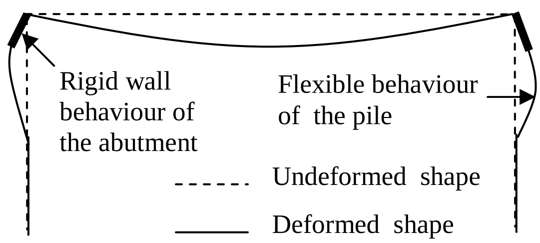

(b)

Figure 2.9 (a) Variation of backfill pressure coefficient as a function of the ratio of the abutment movement to abutment height (actual and linear simulation) **(b)** rigid wall behavior of abutment

Assuming small, uniform lateral abutment displacement of the abutment towards the backfill, the secant slope of the solid curve shown in Fig. 2.9 (a) between *Δ/H*=0 and *Δ/H* =0.001 is used to obtain a set of linear spring constants representing the relationship between the abutment movement and passive resistance of the backfill soil (The dashed line in Fig. 2.9). The uniform lateral abutment displacement is assumed for simplicity considering the general behavior of the bridge under combined loading. A similar approach is also followed in an official NCHRP document (NCHRP 2000) for the derivation of the force deflection curves behind the abutment, for cohesionless soil, non-plastic backfill (fine content less than 30%.). Accordingly, first, the variation of earth pressure, *ΔP*, from at rest (*Δ/H* =0) to passive state at *Δ/H* =0.001 is formulated for an arbitrary location, *z*, measured from the top of the abutment as;

$$\Delta P = \left(K_p - K_0\right) \cdot \gamma \cdot z \tag{2.9}$$

The above equation is divided by the displacement of the wall at *Δ/H* =0.001 to obtain the coefficient of horizontal subgrade reaction modulus, k_{sh}, for the backfill soil as;

$$k_{sh} = \frac{\left(K_p - K_0\right) \cdot \gamma \cdot z}{0.001 \cdot H} \tag{2.10}$$

The values of K_p at *Δ/H* =0.001 and K_0 for the backfill are obtained from Fig. 2.9 as 1.125 and 0.4 respectively. Assuming a unit weight of 20 kN/m^3 for the backfill, the coefficient of horizontal subgrade reaction modulus is computed as;

$$k_{sh} = \frac{14500}{H} \cdot z \tag{2.11}$$

The passive pressure modeling developed above only includes the portion of the passive resistance (that is, the compression stiffness of the backfill) mobilized by the movement of the abutment due to live load effects since the at-rest (or in some cases active depending on the flexibility of the abutment) earth pressure condition is already there at zero temperature state, which is included in the design of the bridge regardless of the presence of the live load.

It is noteworthy that in some instances, a gap may form behind the abutment as a result of the cyclic thermal movements of the bridge. This phenomenon is not taken into consideration in the modeling of the backfill-abutment interaction since the formation of a gap is generally more pronounced in the case of long IBs where the backfill behind the abutment nearly reaches its plastic state due to the considerable movement of the bridge towards the backfill. This is not the case for short IBs considered in this study. Furthermore, formation of a gap behind the abutment takes place after several annual thermal cycles over several years and the effect of the backfill-abutment interaction without a gap should be taken into consideration in design within this initial stage as well. It is also noteworthy that stub abutments are commonly used in IB construction according to the current state of design practice. For that reason, the deformation of the abutment under live load effects may be assumed to be similar to that of a rigid wall due to the large flexural stiffness of the abutment. This assumption is validated in Figs 2.9 (b) and Fig. 2.8. Fig. 2.9 (b) shows the general deformation of the bridge under live load where the abutment rotates almost like a rigid wall due to its relatively higher flexural stiffness compared to that of the piles and the backfill. Fig. 2.8 shows the lateral displacement of the abutment along the abutment height under live load effects for the small and large bridges and for various foundation soil stiffnesses. A linear variation of the abutment lateral displacement along the abutment height is observed in the figure. This linear variation proves that the abutment behaves similar to that of a rigid wall.

Therefore, the derivation of Eq. (2.11) is appropriately based on this assumption.

2.1.3.2.1 Implementation of Abutment-Backfill Interaction Behavior in the Structural Model

The stiffness of the boundary springs connected at the abutment-backfill interface nodes along the height of the abutment are calculated by multiplying k_{sh} by the area tributary to the node in the model. The backfill stiffness model described above considers only the passive resistance of the backfill to the movement of the abutment and excludes the at-rest portion of the backfill pressure which is not directly related to the loading on the bridge. Consequently, only the resistance of the backfill mobilized by live load is taken into consideration in the analyses. Note that under live loads, since the movement of the abutment occurs away from the backfill above the superstructure centroid, no spring is introduced between the superstructure top and the superstructure centroid in the model.

2.1.3.3 VERIFICATION OF LINEAR ELASTIC SOIL AND BACKFILL BEHAVIOR

In the structural modeling of IBs considered in this study, the foundation soil and backfill behavior is assumed to be linear elastic in anticipation of small lateral displacement of abutment and piles under live load effects. In this section this assumption is verified.

Figs. 2.10 (a) and (b) show the variation of the ultimate and calculated soil resistance along the depth of the pile for C_u=40 and 120 kPa respectively. The figures are plotted for the HP250x85 pile, small and large bridge with an abutment height of 3 m. as well as including and excluding the backfill effect. It is observed that for all the cases considered, the maximum calculated soil resistance per unit length of pile varies between 15% and 32% of the ultimate soil resistance. This clearly shows that the assumption of nearly elastic foundation soil behavior under live load effects is correct for short to medium length IBs where thermal effects are assumed to be negligible.

Figs. 2.10 (c) and (d) show the variation of the ultimate (full passive backfill pressure with $K_p=4.0$) and the calculated backfill pressure (with the at rest portion of the backfill pressure added) along the depth of the abutment for 3 and 5 m tall abutments respectively. The figures are plotted for HP250x85 pile, C_u=40 and 120 kPa and small and large bridges. It is observed that the backfill pressure due to live load effects increases nonlinearly as a function of the depth below the deck surface. This is mainly due to the higher stiffness of the backfill and increasing deformations of the abutment due to live load effects at larger depths below the deck surface. Furthermore, as observed from Figs. 2.10 (c) and (d), for the 3 m. tall abutment, the calculated passive backfill pressure under live load effects is relatively larger in spite of the smaller height of the abutment (compared to the 5 m. tall abutment). This mainly results from the more efficient compression of the backfill due to the larger bending stiffness of the shorter, 3.m tall abutment. However, for all the cases considered, the calculated backfill pressure due to live load effects is considerably smaller than the ultimate backfill pressure. This clearly demonstrates that the assumption of nearly elastic backfill behavior under live load effects is correct for short to medium length IBs where thermal effects are assumed to be negligible. The linear elastic modeling assumption for the backfill and foundation soil is further verified including the additional effects of super imposed dead load (SDL) and uniform positive temperature variation. For this purpose, the analyses of the large, 40 m. span IB is repeated under the effect of SDL and uniform positive temperature variation. The SDL is calculated as 5.2 kN/m per girder assuming a 70 mm thick asphalt and typical reinforced concrete traffic barriers used in North America. For the analysis of the bridge under thermal loading, the 27^{o}C maximum uniform positive temperature specified in AASHTO (2007) for concrete bridges located in areas of moderate and cold climates is used. Assuming a typical construction temperature of 15^{o}C, the positive uniform temperature variation used in the analyses is calculated as 12^{o}C. For the analyses under uniform positive temperature effects, the structural model shown in Fig. 3(a) is modified by adding springs above the superstructure centroid to correctly model the resistance of the backfill to the horizontal movement of the superstructure under uniform positive temperature variations. The analyses results are presented in Figs. 2.10 (e) and (f). Fig. 2.10(e) shows the variation of the ultimate and calculated soil resistance due to SDL, temperature variation, live load and total load (SDL + temperature + live load) along the depth of the pile. Fig. 2.10 (f) is similar, but it shows the variation of the ultimate and the calculated backfill pressure. In the plots of Fig. 2.10 (f), the at rest portion of the earth pressure is added to the results obtained for each load case considered. The figures clearly show that even if the effects of the SDL and uniform positive temperature variation are included in the analyses, the maximum calculated soil resistance per unit length of the pile and the calculated backfill pressure are considerably smaller than the ultimate soil resistance and ultimate backfill pressure respectively. This further confirms the assumption of linear elastic soil and backfill behavior under live load effects for short to medium length IBs. Furthermore, using linear elastic properties for the foundation soil and backfill as described here, facilitates the modeling of soil-bridge interaction behavior for the analysis and design of short to medium length IBs in practice.

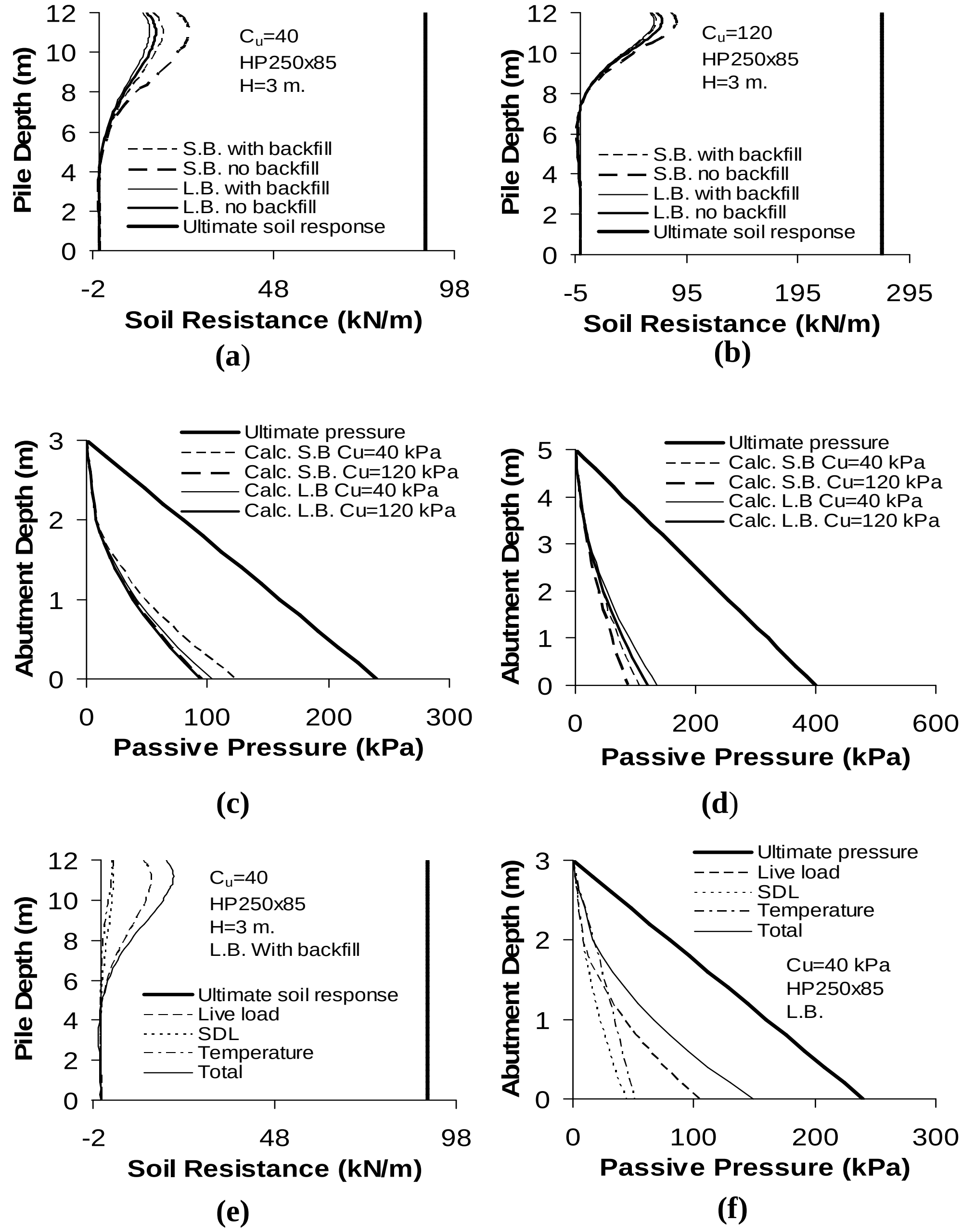

Figure 2.10 Calculated and ultimate soil resistance along the pile for (a) C_u=40 kPa, (b) C_u=120 kPa, Calculated and ultimate backfill pressure distribution for an abutment height of (c) 3 m., (d) 5 m. (e) Ultimate and calculated soil resistance due to SDL, temperature, live load and total load, (f) Ultimate and calculated backfill pressure distribution due to SDL, temperature, live load and total load.

2.2 2-D MODELS

For each 3-D structural model of the SSBs and IBs considered, a corresponding 2-D frame version is also built to enable the calculation of LLDFs. The 2-D structural model of a typical SSBs and IB used in the analyses is shown in Figs. 2(a) and (b). The model is built using 2-D elastic beam elements considering a single interior girder. In the structural models, the tributary width of the slab and abutments is set equal to the spacing of the girders. For the superstructure, full composite action between the slab and the girders is assumed. The stiffness properties of the composite slab-on-girder deck are expressed in terms of the properties of the slab using the transformed section method. The stiffness properties of the pile element in the 2-D model of the IB are calculated as the stiffness properties of a single pile multiplied by the number of piles per girder. The deck-abutment joint in the IB is modeled using a horizontal and a vertical rigid linear elastic beam element (an elastic beam element with large modulus of elasticity). The soil-structure interaction modeling for the 2-D model is similar to that for the 3-D model except the spring constants are calculated using a tributary area equal to the girder spacing times the vertical spacing between the nodes.

The 2-D and 3-D structural models of a typical IB used in the analyses is shown in Fig 2.11.

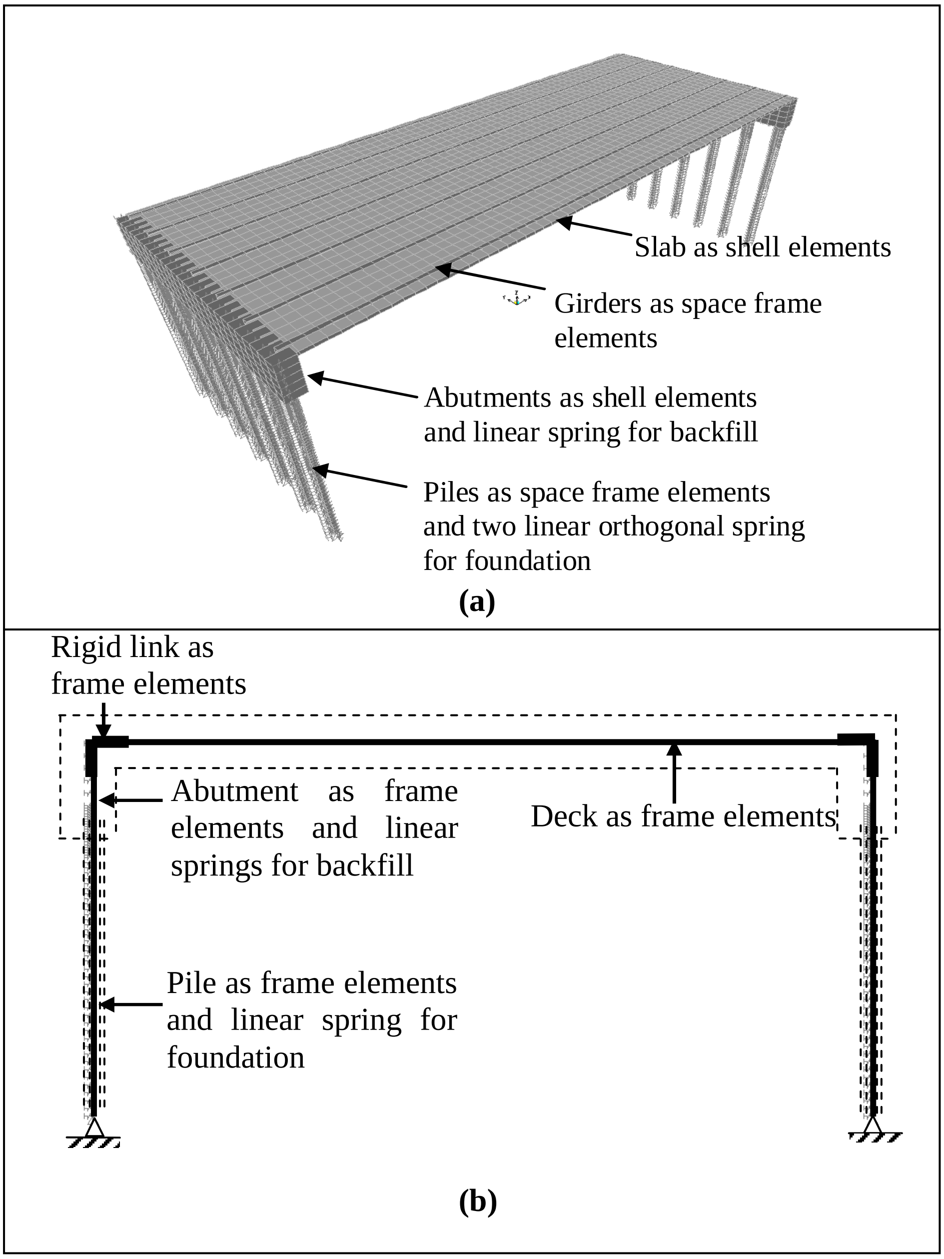

Figure 2.11 2-D and 3-D Structural model of a typical IB

2.3 LIVE LOAD MODEL

Vehicular live loading on highway bridges as descried in AASHTO (1994) LRFD Bridge Design Specifications are designated as HL-93. HL-93 live load consist of a combination of the:

- Design truck or design tandem, and
- Design lane load.

As illustrated in Fig.2.12, the design truck is a model such that the front axle is 35 kN, located 4300 mm behind, the drive axle is 145 kN, and the rear trailer axle is also 145 kN and is positioned at varIBle distance ranging between 4300mm and 9000mm. The design tandem illustrated in Fig.2.13 consists of two axles weighing 110 kN each spaced at 1200mm. The design lane load consists of a uniformly distributed load of 9.3 N/mm and is assumed to be distributed over a width of 3000 mm transversely.

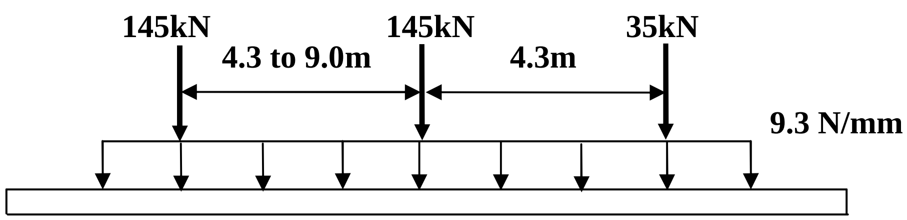

Figure 2.12 Design Truck and Design Lane Load

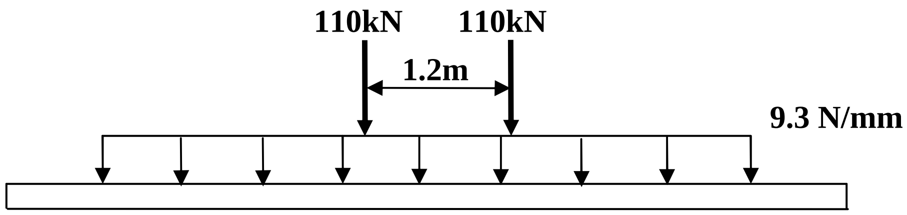

Figure 2.13 Design Tandem and Design Lane Load

The finite element analyses are conducted using the AASHTO design live load. As mentioned earlier, the AASHTO live load includes a design truck or a tandem and a lane load. Influence line analyses conducted on 2-D and 3-D IB models results have revealed that the tandem load does not govern the design for the IBs under consideration (Dicleli and Erhan 2010). Thus, it is not included in the analyses. Furthermore, since the design lane load was not considered in the development of the live load distribution factors in AASHTO (Patrick et al. 2006), the analyses are performed using the design truck alone.

The maximum load effect on a bridge is based on the position of the truck both in the longitudinal and transverse direction, the number of loaded design lanes and the probability of the presence of multiple loaded design lanes (presence of multiple trucks along the transverse direction of the bridge). The probability of the presence of multiple loaded design lanes is taken into consideration in AASHTO by using a multiple-presence factor. In the following sections, the calculation of the number of design lanes as well as the multiple-presence factor is described.

2.3.1. DESIGN LANES

To calculate the live load effects on bridges, the number of lanes a bridge may accommodate must be first determined. The bridge lanes are classified into two categories;

- Traffic lane
- Design lane

The traffic lane is planned by the traffic engineers and is typically taken as 3600mm. However, the number of design lanes is determined by taking the integer part of the ratio *W/3600*, where *W* is the clear roadway width in mm between curbs and/or barriers. In cases where the traffic lanes are less than 3600mm wide, the number of design lanes shall be equal to the number of traffic lanes, and the width of the design lane is taken as the width of the traffic lane. Roadway widths ranging from 6000mm to 7200mm must have two design lanes, each equal to one-half the roadway width.

2.3.2 MULTIPLE PRESENCE OF LIVE LOAD

The maximum live load effects are determined by considering each possible combination of number of loaded lanes multiplied by a corresponding multiple presence factor to account for the probability of simultaneous lane occupations by the full HL93 design live load. (AASHTO 2004). The multiple presence factor for various number of loaded design lanes is given in the table below.

Table 2.6 Multiple presence factors

Number of loaded lanes	Multiple presence factor(m)
1	1.20
2	1.00
3	0.85
>3	0.65

2.3.3 POSITION OF THE TRUCK ON THE BRIGDE

The longitudinal spacing and weights of the axles of HL-93 design truck must be specified as defined earlier. The transverse spacing of the wheels should be taken as 1800 mm. The design truck should be positioned transversely such that the center of any wheel load is not closer than 300 mm from the face of the curb or railing for the design of the deck overhang and 600 mm from the edge of the design lane for the design of all other components as illustrated in Fig.2.14 (AASHTO, 2007).

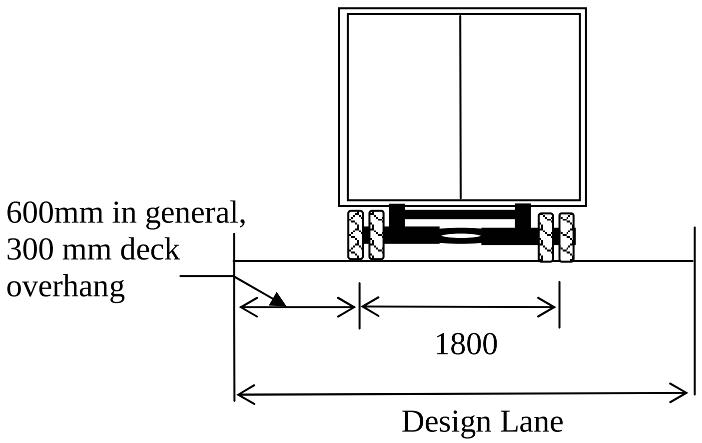

Figure 2.14 transverse position of truck

2.3.4 POSITION OF THE TRUCK ON BRIDGE FOR MAXIMUM LIVE LOAD EFFECTS

The maximum load effect on a bridge is based on the position of the truck both in the longitudinal and transverse direction, the number of loaded design lanes and the probability of the presence of multiple loaded design lanes. To calculate the maximum live load effects on the bridges under consideration, the position of the truck in the longitudinal direction as well as both the position and the number of trucks in the transverse direction are considered. The AASHTO spacing limitations used in the analyses for the transversely positioned trucks is shown in Fig. 2.15.

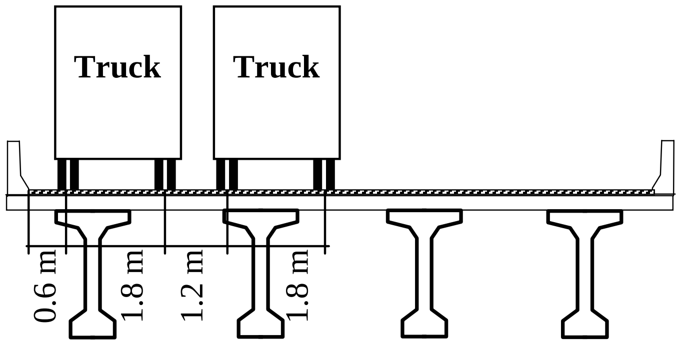

Figure 2.15 Typical slab-on-girder bridge cross-section and minimum clearances for design truck loading.

Influence line analyses conducted for IBs have revealed a truck longitudinal position for maximum girder moment (M_g) similar to that of simple supported brdiges due to the small stiffness of the abutment-pile system relative to that of the superstructure as shown in Table 2.7.

Table 2.7 Longitudinal position of the design truck (m) to produce the maximum girder moment for SSBs and for IBs with various foundation soil properties.

L (m)	Longitudinal Position of the Design Truck's Middle Axle from the Centerline of Left Support (m)				
	IB				SSB
	C_u=20	C_u=40	C_u=80	C_u=120	
20	10.5	10.5	10.5	10.4	10.7
40	20.4	20.4	20.4	20.4	20.7

In the table, the location of the AASHTO design truck's center axle from the centerline of the left support is given for 20 m and 40 m span IBs with various foundation soil properties as well as for SSBs. The truck longitudinal position for a typical IB is shown in Fig. 2.16 (b). To obtain the maximum shear force in the girder (V_g), the design truck is positioned such that the 145 kN rear axle of the truck is placed near the support for SSBs and at the deck abutment interface for the IB as illustrated in Figs. 2.16 (a) and (b). In the estimation of live load effects, the probability of the presence of multiple loaded design lanes is taken into consideration by using the multiple-presence factors defined in AASHTO (2007). The analyses are conducted for the case where one and two or more design lanes are loaded. The transverse loading case producing the maximum girder live load effect after multiplying by the multiple presence factor is used to obtain the LLDFs. A sample of two-and three-lanes transverse truck loading cases to produce the maximum girder moment is shown in Fig. 2.16 (c). In the figure, the hatched girder represents the girder where the maximum live load moment is calculated. Note that the arrangement of transverse truck position to produce the maximum live load effect changes based on the number of girders, girder spacing and the width of the bridge and is shown in Figure 2.16 (c) for a specific case only. For this specific case (for the bridge with seven girders), a sample of transverse direction analyses results to obtain the maximum girder moment is shown in Table 2.8. In the table, the girder moments are reported as a function of the position of the truck from the first girder for various numbers of loaded design lanes and corresponding multiple presence factors of AASHTO. Note that similar girder moments are obtained for the truck position beyond 4.8 m due to symmetry. Therefore calculated girder moments are not given not given in the table. As observed from the table for the truck positions beyond 4.8 m. the maximum interior girder moment occurs in girder # 3 (910.4 kN.m) for the three design lanes loaded case and for a transverse truck position at 1.2 m from the centerline of the first girder (the position of the first of the three transversely placed trucks is 1.2 m from the centerline of the first girder from left as shown in Fig. 2.16 (c)).

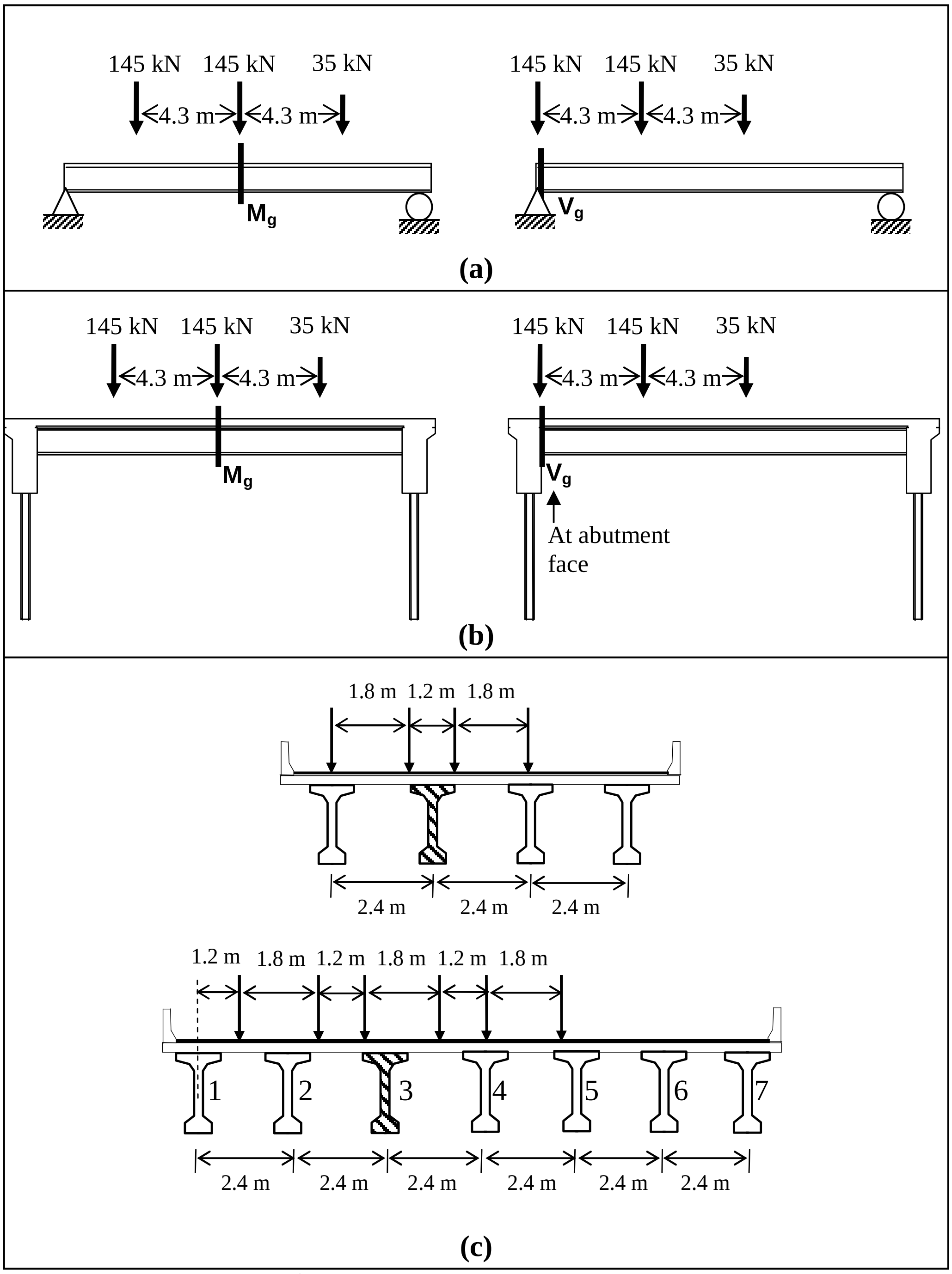

Figure 2.16 Location of calculated maximum girder shear (V_g) and moment (M_g) for (a) SSBs, (b) IB and (c) A sample of transverse position of design trucks to produce maximum moment in the hatched girders for the cases where two or more design lane loaded.

Table 2.8. A sample of transverse direction analyses results to obtain the maximum interior girder moment

Truck Position from the First Beam	Number of Loaded Design Lanes	Multiple Presence Factor	Girder Moment (kN.m)						
			1	2	3	4	5	6	7
0.6	2	1	628.39	875.95	760.78	447.34	280.48	246.48	227.22
	3	0.85	621.60	881.02	906.98	810.54	551.73	365.74	280.53
	4	0.65	548.63	752.30	786.79	784.75	740.06	565.18	329.06
1.2	2	1	502.50	834.38	818.29	527.28	304.50	248.85	224.64
	3	0.85	515.94	831.73	**910.4***	858.67	625.81	394.36	283.40
	4	0.65	468.72	714.50	782.48	795.65	761.95	623.63	359.20
1.8	2	1	401.89	777.43	859.09	612.70	338.72	254.55	221.73
	3	0.85	432.23	774.36	908.30	886.02	701.33	434.13	283.40
	4	0.65	405.65	670.80	778.60	756.50	778.58	670.80	405.35
2.4	2	1	327.98	710.59	867.73	696.79	385.53	264.85	218.60
	3	0.85	371.30	711.36	892.31	905.04	761.57	489.35	291.05
	4	0.65	359.20	623.63	761.95	795.65	782.48	714.50	468.72
3.0	2	1	279.03	623.02	858.22	759.36	449.66	281.44	215.66
	3	0.85	331.49	633.68	864.96	905.99	817.05	557.74	306.05
	4	0.65	329.06	565.18	740.06	784.75	786.79	752.30	548.63
3.6	2	1	247.30	535.27	817.82	812.14	528.14	306.29	213.78
	3	0.85	306.05	557.74	817.05	905.99	864.96	633.68	331.49
	4	0.65	N/A	N/A	N/A	N/A	N/A	N/A	N/A
4.2	2	1	227.61	452.61	757.87	844.74	609.93	340.01	213.55
	3	0.85	291.05	489.35	761.57	905.04	892.31	711.36	371.30
	4	0.65	N/A	N/A	N/A	N/A	N/A	N/A	N/A
4.8	2	1	218.30	398.38	698.97	859.34	698.97	389.38	218.30
	3	0.85	283.40	434.13	701.33	886.02	908.30	774.36	432.23
	4	0.65	N/A	N/A	N/A	N/A	N/A	N/A	N/A

*:Maximum response, N/A: Not Applicable

The design truck is positioned according to influence line analyses results to produce the maximum abutment and pile moments and shears (Dicleli and Erhan 2008). The maximum abutment and pile moments and shears is obtained from the position of the truck where maximum girder moment is obtained in longitudinal direction (Dicleli and Erhan 2008). In addition, the probability of the presence of multiple loaded design lanes is taken into consideration by multiplying the maximum moments and shears obtained from 3-D models under various number of transversely positioned trucks by the multiple-presence factor defined in AASHTO LRFD. A sample of transverse truck loading cases to produce the maximum abutment and pile moment as well as shear is shown in Fig. 2.17. Note that the arrangement of transverse truck position to produce the maximum live load effect changes based on the number of girders, girder spacing and the width of the bridge. For this specific case (for the bridge with seven girders), a sample of transverse direction analyses results to obtain the maximum abutment and pile moment is shown in Tables 2.9 and 2.10. In the tables, the abutment and pile moments are reported as a function of the position of the truck from the first girder for various numbers of loaded design lanes and corresponding multiple presence factors of AASHTO LRFD. As observed from the table, the maximum abutment and pile moments are calculated respectively as 123.74 (within the abutment width tributary to the girder) and 18.55 kN.m, for the three design lanes loaded case and for a transverse truck position at 1.2 m from the centerline of the first girder (the position of the first of the three transversely placed trucks is 1.2 m from the centerline of the first girder from left as shown in Fig. 2.17).

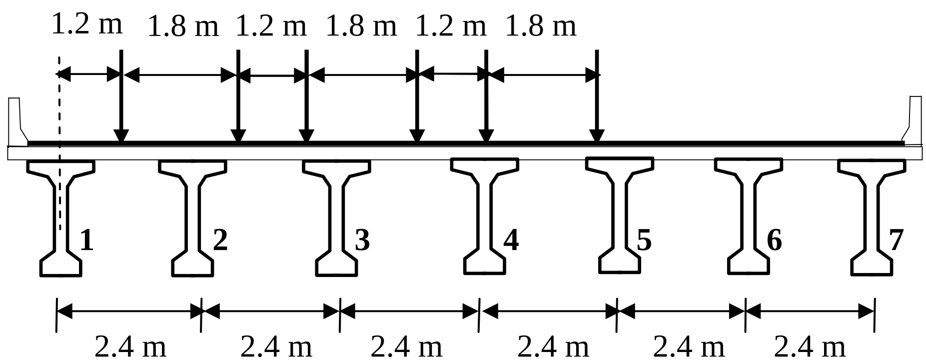

Figure 2.17 A sample of transverse position of design trucks to produce maximum moment in the pile and abutment for the case where three-lanes are loaded.

Table 2.9. A sample of transverse direction analyses results to obtain the maximum abutment moment

Truck Position from the First Girder	Number of Loaded Design Lanes	Multiple Presence Factor	Abutment Moment (kN.m)						
			Girder (Pile) #						
			1	2	3	4	5	6	7
0.6	2	1	37.22	49.58	38.89	42.55	103.16	117.64	101.57
	3	0.85	51.65	47.22	47.71	97.70	122.50	118.91	76.48
	4	0.65	37.60	49.16	82.73	94.48	95.48	86.82	54.59
1.2	2	1	38.37	41.90	45.38	89.31	118.97	89.04	65.56
	3	0.85	52.68	38.01	61.76	107.65	**123.74**	105.04	46.67
	4	0.65	32.22	59.87	88.21	95.66	94.34	78.94	32.28
1.8	2	1	39.70	36.26	49.16	101.32	115.64	71.06	36.08
	3	0.85	51.93	27.24	76.24	114.73	123.49	93.06	23.23
	4	0.65	24.32	70.26	92.22	96.11	92.15	70.04	24.49
2.4	2	1	40.98	37.27	62.73	110.07	109.35	57.67	18.84
	3	0.85	48.94	36.35	89.30	119.56	117.65	79.48	28.56
	4	0.65	32.28	78.94	94.34	95.66	88.21	59.87	32.22
3.0	2	1	41.59	42.22	76.45	114.67	99.03	50.20	26.08
	3	0.85	44.84	50.29	100.27	121.91	110.39	65.28	38.65
	4	0.65	54.59	86.82	95.48	94.48	82.73	49.16	37.60
3.6	2	1	43.56	45.93	89.52	69.22	122.31	46.12	34.32
	3	0.85	38.65	65.28	110.39	121.91	100.27	50.29	44.84
	4	0.65	N/A	N/A	N/A	N/A	N/A	N/A	N/A
4.2	2	1	42.30	50.49	100.98	111.85	73.21	41.18	39.86
	3	0.85	28.56	79.48	117.65	119.56	89.30	36.35	48.94
	4	0.65	N/A	N/A	N/A	N/A	N/A	N/A	N/A
4.8	2	1	42.77	31.14	91.56	122.00	91.04	31.61	43.43
	3	0.85	23.23	93.06	124.49	114.73	76.24	27.24	51.93
	4	0.65	N/A	N/A	N/A	N/A	N/A	N/A	N/A
5.4	2	1	39.86	41.18	73.21	111.85	100.98	50.49	42.30
	3	0.85	46.67	105.04	123.74	107.65	61.76	38.01	52.68
	4	0.65	N/A	N/A	N/A	N/A	N/A	N/A	N/A
6.0	2	1	34.42	46.12	122.31	69.22	89.52	45.93	43.56
	3	0.85	76.48	118.91	122.50	97.70	47.71	47.22	51.65
	4	0.65	N/A	N/A	N/A	N/A	N/A	N/A	N/A
6.6	2	1	26.08	50.20	99.03	114.67	76.45	42.22	41.59
	3	0.85	N/A	N/A	N/A	N/A	N/A	N/A	N/A
	4	0.65	N/A	N/A	N/A	N/A	N/A	N/A	N/A
7.2	2	1	18.84	57.67	109.35	110.07	62.73	37.27	40.98
	3	0.85	N/A	N/A	N/A	N/A	N/A	N/A	N/A
	4	0.65	N/A	N/A	N/A	N/A	N/A	N/A	N/A
7.8	2	1	36.08	71.06	115.64	101.32	49.16	36.26	39.70
	3	0.85	N/A	N/A	N/A	N/A	N/A	N/A	N/A
	4	0.65	N/A	N/A	N/A	N/A	N/A	N/A	N/A
8.4	2	1	65.56	89.04	118.97	89.31	45.38	41.90	38.37
	3	0.85	N/A	N/A	N/A	N/A	N/A	N/A	N/A
	4	0.65	N/A	N/A	N/A	N/A	N/A	N/A	N/A
9.0	2	1	101.57	117.64	103.16	42.55	38.89	49.58	37.22
	3	0.85	N/A	N/A	N/A	N/A	N/A	N/A	N/A
	4	0.65	N/A	N/A	N/A	N/A	N/A	N/A	N/A

Table 2.10. A sample of transverse direction analyses results to obtain the maximum pile moment

Truck Position from the First Girder	Number of Loaded Design Lanes	Multiple Presence Factor	**Pile Moment (kN.m)**						
			Girder (Pile) #						
			1	2	3	4	5	6	7
0.6	2	1	13.60	13.74	13.95	14.23	14.53	14.74	14.82
	3	0.85	17.56	17.73	17.96	18.22	18.43	18.45	18.54
	4	0.65	18.19	18.22	18.25	18.27	18.34	18.46	18.51
1.2	2	1	13.64	13.78	13.99	14.26	14.51	14.67	14.71
	3	0.85	17.65	17.81	18.02	18.23	18.39	**18.55**	18.43
	4	0.65	18.01	18.12	18.21	18.28	18.31	18.29	18.23
1.8	2	1	13.71	13.84	14.04	14.29	14.50	14.60	14.60
	3	0.85	17.74	17.90	18.08	18.25	18.35	18.36	18.30
	4	0.65	18.12	18.21	18.27	18.29	18.27	18.20	18.11
2.4	2	1	13.77	13.91	14.10	14.31	14.47	14.52	14.49
	3	0.85	17.84	17.98	18.14	18.27	18.30	18.27	18.18
	4	0.65	18.23	18.29	18.31	18.28	18.21	18.12	18.01
3.0	2	1	13.84	13.97	14.15	14.34	14.44	14.45	14.39
	3	0.85	17.94	18.07	18.20	18.27	18.25	18.17	18.06
	4	0.65	18.51	18.46	18.34	18.27	18.25	18.22	18.19
3.6	2	1	13.92	14.05	14.21	14.35	14.41	14.37	14.29
	3	0.85	18.06	18.17	18.25	18.27	18.20	18.07	17.94
	4	0.65	N/A	N/A	N/A	N/A	N/A	N/A	N/A
4.2	2	1	14.00	14.13	14.26	14.36	14.36	14.29	14.19
	3	0.85	18.18	18.27	18.30	18.27	18.14	17.98	17.84
	4	0.65	N/A	N/A	N/A	N/A	N/A	N/A	N/A
4.8	2	1	14.10	14.20	14.32	14.37	14.32	14.21	14.10
	3	0.85	18.30	18.36	18.35	18.25	18.08	17.90	17.74
	4	0.65	N/A	N/A	N/A	N/A	N/A	N/A	N/A
5.4	2	1	14.19	14.29	14.36	14.36	14.26	14.13	14.00
	3	0.85	18.43	18.55	18.39	18.23	18.02	17.81	17.65
	4	0.65	N/A	N/A	N/A	N/A	N/A	N/A	N/A
6.0	2	1	14.29	14.37	14.41	14.35	14.21	14.05	13.92
	3	0.85	18.54	18.45	18.43	18.22	17.96	17.73	17.56
	4	0.65	N/A	N/A	N/A	N/A	N/A	N/A	N/A
6.6	2	1	14.39	14.45	14.44	14.34	14.15	13.97	13.84
	3	0.85	N/A	N/A	N/A	N/A	N/A	N/A	N/A
	4	0.65	N/A	N/A	N/A	N/A	N/A	N/A	N/A
7.2	2	1	14.49	14.52	14.47	14.31	14.10	13.91	13.77
	3	0.85	N/A	N/A	N/A	N/A	N/A	N/A	N/A
	4	0.65	N/A	N/A	N/A	N/A	N/A	N/A	N/A
7.8	2	1	14.60	14.60	14.50	14.29	14.04	13.84	13.71
	3	0.85	N/A	N/A	N/A	N/A	N/A	N/A	N/A
	4	0.65	N/A	N/A	N/A	N/A	N/A	N/A	N/A
8.4	2	1	14.71	14.67	14.51	14.26	13.99	13.78	13.64
	3	0.85	N/A	N/A	N/A	N/A	N/A	N/A	N/A
	4	0.65	N/A	N/A	N/A	N/A	N/A	N/A	N/A
9.0	2	1	14.82	14.74	14.53	14.23	13.95	13.74	13.60
	3	0.85	N/A	N/A	N/A	N/A	N/A	N/A	N/A
	4	0.65	N/A	N/A	N/A	N/A	N/A	N/A	N/A

CHAPTER 3

EFFECT OF SOIL-BRIDGE INTERACTION ON THE MAGNITUDE OF INTERNAL FORCES IN INTEGRAL BRIDGE COMPONENTS DUE TO LIVE LOAD EFFECTS

In bridge design, most design engineers prefer using simplified two dimensional (2-D) structural models and live load distribution factors available in current design codes to determine live load effects in bridge components. In the case of IBs, the design engineers generally use a 2-D structural model of the bridge where the effect of the backfill is neglected and the piles are simply modeled as equivalent cantilevers neglecting the effect of the foundation soil stiffness. Accordingly, in this part of the thesis study, an extensive parametric study is conducted to investigate the effect of the backfill and foundation soil stiffness as a function of various geometric and structural parameters on the distribution of internal forces due to live load effects among IB components. The results from such an extensive parametric study is used to present design recommendations to the engineering community at large for building simplified 2-D structural models of IBs for estimating live load effects in IB components using distribution factors. Furthermore, the information acquired from these 2-D studies is used to determine the details of 2-D structural models of IBs which are used together with 3-D models of the same IBs for determining live load distribution factors for IB components. For this purpose, several 2-D structural models of IBs are built including and excluding the effect of backfill and considering a range of foundation soil stiffness values for the piles. In the 2-D structural models studied, several geometric and structural parameters are varied to cover a wide range of possible IB configurations.

The 2-D sensitivity analyses are limited to symmetrical IBs with no skew. The abutments are assumed as supported by end-bearing steel H-piles. A moment connection is assumed between the piles and abutment as well as between the superstructure and abutment. Granular uncompacted material typically used for IB construction is assumed for the backfill behind the abutments while cohesive soil (clay) is assumed for the pile foundations. The water behind the abutment is assumed to be properly drained through the granular material and perforated pipes wrapped with geotextile typically used at the abutment bottom in bridge construction. Moreover, the scope of this research study is limited to short to medium length IBs where the superimposed dead load (SDL) and thermal effects are assumed to be less significant compared to live load effects. Consequently, yielding of the piles is not anticipated under total load effects and the behavior of the backfill and foundation soil is assumed to be within the linear elastic range since small lateral displacements of the abutments and piles are expected under live load effects. This also ensures that potential formation of a gap behind the abutment due to cyclic thermal movements is negligible.

To reach the above stated objective, 2-D structural models of IBs are built including and excluding the effect of backfill and foundation soil. In the 2-D structural models studied, several geometric, structural and geotechnical parameters are varied to cover a wide range of possible IB configurations. This resulted in 200 different IB structural models. The structural models are then analyzed under current AASHTO LRFD Bridge Design Specifications (2007) live loads using the finite element based program SAP2000. Furthermore, to verify the assumption of linear elastic behavior for the backfill and foundation soil, a typical IB is analyzed under thermal, SDL and live load effects and the results from each individual load case and their combination are compared with the ultimate soil resistance. The results from these analyses are then summarized and the conclusions are outlined. The details pertaining to the parameters considered, structural modeling including soil-bridge interaction effects and analyses results are presented in the following sections.

3.1. PARAMETERS CONSIDERED IN THE STUDY

A parametric study is conducted to investigate the effects of backfill and foundation soil on the magnitude of internal forces in IB components due to live loads for various geometric, structural and geotechnical properties of IBs. In the parametric study, the stiffness of the foundation soil (clay) is anticipated to affect the magnitude of the internal forces in IB components due to live loads. Thus, an equivalent pile length neglecting the effect of the foundation soil and four values of clay stiffness are considered in the analyses. Furthermore, to cover a wide range of possible IB configurations, the bridge size, number of span, abutment height as well as pile size and orientation are varied. Details of the parameters considered in the analysis are given in Table 1. The pile sizes presented in Table 3.1 are chosen to cover a wide range of steel H-pile sizes used by many departments of transportation in North America and Europe. The vertical capacity of the end bearing piles is 3270 kN for HP250x85 and 4770 kN for HP310x125. The lateral capacity of the piles varies between 167 kN and 552 kN depending on the pile size and undrained shear strength of the foundation soil.

Table 3.1. Parameters considered in the analyses.

Parameter	Description
Bridge size or stiffness	Small and Large bridge
Number of Spans	1, 2 and 3 (for small bridge only)
Backfill	Including and excluding backfill effect
Soil Stiffness	Excluding soil effect (Equv. pile length) and soft, medium, medium-stiff, stiff clay
Pile Size	HP 250x85, HP 310x125
Pile Orientation	Weak and Strong axis bending
Abutment Height	3m, 5m.

3.2. PROPERTIES OF INTEGRAL BRIDGES USED IN THIS STUDY

Two different existing IBs are considered to investigate the effect of the backfill and foundation soil on the magnitude of internal forces in IB components due to live loads. The bridges are chosen such that the study covers a wide range of superstructure and abutment stiffness properties found in practice. The first bridge is referred to as the small bridge with 20m. span length and 2.4 m. girder spacing. It represents those bridges with relatively smaller superstructure and abutment stiffness. The bridge superstructure is composed of a 190 mm thick reinforced concrete slab supported by W760x173 steel girders. The abutment thickness is 1m. The second bridge is referred to as the large bridge with 40 m. span length and 2.4 m. girder spacing. It represents those bridges with relatively larger superstructure and abutment stiffness. The superstructure is composed of a 225 mm. thick reinforced concrete slab supported by AASHTO Type VI prestressed concrete girders. The abutment thickness is 1.5 m. Please note that the pile sizes used in this study are adequate for both the small and large IBs, even when the number of piles per girder is taken as one for both bridges. Additionally, the pile sizes are already varied as a parameter. This variation results in various pile stiffness values per girder and covers a wide range of design scenarios.

For the 2- and 3-span versions of the small IB, elastomeric bearings are assumed at the intermediate supports. The properties of the 2- and-3 span bridges are assumed to be identical to those of the small bridge. General details of the 2- and 3- span bridges are illustrated in Fig. 3.1 (c) and (d). Moreover, the properties of all the bridges are presented in Table 3.2.

It is noteworthy that in the construction of IBs, the girders are first placed on the supports and then the slab is cast integral with the girders and the abutments. Thus, each span acts as simply supported until the slab hardens. Accordingly, the effect of the dead load of the girder and that of the slab is calculated using a simply supported span while the continuity is taken into consideration only in the calculation of the effects of the superimposed dead loads (such as asphalt) and live load. Therefore, the extrapolation of single span bridge to the multiple span bridges is not going to introduce a large error as far as the superstructure design is concerned (For example, for an IB with a prestressed concrete girder, the girder size will not reduce from AASHTO type IV to AASHTO type III just because of the effect of continuity.). Consequently, it is believed that the effect of this assumption on the outcome of this research study (especially when studying solely the effect of continuity on the distribution of internal live load forces among the IB components) is practically negligible.

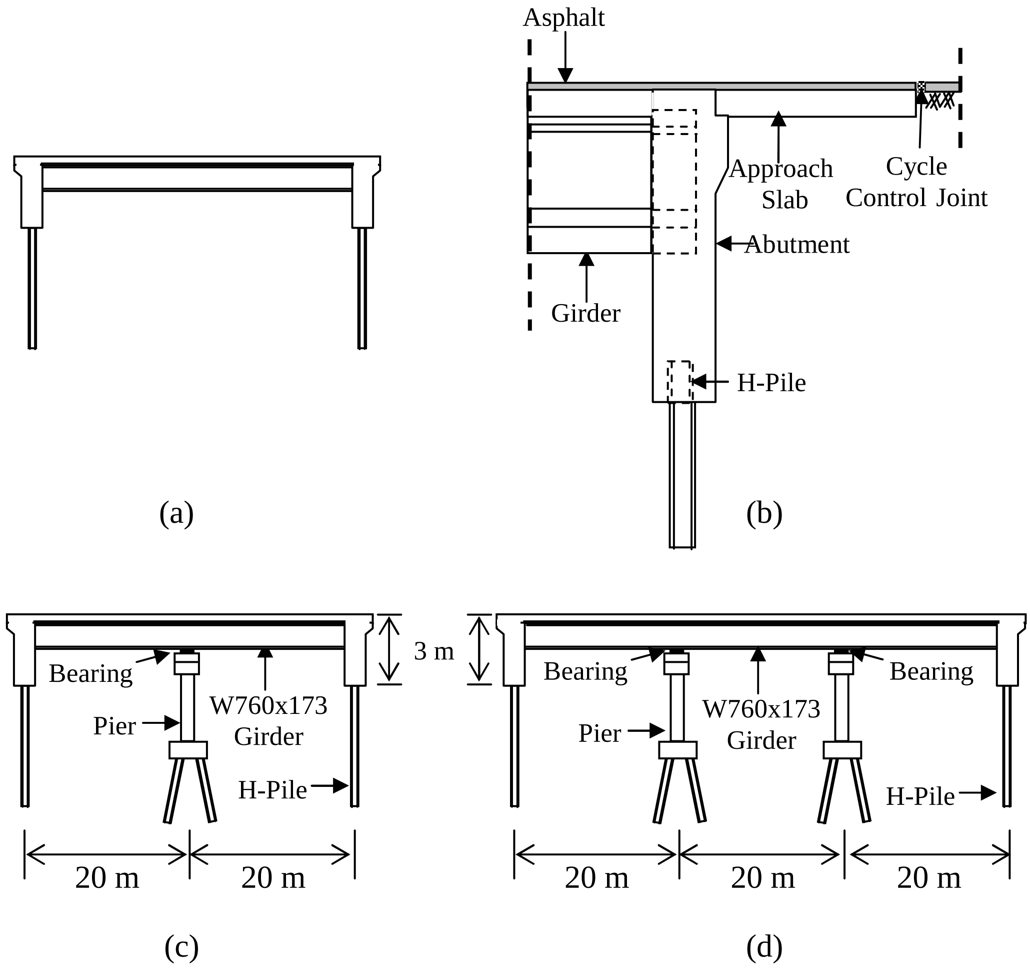

Figure 3.1 (a) A typical single span IB, **(b)** Details of a typical IB at the abutment, **(c)** Two-span version of the small bridge used in the analyses **(d)** Three-span version of the small bridge used in the analyses

Table 3.2 Properties of the IBs used in the analyses

Properties	Small Bridge (1-, 2-, 3-Span)	Large Bridge (Single Span)
Span length (m)	20	40
Superstructure type	Slab-on-girder	Slab-on-girder
Girder spacing (mm)	2400	2400
Girder type	Steel	Prestressed Concrete
Girder size	W760x173	AASHTO VI
Slab thickness (mm)	190	225
Composite girder, A (mm^2)	$0.661x10^6$	$1.174x10^6$
Composite girder, I (mm^4)	$54300x10^6$	$646000x10^6$
Abutment thickness (mm)	1000	1500
Abutment ,A (per girder), (mm^2)	$2.400x10^6$	$3.600x10^6$
Abutment, I (per girder), (mm^4)	$200000x10^6$	$675000x10^6$
Concrete strength (girder) (MPa)	N/A	50
Concrete strength (other) (MPa)	30	30
Type of bearings over piers (for multiple span cases)	Elastomeric	N/A
Number of piles per girder	1	1

3.3. INFLUENCE LINES VERSUS SOIL STIFFNESS

Influence lines are used for the IBs considered in this study to determine the location of the design truck on the bridge producing the maximum internal forces in IB components (Figs 3.2-3.4). To investigate whether the shape of the influence lines and hence the position of the truck on the bridge is affected by the stiffness of the foundation soil, the influence line analyses of the large IB for various foundation soil stiffness values are conducted. The location of the internal forces for which influence lines are plotted, are shown in Fig. 3.2 (a). These locations are chosen to generate the maximum internal forces in the superstructure, abutment and piles. The location for the maximum span (positive) moment (M_d^+) is chosen under one of the truck axels when that axle is as far from one support as the center of gravity of all the axles on the bridge is from the other support (Barker and Puckett 2007). Although this approach seems to be suitable for only simply supported bridges, influence line analyses conducted for IBs have revealed a truck longitudinal position for maximum girder moment (M_d^+) similar to that of a SSB as shown in Table 3.3. This is mainly due to the small base length of the truck relative to the total span length and the symmetrical composition of the bridges. The plots of the influence lines for various soil stiffness ranges are compared in Figs 3.2(b)-(g). Figs. 3.2 ((b) and (c)), ((d) and (e)) and ((f) and (g)) show the influence line plots respectively for the superstructure, abutment and pile bending moment and shear. As observed from the figures, although the maximum amplitude of the influence lines change as a function of the soil stiffness, the shapes of the influence lines remain similar and the influence lines for the superstructure shear overlap for all the soil stiffness ranges considered. In other words, if the influence lines are normalized with respect to their maximum amplitude and plotted, those obtained for various foundation soil stiffness values will all overlap. This clearly demonstrates that the position of the design truck along the bridge to produce the maximum live load effect will not change as a function of the soil stiffness. Thus, for the remainder of the study, the positions of the truck to produce the maximum live load effects in IB components are fixed for all the foundation soil stiffness values used in the analyses.

Influence line plots for the 2 and 3 span IBs are respectively shown in Figs. 3.3 and 3.4 for medium clay (Cu =40 kPa). The AASHTO truck's middle axle (145 kN middle axle) will be placed on the maximum point of the influence line plots to obtain the maximum girder, abutment and pile moment as well as maximum pile and abutment shear. Nevertheless, to obtain the maximum girder shear, the rear axle (145 kN rear axle) should be placed on the maximum point of the influence line plots (near the support).

Table 3.3 Longitudinal position of the design truck (m) to produce the maximum girder moment for SSBs and for IBs with various foundation soil properties.

Number of Spans	**Longitudinal Position of the Design Truck's Middle Axle from the Centerline of Left Support (m)**				
	IB				SSB
	C_u=20	C_u=40	C_u=80	C_u=120	
1 (Small Bridge)	10.5	10.5	10.5	10.4	10.7
1 (Large Bridge)	20.4	20.4	20.4	20.4	20.7
2	10.4	10.4	10.4	10.4	10.7
3 (Truck is in mid-span)	10.4	10.4	10.4	10.4	10.7
3 (Truck is in side-span)	10.4	10.4	10.4	10.4	10.7

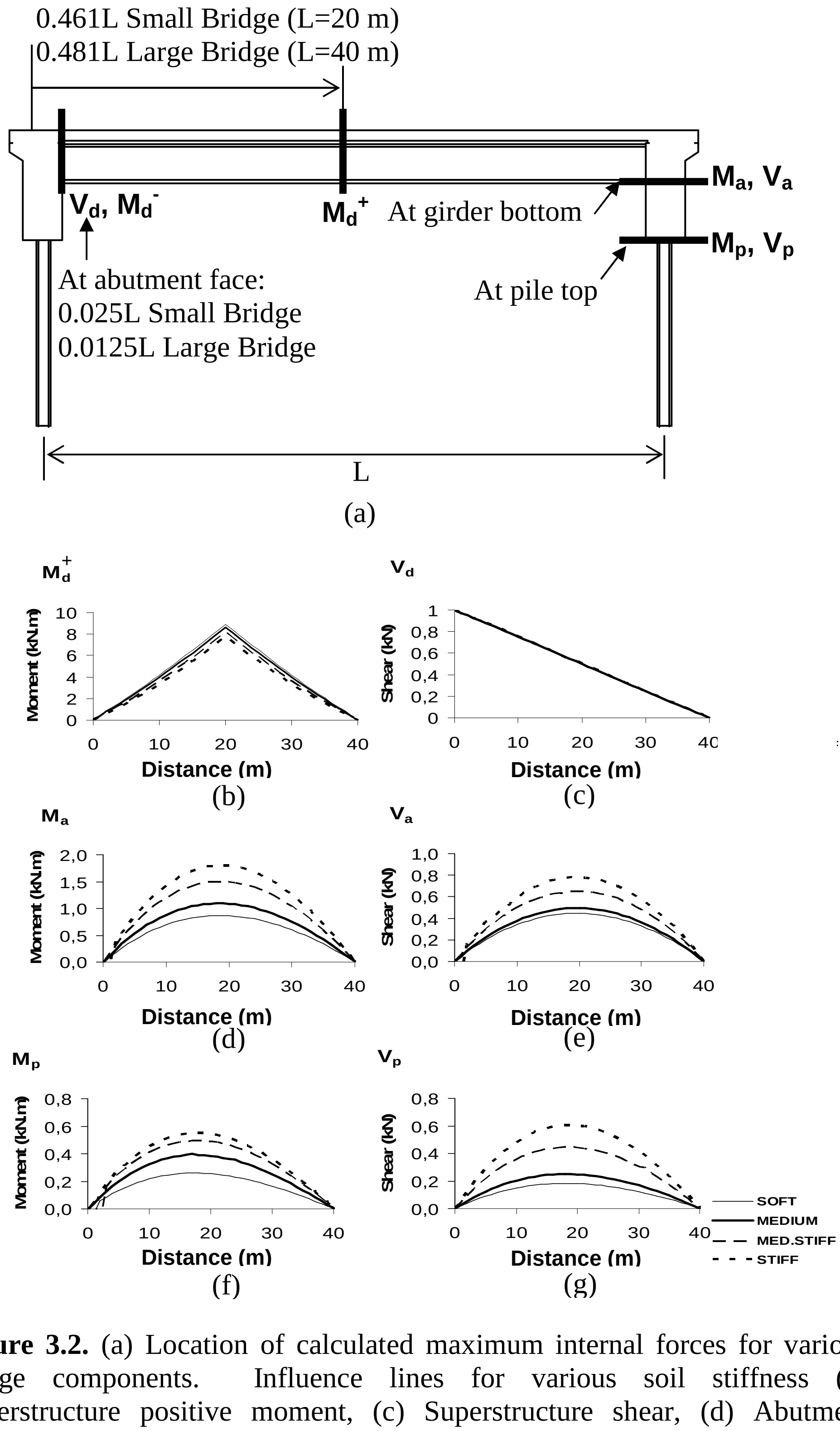

Figure 3.2. (a) Location of calculated maximum internal forces for various bridge components. Influence lines for various soil stiffness (b) Superstructure positive moment, (c) Superstructure shear, (d) Abutment moment, (e) Abutment shear, (f) Pile moment, (g) Pile shear.

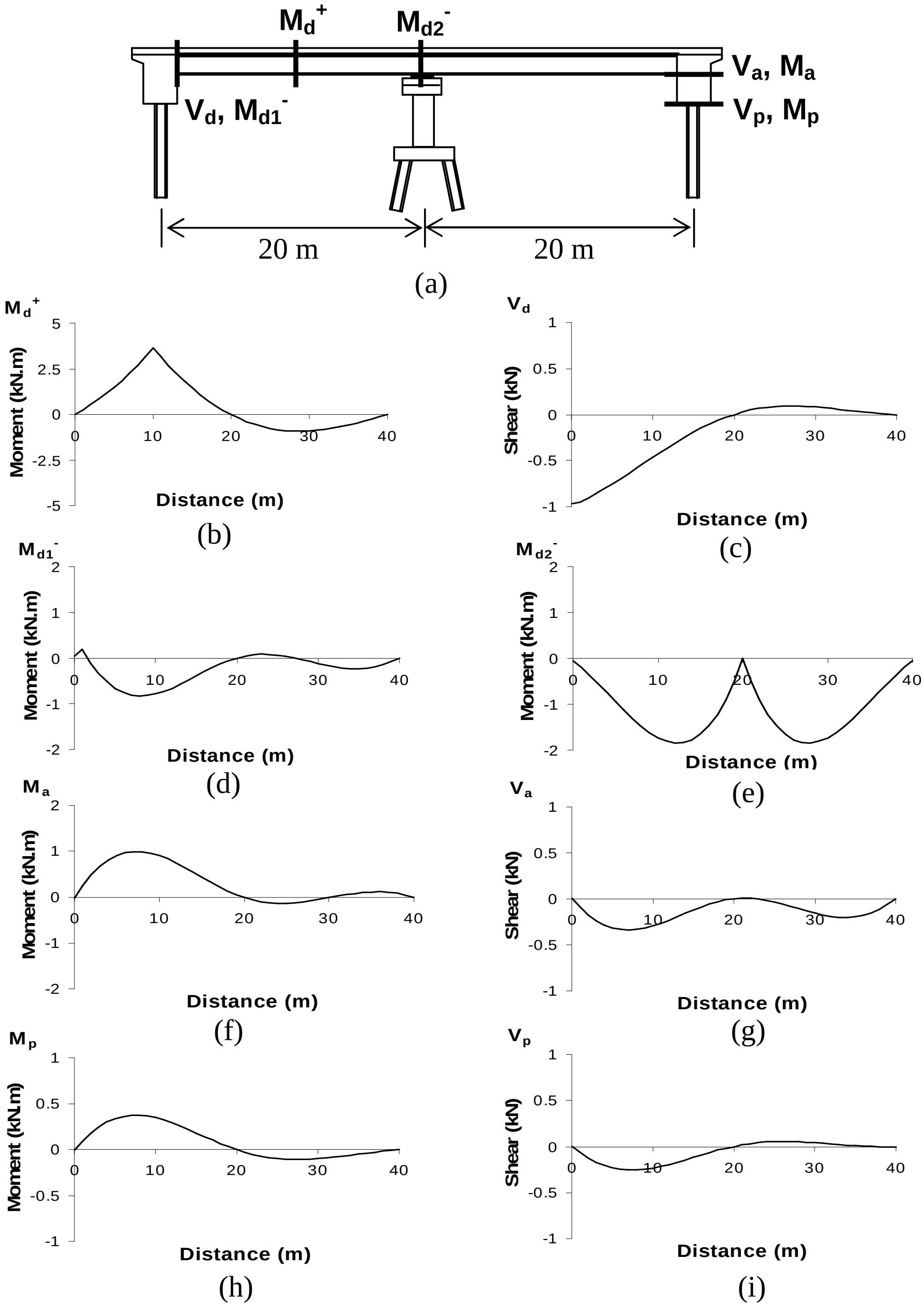

Figure 3.3. (a) Location of calculated maximum internal forces for various bridge components. Influence lines for 2 span IB with HP 250x85 pile and medium stiffness (b) Superstructure positive moment, (c) Superstructure shear, (d) Superstructure negative moment at abutment, (e) Superstructure negative moment at pier, (f) Abutment moment, (g) Abutment shear (h) Pile moment, (i) Pile shear.

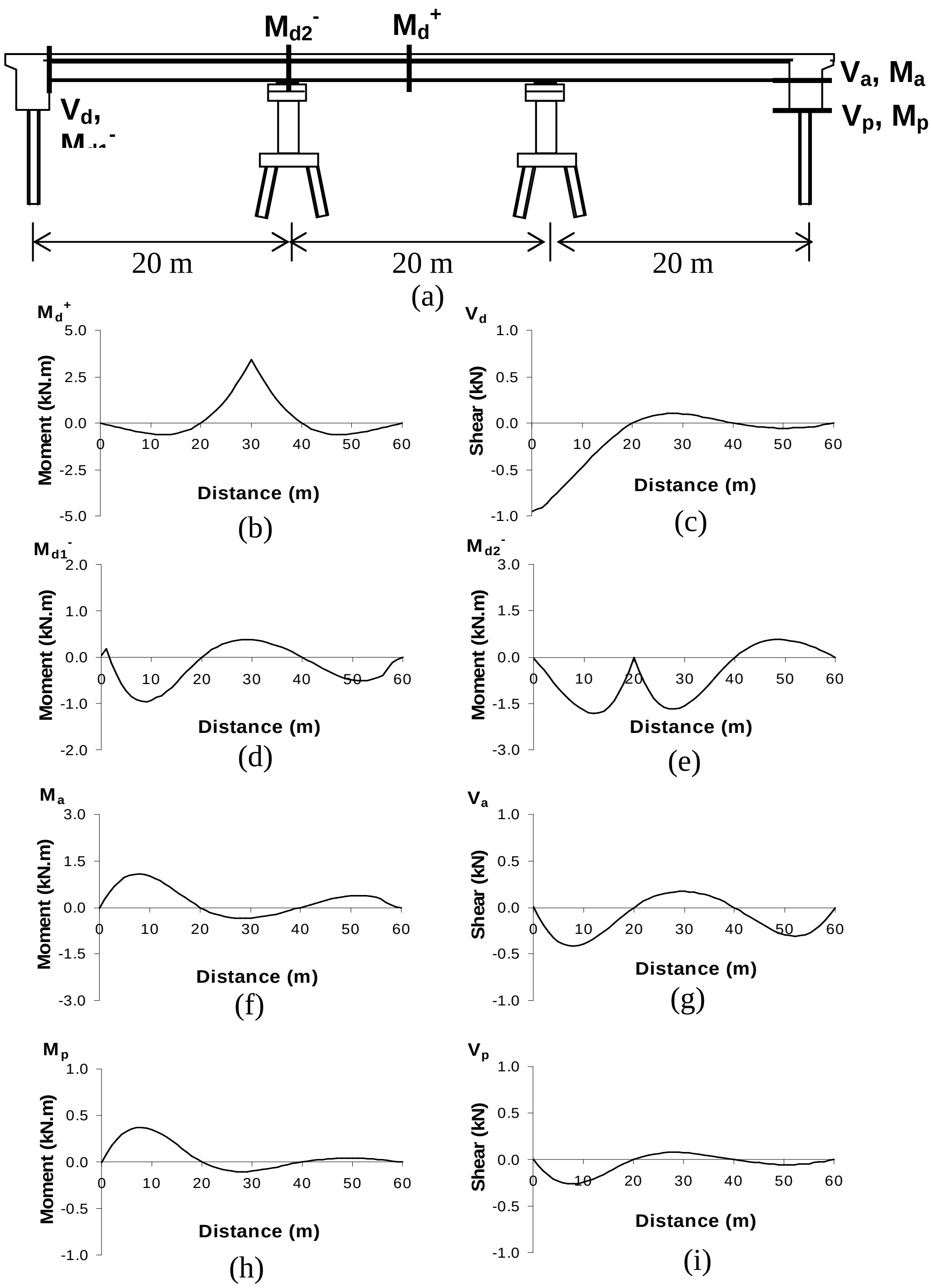

Figure 3.4. (a) Location of calculated maximum internal forces for various bridge components. Influence lines for 3 span IB with HP 250x85 pile and medium stiffness (b) Superstructure positive moment, (c) Superstructure shear, (d) Superstructure negative moment at abutment, (e) Superstructure negative moment at pier, (f) Abutment moment, (g) Abutment shear (h) Pile moment, (i) Pile shear.

2-D structural models of the IBs considered in this study are built using the modeling technique given in Chapter 2. and analyzed using the finite element based software SAP2000. In the 2-D structural models studied, several geometric, structural and geotechnical parameters are varied to cover a wide range of possible IB configurations. This resulted in 200 different IB structural models. The analyses results are then used to assess the effects of the backfill and foundation soil on the magnitude of the internal forces in IB components for various structural, geometric and geotechnical parameters such as bridge size, abutment height and thickness, pile size and orientation, number of spans. The analyses results are summarized in the following sections.

3.4 EFFECT OF FOUNDATION SOIL STIFFNESS ON INTERNAL FORCES

The effects of the foundation soil stiffness on the magnitude of the internal forces in the components of IBs due to live load are illustrated in Figs.3.5-3.14 for different pile sizes and orientations as well as abutment heights and number of spans. The analyses results are discussed in the following subsections.

3.4.1 EFFECT OF FOUNDATION SOIL STIFFNESS ON INTERNAL FORCES FOR VARIOUS PILE SIZES AND ORIENTATIONS

Internal forces in IB components due to live load are plotted in Figs. 3.5-3.8 as a function of the undrained shear strength, C_u, of clay for various pile sizes and orientations as well as for the small and large single span IBs considered in the analyses. The figures are plotted for an abutment height of 5 m. Since the clay stiffness is directly proportional to its undrained shear strength, the figures also demonstrate the relationship between the internal forces and the foundation soil stiffness. The location of the internal forces plotted in Figs. 3.5-3.8 (for the superstructure, abutment and pile moments and shears) are shown in Fig. 3.2(a).

Fig. 3.5 displays the internal forces in the superstructure as a function of C_u. It is observed that the stiffness of the foundation soil has a remarkable effect on the positive (M_d^+) and negative (M_d^-) superstructure moments in single span IBs regardless of the pile size. The figure reveals that larger clay stiffness values produce smaller positive, but larger negative superstructure moments. This is mainly due to the increasing stiffness of the pile-soil system that produces larger rotational resistance at the ends of the bridge superstructure. For instance, in a large IB with HP310x125 piles, 5m tall abutment and considering the effect of the backfill, M_d^+ is 3290 kN.m for soft clay whereas, it is 2734 kN.m for stiff clay. Similar differences are also observed for the negative superstructure moment. For instance, M_d^- is 1236 kN.m for soft clay, whereas, it is 1793 kN.m for stiff clay. However, the variation of the positive (M_d^+) and negative (M_d^-) superstructure moments as a function of the foundation soil stiffness is not as much in the case of the small IB when the backfill effect is included in the structural model. This results from the large stiffness of the backfill relative to the stiffness of the small bridge that imposes a rotational restraint on the superstructure-abutment joint and hence reduces the effect of the foundation soil stiffness on the response of the IB to live loads. As expected, the effect of the foundation soil stiffness on the positive (M_d^+) and negative (M_d^-) superstructure moments of IBs becomes more pronounced when the effect of the backfill is excluded from the structural model. However, the foundation soil stiffness has no effect on the maximum superstructure shear as observed from Fig. 3.5. For the calculation of the maximum live load superstructure shear, the design truck is placed near the abutment. This particular position of the design truck produces smaller deformations in the abutment and the piles. Consequently, soil bridge interaction effects become insignificant in the calculations of the maximum superstructure shear.

Fig. 3.6 displays the internal forces in the substructures (abutment and piles) as a function of C_u. It is observed that the stiffness of the foundation soil has a remarkable effect on the bending moment and shear in the abutment (M_a and V_a) and piles (M_p and V_p) in single span IBs regardless of the pile size. The figure reveals that larger clay stiffness values generally produce larger internal forces in the substructure components with only a few exceptions in the case of the small IB. For instance, in a large IB with HP250x85 piles, 5m tall abutment and considering the effect of the backfill, M_a is 1158 kN.m for soft clay whereas, it is 1647 kN.m for stiff clay. Similar differences are also observed for the pile moment. For instance, M_p is 79 kN.m for soft clay, whereas, it is 165 kN.m for stiff clay. The rotation and displacement at the pile top are respectively 0.00180 radian and 0.00725 m for soft clay and 0.00164 radian and 0.0066 m. for stiff clay. Note that the calculated pile moments are much smaller than the 267 kN.m plastic moment capacity of the pile including the axial load effect (1051 kN) due to dead plus live loads. This difference becomes even larger for the larger pile size and/or for the small bridge.

Furthermore, the calculated pile moments and rotations/displacements are for a full truck load. In reality, a part of the truck load is also distributed to other piles supporting the abutments. In live load analyses, this is taken into consideration by using a live load distribution factor which is smaller than 1 (usually varying between 0.5 and 0.8 depending on the bridge configuration and number of piles). Hence the actual live load effects are much smaller than those calculated by 2-D analyses.

Fig. 3.7 displays the internal forces in the superstructure as a function of C_u for HP 250x85 pile oriented to bend about its strong and weak axes as well as for the small and large single span IBs considered in the analyses. Fig. 3.8 displays similar information but, for the internal forces in the substructure components. It is observed from the figures that the foundation soil stiffness has a remarkable effect on the magnitude of internal forces (except the maximum superstructure shear) in IB components regardless of the pile orientation.

3.4.2 EFFECT OF FOUNDATION SOIL STIFFNESS ON INTERNAL FORCES FOR VARIOUS ABUTMENT HEIGHTS

Fig. 3.9 displays the internal forces in the superstructure as a function of C_u for HP 250x85 pile oriented to bend about its strong axes, for abutment heights of 3 m. and 5 m. and for the small and large single span IBs considered in the analyses. Fig. 3.10 displays similar information but, for the internal forces in the substructure components. It is observed from the figures that the foundation soil stiffness has a remarkable effect on the magnitude of internal forces in IB components regardless of the abutment height except the maximum superstructure shear.

3.4.3 EFFECT OF FOUNDATION SOIL STIFFNESS ON INTERNAL FORCES FOR VARIOUS NUMBERS OF SPANS

Fig. 3.11 displays the internal forces in the superstructure of the two and three span versions of the small bridge considered in the analyses with HP 250x85 piles oriented to bend about their strong axis and an abutment height of 3 m, as a function of C_u. Fig. 19 displays similar information but, for the internal forces in the substructure components.

It is observed from Fig. 3.11 that the effect of the foundation soil stiffness on the maximum positive (M_d^+) and negative (M_d^-) (at the intermediate support) superstructure moments loses its importance in the case of multiple-span IBs. This mainly results from the much larger rotational rigidity provided at the superstructure ends over the inner supports due to the effect of continuity, negating the effect of the pile-soil system. Similar to the single span IB cases, the foundation soil stiffness does not affect the maximum superstructure shear force due to the reasons stated earlier. However, Fig. 3.12 reveals that the stiffness of the foundation soil has a considerable effect on the abutment and pile moments as well as shear forces regardless of the number of spans.

3.4.4 EQUIVALENT PILE LENGTH VERSUS FOUNDATION SOIL STIFFNESS

In the analysis of IBs under live load effects, the pile-soil system is usually modeled as an equivalent pile with a length equal to ten times the pile diameter and the effect of the foundation soil and backfill is neglected. To investigate the effect of this simplifying assumption on the magnitude of the internal forces in IB components, the IBs considered in this study are analyzed using the equivalent pile length concept excluding the backfill effect and the analyses results are compared with the cases where the foundation soil is taken into consideration and the backfill is included and excluded. The analyses results are presented in Figs. 3.13 and 3.14 for the internal forces in superstructure and substructure components of the small bridge with HP250x85 and HP310x15 piles respectively.

It is found that the analyses performed using the equivalent pile length concept inconsistently yield either conservative or unconservative estimates of the internal forces in the components of IBs except for the superstructure shear where the results of the equivalent pile length model coincide with those of the models including soil-bridge interaction effects. The discrepancy between the analyses results of structural models built using the equivalent pile length concept and more complicated soil-bridge interaction modeling techniques increases for stiff foundation soil conditions and larger pile sizes. Thus, in live load analyses of IBs, the equivalent pile concept should be used cautiously especially in the cases of stiff soil conditions at the bridge site. However, generally in stiff soil conditions, pre-drilled oversize holes filled with loose sand is provided along the top portion of the pile to reduce the resistance of the surrounding stiff soil to lateral movements of the pile. Thus, in such cases the equivalent pile length concept may yield more reasonable estimates of the internal forces in IB components due to live load effects.

3.5. EFFECT OF BACKFILL ON INTERNAL FORCES

The effects of the backfill on the magnitude of the internal forces in the components of IBs due to live loads are illustrated in Figs. 3.5-3.12 for different pile sizes and orientations as well as abutment heights and number of spans. The figures display the analysis cases considering and neglecting the effect of the backfill. The analyses results are discussed in the following subsections.

3.5.1 EFFECT OF BACKFILL ON INTERNAL FORCES FOR VARIOUS PILE SIZES AND ORIENTATIONS

Internal forces in IB components due to live load are plotted in Figs. 3.5-3.8 as a function of C_u, for various pile sizes and orientations as well as for the small and large single span IBs considered in the analyses for the cases where the effect of the backfill is included in and excluded from the structural model

As observed from the figures, all the internal forces in the bridge components, except the superstructure shear force show significant differences when the presence of the backfill is taken into consideration in the structural model of single span IBs regardless of the pile size and orientation. Including the effect of the backfill in the structural model produces smaller positive (M_d^+) and larger negative (M_d^-) superstructure moments for all the cases considered (Figs. 3.5 and 3.7). This is mainly due to the larger stiffness of the abutment with the presence of the backfill that produces larger rotational resistance at the ends of the bridge superstructure. For instance, for a small bridge with 5m abutment height and HP310x125 pile driven in soft clay and oriented to bend about its strong axis, the positive superstructure moment, M_d^+ is 772 kN.m when the presence of the backfill is included in the model however, it is 1050 kN.m when the backfill is excluded from the model. Similarly, the negative superstructure moment, M_d^- is calculated as 813 kN.m in the structural model with the backfill but it is calculated as 527 kN.m in the structural model without the backfill. Moreover, it is observed that including the effect of the backfill in the analyses, reduces the sensitivity of the internal forces in IB components to the stiffness of the foundation soil regardless of the pile size and orientation.

Figs. 3.6 and 3.8 display the internal forces in the substructures (abutment and piles) as a function of C_u for various pile sizes and orientations for the cases where the effect of the backfill is included in and excluded from the structural model. It is observed that in the substructures, the abutment moment (M_a) and shear force (V_a) becomes larger and the pile moment (M_p) and shear force (V_p) becomes smaller when the presence of the backfill is considered in the structural model regardless of the pile size and orientation.

3.5.2 EFFECT OF BACKFILL ON INTERNAL FORCES FOR VARIOUS ABUTMENT HEIGHTS

Fig. 16 displays the internal forces in the superstructure as a function of C_u for abutment heights of 3 m. and 5 m. and for the cases where the effect of the backfill is included in and excluded from the structural model. Fig. 3.10 displays similar information but, for the internal forces in the substructure components. It is observed from the figures that the internal forces in the bridge components, except the superstructure shear force show significant differences when the presence of the backfill is taken into consideration in the structural model of single span IBs regardless of the abutment height. Nevertheless, the effect of the backfill becomes more pronounced for taller abutments.

3.5.3 EFFECT OF BACKFILL ON INTERNAL FORCES FOR VARIOUS NUMBER OF SPANS

Fig. 3.11 displays the internal forces in the superstructure as a function of C_u for two and three span versions of the small bridge considered in the analyses considering and neglecting the effect of the backfill in the structural model. Fig. 3.12 displays similar information but, for the internal forces in the substructure components.

As observed from the figures, the presence of the backfill does not significantly affect the superstructure moments in the case of multiple-span IBs. This mainly results from the much larger rotational rigidity provided at the superstructure ends over the inner supports due to the effect of continuity, negating the effect of the abutment-backfill system. However, in the substructures, the abutment moment (M_a) and shear force (V_a) becomes larger and the pile moment (M_p) and shear force (V_p) becomes smaller when the presence of the backfill is considered in the structural model for multiple-span IBs

3.6. SUMMARY

In this chapter, a parametric study is conducted to investigate the effects of the backfill and foundation soil on the magnitude of internal forces in IB components due to live loads for various geometric, structural and geotechnical properties of IBs. For this purpose, 2-D structural models of IBs including and excluding the effect of the backfill as well as including and excluding the effect of the foundation soil by using an actual pile-soil model with four values of clay stiffness and an equivalent pile model neglecting the effect of the foundation soil are built and analyzed. Furthermore, the effect of foundation soil stiffness on the shape of the influence lines for live load analysis is investigated and the assumption of linear elastic modeling of soil-bridge interaction behavior is verified. Followings are the conclusions:

1. For live load analysis of IBs, linear backfill and foundation soil behavior may be assumed in the structural model for short to medium length IBs. Such an assumption is anticipated to facilitate the modeling of soil-bridge interaction behavior for the analysis and design of short to medium length IBs in practice. This will lead to more accurate estimations of live load effects in the design of IBs.

2. The foundation soil stiffness is found to have no effect on the shape of the influence lines for live load analyses.

3. The analyses results revealed that including the soil-bridge interaction behavior in the structural model for live load analysis has a significant effect on the magnitude of the live load moments in the superstructure and the substructures (abutments and piles) and the magnitude of the shear force in the piles and abutments of single span IBs. However, soil-bridge interaction is found to have only a negligible effect on the live load shear force in the superstructure of IBs.

4. Including the effect of the backfill behind the abutments in the structural model is generally found to result in larger superstructure support and abutment moments and smaller superstructure span and pile moments.

5. The difference between the internal forces due to live load effects for the cases with and without soil-bridge interaction effects is found to be a function of the foundation soil stiffness. More specifically, it is observed that generally larger foundation soil stiffness values produce smaller positive, but larger negative superstructure moments and larger pile shear forces.

6. For multiple span IBs, the effect of the backfill and foundation soil stiffness on the internal forces in the superstructure becomes less significant.

7. Furthermore, it is found that the analyses performed using the equivalent pile length concept inconsistently yield either conservative or unconservative estimates of the internal forces in the components of IBs

except for the superstructure shear where the results of the equivalent pile length model coincide with those of the models including soil-bridge interaction effects. Thus, in live load analyses of IBs, the equivalent pile length concept should be used cautiously especially in the cases of stiff soil conditions at the bridge site.

8. Based on the findings of this research study, it may be recommended to include the abutment-backfill and soil-pile interaction behavior in the structural model of short to medium length IBs for the purpose of live load analyses. The linear soil-bridge interaction modeling techniques presented in this paper may be used for this purpose.

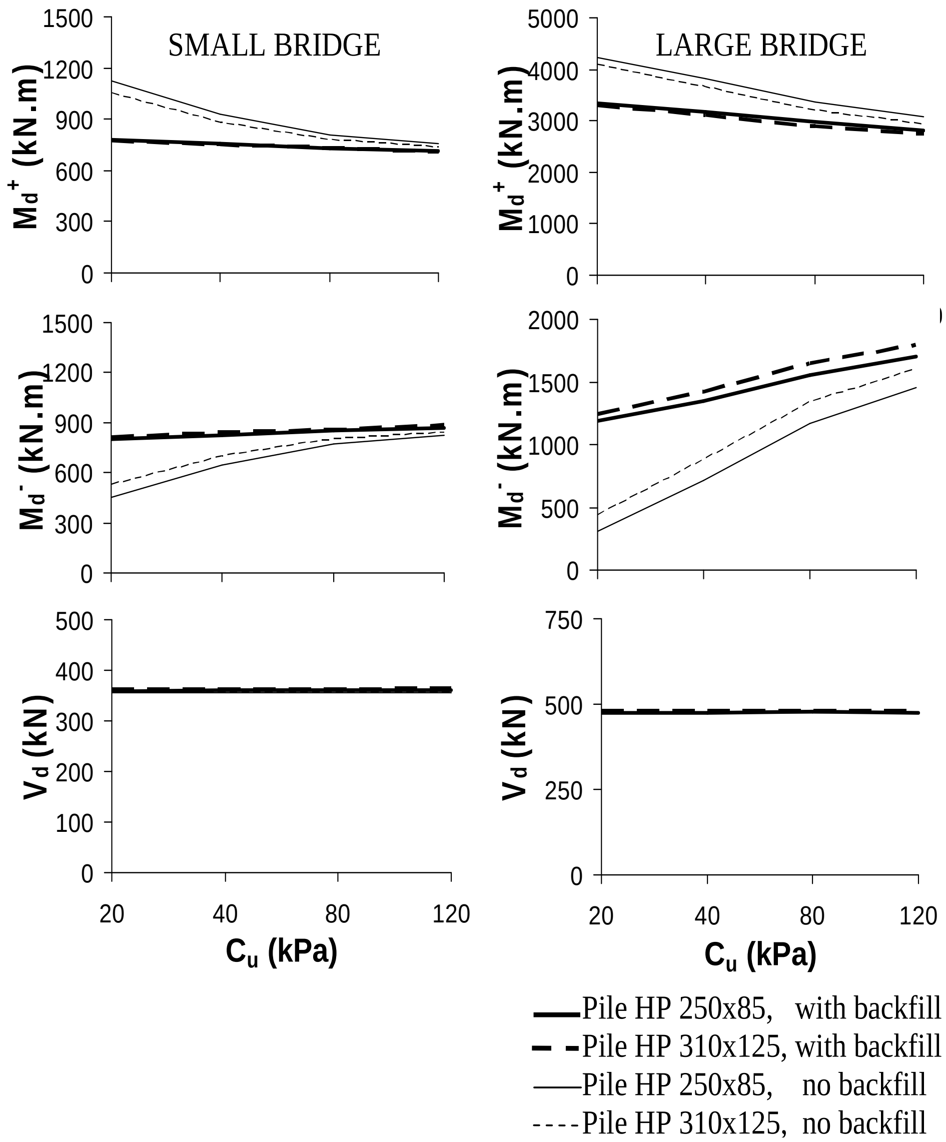

Figure 3.5 Superstructure internal forces, vs. Cu for small and large single-span IBs with an abutment height of 5m and strong axis bending of various piles.

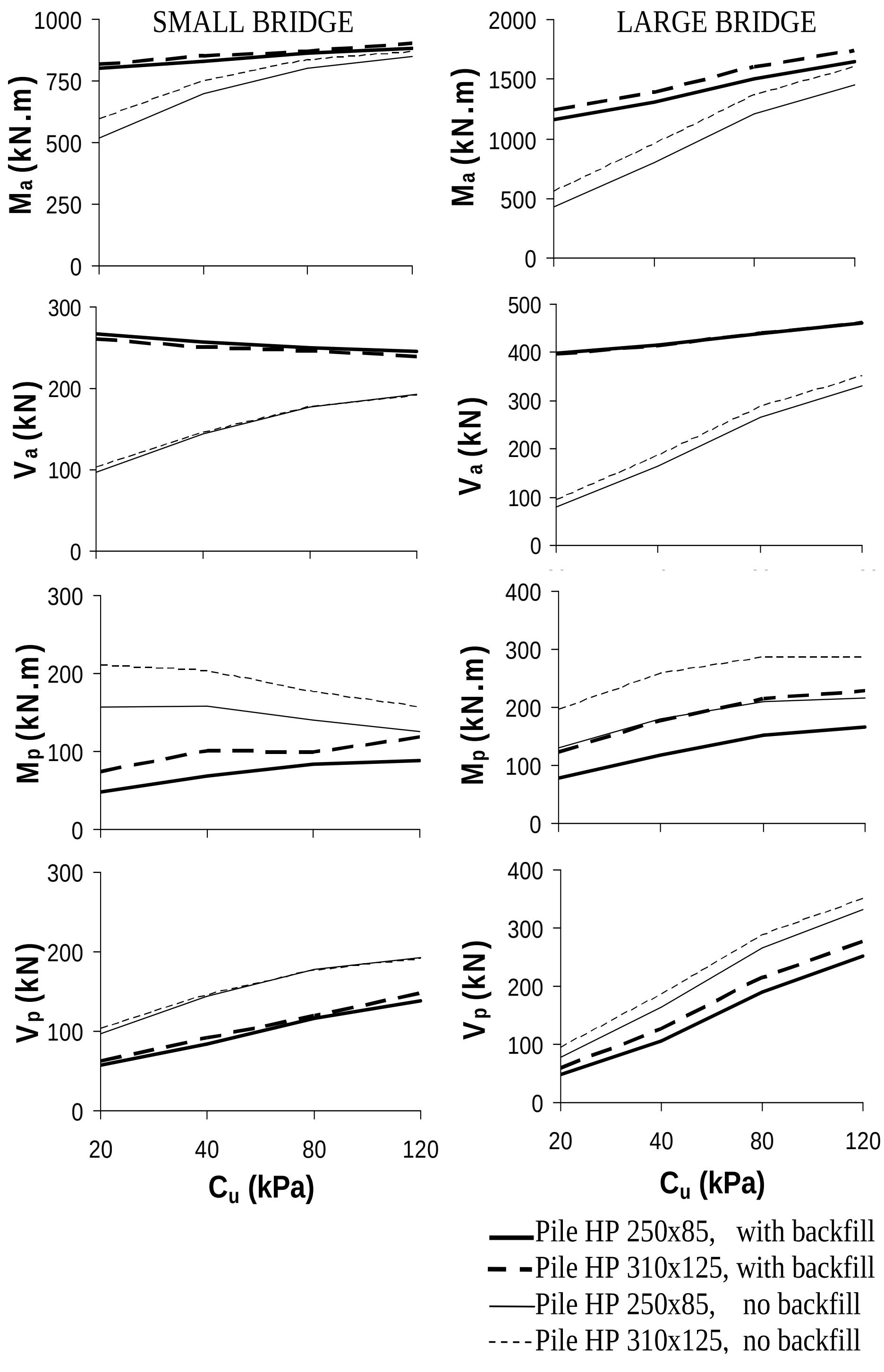

Figure 3.6 Substructure internal forces, vs. C_u for small and large single-span IBs with an abutment height of 5m and strong axis bending of various piles.

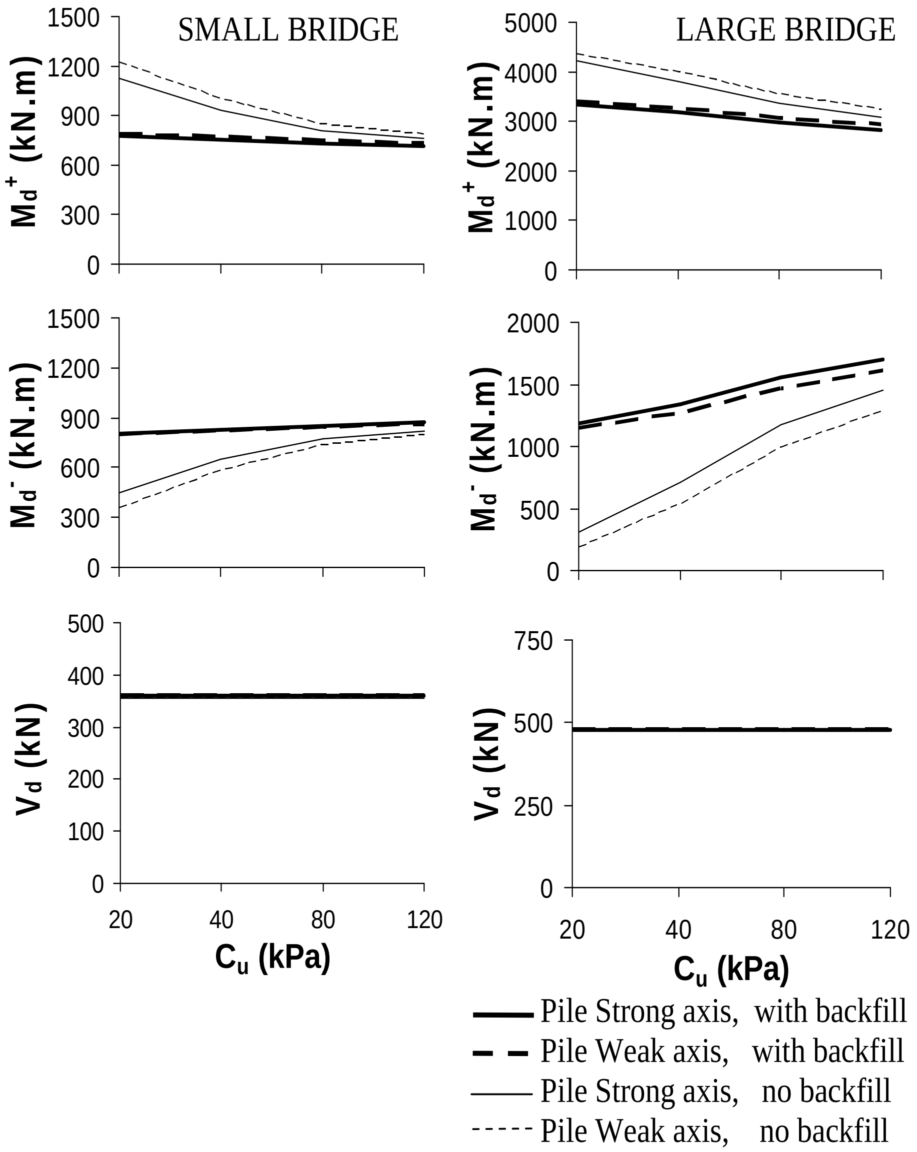

Figure 3.7 Superstructure internal forces, vs. C_u for small and large single-span IBs with an abutment height of 5m and an HP250x85 pile oriented to bend about its strong and weak axes.

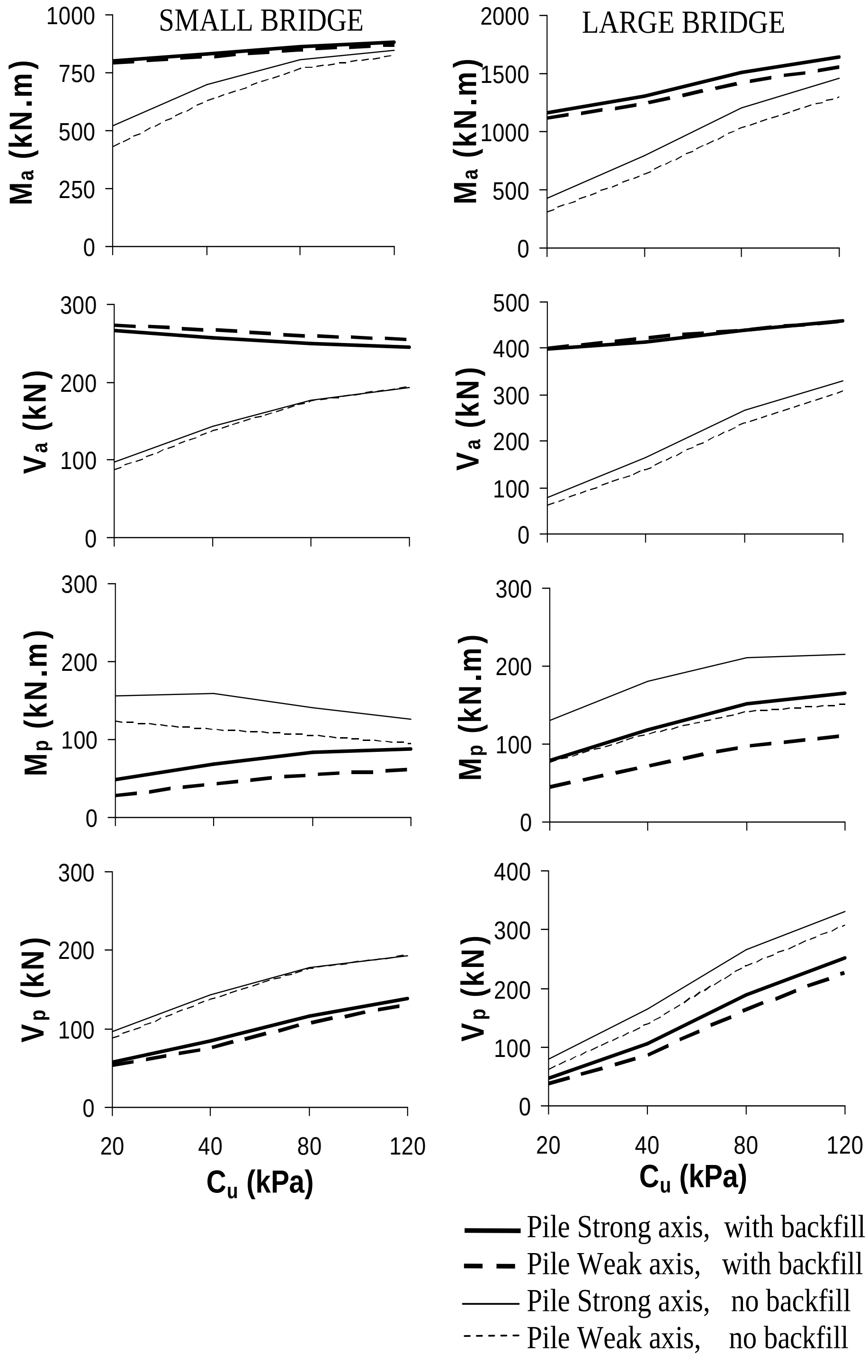

Figure 3.8 Substructure internal forces, vs. Cu for small and large single-span IBs with an abutment height of 5m and an HP250x85 pile oriented to bend about its strong and weak axes.

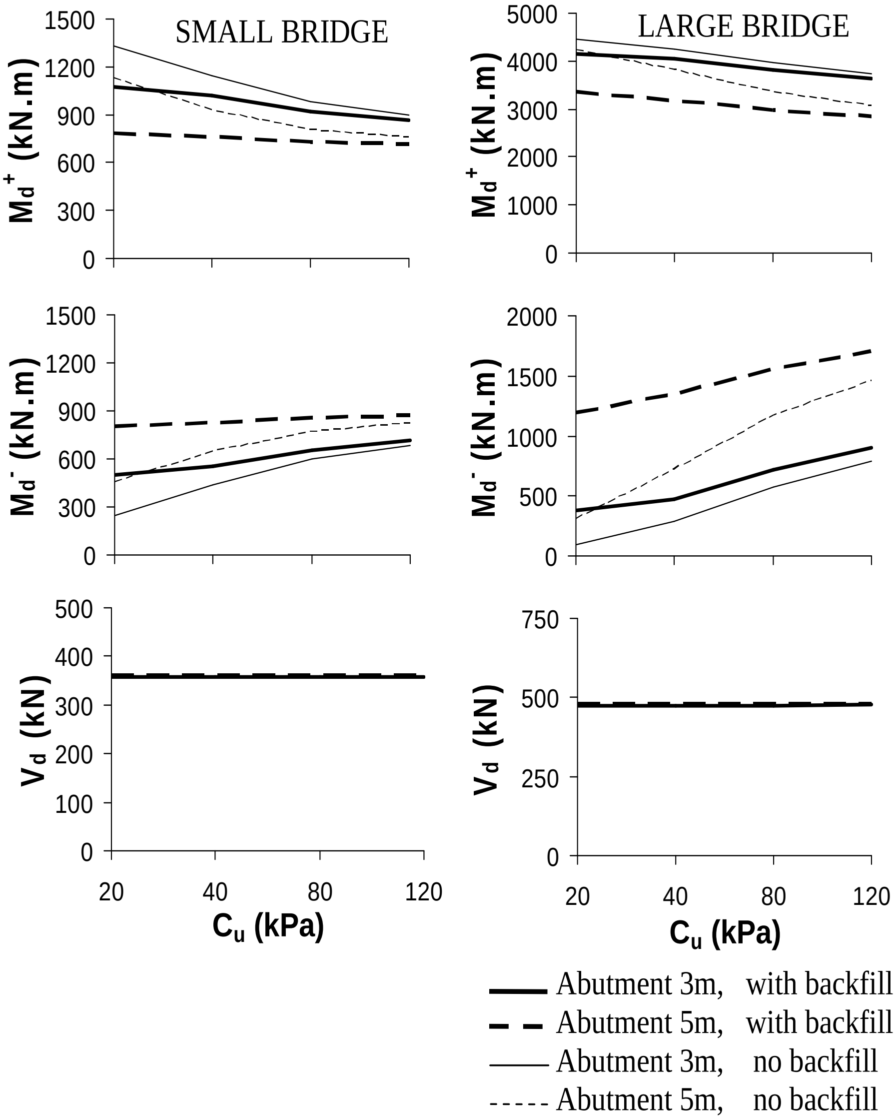

Figure 3.9 Superstructure internal forces, vs. C_u for small and large single-span IBs with an HP250x85 pile oriented to bend about its strong axis and various abutment heights.

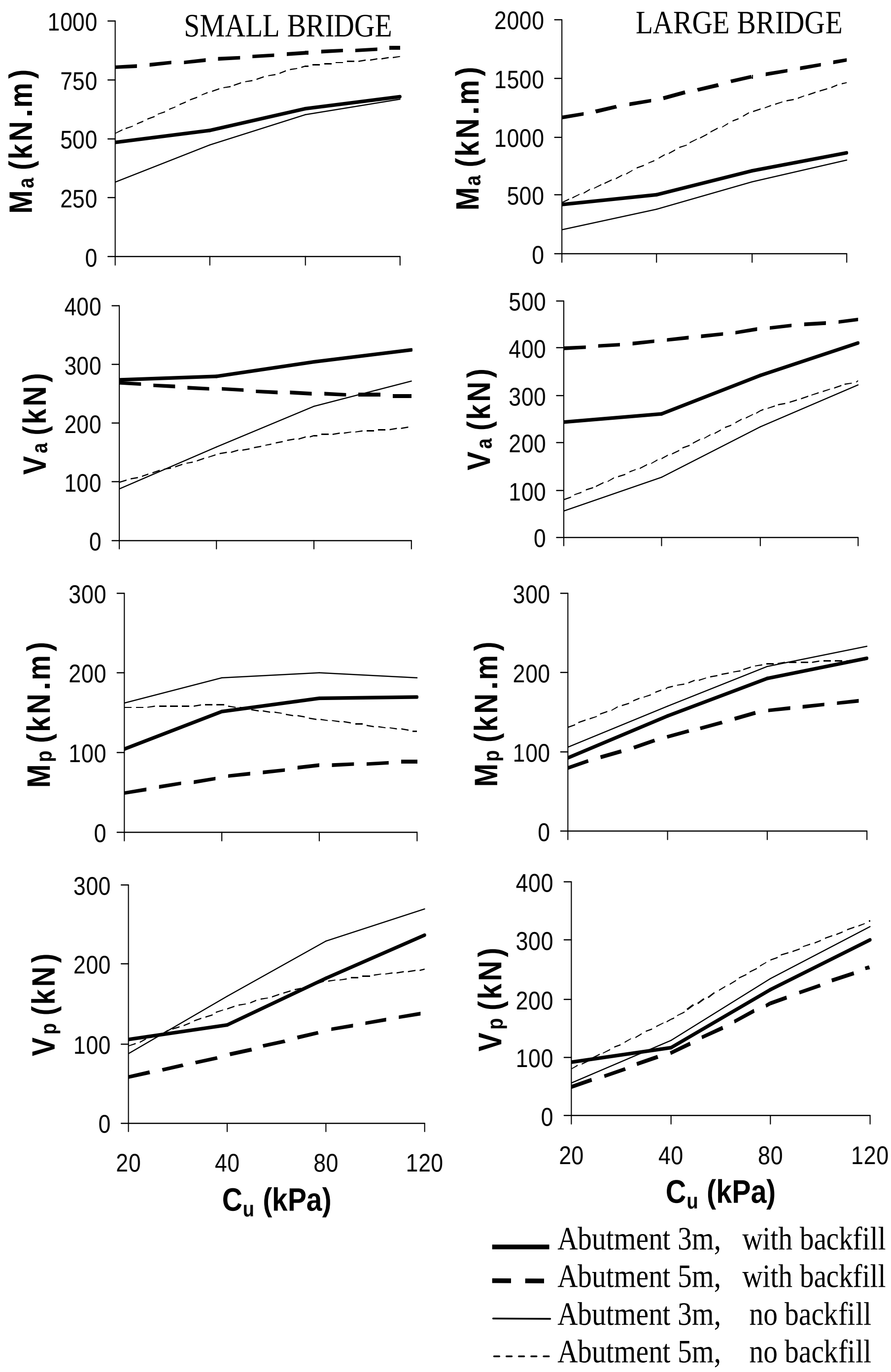

Figure 3.10 Substructure internal forces, vs. C_u for small and large single-span IBs with an HP250x85 pile oriented to bend about its strong axis and various abutment heights.

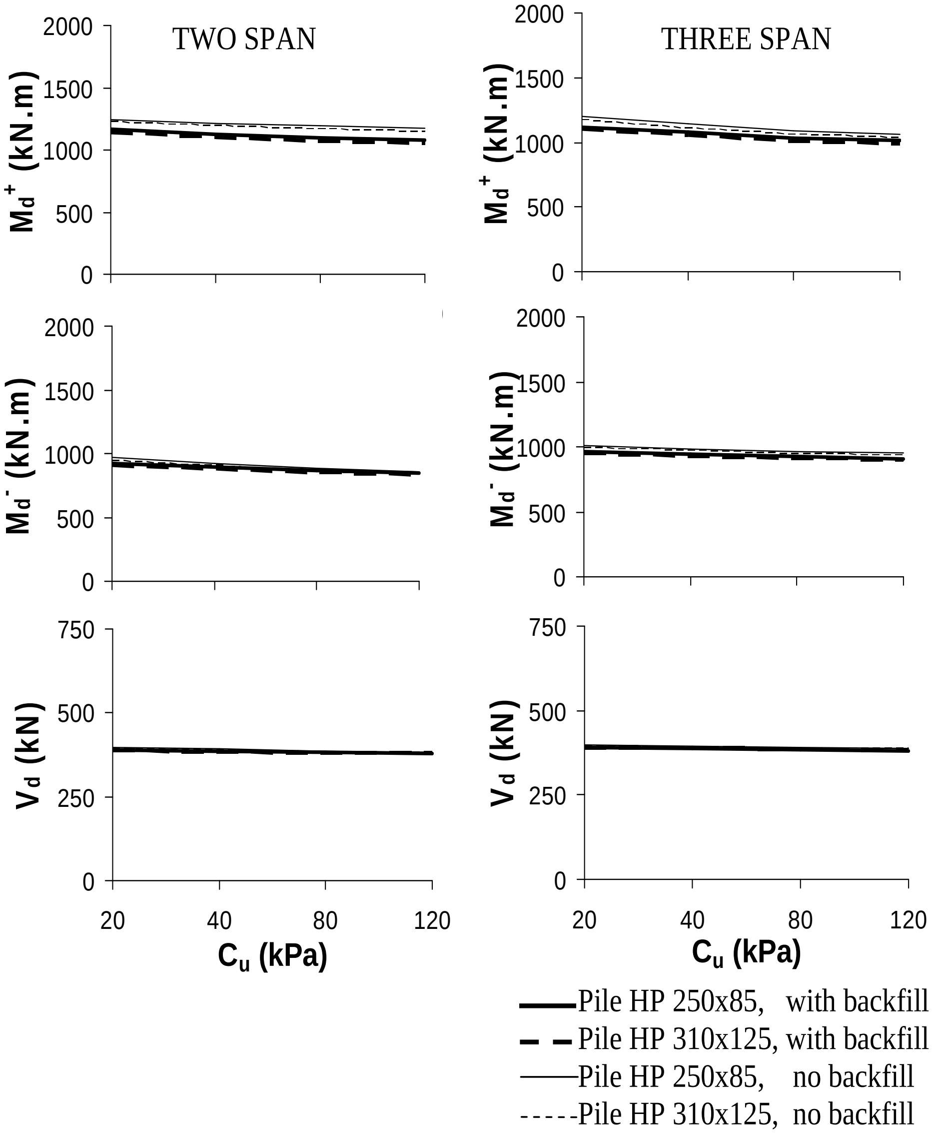

Figure 3.11 Superstructure internal forces, vs. C_u for small multiple span IBs with an abutment height of 3 m. and strong axis bending of various piles.

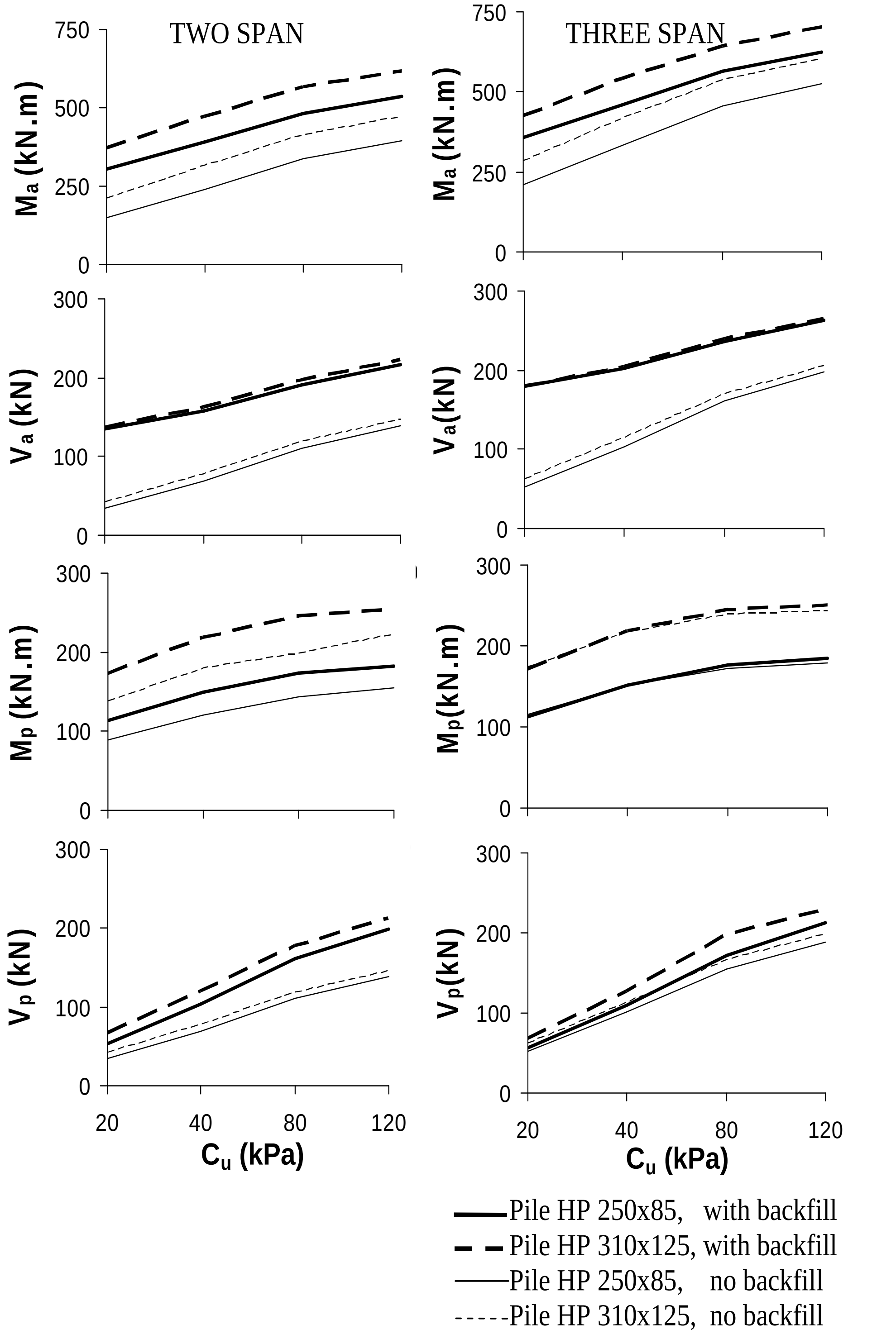

Figure 3.12 Substructure internal forces, vs. C_u for small multiple span IBs with an abutment height of 3 m. and strong axis bending of various piles.

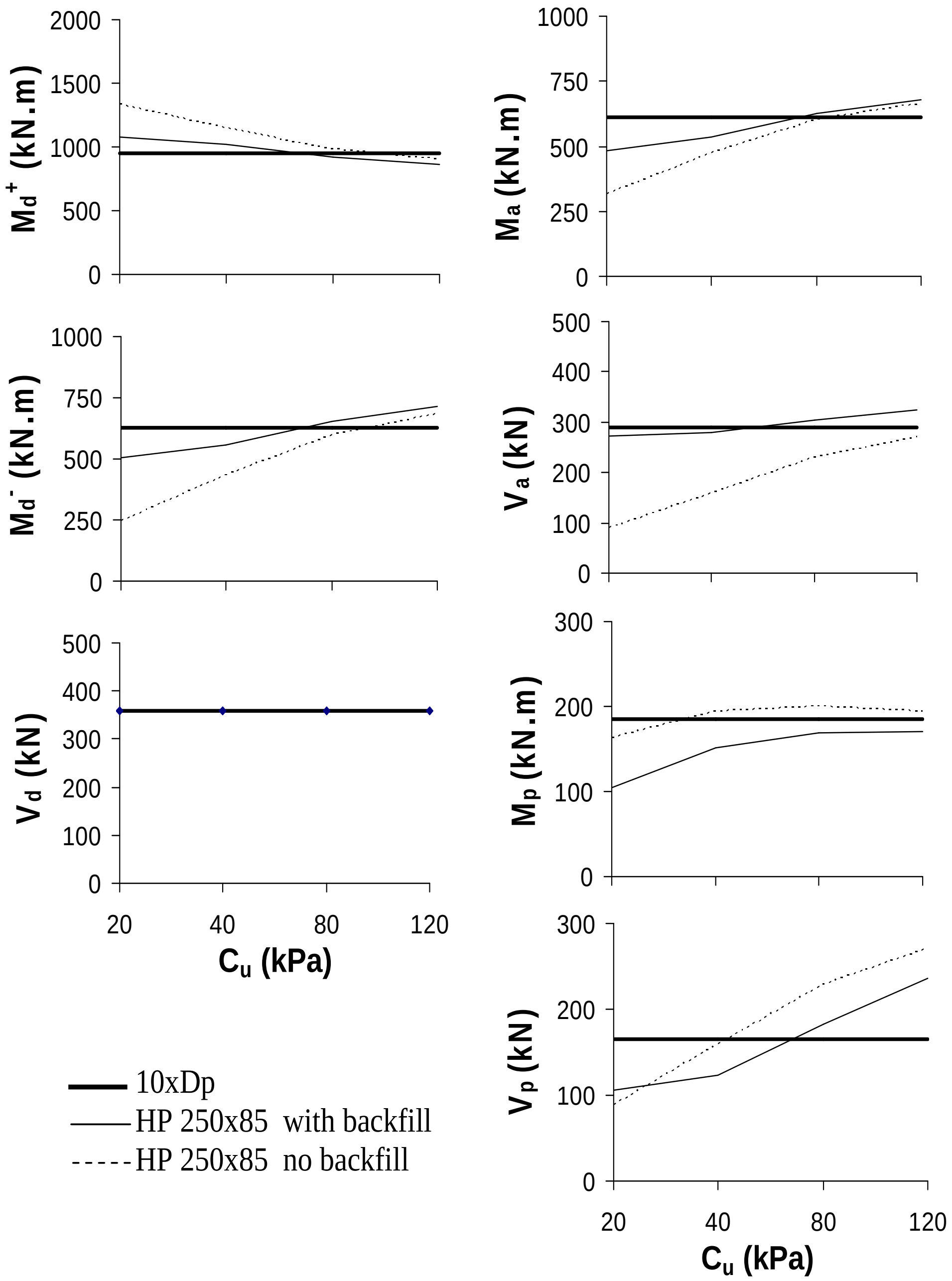

Figure 3.13 Superstructure and substructure internal forces including soil effect with various C_u and equivalent pile length concept for the HP250x85 pile oriented to bend about its strong axis.

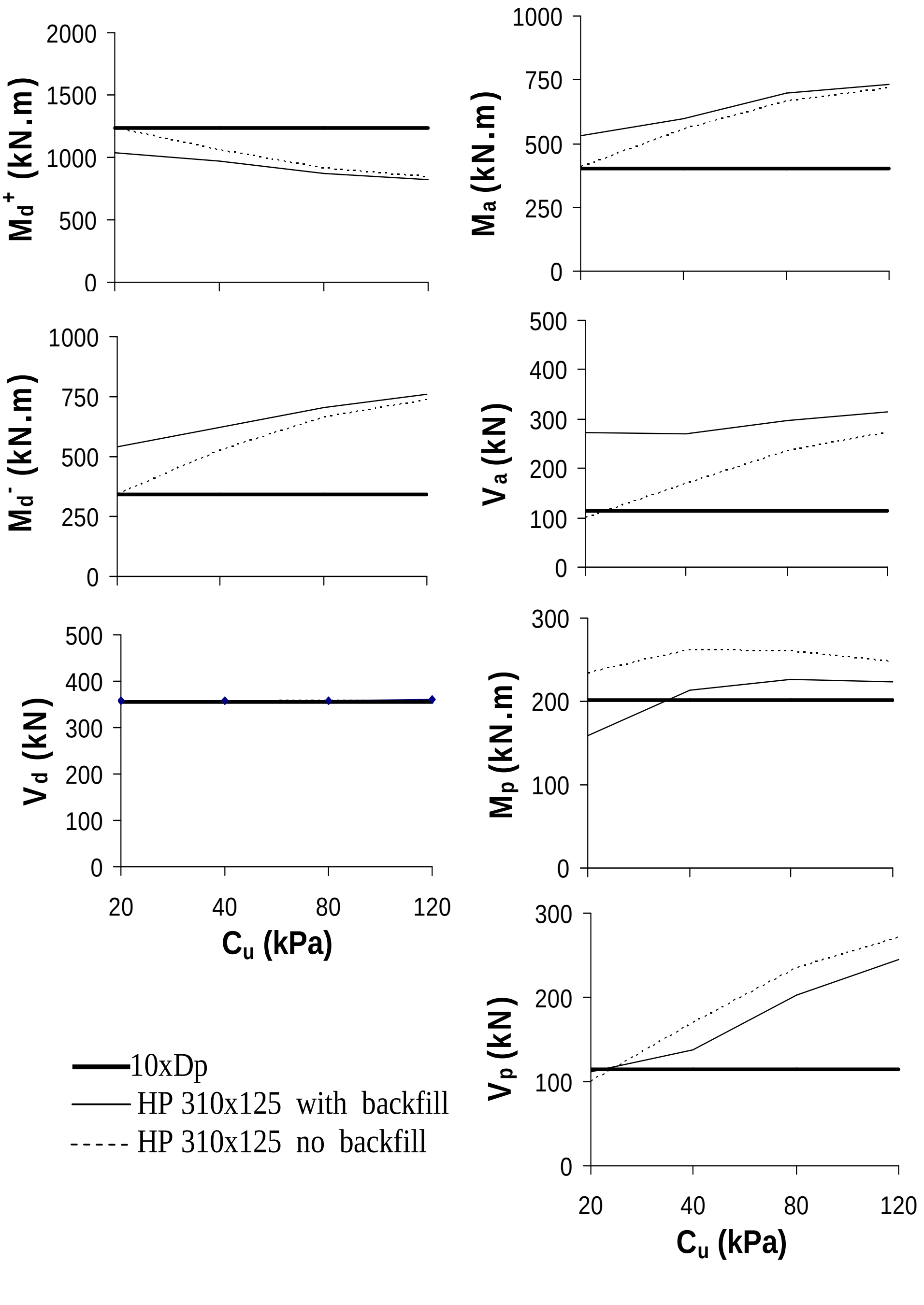

Figure 3.14 Superstructure and substructure internal forces including soil effect with various C_u and equivalent pile length concept for the HP310x125 pile oriented to bend about its strong axis.

CHAPTER 4

EFFECT OF SOIL AND SUBSTRUCTURE PROPERTIES ON LIVE LOAD DISTRIBUTION IN INTEGRAL BRIDGES

In this part of thesis study, the effect of soil-structure interaction and substructure properties at the abutments on the distribution of live load effects in IB components is studied. For this purpose, numerous three dimensional (3-D) and corresponding two dimensional (2-D) structural models of typical IBs are built and analyzed under AASHTO (2007) live load. In the analyses, the effect of various geotechnical and substructure properties such as foundation soil stiffness, considering and neglecting the effect of backfill, backfill compaction level, considering and neglecting the effect of wingwalls, abutment height and thickness as well as size, orientation and number of piles are considered. This resulted in over 260 different 2-D and 3-D structural models and analysis cases. The results from 2-D and 3-D analyses of IBs are then used to calculate the LLDFs for the components of IBs as a function of the above mentioned properties. The results from this research study are intended to evaluate some of the previously mentioned uncertainties regarding the distribution of live load effects in IB components and to form a basis for the development of live load distribution formulae for IB components.

4.1 INTEGRAL ABUTMENT BRIDGES AND PARAMETERS CONSIDERED

Two different existing IBs are considered to investigate the effect of soil-structure interaction and substructure properties at the abutments on the distribution of live load effects in IB components. The bridges are chosen such that the study covers a wide range of deck and substructure stiffness properties found in practice. The first bridge is referred to as the flexible bridge (FB) with 19.8 m. span length. It represents those bridges with relatively smaller deck and substructure stiffness. The second bridge is referred to as the stiff bridge (SB) with 39.6 m. span length. It represents those bridges with relatively larger deck and substructure stiffness. The deck cross-section for both bridges and the side view of the SB are shown in Fig. 4.1. The properties of the IBs are presented in Table 4.1. For both IBs, a range of various geotechnical and substructure properties mentioned earlier are considered to investigate the effect of soil-structure interaction and substructure properties at the abutments on the distribution of live load effects in IB components. The details of these parameters are presented in Table 4.2.

4.2 ESTIMATION OF LIVE LOAD DISTRIBUTION FACTORS

Numerous 3-D and corresponding 2-D structural models of typical IBs are built using the modeling technique given in Chapter 2 and analyzed under AASHTO live load. In the structural models, several geometric, structural and geotechnical parameters are varied to cover a wide range of possible IB configurations.

LLDFs are calculated for the composite interior girders, abutment and piles using the analyses results of 3-D and 2-D models. For the composite interior girders, the maximum live load effects (moment and shear) from 3-D analyses are calculated as the summation of the maximum effects in the girder element and within the tributary width of the slab (equal to the girder spacing) at the same location along the bridge. For the abutment, the maximum live load effects from 3-D analyses are calculated as the summation of the forces within the tributary width of the abutment set equal to the girder spacing. The maximum live load effects for the piles from 3-D analyses are directly obtained as the related effect (shear or moment) at the top of the pile. The live load distribution factors are then calculated as the ratio of the maximum live load effects obtained from 3-D analyses to those obtained from 2-D analyses under a single truck load.

The calculated LLDFs are then used to assess the effects of the backfill and foundation soil on the LLDFs in IB components for various structural, geometric and geotechnical parameters. The analyses results are summarized in the following sections.

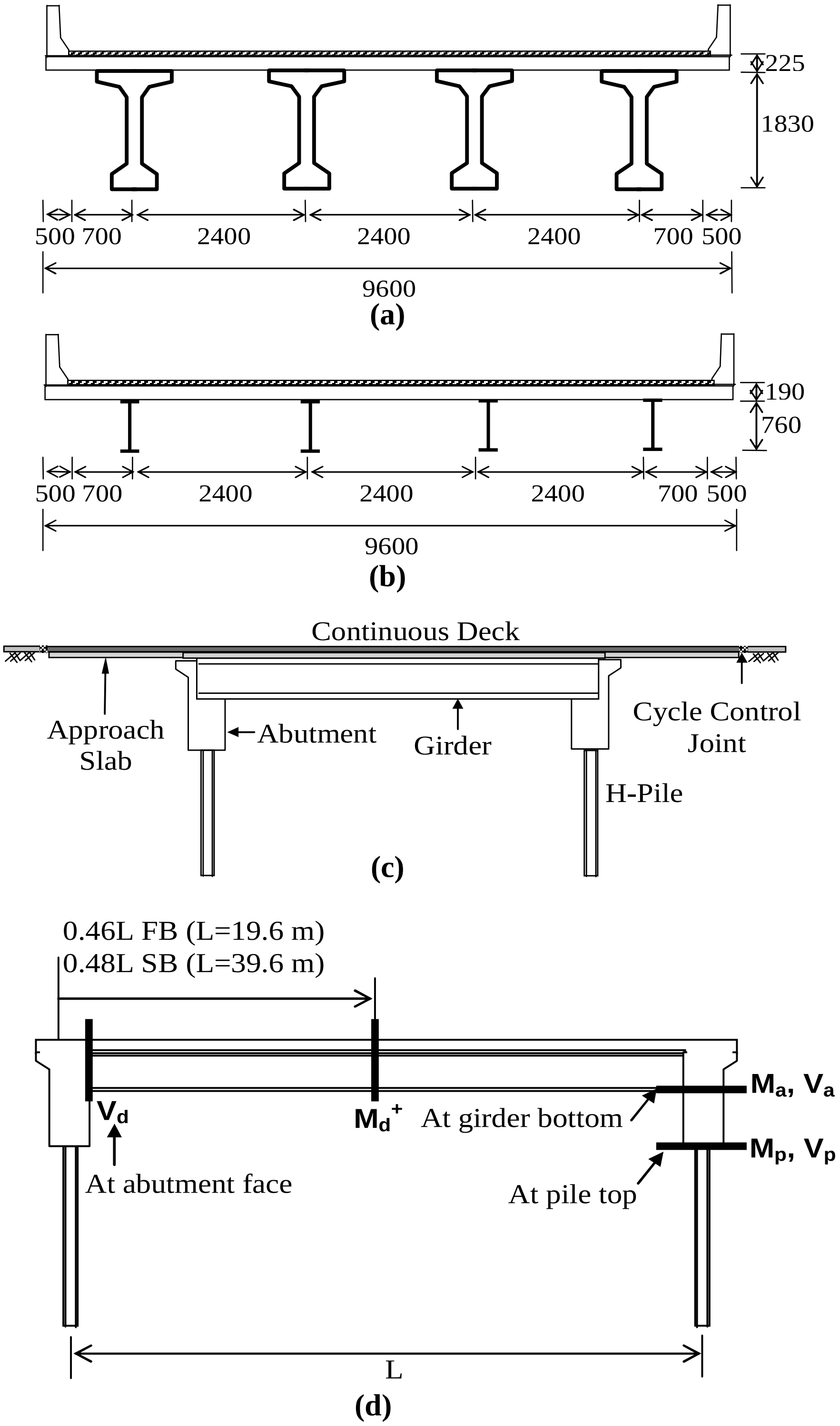

Figure 4.1. (a) Deck cross-section for the stiff bridge, (b) Deck cross-section for the flexible bridge, (c) Side view of the stiff bridge. (d) Location of calculated live load effects for various components

Table 4.1. Properties of the IBs used in the analyses

Properties	**Flexible Bridge (FB)**	**Stiff Bridge (SB)**
Span length (m)	19.8	39.6
Width (m)	9.6	9.6
Net width excluding barriers (m)	8.6	8.6
Deck type	Slab-on-girder	Slab-on-girder
Girder spacing (mm)	2400	2400
Girder type	Steel	Prestressed Concrete
Girder size	W760x173	AASHTO VI
Slab thickness (mm)	190	225
Composite girder, A (mm^2)	0.661×10^6	1.174×10^6
Composite girder, I (mm^4)	54300×10^6	646000×10^6
Abutment thickness (mm)	1000	1500
Abutment, A (per girder), (mm^2)	2.400×10^6	3.600×10^6
Abutment, I (per girder), (mm^4)	200000×10^6	675000×10^6
Concrete strength (girder) (MPa)	N/A	50
Concrete strength (other) (MPa)	30	30
Number of piles per girder	1	1
Pile length (m)	12	12

Table 4.2. Geotechnical and substructure properties considered in the analyses.

Parameter	Description
Backfill	Including (WB) and excluding backfill effect (NB)
Backfill Compaction Level	Simulated using unit weights of 18, 20, 22 kN/m^3 for the backfill
Soil Stiffness	soft, medium, medium-stiff, stiff clay
Pile Size	HP 250x85 (SP), HP 310x125 (LP)
Pile Orientation	Weak axis (WA) and Strong axis (SA) bending
Number of Piles	4, 6 piles (1 and 1.5 piles per girder)
Abutment Height (m)	3.0, 5.0
Abutment Thickness (m)	1.0, 1.5
Wingwall	Including and excluding the wingwalls

NB: No backfill, WB: With Backfill ,SP: Small Pile , LP: Large pile, WA: Weak axis, SA: Strong axis

4.3 EFFECT OF SOIL STRUCTURE INTERACTION ON LLDFs FOR IB COMPONENTS

The analyses results for the effect of foundation soil stiffness, considering and neglecting the effect of backfill as well as backfill compaction level on LLDFs for IB components are summarized in the following subsections.

4.3.1. FOUNDATION SOIL STIFFNESS

The effect of the foundation soil stiffness on LLDFs for girder, abutment and pile moments (M_d^+, M_a, M_p) and shears (V_d, V_a, V_p) for the stiff (SB) and flexible (FB) bridges are illustrated in Figs. 4.2-4.7 for different pile sizes (SP: HP250x85, LP: HP310x125) , pile orientations (WA: Weak Axis, SA: Strong Axis) and abutment thicknesses (1 m, 1.5 m) respectively. In the figures, the variations of LLDFs are plotted as a function of the undrained shear strength, C_u, of clay. Since larger C_u values correspond to larger clay stiffness values, the figures also display the variation of LLDFs as a function of the stiffness of the foundation soil. The figures also include the cases where the effect of the backfill is considered (WB) and neglected (NB) in the analyses. Fig. 4.9 display similar information for the stiff bridge only and for various abutment heights (3 m., 5 m.).

It is observed from the figures that the effect of the foundation soil stiffness on the LLDFs for the girder moment and shear is negligible regardless of the bridge size, pile size and orientation, abutment thickness and height as well as considering and neglecting the backfill effect. For instance, for the stiff IB with HP250x85 piles and considering the effect of the backfill (Fig. 4.2 and 4.3), the LLDFs for the interior girder positive moment (M_d^+) are found as 0.577, 0.576, 0.576 and 0.576 for soft, medium, medium-stiff and stiff clay (C_u= 20, 40, 80 and 120 kPa) respectively. Similarly, for the same IB, the LLDFs for the girder shear (V_d) are found as 0.782, 0.782, 0.782and 0.781 for soft, medium, medium-stiff and stiff clay respectively.

Nevertheless, the stiffness of the foundation soil is found to have a significant effect on the LLDFs for the abutment moment (M_a) as observed from the same figures. For instance, for the stiff IB with HP250x85 piles and considering the effect of the backfill (Fig. 4.2), the LLDFs for the abutment moment are calculated as 0.881, 0.799, 0.723 and 0.685 for soft, medium, medium-stiff and stiff clay respectively. The stiffness of the foundation soil is also found to affect the LLDFs for the abutment shear (V_a) (Fig. 4.3), but to a lesser extent compared to that of the moment. For instance, for the same IB, the LLDFs for the abutment shear are found as 0.698, 0.654, 0.614 and 0.612 for soft, medium, medium-stiff and stiff clay respectively. The difference between the LLDFs for the cases corresponding to stiff and soft foundation soils is 30% for the moment and 14% for the shear. It is also observed from the figures that the distribution of live load moment and shear in the abutment improves (LLDF becomes smaller) as the stiffness of the foundation soil increases. This is because larger foundation soil stiffness provides larger translational and rotational restraint at the bottom of the abutment. This, in turn, produces a more uniform distribution of the translational and rotational effects across the width of the abutment.

It is also found that the stiffness of the foundation soil has only a minor effect on the LLDFs for the pile moment (M_p) and shear (V_p). For instance, for the stiff IB with HP250x85 piles and considering the effect of the backfill, (Fig. 4.2 and 4.3) the LLDFs for the pile moment are calculated as 0.588, 0.575, 0.555, and 0,565 for soft, medium, medium-stiff and stiff clay respectively. Similarly, for the same IB, the LLDFs for the pile shear are found as 0.595, 0.578, 0.560, and 0,574 for soft, medium, medium-stiff and stiff clay respectively.

In summary, the effect of the foundation soil stiffness on the LLDFs for the girder and pile moments and shear is negligible. However, the foundation soil stiffness is found to have a significant effect on the LLDFs for the abutment moment and to a lesser extent on those for the abutment shear. Therefore, the foundation soil stiffness must be considered in estimating the distribution of live load effects within the abutments of IBs.

4.3.2 CONSIDERING AND NEGLECTING THE BACKFILL EFFECT

In this section, the effect of including and excluding the effect of the backfill on LLDFs for IB components is investigated. Figs. 4.2-4.7, display the LLDFs for various IB components as a function of C_u considering (WB) and neglecting (NB) the effect of the backfill for various pile sizes (SP, LP), pile orientations (WA, SA) and abutment thicknesses (1 m., 1.5 m.) respectively. The figures reveal that the effect of the backfill on the LLDFs for girder moment (M_d^+) and shear (V_d) is negligible regardless of the bridge size, pile size and orientation, abutment thickness as well as the stiffness of the foundation soil. For instance, for an IB with HP250x85 pile (SP), 1m thick abutment and soft clay (C_u =20 kPa), the LLDFs for the girder moment considering and neglecting the effect of the backfill are found to be identical (0.577). Similarly, for the same IB, the LLDFs for the girder shear are calculated as 0.782 and 0.781 for the cases including and excluding the backfill effect respectively.

However, it is found that the backfill has a considerable effect on the LLDFs for the abutment moment (M_a) and to a lesser extent on those for the abutment shear (V_a) for all the cases considered. For instance, for the stiff IB with HP250x85 piles (SP), 1m thick abutment and soft foundation clay, the LLDFs for the abutment moment considering and neglecting the effect of the backfill are found as 0.881 and 1.011 respectively. Similarly, for the same IB, the LLDFs for the abutment shear are found as 0.698 and 0.622 for the cases including and excluding the backfill effect respectively. It is also observed that the distribution of live load moment and shear across the width of the abutment improves (i.e. LLDFs become smaller) when the effect of the backfill is included in the structural model. This is due to the fact that including the backfill effect in the structural model produces a larger rotational and translational resistance and a more uniform distribution of the rotational and translational live load effects across the width of the abutment.

For the piles, it is found that the backfill has only a negligible effect on the LLDFs for the moment (M_p) and shear (V_p). For instance, for the stiff IB with HP250x85 piles, 1m thick abutment and soft foundation clay, the LLDFs for the pile moment considering and neglecting the effect of the backfill are found as 0.588 and 0.585 respectively. Similarly, for the same IB, the LLDFs for the pile shear are found as 0.595 and 0.584 for the cases including and excluding the backfill effect respectively.

In summary, the effect of the backfill on the LLDFs for the girder and pile moments and shears is negligible. However, the backfill is found to have a notable effect on the LLDFs for the abutment moment and shear. Therefore, the backfill must be considered in estimating the distribution of live load effects within the abutments of IBs.

4.3.3 BACKFILL COMPACTION LEVEL

In the construction of IBs, the compaction level, hence the unit weight of the backfill behind the abutment can be different. For this reason, the effect of the backfill compaction level on the distribution of live load effects for various components of IBs is investigated considering three different unit weight of the backfill (18, 20 and 22 kN/m^3) corresponding to different compaction levels. The analyses results are shown in Fig. 4.8. The figure displays the LLDFs for the girder, abutment and pile moments and shears as a function of the backfill unit weight used in the structural models. The figure is obtained for the stiff IB with 3 m tall abutment supported on four HP250x85 piles oriented to bend about their strong axis and driven in medium clay. The figure reveals that the effect of the backfill compaction level on the LLDFs for the girder, abutment and pile moment and shear is negligible. For the cases where the backfill unit weight is 18, 20 and 22 kN/m^3, the LLDFs are found to be nearly identical and equal to 0.575 for the girder moment, 0.798, 0.792 and 0.791 for the abutment moment and 0.582, 0.578 and 0.582 for the pile moment. Similarly, for the cases where the backfill unit weight is 18, 20 and 22 kN/m^3, the LLDFs are calculated as 0.784, 0.782 and 0.781 for the girder shear, 0.651, 0.655 and 0.665 for the abutment shear and 0.592, 0.591 and 0.590 for the pile shear.

4.4. EFFECT OF SUBSTRUCTURE PROPERTIES ON LLDFs FOR IB COMPONENTS

4.4.1 ABUTMENT THICKNESS AND HEIGHT

The effects of abutment thickness and height on the distribution of live load effects for various IB components are illustrated in Figs. 4.6, 4.7 and 4.9 respectively. Fig. 4.6 and 4.7 displays the LLDFs for the girder, abutment and pile moments and shears as a function of C_u for abutment thicknesses of 1.0 m and 1.5 m. The figure is obtained for the stiff (SB) and flexible (FB) bridges with 3.0 m tall abutments supported on four HP250x85 piles. Fig. 10 is similar but displays the same information for abutment heights of 3 m. and 5 m for the stiff bridge only and for small (SP) and large (LP) pile sizes

(HP250x85 and HP310x125). The effect of the backfill is considered in Fig. 4.9.

It is observed from Fig. 4.6 and 4.7 that the effect of the abutment thickness on the LLDFs for the girder, abutment and pile moment and shear is negligible. For instance, for the stiff IB supported on soft clay and considering the effect of the backfill, the LLDFs for abutment thicknesses of 1 m. and 1.5 m. are obtained as 0.577 and 0.576 for the girder moment, 0.781 and 0.799 for the girder shear, 0.881 and 0.863 for the abutment moment, 0.698 and 0.691 for the abutment shear, 0.588 and 0.586 for the pile moment, and 0.595 and 0.593 for the pile shear. Therefore the abutment thickness need not be considered as a parameter for estimating the LLDFs for IB components.

The analyses results presented in Fig. 4.9 reveal that the effect of the abutment height on the LLDFs for the girder moment and shear is negligible. For instance, for the stiff IB with HP250x85 piles (SP) driven in soft clay, the LLDFs for the girder moment are calculated as 0.577 and 0.585 for the cases of 3 m. and 5 m. tall abutments respectively. Similarly, for the same IB, the LLDFs for the girder shear are calculated as 0.782 and 0.775 for the cases of 3 m. and 5 m. tall abutments respectively.

However, it is found that the abutment height has a notable effect on the LLDFs for the abutment moment and shear and to a lesser extent on those for the pile moment and shear. For instance, for the stiff IB with HP250x85 piles (SP) driven in medium clay, the LLDFs for the cases of 3 m. and 5 m. tall abutments are calculated as 0.799 and 0.665 for the abutment moment and 0.657 and 0.575 for the pile moment. Similarly, for the same IB, the LLDFs for the cases of 3 m. and 5 m. tall abutments are calculated as 0.654 and 0.602 for the abutment shear and 0.578 and 0.611 for the pile shear. It is also observed that the effect of abutment height on the LLDFs for the abutment moment and shear becomes more pronounced for softer foundation soil. Moreover, it is observed that the distribution of live load moment and shear across the width of the abutment improves for larger abutment heights (i.e. LLDFs becomes smaller). However the opposite is true for the piles. That is, the effect of abutment height on the LLDFs for the pile moment and shear becomes less pronounced for softer foundation soil and the distribution of live load moment and shear to the piles improves for shorter abutment heights.

In summary, the effect of the abutment height on the LLDFs for the girder moments and shears is negligible. However, the abutment height is found to have a notable effect on the LLDFs for the abutment and pile moment and shear. Therefore, the abutment height must be considered in estimating the live load effects in the abutments and piles of IBs.

4.4.2. CONSIDERING AND NEGLECTING THE WINGWALLS

In regular jointed bridges, the superstructure is separated from the substructure via joints and bearings. Therefore, the wingwalls do not influence the distribution of live load effects to bridge components. However, in the case of IBs, due to the monolithic construction of the deck with the abutments, the wingwalls may influence the distribution of live load effects to the components of IB s. This is investigated in this section. For this purpose, the live load analyses of the stiff IB is conducted by including and excluding the wingwalls from the 3-D structural models. The analyses results for the cases with and without the wingwalls are then compared. For the IBs with and without the wingwalls, the abutment height is taken as 5 m. The bridges are assumed to be supported by four HP250x85 piles oriented to bend about their strong axis. For the IB with wingwalls, two (trapezoidal), 0.43 m thick and 3.5 m. long wingwalls with vertical dimensions of 3 m and 1.25 m respectively at the abutment interface and at the wingwall end are considered at each end of the bridge. The wingwalls are modeled using quadrilateral and triangular shell elements with six DOFs at each node. Backfill-abutment interaction effects are also considered in the analyses. The analyses results are displayed in Fig. 4.10. The figure displays the LLDFs for the girder, abutment and pile moments and shears as a function of C_u for the cases including and excluding the wingwalls in the 3-D structural model.

The analyses results presented in Fig. 4.10 reveal that the effect of the wingwall on the LLDFs for the girder, abutment and pile moments and shears is negligible. For the cases where the effect of the wingwalls is included in and excluded from the analyses, the LLDFs are found to be equal to 0.583 and 0.577 for the girder moment, 0.875 and 0.881 for the abutment moment and 0.590 and 0.588 for the pile moment. Similarly, for the cases where the effect of the wingwalls is included in and excluded from the analyses, the LLDFs are calculated as 0.794 and 0.781 for the girder shear, 0.701 and 0.689 for the abutment shear and 0.606 and 0.595 for the pile shear.

In summary, the effect of the wingwalls on the LLDFs for the components of IBs is negligible. Thus, the wingwalls need not be considered in estimating the live load effects in IB components.

4.4.3. SIZE, ORIENTATION AND NUMBER OF PILES

In this section the effect of the size, orientation and number of piles on the distribution of live load effects in IBs is studied. The analyses results are presented in Figs. 4.4-4.7. Figs. 4.4-4.7 show the LLDFs as a function of C_u respectively for various pile sizes (HP250x85 (SP) and HP310x125 (LP) piles) oriented to bend about their strong axis and orientations (HP250x85 pile oriented to bend about weak axis (WA) and strong axis (SA)) for the stiff (SB) and flexible (FB) bridges with 3 m. tall abutments. Both figures are obtained for the cases where the effect of the backfill is included in and excluded from the analyses. Fig. 4.11 displays the LLDFs for various numbers of piles (4 and 6) supporting the abutments. The figure is obtained for the stiff IB with 3 m tall abutments supported on HP250x85 piles oriented to bend about their strong axis and driven in medium clay.

Figs. 4.4-4.7 reveal that the size and orientation of the piles has a negligible effect on the girder, abutment and pile moments and shears. For instance, for the flexible IB supported on medium clay and considering the effect of the backfill, the LLDFs for the HP250x85 (SP) and HP310x125 (LP) piles are obtained as 0.612 and 0.612 for the girder moment, 0.709 and 0.711 for the girder shear, 0.623 and 0.625 for the abutment moment, 0.484 and 0.489 for the abutment shear, 0.492 and 0.520 for the pile moment, and 0.498 and 0.528 for the pile shear. Similarly for the same IB, the LLDFs for the strong and weak axis orientation of the piles are obtained as 0.612 and 0.608 for the girder moment, 0.709 and 0.708 for the girder shear, 0.620 and 0.646 for the abutment moment, 0.484 and 0.485 for the abutment shear, 0.492 and 0.503 for the pile moment and 0.498 and 0.507 for the pile shear.

The analyses results presented in Fig. 4.11 reveal that the effect of the number of the piles on the LLDFs for the girder moment and shear, abutment shear and pile moment is negligible. For instance, the LLDFs for the cases of 4 and 6 piles are calculated as 0.580 and 0.590 for the girder moment, 0.781 and 0.781 for the girder shear, 0.570 and 0.560 for the abutment shear and 0.581 and 0.575 for the pile moment. However, it is observed that the number of piles has a considerable effect on the LLDFs for the abutment moment and pile shear. The LLDFs for the cases of 4 and 6 piles are calculated as 0.711 and 0.598 for the abutment moment and 0.584 and 0.393 for the pile shear. It is also observed that a better distribution of live load effects for the abutment moment and pile shear is obtained with increasing number of piles.

In summary, while the effect of the pile size and orientation on the distribution of live load effects among the components of IBs can be neglected, the number (or spacing) of piles supporting the abutments need to be considered in estimating the distribution of live load effects within the substructure components of IBs.

4.5 SUMMARY

In this chapter, the effect of soil-structure interaction and substructure properties at the abutments on the distribution of live load effects in IB components is investigated. Followings are the conclusions deduced from this research study.

1. The effect of the foundation soil stiffness on the LLDFs for the girder and pile moments and shear is found to be negligible. However, the foundation soil stiffness is found to have a significant effect on the LLDFs for the abutment moment and to a lesser extent on those for the abutment shear. Therefore, the foundation soil stiffness must be considered in estimating the distribution of the live load effects within the abutments of IBs.

2. The effect of the backfill on the LLDFs for the girder and pile moments and shears is found to be negligible. However, the backfill is found to have a notable effect on the LLDFs for the abutment moment and shear. Therefore, the backfill must be considered in estimating the distribution of live load effects within the abutments of IBs. Nevertheless, the distribution of live load effects in IBs is found to be insensitive to the compaction level of the backfill.

3. Furthermore, the distribution of live load effects in IBs is found to be insensitive to the size and orientation of the piles, abutment thickness and the wingwalls. However, the abutment height and number of piles is found to affect the distribution of live load effects in the piles and abutments. It is observed that while taller abutments enhance the distribution of live load effects within the abutment, using shorter abutment is more suited for better distribution of live load effects to the piles. Moreover, increasing the number of piles is found to improve the distribution of live load effects among the piles.

4. LLDFs for IB abutments and piles are still needed to estimate live load effects in these components for design purposes. The findings from this research study can be used as a starting point to formulate the LLDFs for the abutment and piles of IBs.

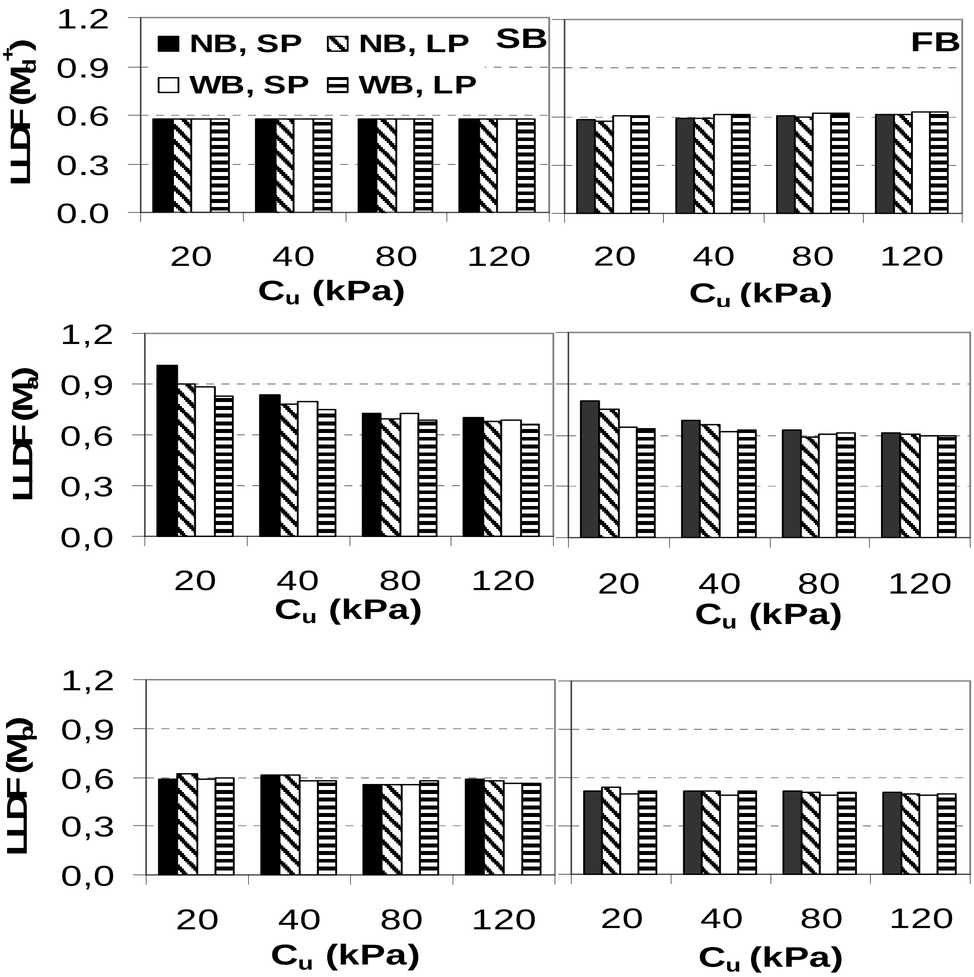

Figure 4.2 LLDFs for girder, abutment and pile moments (M_d, M_a, M_p) versus C_u for the stiff (SB) and flexible (FB) bridges with 3 m. tall abutments supported on HP250x85 (SP) and HP310x125 (LP) piles oriented to bend about their strong axes and considering (WB) and neglecting (NB) the backfill effect.

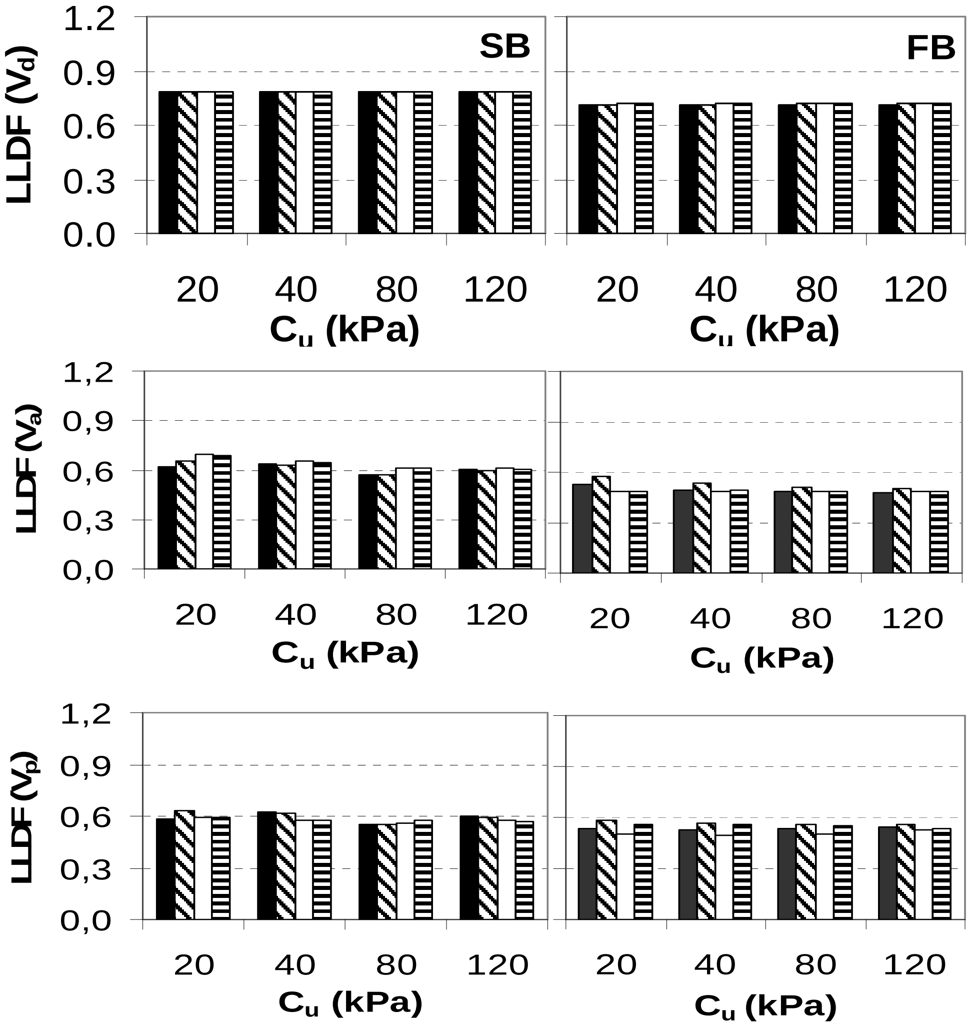

Figure 4.3 LLDFs for girder, abutment and pile shears (V_d, V_a, V_p) versus C_u for the stiff (SB) and flexible (FB) bridges with 3 m. tall abutments supported on HP250x85 (SP) and HP310x125 (LP) piles oriented to bend about their strong axes and considering (WB) and neglecting (NB) the backfill effect.

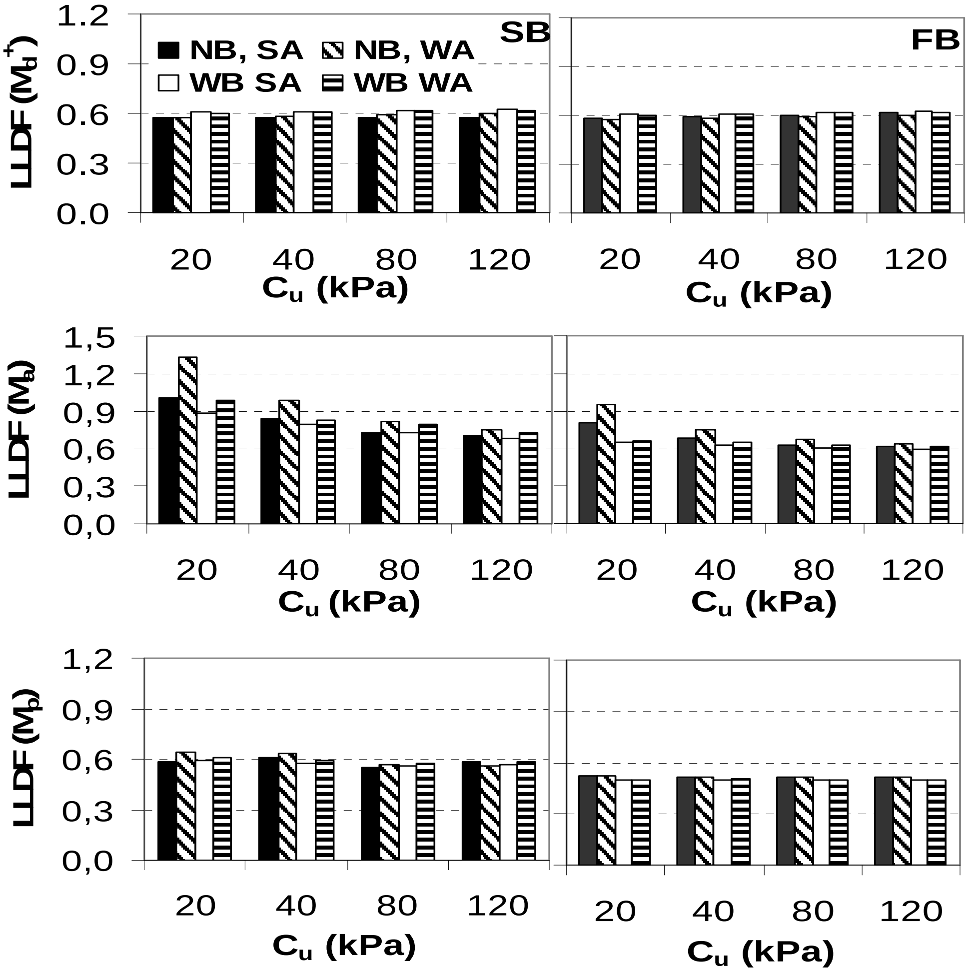

Figure 4.4 LLDFs for girder, abutment and pile moments (M_d, M_a, M_p) versus C_u for the stiff (SB) and flexible (FB) bridges with 3 m. tall abutments supported on HP250x85 piles oriented to bend about their strong (SA) and weak (WA) axes and considering (WB) and neglecting (NB) the backfill effect.

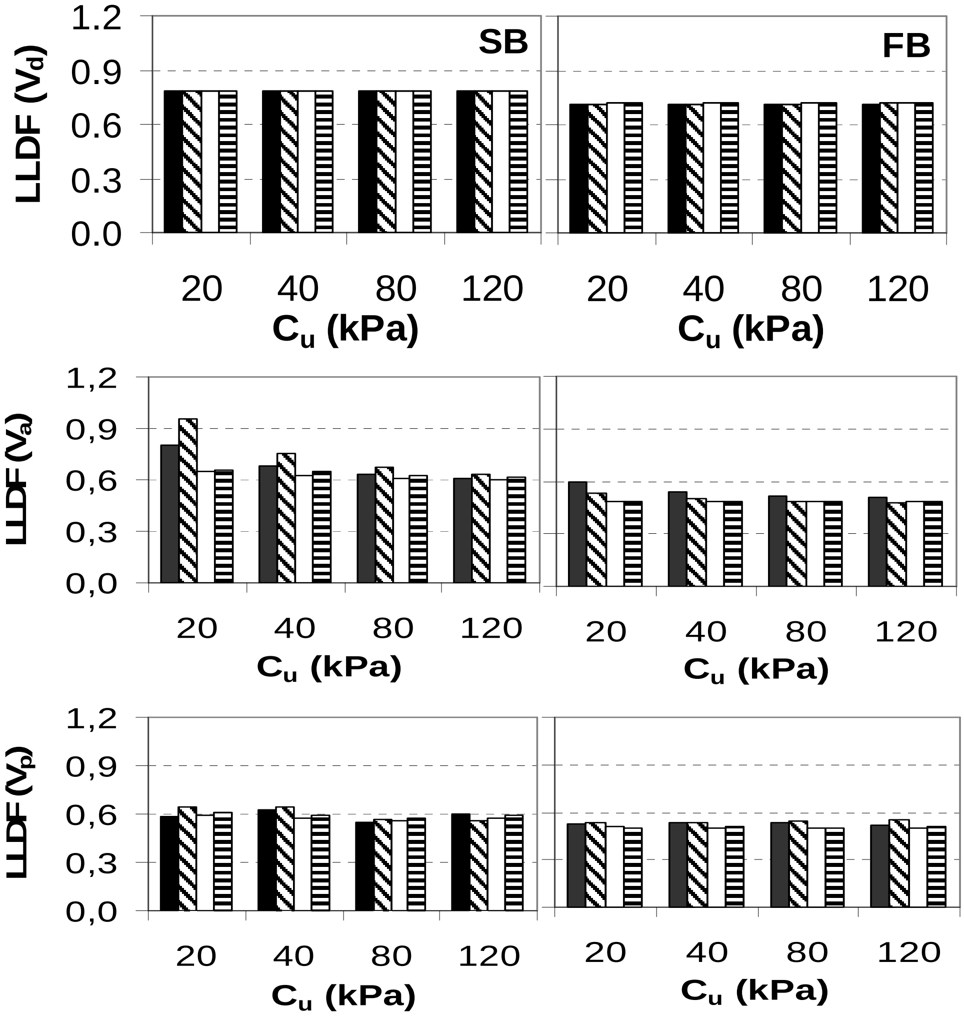

Figure 4.5 LLDFs for girder, abutment and pile shears (V_d, V_a, V_p) versus C_u for the stiff (SB) and flexible (FB) bridges with 3 m. tall abutments supported on HP250x85 piles oriented to bend about their strong (SA) and weak (WA) axes and considering (WB) and neglecting (NB) the backfill effect.

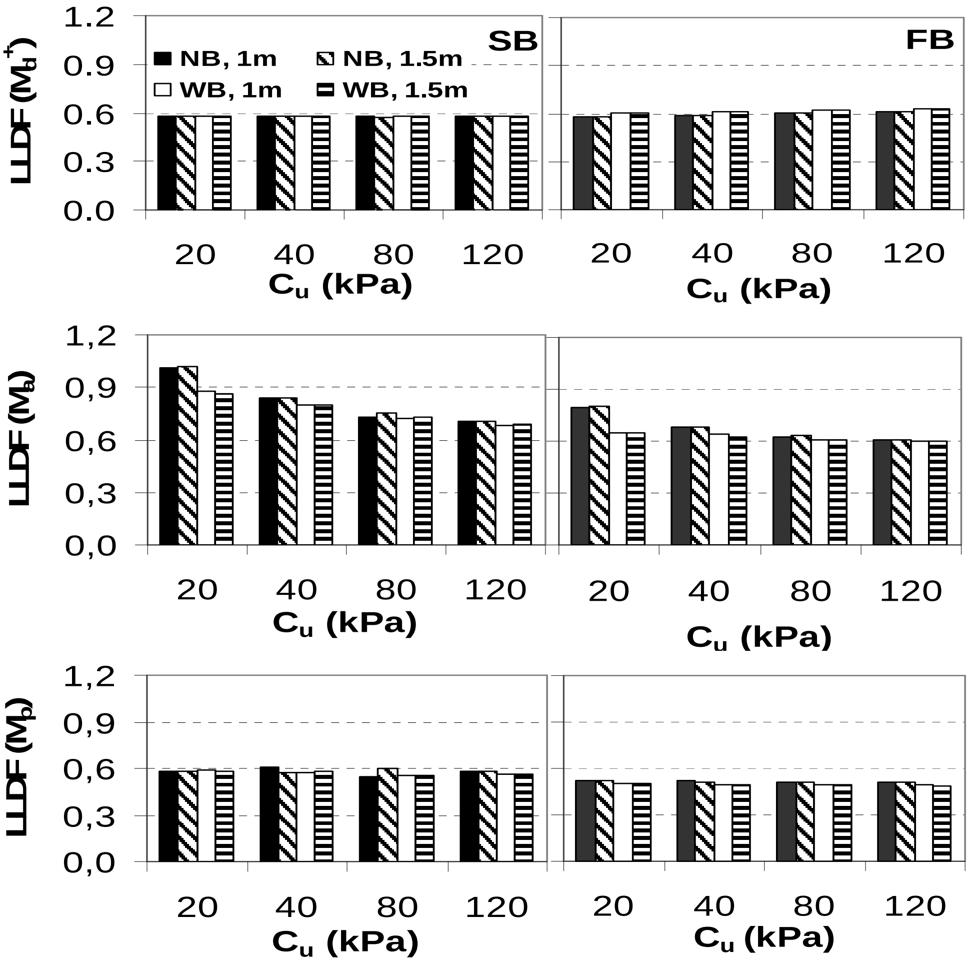

Figure 4.6 LLDFs for girder, abutment and pile moments (M_d, M_a, M_p) versus Cu for the stiff (SB) and flexible (FB) bridges with 3 m. tall and 1.0 and 1.5 m. thick abutments supported on HP250x85 piles oriented to bend about their strong axes and considering (WB) and neglecting (NB) the backfill effect.

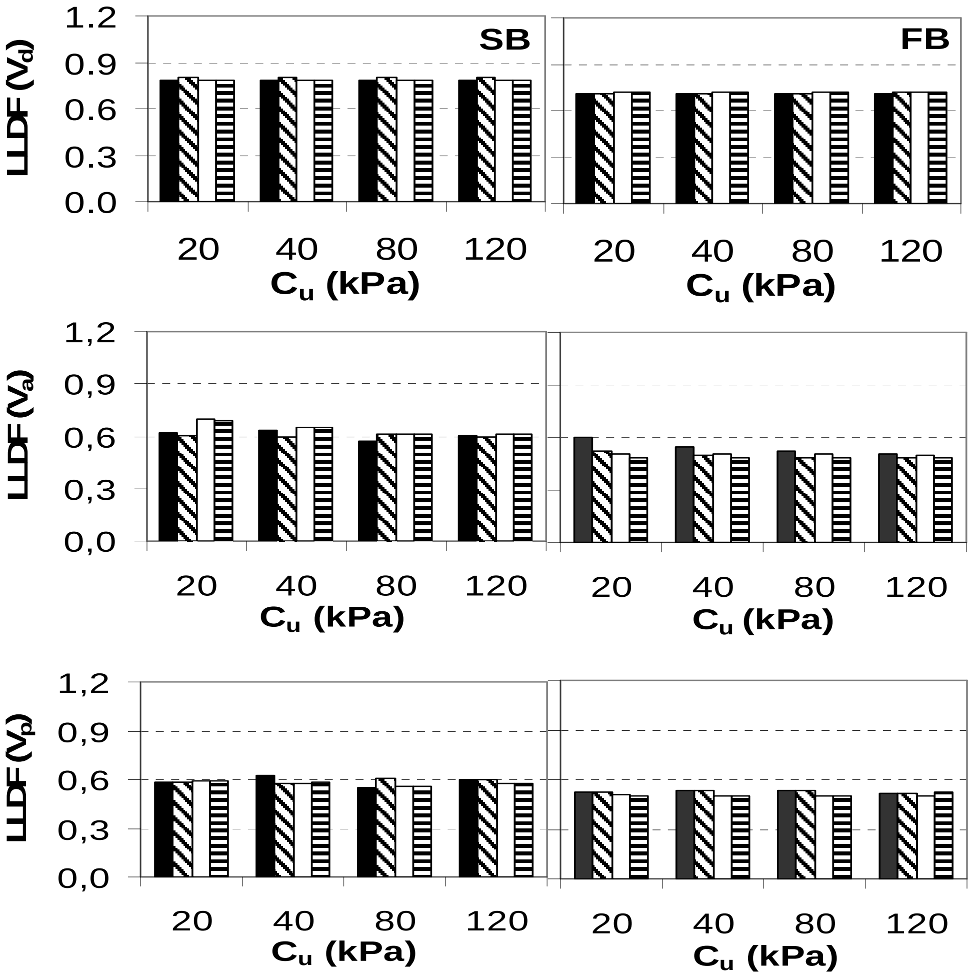

Figure 4.7 LLDFs for girder, abutment and pile moments (M_d, M_a, M_p) versus Cu for the stiff (SB) and flexible (FB) bridges with 3 m. tall and 1.0 and 1.5 m. thick abutments supported on HP250x85 piles oriented to bend about their strong axes and considering (WB) and neglecting (NB) the backfill effect.

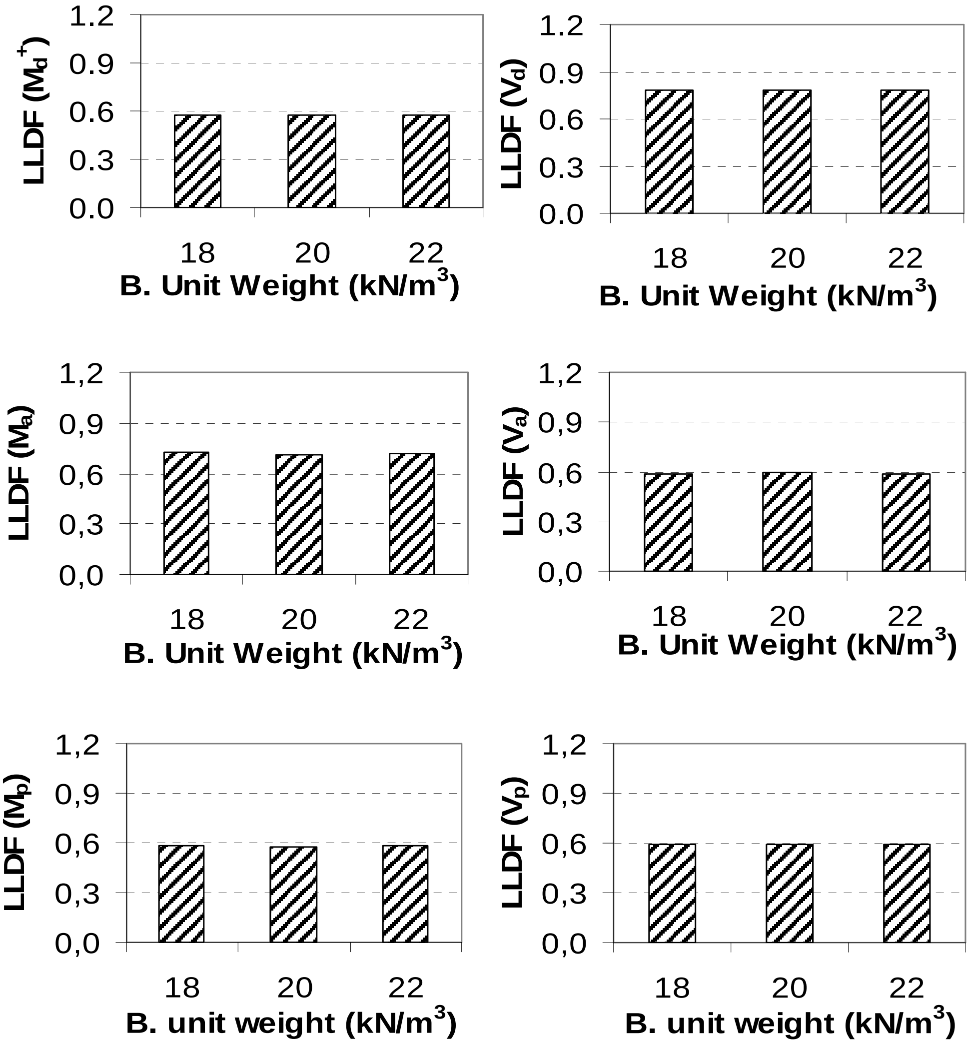

Figure 4.8. LLDFs for girder, abutment and pile moments (M_d, M_a, M_p) and shears (V_d, V_a, V_p) versus unit weight of backfill for the stiff bridge with 3 m. tall abutments supported on HP250x85 piles oriented to bend about their strong axes.

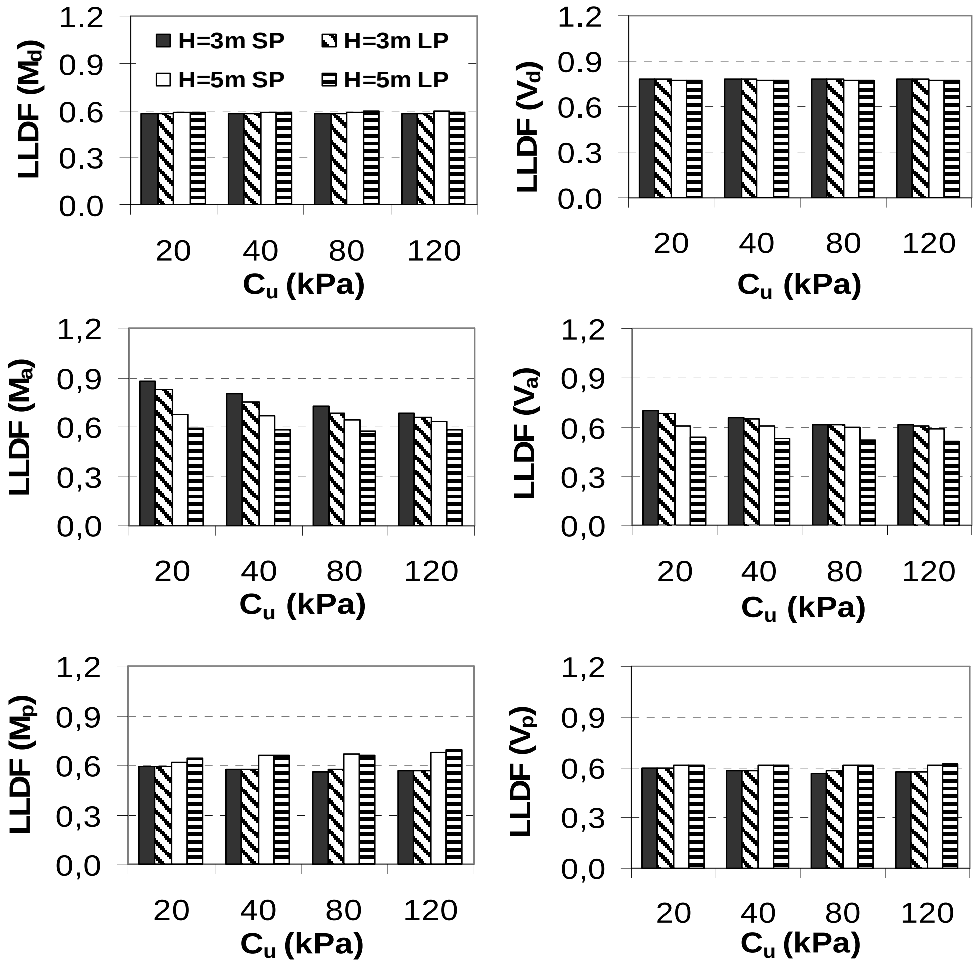

Figure 4.9. LLDFs for girder, abutment and pile moments (M_d, M_a, M_p) and shears (V_d, V_a, V_p) versus Cu for the stiff bridge with 3 and 5 m. tall abutments supported on HP250x85 (SP) and HP310x125 (LP) piles oriented to bend about their strong axes and considering the backfill effect.

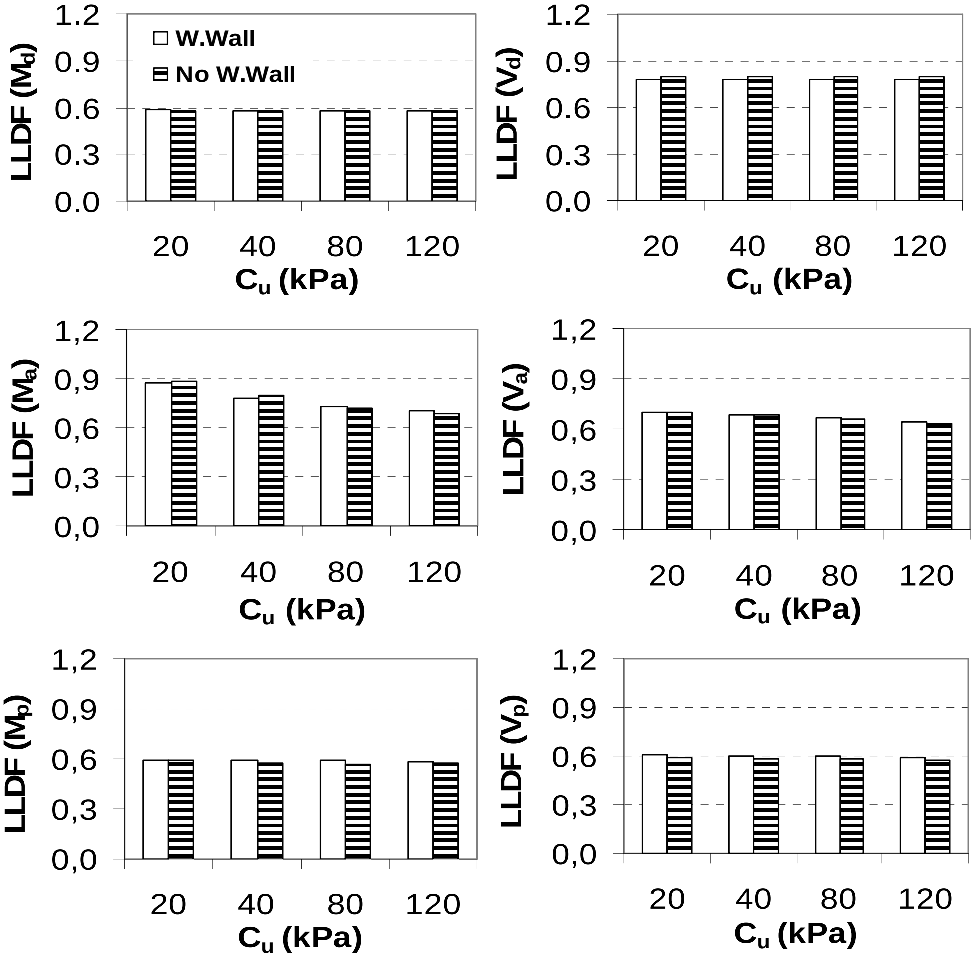

Figure 4.10. LLDFs for girder, abutment and pile moments (M_d, M_a, M_p) and shears (V_d, V_a, V_p) versus C_u for the stiff bridge with 3 m. tall abutments supported on HP250x85 piles oriented to bend about their strong axis and considering the backfill effect for the cases with and without wingwalls.

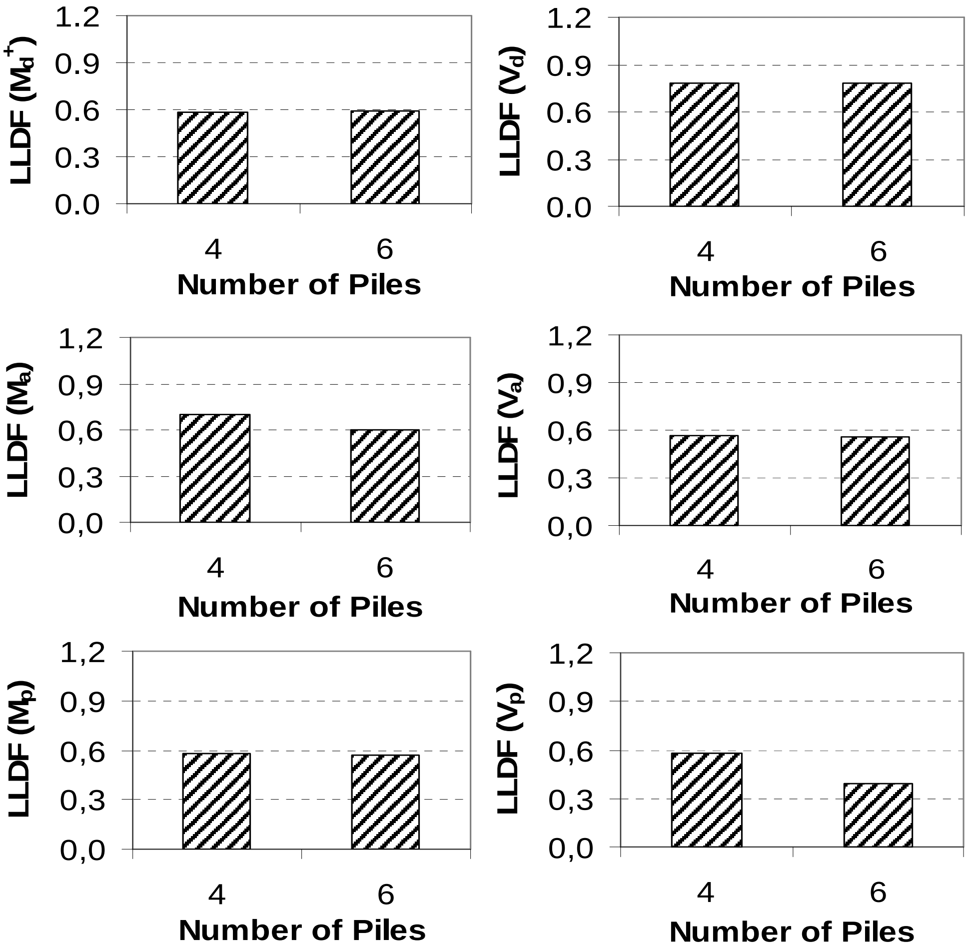

Figure 4.11. LLDFs for girder, abutment and pile moments (M_d, M_a, M_p) and shears (V_d, V_a, V_p) versus number of HP250x85 piles oriented to bend about their strong axis for the stiff bridge with 3 m. tall abutments and considering the effect of the backfill.

CHAPTER 5

EFFECT OF SUPERSTRUCTURE-ABUTMENT CONTINUITY ON LIVE LOAD DISTRIBUTION IN INTEGRAL ABUTMENT BRIDGE GIRDERS

This part of the thesis study is aimed at investigating the effect of superstructure-abutment continuity on the distribution of live load effects in IB girders. For this purpose, two (2-D) and three (3-D) dimensional finite element models of several single-span, symmetrical integral abutment and regular jointed SSBs are built and analyzed under AASHTO live load. In the analyses, the effect of various superstructure properties such as span length, number of design lanes, girder size and spacing as well as slab thickness is considered. The results from the analyses of 2-D and 3-D finite element models are then used to calculate the LLDFs for the girders of IBs and SSBs as a function of the above mentioned parameters. LLDFs for the girders are also calculated using the AASHTO formulae developed for SSBs (AASHTO 2007). The girder LLDFs for IBs are then compared with those of SSBs and AASHTO to assess the effect of superstructure-abutment continuity on the distribution of live load effects among the girders of IBs.

5.1. BRIDGES AND PARAMETERS CONSIDERED IN THE ANALYSES

To investigate the effect of superstructure-abutment continuity on the distribution of live load effects among the girders of IBs, comparative live load analyses of both SSBs and IBs with various properties are conducted. For the SSBs, the diaphragms at the supports are assumed to have a 0.4 m wide rectangular cross-section. The depth of the diaphragms is varied based on the type of AASHTO prestressed concrete girders used in the analyses. The abutments of the IBs considered in this study are assumed to be 3 m. tall (same as the height of the backfill) and supported by 12 m. long end-bearing steel HP250x85 piles. The number of piles is set equal to the number of girders (i.e. one pile is assumed underneath each girder). It is noteworthy that in an earlier research study conducted by Dicleli and Erhan (2008), the number of piles per girder was found to have only a negligible effect on the LLDFs for IB girders. The strength of the concrete used for the prestressed concrete girders are assumed to be 50 MPa while those of the slab, diaphragms (for SSBs) and the abutments (for IBs) are assumed to be 30 MPa. The granular backfill behind the abutments is assumed to have a unit weight of 20 kN/m^3. The foundation soil surrounding the piles is assumed to be medium-stiff clay with an undrained shear strength of C_u=40 kPa. The assumed clay stiffness is typical for IB construction as in stiffer soils; pre-drilled oversize holes filled with loose sand is generally provided along the top portion of the pile to reduce the resistance of the surrounding stiff soil to the lateral movements of the pile. A parametric study is conducted to cover a broad range of bridge properties found in practice. Nevertheless, the parameters included in this study are limited to superstructure properties since in an earlier research study conducted by Dicleli and Erhan (2008), the variations in substructure (abutments and piles), backfill and foundation soil properties are found to have negligible effects on the distribution of live load moment and shear among the girders of IBs. The superstructure properties considered in the analyses include the span length (10, 15, 20, 25, 30, 35, 40, 45 m.), number of design lanes (1, 2, 3, 4 design lanes), girder size (Girder type I, II, III, IV, V, VI) and spacing (1.2, 2.4, 3.6, 4.8 m.) as well as slab thickness (0.15, 0.20, 0.25, 0.30 m.). This resulted in a total of 324 different 3-D and corresponding 2-D structural models of SSBs and IBs and more than 2000 analyses cases. The 2000 analyses cases include the analyses of both 2-D and 3-D models, the analyses for various longitudinal positions of the truck for shear and moment and the analyses for various transverse positions of two or more trucks in the analyses of 3-D models. Note that the combination of various parameters presented above may not always be realistic (e.g. the combination of girder type VI and a span length of 15 m). Although such unrealistic combinations may result in biased interpretations of analysis results for LLDFs due to the combination of unrealistic girder sizes with various span lengths, this was done deliberately to solely study the effect of a certain parameter on the distribution of live load moment and shear among the girders by keeping the other parameters constant and to have adequate data covering the full range of possible variation of the parameters to incorporate all possible cases of scenarios. A similar approach was also used in the development of AASHTO LLDFs.

5.2 ESTIMATION OF LIVE LOAD DISTRIBUTION FACTORS

LLDFs are calculated for the composite interior girders of the SSBs and IBs. For this purpose, first the maximum live load effects (moment and shear) from the analyses of the 3-D FEM models (for SSBs the 3-D FEM model in Figure 5.1 (a) and for IBs the 3-D FEM model in Figure 5.2 (b)) for the composite interior girders are calculated as the summation of the maximum effects in the girder element and within the tributary width of the slab (equal to the girder spacing) at the same location along the bridge. The live load effects (moment and shear) due to a single truck loading at the same longitudinal location as the position of the trucks in the 3-D model is also calculated using the 2-D models presented for SSBs and IBs respectively in Figs. 5.1 (a) and 5.2 (b). The live load distribution factors are then calculated as the ratio of the maximum live load effects obtained from 3-D analyses to those obtained from 2-D analyses. Analytically, the LLDFs for girder moment ($LLDF_M$) and shear ($LLDF_V$) are expressed as follows;

$$LLDF_M = \frac{M_{3D}}{M_{2D}} \tag{5.1}$$

$$LLDF_V = \frac{V_{3D}}{V_{2D}} \tag{5.2}$$

where M_{3D} and V_{3D} are respectively the maximum girder live load moment and shear force obtained from the analyses of the 3-D FEMs for the most unfavorable longitudinal and transverse positions of multiple trucks (i.e based on the number of design lanes, several analyses are conducted for two or more trucks placed at the same longitudinal location along the bridge and the maximum effect is picked after multiplying each result by the multiple presence factors of AASHTO (2007) to take into consideration the reduced probability of the presence of a number of trucks at the same longitudinal location) and M_{2D} and V_{2D} are respectively the maximum girder live load moment and shear force obtained from the analysis of the 2-D FEMs under a single truck load placed at the same longitudinal position as that of the trucks in the 3-D model.

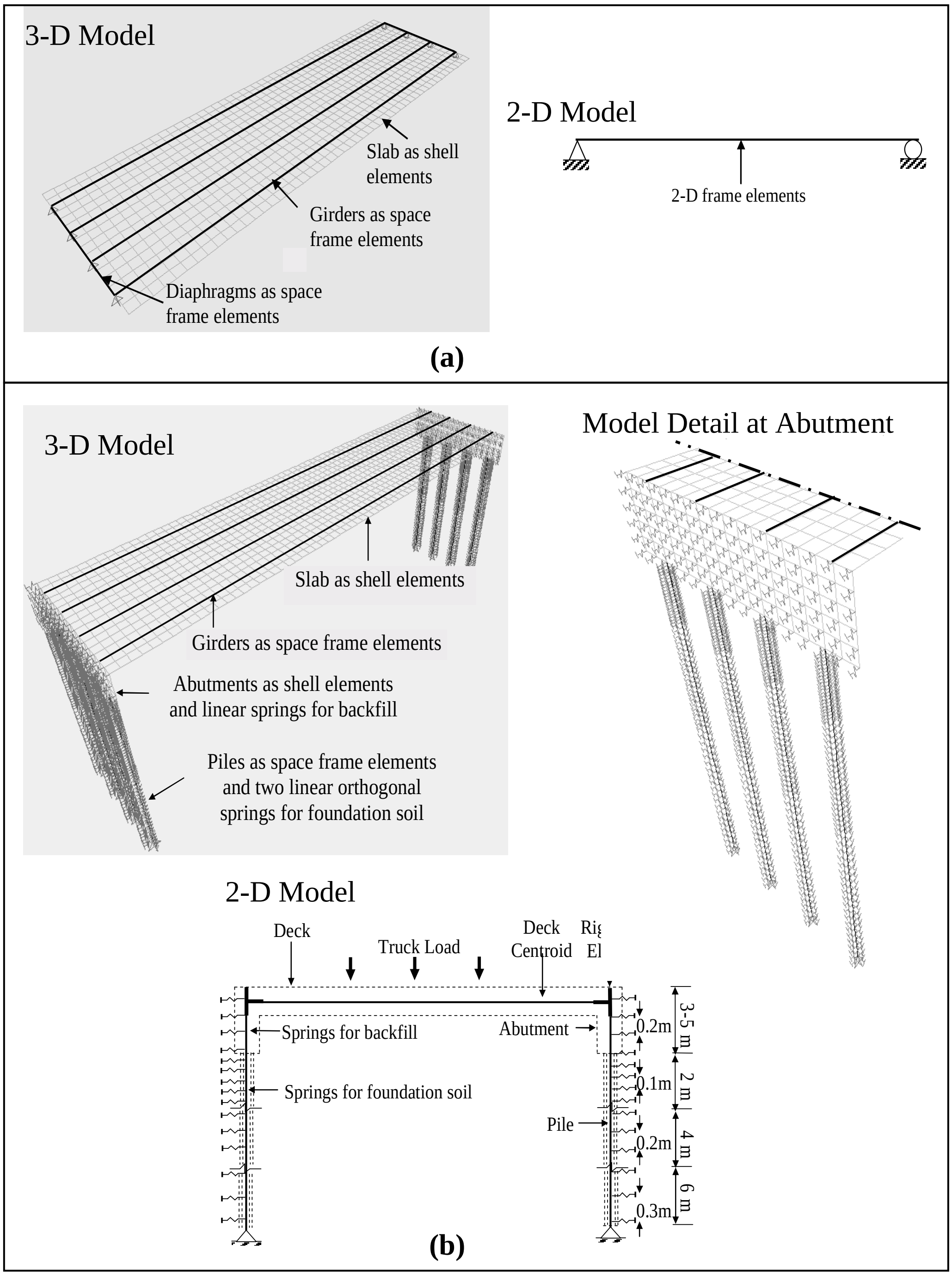

Figure 5.1 3-D and 2-D Structural models of (a) SSB, (b) IB.

5.3 CONTINUITY EFFECT: LONG-NARROW VERSUS SHORT-WIDE BRIDGES

In this section, preliminary comparative sensitivity analyses are conducted to investigate whether the superstructure-abutment continuity in IBs influences the distribution of live load shear and moment among the girders. A long-and-narrow and a short-and-wide SSB and IB are considered in the analyses to cover a broad range of possibilities. For this purpose, 45 m long SSB and IB with four girders spaced at 2.4 m (long and narrow bridges) and 15 m long SSB and IB with seven girders spaced at 2.4 m (short and wide bridges) are considered. The overhang and the total width of the bridges are respectively 1.2 m and 9.6 m for the long and narrow bridge and 0.6 m and 15.6 m for the short and wide bridge. For the long and narrow bridges, AASHTO prestressed concrete girder types (GT) II and VI and for the short and wide bridges AASHTO prestressed concrete girder types (GT) I and IV are considered to examine the impact of the variation of girder size, on the effect of superstructure-abutment continuity on live load distribution among the girders. This resulted in eight analyses cases. The design trucks are transversely located on the bridge to produce the maximum interior girder moment and shear for the long and narrow bridge with four girders and for the short and wide bridge with seven girders. For the long and narrow bridge only two trucks are required to produce the maximum live load effects in one of the girders while for the short and wide bridge three trucks are required as shown in the figure. The live load shear/moment in each girder is then calculated and divided by the corresponding shear/moment obtained from 2-D analyses under a single truck load to normalize the live load effect in each girder with respect to a single truck load. The analyses results are presented in Figs. 5.2 (a) and (b) for long and narrow and short and wide bridges respectively. The figures display the distribution of live load moment (M_g) and shear (V_g) (LLDF) to each girder, (for certain truck transverse positions producing the maximum interior girder shear and moment) which are presented on the horizontal axis and depicted on the picture representing superstructure cross-section placed on the graph.

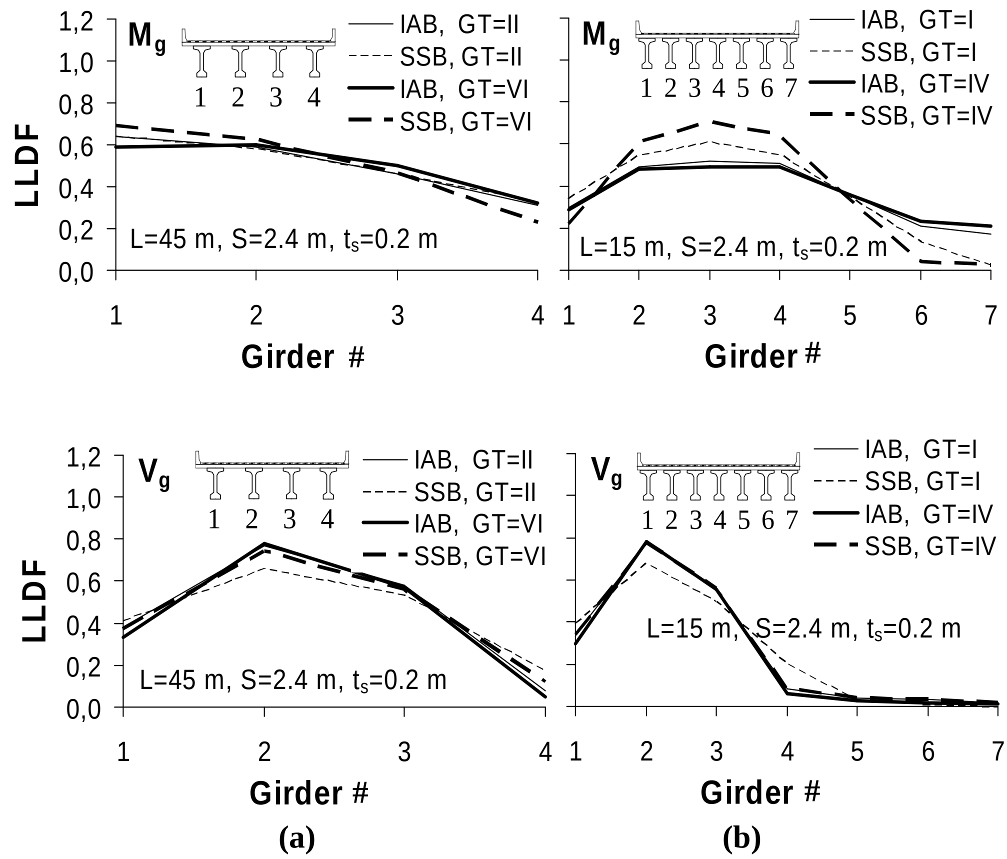

Figure 5.2 Effect of superstructure-abutment continuity on the distribution of live load moment and shear among the girders of (a) long and narrow bridges (b) short and wide bridges.

It is observed from the figures that the superstructure-abutment continuity in IBs improves the distribution of live load moment among the girders. That is, the plots for IBs are relatively more uniform and have smaller peaks compared to those of the SSB. The figures reveal that the effect of superstructure-abutment continuity on live load moment distribution among the girders of IBs is more pronounced for short span bridges. The better distribution of live load moment in IBs may be mainly due to the torsional rotational rigidity provided by the monolithic abutments to the girders and the slab, which is more predominant for shorter span bridges. Furthermore, the overhanging portion of the slab, which is free over the supports in SSBs, is fixed to the abutments (cast monolithically) in the case of IBs. This may also enhance the distribution of live load moment among the girders of IBs. However, the effect of superstructure-abutment continuity on the distribution of live load shear among the girders is found to be less significant. In fact, the live load shear distribution in the girders of IBs is found to be slightly poorer than that in the girders of SSBs. The location of the calculated live load shear, which is at the face of the abutment in IBs rather than the immediate vicinity of the end supports underneath the girders in SSBs, may be the main reason for this type of a behavior. It is also observed that while smaller girder sizes enhances the distribution of live load effects among the girders of SSBs, the effect of girder size on the distribution of live load among the girders of IBs is less significant. Accordingly, the effect of continuity is more pronounced for larger girder sizes.

In summary, the preliminary sensitivity analyses indicated that superstructure-abutment continuity affects the distribution of live load moment among the girders. However, continuity does not have a significant effect on the distribution of live load shear. The continuity effect is found to be a function of the span length and girder size. Accordingly, the effect of superstructure-abutment continuity as a function of the above mentioned parameters as well as the girder spacing, number of design lanes and slab thickness will be investigated in detail in the following sections.

5.4. CONTINUITY EFFECT VERSUS SPAN LENGTH

The effects of the superstructure-abutment continuity on the distribution of girder live load moment and shear are illustrated in Figs. 5.3 and 5.4 as a function of span length (10, 15, 20, 25, 30, 35, 40 and 45 m.) for various girder spacings (1.2 m, 2.4 m, 3.6 m) and girder types (II, IV, VI) respectively. The data presented in the figures are obtained for bridges with two lanes, slab thickness of 0.2 m, deck widths of 9.6 m for 1.2 (7 girders) and 2.4 m (4 girders) girder spacing and 13.2 m for 3.6 m (4 girders) girder spacing and overhang width of 1.2 m. In the figures, the LLDFs obtained for IBs, SSBs and those calculated from the AASHTO formulae for the interior girders of slab-on-girder bridges are compared. The AASHTO (2007) LLDF for the composite interior girder moments ($LLDF_{M\text{-}AASHTO}$) and shears ($LLDF_{V\text{-}AASHTO}$) of slab-on-girder jointed bridges with two or more design lanes loaded is given as;

$$LLDF_{M-AASHTO} = 0.075 + \left(\frac{S}{2900}\right)^{0.6}\left(\frac{S}{L}\right)^{0.2}\left(\frac{K_g}{Lt_s^3}\right)^{0.1} \tag{5.3}$$

$$LLDF_{V-AASHTO} = 0.2 + \frac{S}{3600} - \left(\frac{S}{10700}\right)^{2.0} \tag{5.4}$$

where S is the girder spacing, L is the span length, t_s is the slab thickness and K_g is a parameter representing the longitudinal stiffness of the composite slab-on-girder section of the bridge expressed as (AASHTO 2007);

$$K_g = n\left(I + Ae_g^2\right) \tag{5.5}$$

In the above equation, n is the ratio of the modulus of elasticity of the girder material to that of the slab material, I is the moment of inertia of the girder, A is the cross-sectional area of the girder and e_g is the distance between the centers of gravity of the girder and the slab.

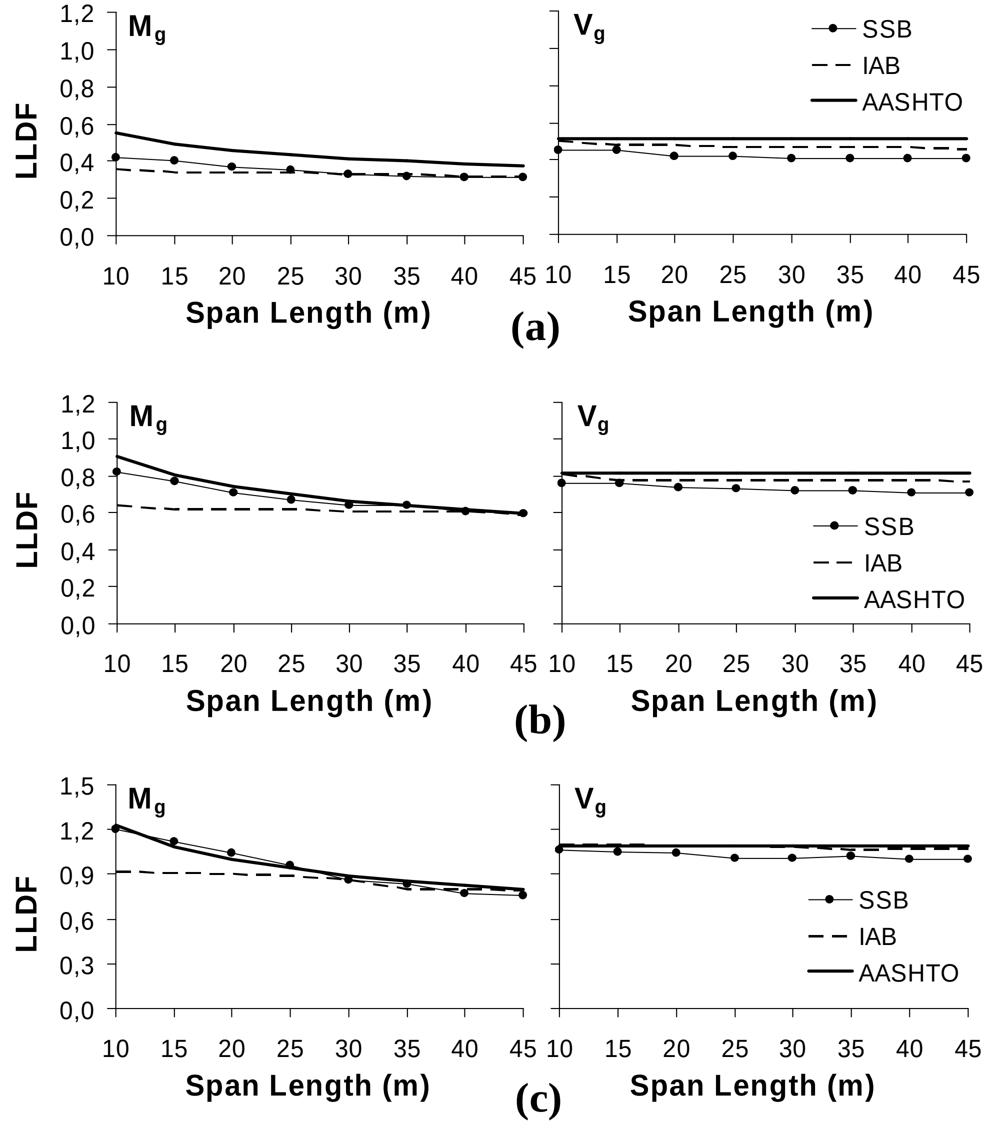

Figure 5.3 Distribution factor vs. span length for (a) Girder Type II, (b) Girder Type IV, (c) Girder Type VI (For all the graphs; girder spacing = 2.4 m and slab thickness = 0.2 m).

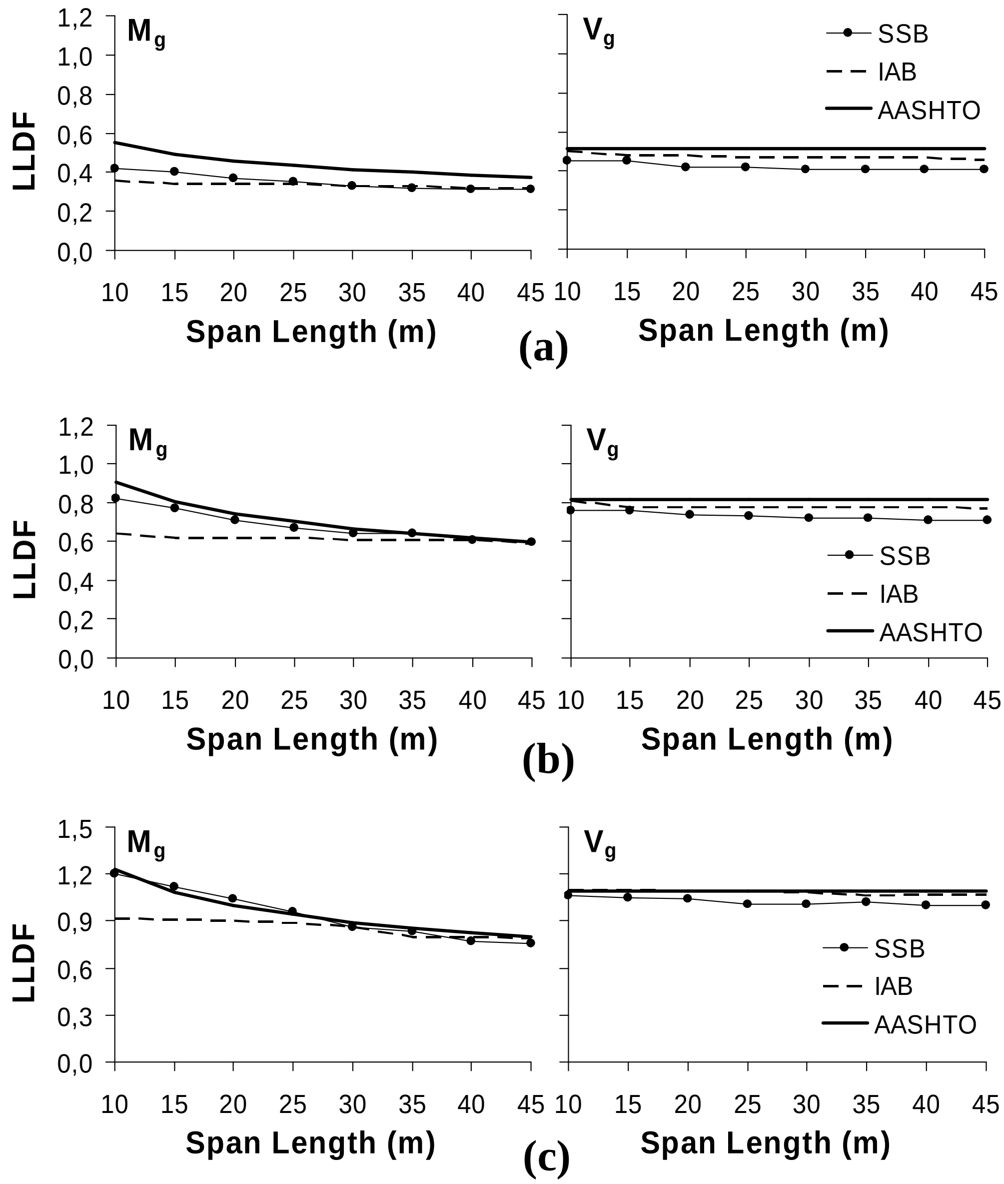

Figure 5.4 Distribution factor vs. span length for (a) 1.2 m girder spacing, (b) 2.4 m girder spacing, (c) 3.6 m girder spacing (For all the graphs; girder type = IV and slab thickness = 0.2 m).

It is observed from the figures that the effect of the superstructure-abutment continuity on the LLDFs for the girder moment is significant especially in the case of short span bridges. For instance, for an IB and SSB with 10 m span length, 0.2 m thick slab and AASHTO Type IV girders spaced at 2.4 m, the LLDFs for the interior girder moment (M_g) are calculated as 0.636 and 0.845 respectively. The LLDF calculated from the AASHTO formulae is 0.973. The difference between the LLDFs of the IB and SSB as well as that calculated using AASHTO formulae are 33%. and 53% respectively. This clearly demonstrates that using AASHTO formulae for short span IBs will produce conservative estimates of live load moment in the girders. However, for the same IB and SSB, but with 45 m span length, the LLDFs for the interior girder moment (M_g) are calculated as 0.596 and 0.586 respectively. The LLDF calculated from the AASHTO formulae is 0.640. The difference between the LLDFs of the IB and the SSB as well as that calculated using AASHTO formulae are 1.7%. and 7.4% respectively. This indicates that the effect of superstructure-abutment continuity ceases for longer span bridges. It is also observed that AASHTO LLDFs produces reasonable estimates of the live load moments in the girders of IBs with longer spans. Furthermore, Figs. 5.3 and 5.4 reveal that for IBs, the variation of the LLDFs for the girder moment is less sensitive to the span length due to superstructure-abutment continuity. The plots in Figs. 5.3 (a), (b), (c) and 5.4 (a), (b), (c) reveal that the above observations are valid regardless of the girder type and spacing.

For the girder shear, the superstructure-abutment continuity is found to have negligible effects on live load distribution for short span bridges, but such effects become slightly more noticeable as the span length increases. For instance, for the IB and SSB with 10 m span length, AASHTO girder type IV and girder spacing of 2.4 m, the LLDFs for the interior girder shear (V_g) are found as 0.769 and 0.781 respectively. However, for the same IB and SSB, but with a 40 m span length, the LLDFs for the interior girder shear (V_g) are obtained as 0.783 and 0.714 respectively. For the same bridges, the LLDF calculated from AASHTO formulae is 0.816 for the range of span lengths considered (AASHTO formula for LLDFs for girder shear is not a function of span length). As observed from the figures, for IBs, the LLDFs for girder shear are in close agreement with those calculated from AASHTO formulae. Thus, for the range of span lengths considered, AASHTO LLDFs for girder shear may be used for the design of IB girders regardless of the girder type. However, AASHTO LLDFs for girder shear seem to be overly conservative for SSBs.

5.5 CONTINUITY EFFECT VERSUS GIRDER SPACING

The effects of the superstructure-abutment continuity on the distribution of girder live load moment and shear are illustrated in Figs. 5.5 and 5.6 as a function of girder spacing (1.2, 2.4, 3.6 and 4.8 m.) for various span lengths (15 m, 30 m, 40 m) and girder types (II, IV, VI) respectively. The data presented in the figures are obtained for bridges with four lanes, slab thickness of 0.2 m, deck width of 15.6 m and overhang width of 0.6 m. In the figures, LLDFs obtained for IBs, SSBs and those calculated from the AASHTO formulae for slab-on-girder bridges are compared.

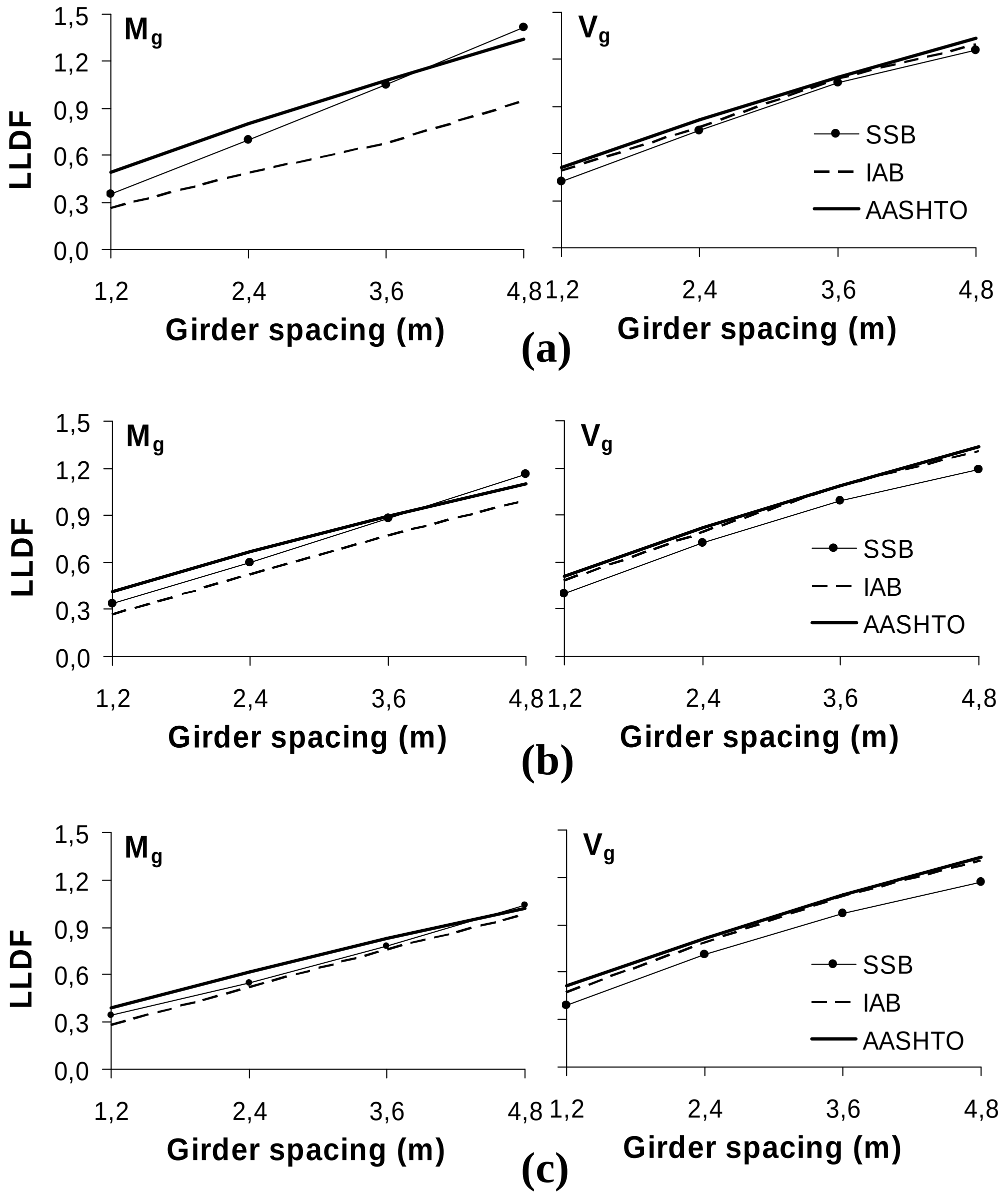

Figure 5.5 Distribution factor vs. girder spacing for (a) 15 m span length, (b) 30 m span length, (c) 40 m span length, (For all the graphs; girder type = IV and slab thickness = 0.2 m).

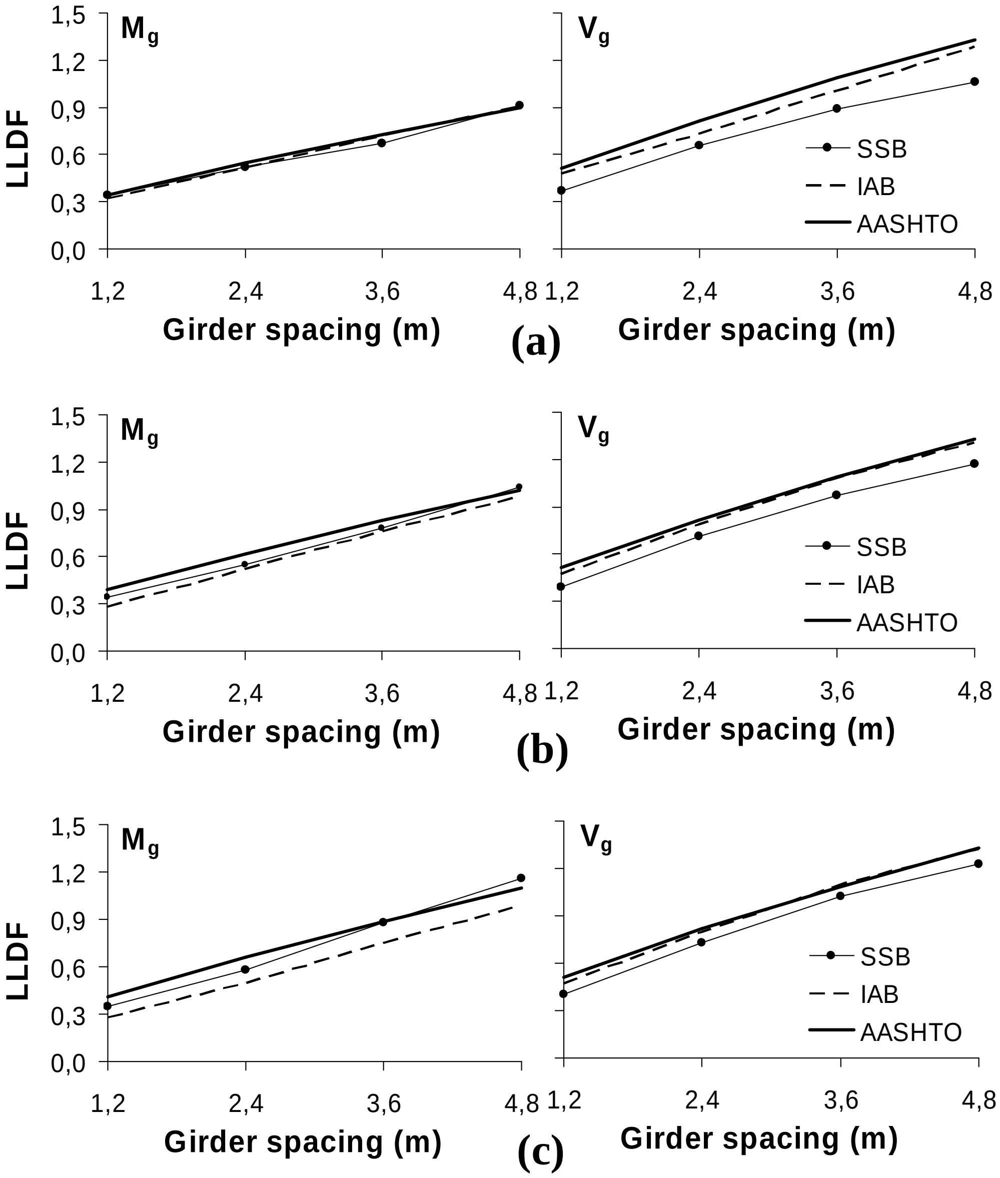

Figure 5.6 Distribution factor vs. girder spacing for (a) Girder Type II, (b) Girder Type IV, (c) Girder Type VI (For all the graphs; span length = 40 m and slab thickness = 0.2 m).

It is observed from the figures that the superstructure-abutment continuity affects the distribution of live load moment among the girders regardless of the girder spacing. The continuity effect is somewhat more noticeable for shorter span bridges (Fig. 5.5) and larger girder sizes (Figs. 5.6) for the range of girder spacings considered. However, the continuity effect generally becomes more noticeable at larger girder spacings especially for shorter span bridges. It is also found that, the LLDFs calculated from AASHTO formulae yield conservative estimates of LLDF for girder moment especially for larger girder spacings and for shorter span bridges. This effect diminishes for smaller girder sizes and larger span lengths. The difference between the LLDFs for the girder moment of IBs and SSBs considered in Figs. 5.5 and 5.6 is estimated to range between 0% and 54.4% while the difference between the LLDFs for the girder moment of IB and those calculated from AASHTO formulae is estimated to range between 0.8% and 63%. Thus, designing the girders of IB using the AASHTO formulae for girder moments expected to be uneconomical especially for short span bridges for the range of girder spacings considered.

However, in the case of LLDFs for girder shear, it is found that the superstructure-abutment continuity effect is less noticeable compared to that of the LLDFs for girder moment for the range of girder spacings considered. The continuity effect for the girder shear is observed to become slightly more noticeable only for longer span bridges and smaller girder sizes. The difference between the LLDFs for the girder shear of IBs and SSBs considered in Figs. 5.5 and 5.6 is estimated to range between 2.3% and 22.9% while the difference between the LLDFs for the girder shear of IB and those calculated from AASHTO formulae is estimated to range between 0.3%.and 8.9%. Since the difference between the IB and AASHTO LLDFs for girder shear is small, using the AASHTO formulae will produce reasonable estimates of live load shear in the girders of IBs regardless of the girder spacing. However, AASHTO LLDFs for girder shear seem to be overly conservative for SSBs.

5.6. CONTINUITY EFFECT VERSUS GIRDER TYPE (SIZE)

The effects of the superstructure-abutment continuity on the distribution of girder live load moment and shear are illustrated in Figs. 5.7 and 5.8 as a function of the girder type (I, II, III, IV, V,) for various span lengths (15, 30, 45 m) and girder spacings (1.2 m, 2.4 m, 3.6 m) respectively. The data presented in the figures are obtained for bridges with two lanes, slab thickness of 0.2 m, deck widths of 9.6 m for 1.2 (7 girders) and 2.4 m (4 girders) girder spacing and 13.2 m for 3.6 m (4 girders) girder spacing and overhang width of 1.2 m. In the figures, LLDFs obtained for IBs, SSBs and those calculated from the AASHTO formulae for slab-on-girder bridges are compared.

It is observed from the figures that the superstructure-abutment continuity affects the distribution of live load moment among the girders regardless of the girder type (size). However, the continuity effect is noticeable only in the case of short span bridges or bridges with larger girder sizes. However, the girder size effect is less noticeable compared to that of the other parameters studied. For instance, for 30 m long IB and SSB with 0.2 m thick slab and AASHTO Type III girders spaced at 2.4 m, the LLDFs for the interior girder moment are calculated as 0.607 and 0.626 respectively. The LLDF calculated from the AASHTO formulae is 0.628. The difference between the LLDFs of the IB and SSB as well as that calculated using AASHTO formulae are 3.1%. and 3.5% respectively. However, for the same IB and SSB, but with AASHTO

Type VI girders, the LLDFs for the interior girder moment are calculated as 0.624 and 0.684 respectively. The LLDF calculated from the AASHTO formulae is 0.713. The difference between the LLDFs of the IB and SSB as well as that calculated using AASHTO formulae are 8.8% and 12.5% respectively. These differences become even larger for shorter span bridges. Accordingly, the continuity effect should be included in the estimation of live load moments in the girders of IBs. Furthermore, Figs. 5.7 and 5.8 reveal that for IBs, the variation of the LLDFs for the girder moment is less sensitive to the girder size due to the effect of continuity as the LLDF vs. girder type plots for IBs have very small gradients compared to those for the SSBs.

It is also found that the effect of superstructure-abutment continuity on the LLDFs for girder shear is more noticeable than that for girder moment especially for bridges with, longer spans and smaller girder sizes. However, the shear LLDFs for IB girders are found to be in close agreement with those calculated using the AASHTO formulae. The difference between the LLDFs for the girder shear of IB and those calculated from AASHTO formulae is estimated to range between 0.65% and 8.9%. Since the difference between the IB and AASHTO LLDFs for girder shear is small, using the AASHTO formulae will produce reasonable estimates of live load shear in the girders of IBs regardless of the girder size. However, AASHTO LLDFs for girder shear seem to be overly conservative for SSBs.

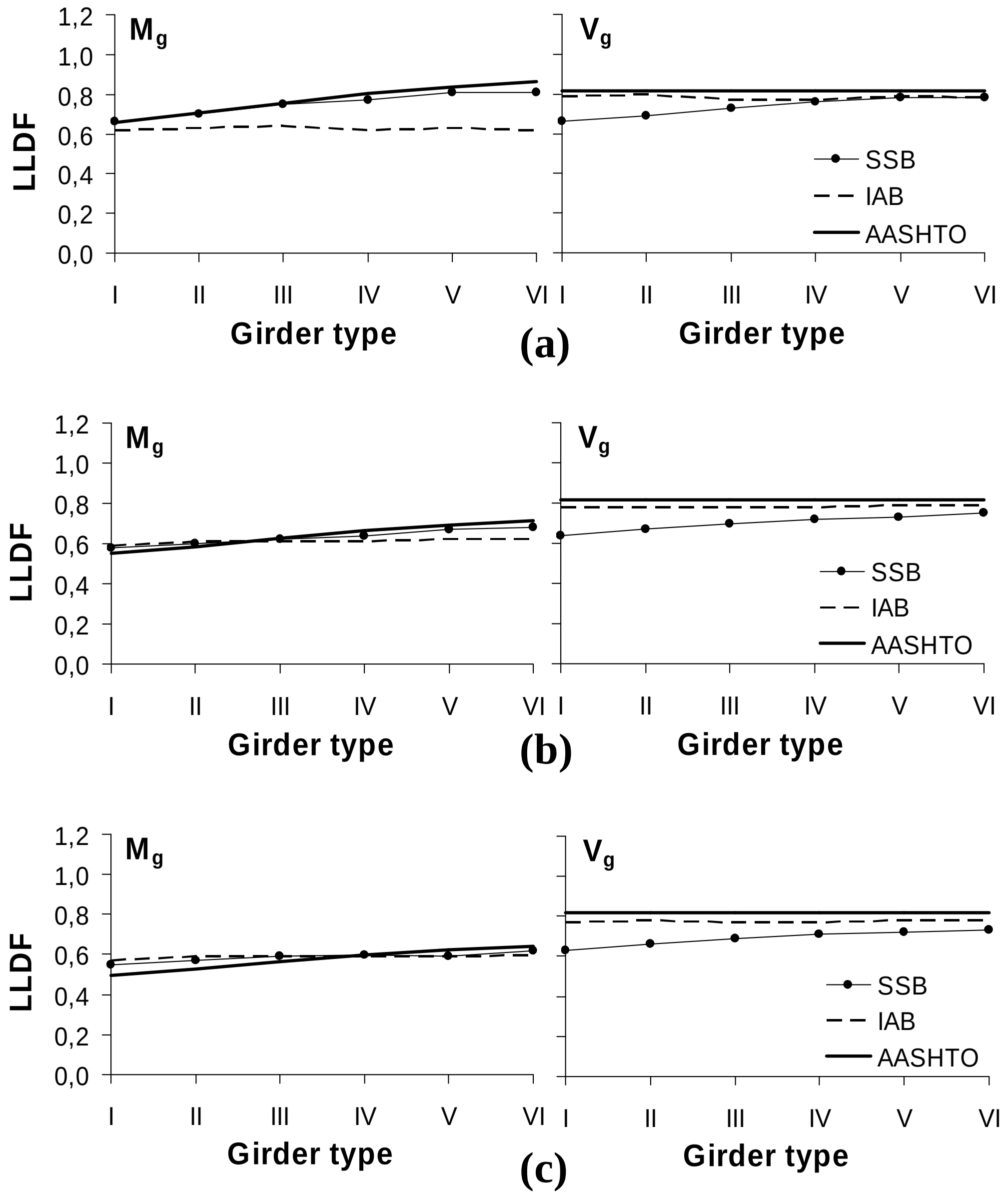

Figure 5.7 Distribution factor vs. girder type for (a) 15 m span length, (b) 30 m span length, (c) 45 m span length, (For all the graphs; girder spacing = 2.4 m and slab thickness = 0.2 m).

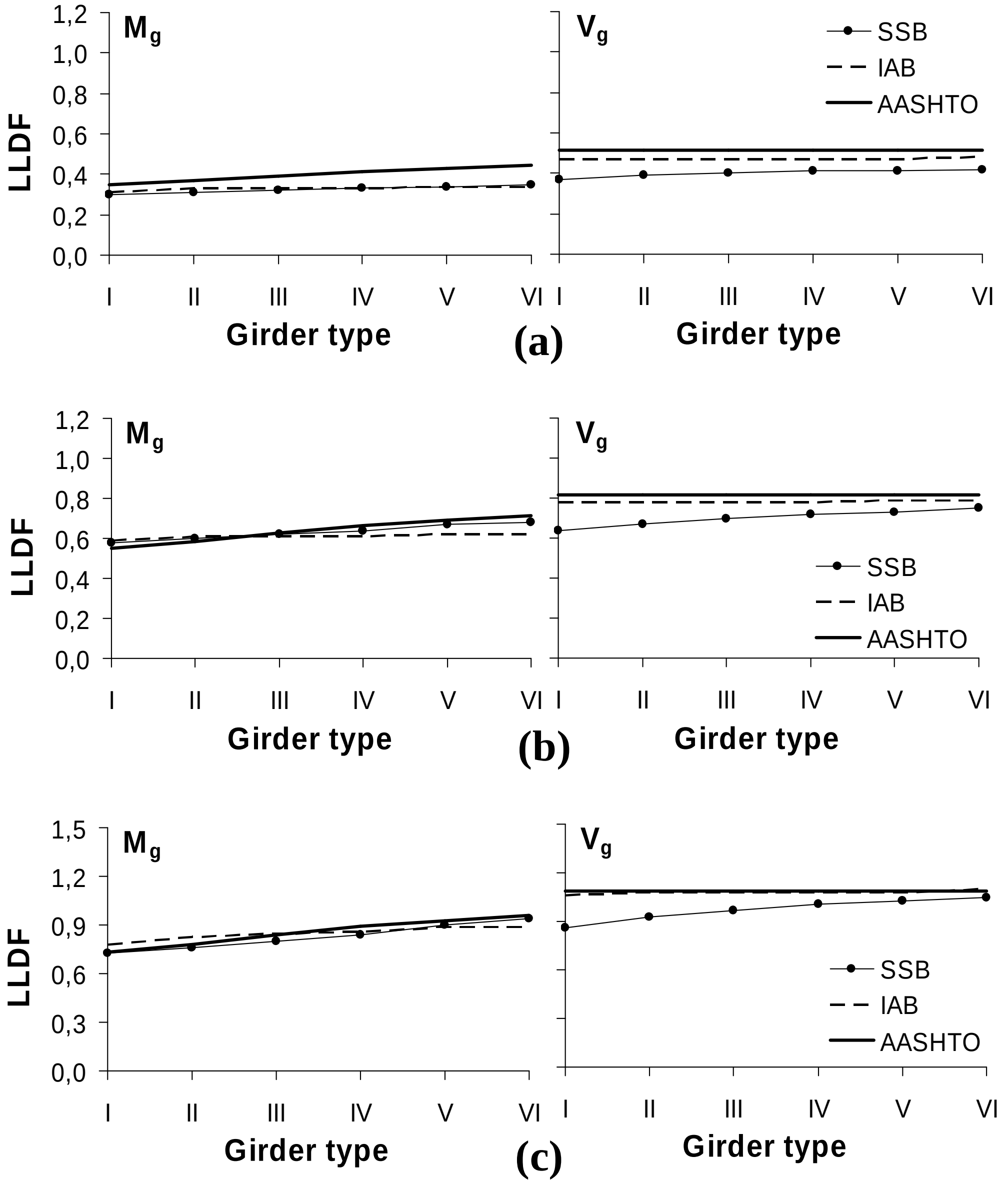

Figure 5.8 Distribution factor vs. girder type for (a) 1.2 m girder spacing, (b) 2.4 m girder spacing, (c) 3.6 m girder spacing, (For all the graphs; span length = 30 m and slab thickness = 0.2 m).

5.7. CONTINUITY EFFECT VERSUS SLAB THICKNESS

The effects of the superstructure-abutment continuity on the distribution of girder live load moment and shear are illustrated in Figs. 5.9 and 5.10 as a function of the slab thickness (0.15, 0.20, 0.25, 0.30 m.) for various span lengths (15, 30, 45 m) and girder spacings (1.2 m, 2.4 m, 3.6 m) respectively. The data presented in the figures are obtained for bridges with two lanes, girder type IV, deck widths of 9.6 m for 1.2 (7 girders) and 2.4 m (4 girders) girder spacing and 13.2 m for 3.6 m (4 girders) girder spacing and overhang width of 1.2 m. In the figures, LLDFs obtained for IBs, SSBs and those calculated from the AASHTO formulae for slab-on-girder bridges are compared.

It is observed from the figures that the superstructure-abutment continuity affects the distribution of live load moment among the girders regardless of the slab thickness. However, the variation of the LLDF as a function of the slab thickness is modest (compared to the variation of the LLDF as a function of other parameters considered so far), for both IB and SSB. Furthermore, the continuity effect becomes more noticeable only in the case of short span bridges and smaller slab thicknesses. For instance, for 30 m long IB and SSB with 0.2 m thick slab and AASHTO Type IV girders spaced at 2.4 m, the LLDFs for the interior girder moment are calculated as 0.612 and 0.643 respectively. The LLDF calculated from the AASHTO formulae is 0.666. The difference between the LLDFs of the IB and SSB as well as that calculated using AASHTO formulae are 5% and 8.8% respectively. However, for the same IB and SSB, but with a 0.3 m thick slab, the LLDFs for the interior girder moment are calculated as 0.585 and 0.609 respectively. The LLDF calculated from the AASHTO formulae is 0.603. The difference between the

LLDFs of the IB and the SSB as well as that calculated using AASHTO formulae are 3.9% and 3.0% respectively. This indicates that the effect of superstructure-abutment continuity decreases for bridges with thicker slab. Figs. 5.9 and 5.10 also reveal that for IBs, the variation of the LLDFs for the girder moment is less sensitive to the slab thickness due to the effect of continuity.

It is also found that the effect of superstructure-abutment continuity on the LLDFs for girder shear is more noticeable than that for girder moment for bridges with longer spans However, the shear LLDFs for IB girders are found to be in close agreement with those calculated using the AASHTO formulae regardless of the slab thickness. Furthermore, the variation of the LLDF for girder shear as a function of the slab thickness is modest for SSBs and nearly negligible for IBs.

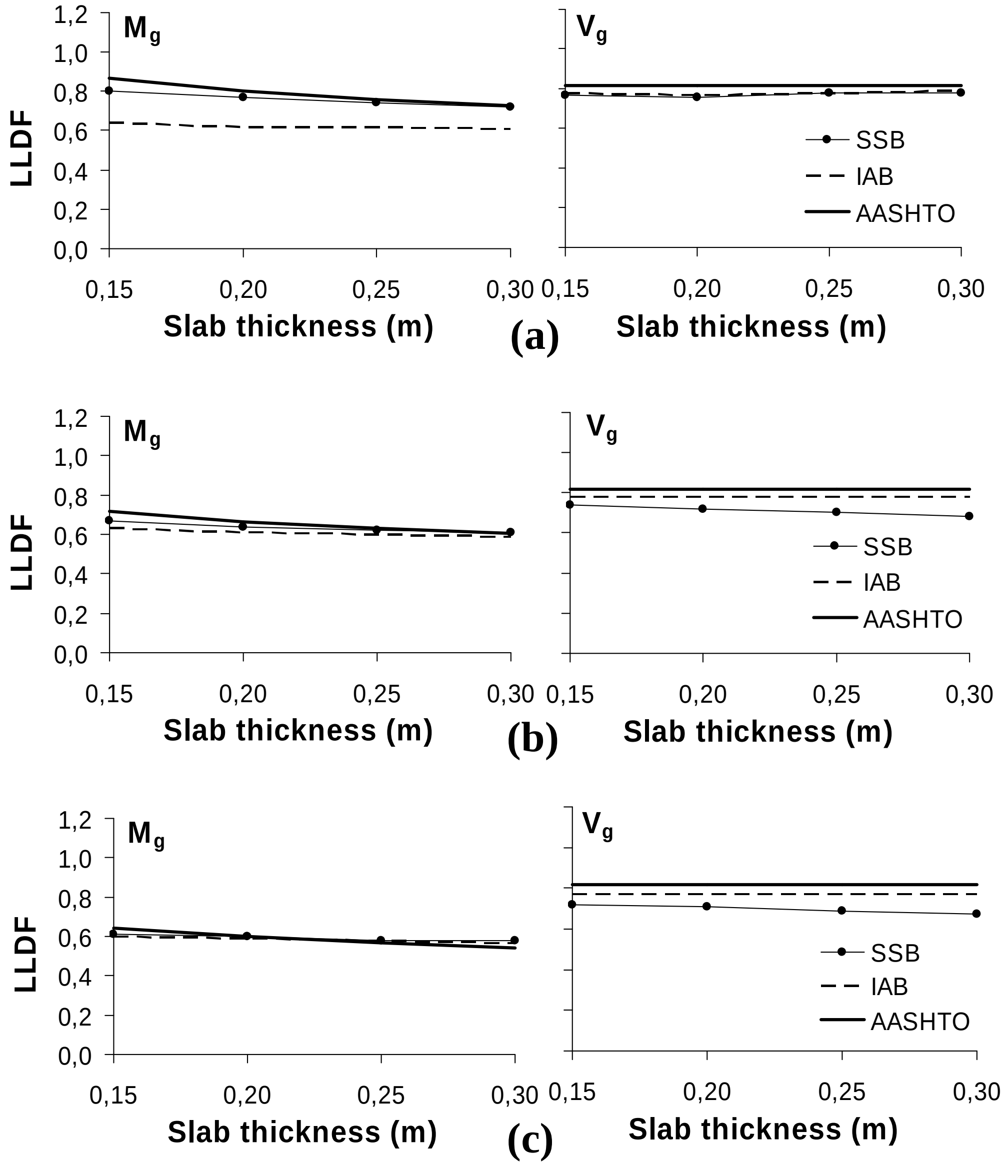

Figure 5.9 Distribution factor vs. slab thickness for (a) 15 m span length, (b) 30 m span length, (c) 45 m span length, (For all the graphs; girder spacing = 2.4 m and girder type = IV).

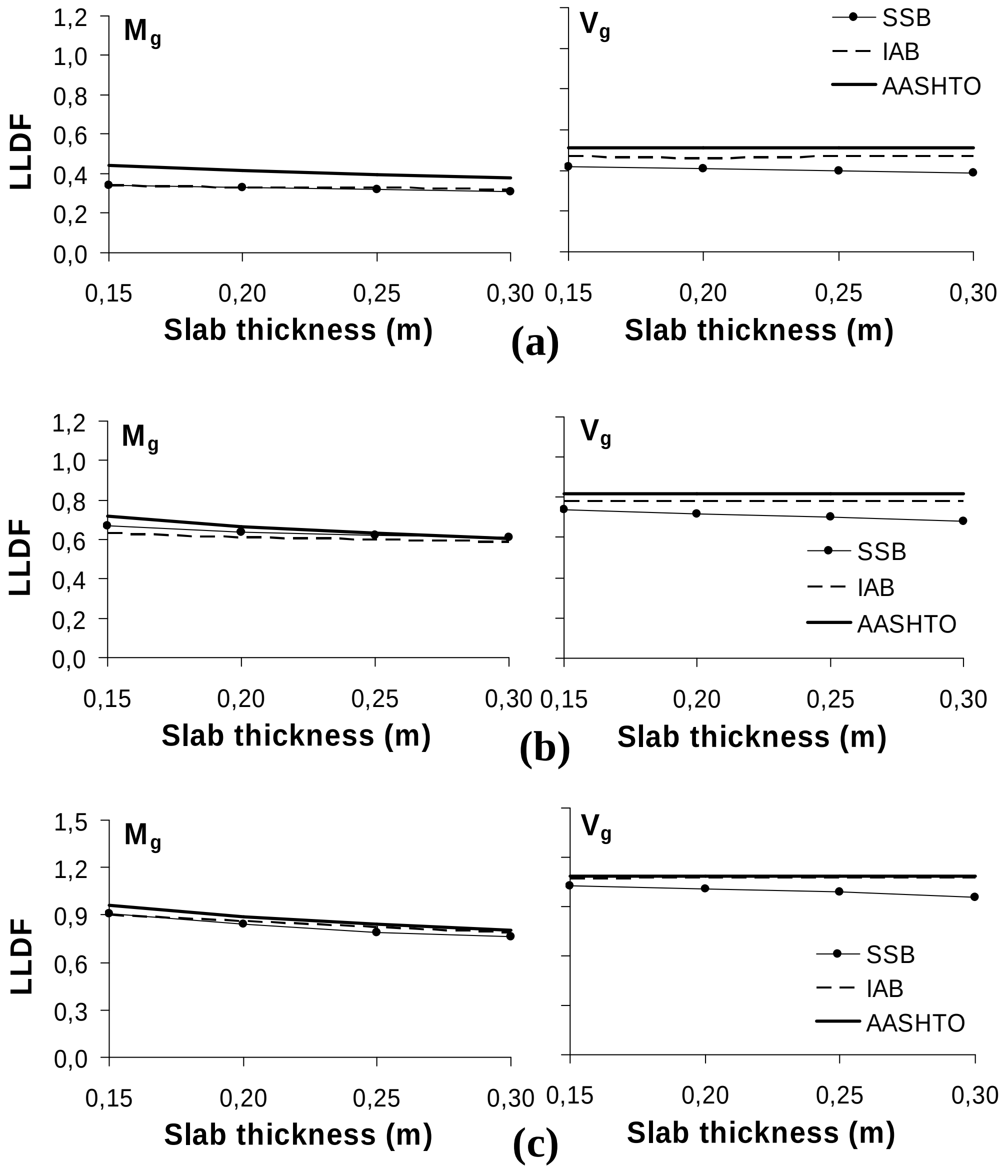

Figure 5.10 Distribution factor vs. slab thickness for (a) 1.2 m girder spacing, (b) 2.4 m girder spacing, (c) 3.6 m girder spacing, (For all the graphs; span length = 30 m and girder type = IV).

5.8. CONTINUITY EFFECT VERSUS NUMBER OF DESIGN LANES

The effects of the superstructure-abutment continuity on the distribution of girder live load moment and shear are illustrated in Figs. 5.11 and 5.12 as a function of the number of design lanes (1, 2, 3 and 4 design lanes) for various span lengths (15, 30, 40 m) and girder types (II, IV and VI) respectively. The data presented in the figures are obtained for bridges with slab thickness of 0.2 m, girder spacing of 2.4 m, overhang width of 0.6 m and deck widths of 6, 8.4, 10.8 and 13.2 m. respectively for 1, 2, 3 and 4 design lanes. In the figures, LLDFs obtained for IBs, SSBs and those calculated from the AASHTO formulae for slab-on-girder bridges are compared.

It is observed from the figures that the superstructure-abutment continuity affects the distribution of live load moment among the girders regardless of the number of design lanes. However, the continuity effect generally becomes slightly more noticeable in the case of short span bridges and larger number of design lanes. (only in Fig. 5.11(b)) The difference between the LLDFs for girder moment of single-lane and multiple-lane IBs is less than that of SSBs due to the continuity effect.

Figs 5.11 and 5.12 reveal that the superstructure-abutment continuity affects the distribution of live load shear among the girders regardless of the number of design lanes. Although, the continuity effect for the girder shear generally becomes more noticeable for smaller girder sizes, the trend of the shear LLDF plots in the figures for IB, SSB and AASHTO are similar. Nevertheless, the shear LLDFs for IB girders are found to be in close agreement with those calculated using the AASHTO formulae regardless of the number of design lanes.

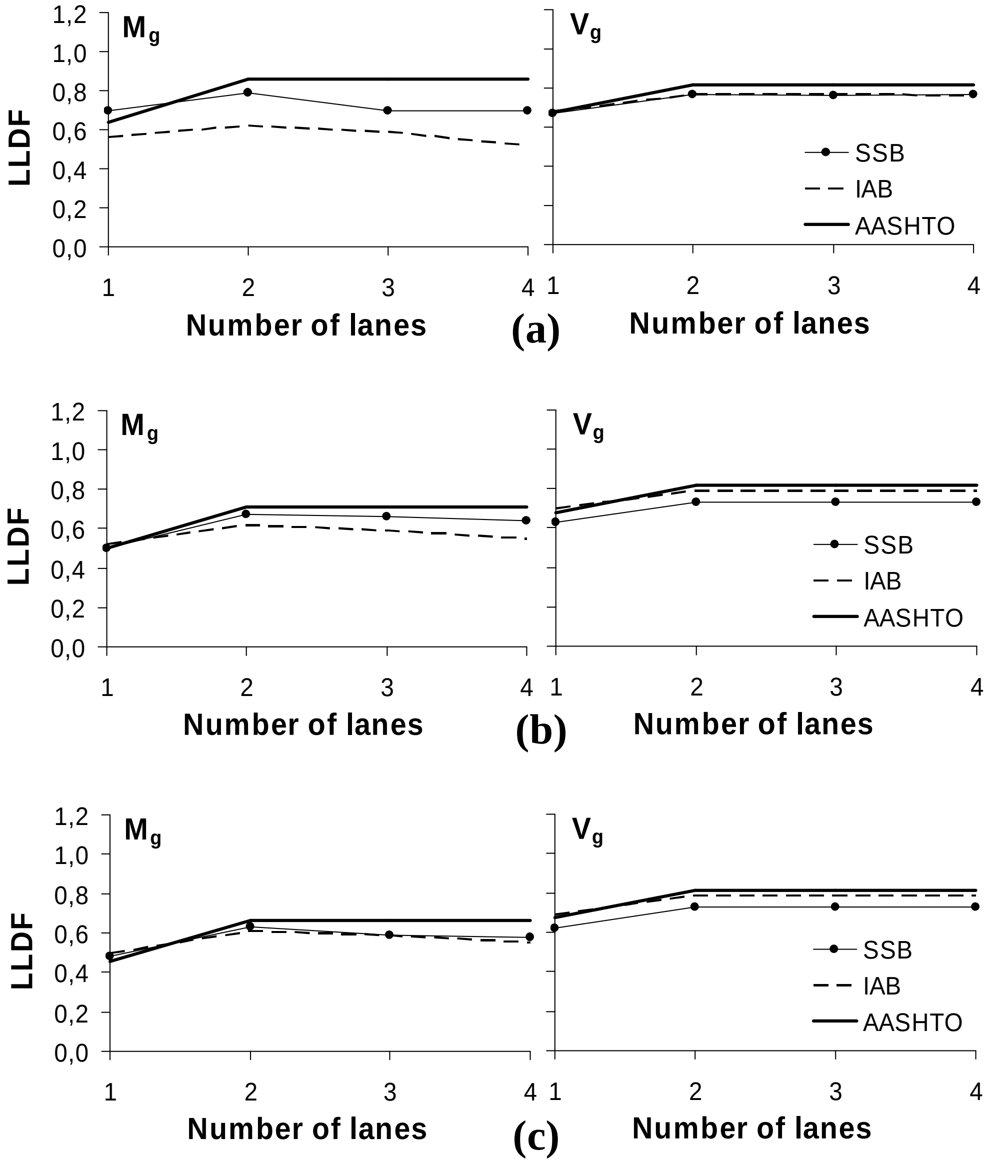

Figure 5.11 Distribution factor vs. number of lanes for (a) 15 m span length, (b) 30 m span length, (c) 40 m span length, (For all the graphs; girder spacing = 2.4 m, girder type = IV and slab thickness = 0.2 m).

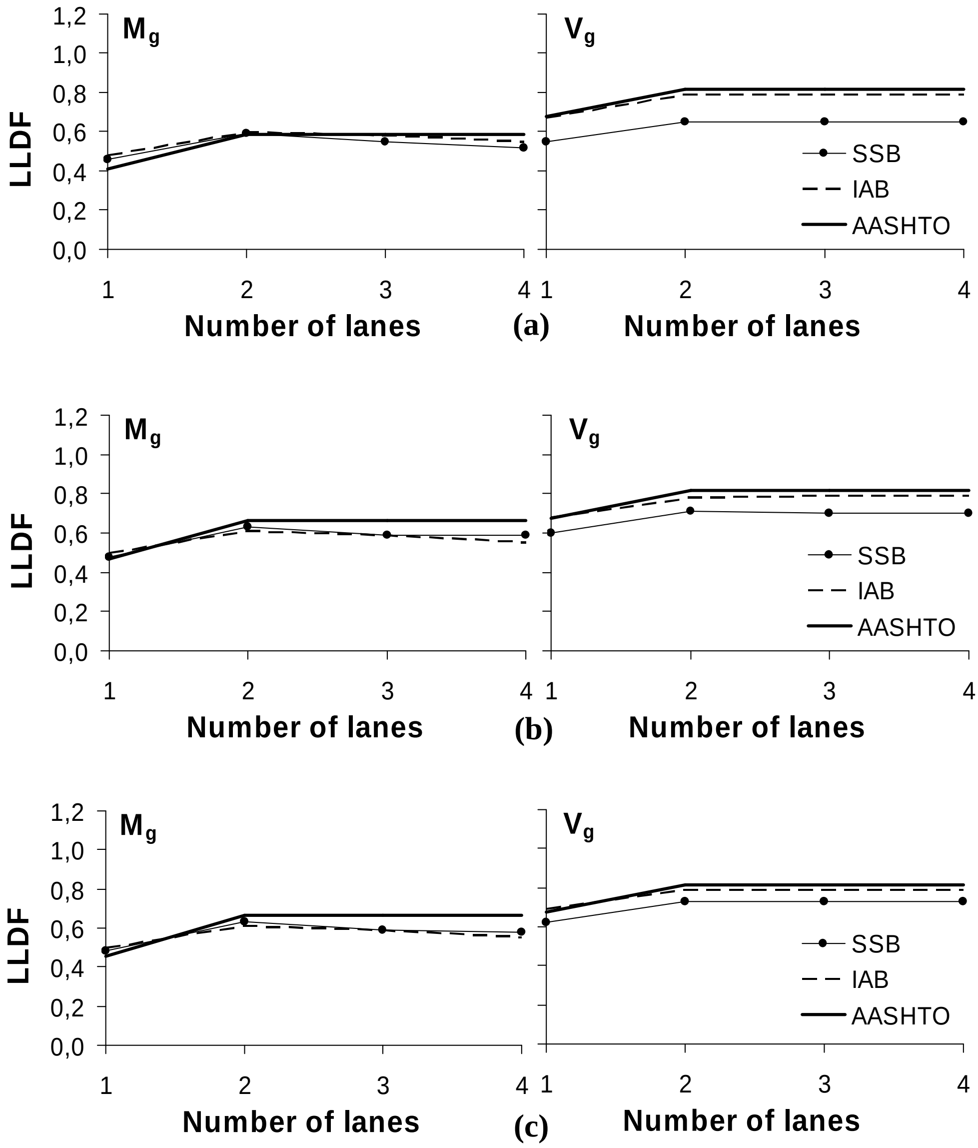

Figure 5.12 Distribution factor vs. number of lanes for (a) Girder Type II, (b) Girder Type IV, (c) Girder Type VI (For all the graphs; girder spacing = 2.4 m, span length = 30 m and slab thickness = 0.2 m)

5.9. SUMMARY

In this chapter, a parametric study is conducted to investigate the effects of superstructure-abutment continuity on the distribution of live load shear and moment among the girders of IBs. The LLDFs obtained for IBs are also compared with those calculated using AASHTO formulae to assess the applicability of AASHTO procedure to the design of IB girders. Followings are the conclusions deduced from this study.

1. The superstructure-abutment continuity in IBs improves the distribution of live load moment among the girders. The better distribution of live load moment in IBs may be mainly due to the torsional rotational rigidity provided by the monolithic abutments to the girders and the slab. Furthermore, the overhanging portion of the slab, which is free over the supports in SSBs, is fixed to the abutments (cast monolithically) in the case of IBs. This may also enhance the distribution of live load moment among the girders of IBs.

2. The lack of superstructure-abutment continuity in SSBs improves the distribution of live load shear among the girders.

3. The effect of the superstructure-abutment continuity in IBs in relation to SSBs on the LLDFs for the girder moment is observed to be significant for bridges with shorter spans (10-20 m) or larger girder sizes, It is observed that the difference between the LLDFs for the girder moment due to continuity effect in IBs may be as much as 54.4% compared to SSBs.

4. However, the effect of the superstructure-abutment continuity on the LLDFs for the girder shear is observed to become more noticeable for smaller girder sizes. The difference between the LLDFs for the girder shear due to continuity effect in IBs in relation to SSBs. may be as much as 22%.

5. It is also observed that the variation of the LLDFs for the girder moment is less sensitive to the span length, girder size and spacing, slab thickness and number of design lanes in IBs. This is the main reason for the differences between the LLDFs of IB and SSBs as in the case of SSBs, LLDFs for the girder moment vary greatly as a function of the above mentioned parameters.

6. LLDFs for the girder moment and shear are also calculated using the AASHTO formulae developed for regular jointed bridges. Comparison of the AASHTO LLDFs for the girder moment with those obtained for IBs revealed that, for short span IBs (10-20m), AASHTO formulae will produce very conservative estimates of live load moment in the girders. The difference between the LLDFs for girder moment of IBs and those calculated using the AASHTO formulae range between 0.3%. and 63%. These differences become smaller when realistic combinations of girder size and span length are considered. Since the AASHTO LLDF formulae for moment are developed for SSBs, they are not suitable for IB girder design. Thus, live load distribution formulae for IBs are needed for reasonable estimation of live load moments in IB girders especially for short span bridges. However, for IBs, the LLDFs for interior girder shear are in close agreement with those calculated from AASHTO formulae for the range of superstructure properties considered. Thus, AASHTO LLDFs for the interior girder shear may be used for the design of IB girders.

Furthermore, AASHTO LLDFs for girder shear seem to be overly conservative for SSBs and need to be reevaluated.

CHAPTER 6

INVESTIGATION OF THE APPLICABILITY OF AASHTO LRFD LIVE LOAD DISTRIBUTION EQUATIONS FOR INTEGRAL BRIDGE SUBSTRUCTURES

In the design of IBs, design engineers generally calculate the live load effects in the abutments and piles of IBs by using the LLDEs developed for the interior girders of jointed bridges. This approach is based on the assumption that the same rotations about a transverse axis perpendicular to the longitudinal direction of the bridge occur both in the abutments and the girders under live load due to the monolithic construction of the superstructure-abutment joint in IBs. However, it is anticipated that the concentrated rigidity of a particular girder combined with those of the adjacent girders connected to the abutment having a smeared rigidity, may produce a live load distribution within the abutment and piles different than that calculated using the LLDEs developed for the girders of jointed bridges. Therefore, using AASHTO LRFD LLDEs may results in either conservative or unconservative estimates of the live load effects in the piles and abutments of IBs . Consequently, in this part of the thesis study, a research study on the suitability of the current AASHTO LRFD LLDEs for the abutment and piles is conducted to address the above-mentioned uncertainties. For this purpose, 2-D and 3-D finite element models (FEMs) of numerous IBs are built and analyzed under AASHTO LRFD live load. In the analyses, the effect of various superstructure properties such as span length, girder size and spacing as well as slab thickness (i.e. the parameters, which the AASHTO LRFD LLDEs are based on) are considered to broadly investigate the applicability of the AASHTO LRFD's girder LLDEs to the abutments and piles of IBs. The results from the analyses of 2-D and 3-D FEMs are then used to calculate the live load distribution factors (LLDFs) for the piles and abutments of IBs as a function of the above mentioned parameters. LLDFs for the girders are also calculated using the AASHTO LRFD LLDEs developed for conventional bridges. The LLDFs for the IB abutments and piles obtained from the analyses are then compared with those calculated using AASHTO LRFD LLDEs to assess the suitability of AASHTO LRFD LLDFs for the design of abutments and piles of IBs.

6.1 INTEGRAL BRIDGE PARAMETERS CONSIDERED IN THE ANALYSES

A parametric study is conducted to cover a broad range of bridge properties found in practice. The superstructure properties considered in the analyses include the span length (*L*), girder type (*GT*) (or size), girder spacing (*S*) and slab thickness (t_s). The range of values considered for each parameter is given in Table 6.1. Four sets of analyses are considered as shown in the first column of Table 6.1. In each analysis set one of the parameters is considered to be dominant. For instance, the first row of the table, where the span length is taken as the dominant parameter, indicates that girder types II, IV and VI, a slab thickness of 0.2 m, and girder spacings of 1.2, 2.4 and 3.6 m. are considered with span lengths of 10, 15, 20, 25, 30, 35, 40 and 45 m, while in the second row where the girder type is taken as the dominant parameter, the span lengths of 15, 30 and 45 m, a slab thickness of 0.2 m and girder spacing of 1.2, 2.4 and 3.6 m are considered with girder types I, II, III, IV, V and VI. This leads to nearly 200 different 3-D and corresponding 2-D structural models of IBs. In these models, the abutments of the IBs are assumed to be 3 m. tall and supported by 12 m. long end-bearing steel HP250x85 piles typically used in IB construction. The number of piles is set equal to the number of girders (i.e. one pile is assumed underneath each girder). The granular backfill behind the abutments is assumed to have a unit weight of 20 kN/m^3 (sensitivity analyses are conducted using 18 and 22 kN/m^3 unit weight as well). The foundation soil surrounding the piles is assumed to be medium and medium-stiff clay with an undrained shear strength of C_u=40 and 80 kPa (80 kPa is used only in sensitivity analyses).

Table 6.1. Superstructure parameters considered in the analyses.

PARAMETER	Span Length (m)	Girder Type	Slab Thickness (m)	Girder Spacing (m)
Span Length (m)	**10, 15, 20, 25, 30, 35, 40, 45**	II, IV, VI	0.20	1.2, 2.4, 3.6
Girder Type	15, 30, 45	**I, II, III, IV, V, VI**	0.20	1.2, 2.4, 3.6
Slab Thickness (m)	**15, 30, 45**	IV	**0.15, 0.20, 0.25, 0.30**	1.2, 2.4, 3.6
Girder Spacing (m)	15, 30, 40	**II, IV, VI**	0.20	1.2, 2.4, 3.6, 4.8

6.2 BEHAVIOUR OF ABUTMENTS AND PILES OF IBs UNDER LIVE LOAD EFFECTS

In this section, the distribution of live load effects within the abutment and piles of IBs is studied in detail. For this purpose, a short and a long IB, with span lengths of 15 m and 45 m, are considered to cover a broad range of deck stiffness properties found in practice. Both bridges have seven AASHTO LRFD Type IV girders spaced at 2.4 m. Although AASHTO LRFD Type IV girders may not be suitable for both the 15 m and 45 m long IBs, this average girder size is deliberately considered to assess the distribution of live load effects for very short, stiff and very long, flexible IB superstructures. The slab is assumed to be 0.2 m thick. For both bridges, their 3 m tall and 1 m thick abutments are supported by seven HP250x85 piles. Both bridges are then subjected to AASHTO LRFD truck loading. The analysis results are depicted in Figs. 6.1 and 6.2. Figs. 6.1 (a) and (b) display the LLDF for abutment and pile moments *(M)* and shears *(V)* across the width of the 15 m and 45 m long IBs respectively. In the horizontal axis, the girder numbers (note that the piles are also aligned with the girder locations and hence the girder number refers to the position of each pile as well) are used to determine the position across the width of the bridge. Such an illustration will enable the reader to assess the concentrated effects transferred from specific girders to the abutment. For both bridges, the influence line analyses revealed a truck position in the vicinity of the mid-span to produce the maximum moment and shear within the abutment and piles. Consequently, in the case of the longer span IB, the larger distance of the truck axles to the abutment produces a flared, more uniform distribution of live load moment across to width of the abutment. The live load flexural stress distribution within the abutment shown in Fig. 6.2 (a) also confirms this statement. However, in the case of the shorter span IB, because of the shorter distance of the truck axles to the abutment, the distribution of the live load effects are relatively more concentrated. This obviously results in larger LLDFs for the abutments of shorter IBs as observed from the live load flexural stress distribution within the abutment shown in Fig. 6.2 (b). For instance, for the 15 m long IB, the LLDF for the abutment moment (M_a) obtained from FEAs is 0. 95. However, for the longer, 45 m span IB, the LLDF for the abutment moment is obtained as 0.61. Also, note that as observed from Figs.

6.2 (a) and (b) the flexural live load distribution (stresses) become more uniform away from the girder tips, closer to the bottom of the abutment. This leads to a more uniform distribution of the live load effects among the piles as observed from Figs. 6.1 (a) and (b). In the case of the abutment shear, the live load distribution is also more uniform than that of the moment. This is because, the shear effects within the abutment are largely produced by the horizontal resistance of the piles supporting the abutment which also have a more uniform distribution of live load effects regardless of the span length. The finding about a more uniform live load shear distribution regardless of the span length is also in agreement with AASHTO LRFD shear LLDE for girders, which is independent of the span length, *L*.

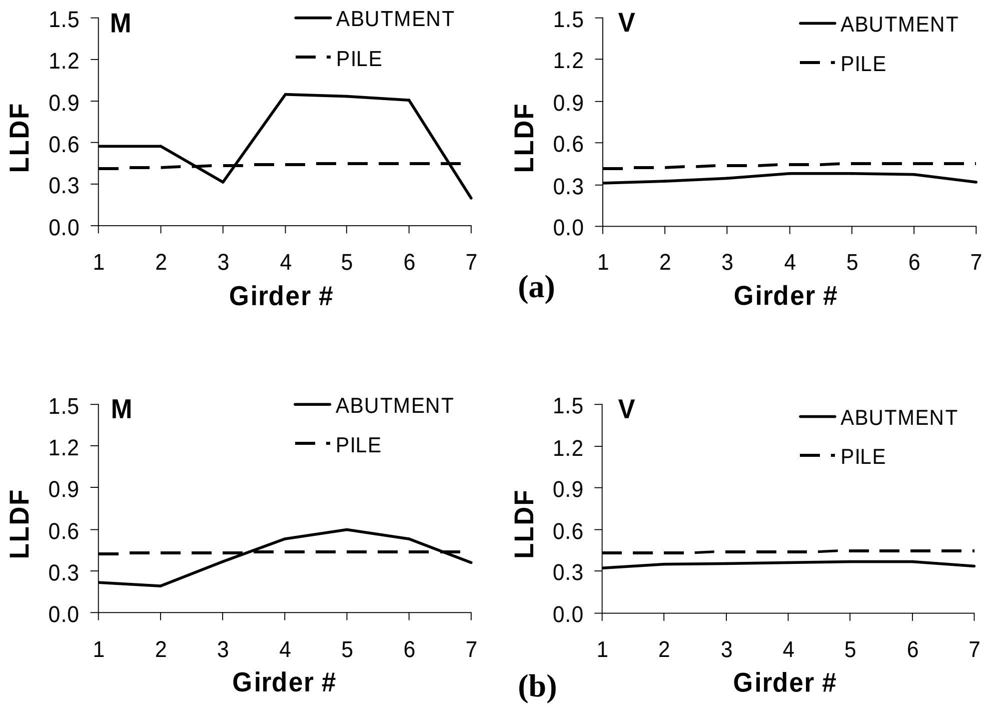

Figure 6.1 Distribution of live load effects among the piles and abutment for the IBs with span lengths of (a) 15 m (b) 45 m

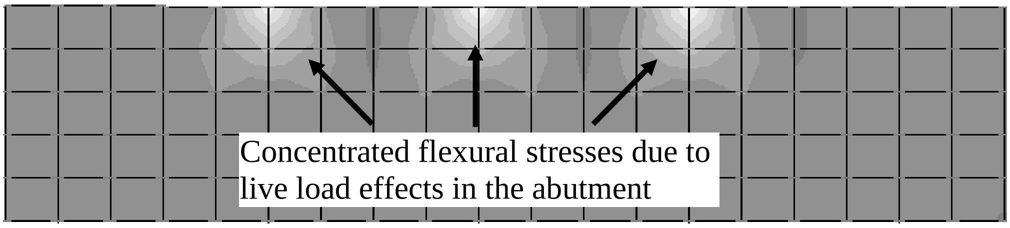

(a)

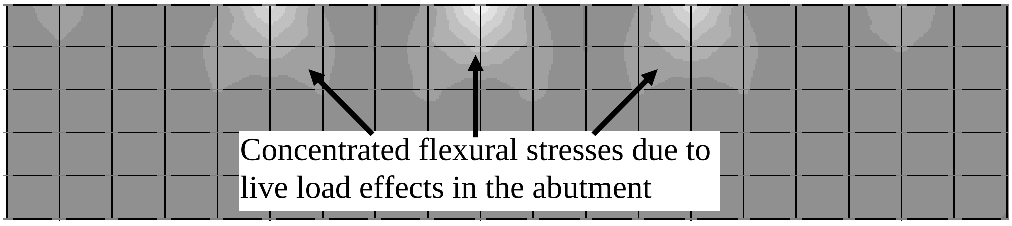

(b)

Figure 6.2 Flexural stresses distribution due to live load effects in the abutment **(a)** flexible superstructure- abutment case **(b)** rigid superstructure-abutment case

6.3. APPLICABILITY OF AASHTO LRFD LLDEs VERSUS SPAN LENGTH

In this section, the effect of the span length on the distribution of live load moment and shear within the IB abutment and piles is studied. In addition, the suitability of the AASHTO LRFD girder LLDFs to the abutments and piles of IBs is investigated. For this purpose, IBs with 10, 15, 20, 25, 30, 35, 40 and 45 m spans are considered. The FEAs of these bridges are conducted to calculate the LLDFs for the abutments and piles. The analyses are repeated for IBs with various girder spacings (1.2 m, 2.4 m, 3.6 m) and girder types (II, IV, VI) to extend the range of applicability of the findings for various bridge properties. This resulted in 72 FEMs and more than 1400 analyses cases for various transverse truck positions and number of transversely placed trucks. Some of these analyses results are illustrated in Figs. 6.3 (a) and (b). The figures display the LLDF for abutment moment *(M_a)* and shear *(V_a)* as well as for pile moment *(M_p)* and shear *(V_p)* as a function of span length. In the figures, LLDFs obtained for the abutments and piles of IBs, and those calculated from the AASHTO LRFD LLDEs are compared.

The analyses results presented in Figs. 6.3 (a) and (b) reveal that AASHTO LRFD girder LLDEs may generally lead to unconservative estimates of live load moments particularly in the abutments of short span IBs. For instance, for an IB with 10 m span length, 0.2 m thick slab and AASHTO LRFD Type IV girders spaced at 2.4 m, the LLDF for the abutment moment (M_a) obtained from FEAs is 1.230. The LLDF calculated from the AASHTO LRFD LLDE is 0.897. The difference between the LLDFs obtained from the FEA of the IB and that calculated using the associated AASHTO LRFD LLDE is 37%. This clearly demonstrates that using AASHTO LRFD LLDEs for short span IBs will produce unconservative estimates of flexural live load effects in the abutments for the range of superstructure and substructure parameters considered .However, for the same IB, but with 45 m span length, the LLDFs for the abutment moment (M_a) obtained from FEAs is 0.610. The LLDF calculated from the AASHTO LRFD LLDE is 0.598. The difference between the LLDFs obtained from the FEA of the IB and that calculated using AASHTO LRFD LLDE are 2%. This indicates that AASHTO LRFD LLDEs are more suited for longer span IBs for the calculation of flexural live load effects in the abutments.

The analyses results also reveal that using AASHTO LRFD LLDEs may lead to quite conservative estimates of live load shear (V_a) in the abutments as well as moments (M_p) and shears (V_p) in the piles of IBs for the range of superstructure and substructure parameters considered. For instance, for the 15 m. long IB, the LLDFs for the abutment shear (V_a), pile moment (M_p) and pile shear (V_p) obtained from FEAs are 0.47, 0.49 and 0.50 respectively. The LLDF calculated from the AASHTO LRFD girder LLDEs are 0.816, 0.897 and 0.816 respectively. The difference between the LLDFs obtained from the FEA of the IB and those calculated using AASHTO LRFD LLDEs are 74%, 91% and 61% for the abutment shear as well as pile moment and shear respectively. Similar results are also observed for IBs with other span lengths. This obviously indicates that using AASHTO LRFD LLDEs for IBs may lead to exceedingly conservative estimates of live load shear in the abutments as well as live load moment and shear in the piles.

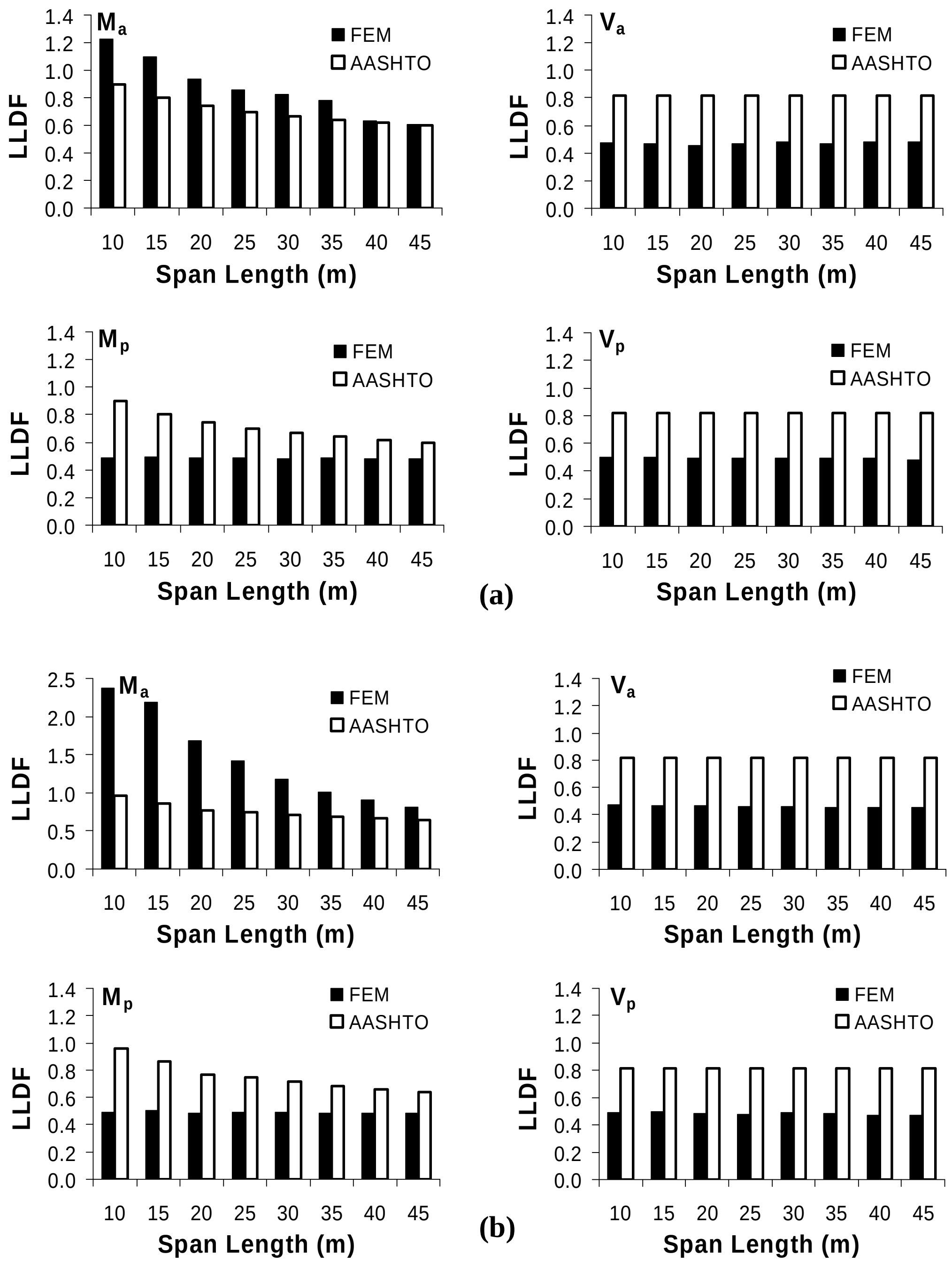

Figure 6.3 LLDFs vs. span length for (a) Girder spacing of 2.4 m, girder type IV and slab thickness of 0.2 m. (b) Girder spacing of 2.4 m, girder type VI and slab thickness of 0.2 m.

6.4 APPLICABILITY OF AASHTO LRFD LLDEs VERSUS GIRDER SPACING

In this section, the effect of the girder spacing on the distribution of live load moment and shear within the IB abutment and piles is studied. In addition, the suitability of the AASHTO LRFD girder LLDFs to the abutments and piles of IBs is investigated for various girder spacings. For this purpose, IBs with 1.2, 2.4, 3.6 and 4,8 m girder spacings are considered. The FEA of these bridges are conducted to calculate the LLDFs for the abutments and piles. The analyses are repeated for IBs with various span length (15, 30, 45 m) and girder types (II, IV, VI) to extend the range of applicability of the findings for various bridge properties. This resulted in 36 FEMs and more than 700 analyses cases for various transverse truck positions and number of transversely placed trucks. Some of these analyses results are illustrated in Figs. 6.4 (a) and (b). The figures display the LLDF for abutment moment (M_a) and shear (V_a) as well as for pile moment (M_p) and shear (V_p) as a function of girder spacing. In the figures, LLDFs obtained for the abutments and piles of IBs, and those calculated from the AASHTO LRFD LLDEs are compared.

It is observed from the figures that AASHTO LRFD girder LLDEs may generally lead to unconservative estimates of live load moments particularly in the abutments of IBs having wider girder spacing. For instance, for 30 m long IB with 0.2 m thick slab and AASHTO LRFD Type IV girders spaced at 4.8 m, the LLDF for the abutment moment (M_a) obtained from FEAs is 1.46. The LLDF calculated from the AASHTO LRFD LLDE is 1.1. The difference between the LLDFs obtained from the FEA of the IB and that calculated using AASHTO LRFD LLDE is 33%. This clearly demonstrates that using AASHTO LRFD LLDEs for IBs having wider girder spacing will produce unconservative estimates of flexural live load effects in the abutments for the range of superstructure and substructure parameters considered. However, for the same IB, but with 1.2 m girder spacing, the LLDF for the abutment moment (M_a) obtained from FEAs is 0.67. The LLDF calculated from the AASHTO LRFD LLDE is 0.70. The difference between the LLDFs obtained from the FEA of the IB and that calculated using AASHTO LRFD LLDE is 4%. This indicates that AASHTO LRFD LLDEs are more suitable for IBs with shorter girder spacing for the calculation of live load effects in the abutments.

It is also observed from the Figs. 6.4 (a) and (b) that AASHTO LRFD LLDEs may lead to fairly conservative estimates of live load shear (V_a) in the abutments as well as moments (M_p) and shears (V_p) in the piles of IBs for the range of superstructure and substructure parameters considered. For instance, for a 30 m long IB with 2.4 m girder spacing, the LLDFs for the abutment shear (V_a), pile moment (M_p) and pile shear (V_p) obtained from FEAs are 0.37, 0.44 and 0.44 respectively. The LLDF calculated from the AASHTO LRFD LLDEs are 0.816, 0.670 and 0.816 respectively. The difference between the LLDFs obtained from the FEA of the IB and those calculated using AASHTO LRFD LLDEs are 105%, 52% and 85%. Similar results are also observed for IBs with other girder spacings. This obviously indicates that using AASHTO LRFD LLDEs for IBs may result in extremely conservative estimates of live load shear in the abutments as well as live load moment and shear in the piles.

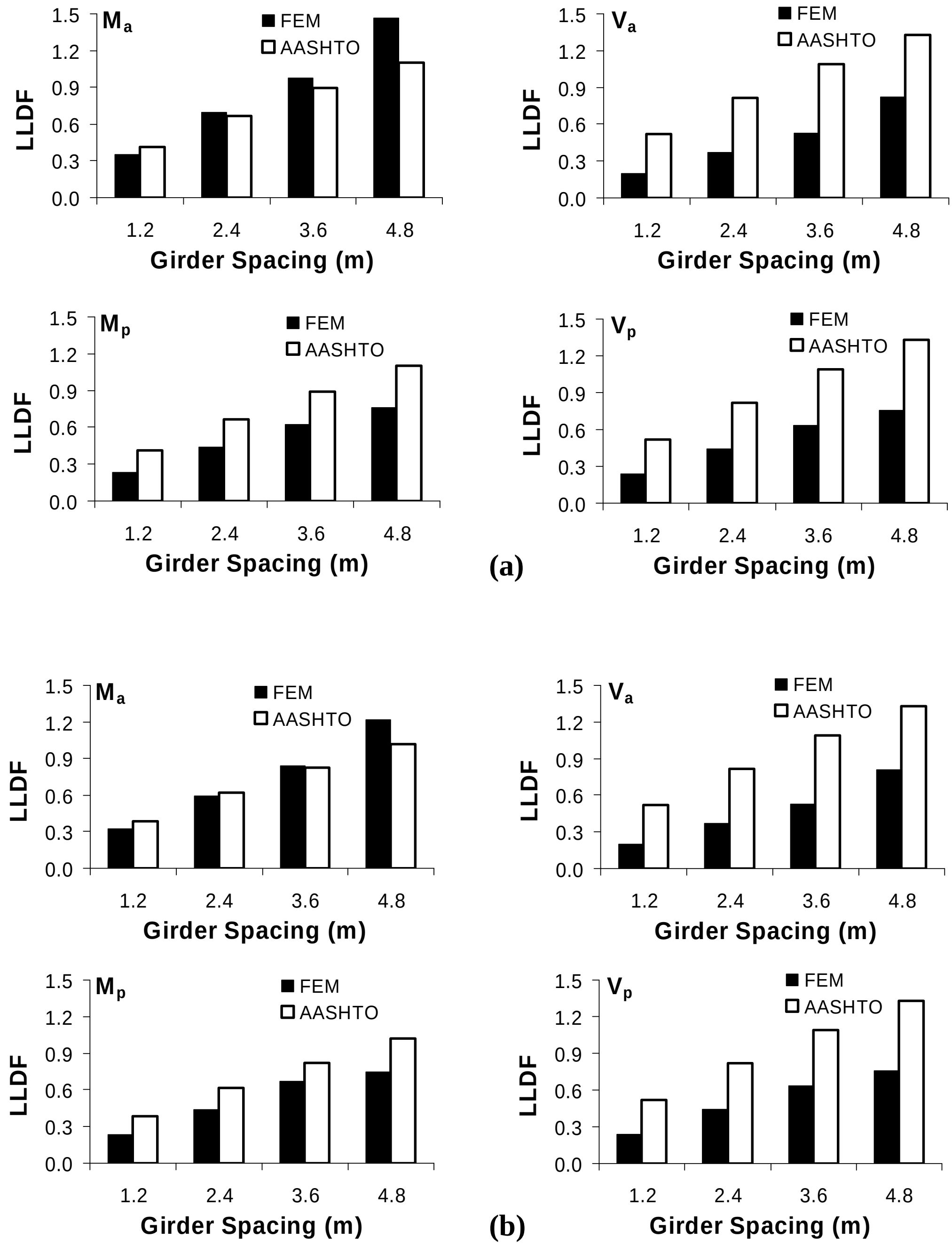

Figure 6.4 LLDFs vs. girder spacing for **(a)** Span length of 30 m, girder type IV and Slab thickness of 0.2 m. **(b)** Span length of 40 m, girder type IV and slab thickness of 0.2 m.

6.5 APPLICABILITY OF AASHTO LRFD LLDEs VERSUS GIRDER TYPE (STIFFNESS)

In this section, the effect of the girder type (stiffness) on the distribution of live load moment and shear within the IB abutment and piles is studied. In addition, the suitability of the AASHTO LRFD girder LLDFs to the abutments and piles of IBs is investigated for various girder types. For this purpose, IBs with AASHTO LRFD Type I, II, III, IV, V and VI girders are considered. The FEA of these bridges are conducted to calculate the LLDFs for the abutments and piles. The analyses are repeated for IBs with various girder spacing (1.2, 2.4, 3.6 m) and span length (15, 30, 45 m) to extend the range of applicability of the findings for various bridge properties. This resulted in 54 FEMs and more than 1000 analyses cases for various transverse truck positions and number of transversely placed trucks. Some of these analyses results are illustrated in Figs. 6.5 (a) and (b). The figures display the LLDF for abutment moment (M_a) and shear (V_a) as well as for pile moment (M_p) and shear (V_p) as a function of girder type. In the figures, LLDFs obtained for the abutments and piles of IBs, and those calculated from the AASHTO LRFD LLDEs are compared.

It is observed from the figures that AASHTO LRFD girder LLDEs may generally lead to unconservative estimates of live load moments particularly in the abutments of IBs supported by stiffer girders. For instance, for a 30 m long IB with 0.2 m thick slab and AASHTO LRFD Type VI girder spaced at 2.4 m, the LLDF for the abutment moment (M_a) obtained from FEAs is 1.17. The LLDF calculated from the AASHTO LRFD LLDE is 0.713. The difference between the LLDFs obtained from the FEAs of the IB and that calculated using AASHTO LRFD LLDE is 64%. This clearly demonstrates that using AASHTO LRFD LLDEs for IBs supported by stiffer girders will produce unconservative estimates of flexural live load effects in the abutments for the range of superstructure and substructure parameters considered. However, for the same IB, but with AASHTO LRFD Type I girder, the LLDFs for the abutment moment (M_a) obtained from FEAs is 0.58. The LLDF calculated from the AASHTO LRFD LLDE is 0.55. The difference between the LLDFs obtained from the FEA of the IB and that calculated using AASHTO LRFD LLDE is 5.5%. This demonstrates that AASHTO LRFD LLDEs are more suitable for IBs having smaller size girders for the calculation of flexural live load effects in the abutments.

It is also found that AASHTO LRFD LLDEs may lead to fairly conservative estimates of abutment live load shear as well as pile live load moment and shear as observed from Figs. 6.5 (a) and (b).

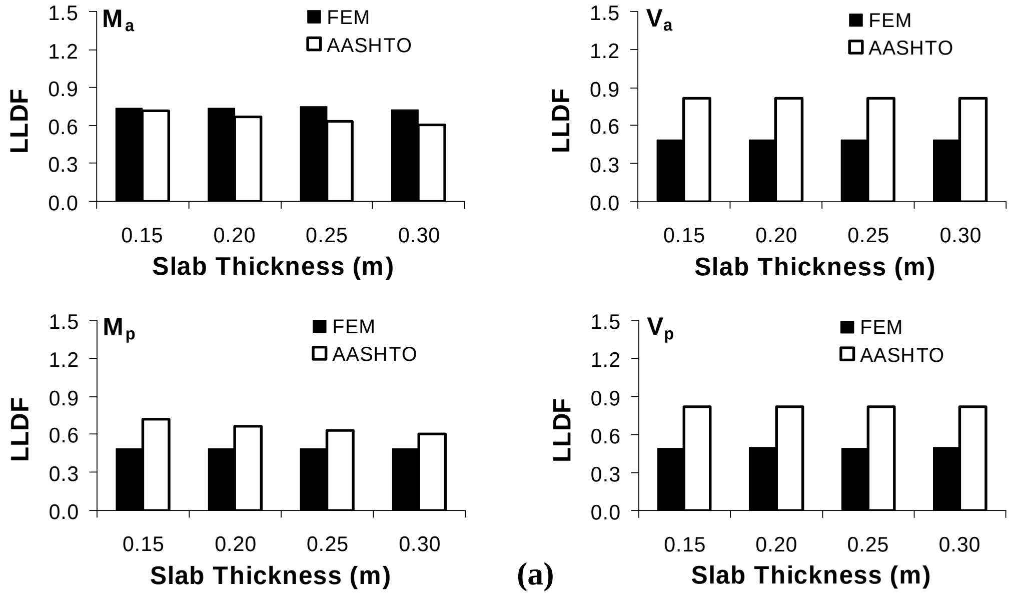

(a)

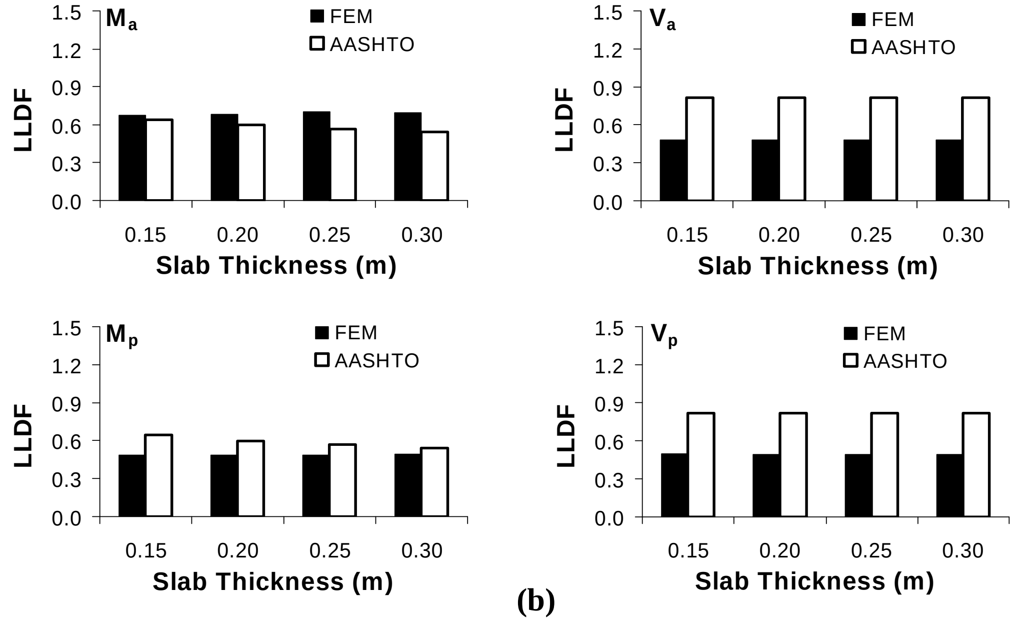

(b)

Figure 6.5 LLDFs vs. girder type for **(a)** Span length of 30 m, girder spacing of 2.4 m and slab thickness of 0.2 m. **(b)** Span length of 45 m, girder spacing of 2.4 m and slab thickness of 0.2 m.

6.6 APPLICABILITY OF AASHTO LRFD LLDEs VERSUS SLAB THICKNESS

In this section, the effect of the slab thickness on the distribution of live load moment and shear within the IB abutment and piles is studied. In addition, the suitability of the AASHTO LRFD girder LLDEs to the abutments and piles of IBs is investigated for various slab thicknesses. For this purpose, IBs with 0.15, 0.20, 0.25 and 0.30 m slab thicknesses are considered. The FEA of these bridges are conducted to calculate the LLDFs for the abutments and piles. The analyses are repeated for IBs with various girder spacing (1.2, 2.4, 3.6 m) and span length (15, 30, 45 m) to extend the range of applicability of the findings for various bridge properties. This resulted in 36 FEM and more than 700 analyses cases for various transverse truck positions and number of transversely placed trucks. Some of these analyses results are illustrated in Figs. 6.6 (a) and (b). The figures display the LLDF for abutment moment (M_a) and shear (V_a) as well as for pile moment (M_p) and shear (V_p) as a function of girder type. In the figures, LLDFs obtained for the abutments and piles of IBs, and those calculated from the AASHTO LRFD LLDEs are compared.

The analyses results reveal that AASHTO LRFD girder LLDEs may generally lead to unconservative estimates of live load moments particularly in the abutments of IBs with thicker slabs. For instance, for a 30 m long IB with 0.3 m thick slab and AASHTO LRFD Type IV girder spaced at 2.4 m, the LLDF for the abutment moment (M_a) obtained from FEAs is 0.73. The LLDF calculated from the AASHTO LRFD LLDE is 0.60. The difference between the LLDFs obtained from the FEA of the IB and that calculated using AASHTO LRFD LLDE is 22%. This clearly demonstrates that using AASHTO LRFD LLDEs for IBs having larger slab thickness will produce unconservative estimates of flexural live load effects in the abutments for the range of superstructure and substructure parameters considered. However, for the same IB, with 0.15 m slab thickness, the LLDF for the abutment moment (M_a) obtained from FEAs is 0.74. The LLDF calculated from the AASHTO LRFD LLDE is 0.72. The difference between the LLDFs obtained from the FEA of the IB and that calculated using AASHTO LRFD LLDE is only 3%. This demonstrates that AASHTO LRFD LLDEs are more suitable for IBs having smaller slab thickness for the calculation of flexural live load effects in the abutments.

The analyses results also reveal that compared to FEA results, AASHTO LRFD LLDEs produce very conservative estimates of abutment live load shear as well as pile live load moment and shear as observed from the Figs. 6.6 (a) and (b).

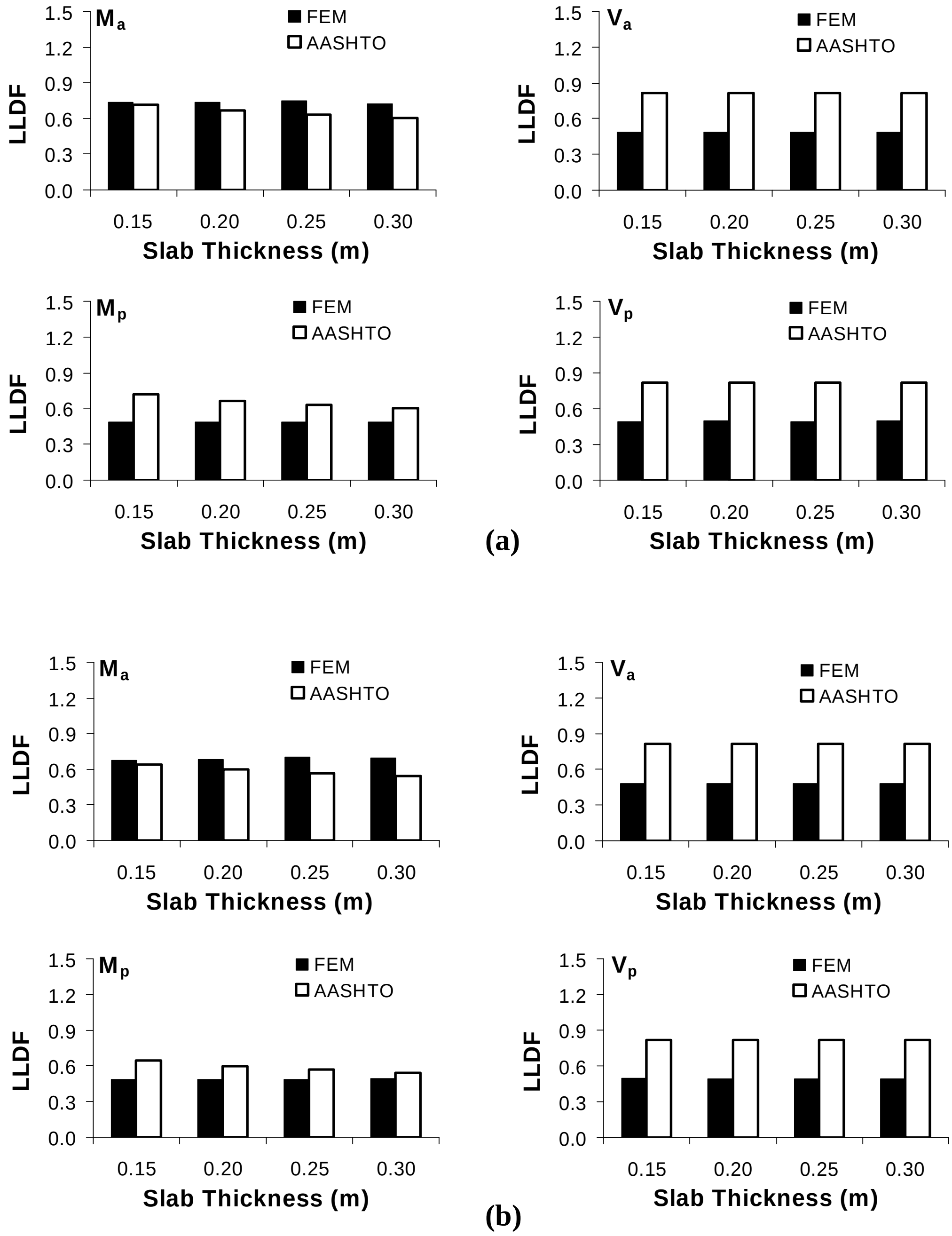

Figure 6.6 LLDFs vs. slab thickness for **(a)** span length of 30 m, girder spacing of 2.4 m and girder type IV. **(b)** Span length of 45 m, girder spacing of 2.4 m and girder type IV.

6.7. APPLICABILITY OF THE ABOVE FINDINGS FOR VARIOS SUBSTRUCTURE AND SOIL PROPERTIES

In the previous sections (Sections 6.3–6.6) the live load analyses of IBs are conducted assuming an abutment height (*H*) of 3 m, a pile size (*PS*) of HP250x85, backfill unit weight of 20 kN/m^3 and a soil strength of C_u=40 kPa. In this section, the findings of Sections 6.3–6.6 are assessed for substructure and soil properties different than those used earlier. For this purpose, two IBs with span lengths of 20 m with AASHTO LRFD Type II girders spaced at 2.4 m. and 40 m with AASHTO LRFD Type VI girders spaced at 2.4 m. are considered. The IBs are assumed to have 3 m and 5 m tall abutments supported by seven HP250x85 and HP310x125 piles. The undrained shear strength of the foundation soil (C_u) of the IBs is assumed as 40 kPa and 80 kPa respectively. In addition, to study the effect of the backfill stiffness on LLDFs, the 20 m span IB model is also built by assuming backfill unit weights of 18 and 22 kN/m^3 (this corresponds to a 10% decrease and increase in backfill stiffness compared to γ=20 kN/m^3). The IB models mentioned above are then analyzed under AASHTO LRFD truck loading. The analysis results are illustrated in Figs. 6.7-6.9. The figures display the LLDFs for abutment moment (M_a) and shear (V_a) as well as for pile moment (M_p) and shear (V_p) as functions of abutment height (*H*), undrained shear strength of foundation soil (C_u), backfill unit weight (γ) and pile size (*PS*). In the figures, LLDFs obtained for the abutments and piles of IBs, and those calculated from the AASHTO LRFD LLDEs are compared.

The analyses results reveal that the findings of Sections 6.3–6.6 are generally valid for substructure and soil properties different than those used earlier with the exception that taller abutments produce a better distribution of flexural live load effects within the abutment. Consequently, it may be stated that the AASHTO LRFD girder LLDEs are generally not applicable to IB abutments and piles regardless of the substructure and soil properties.

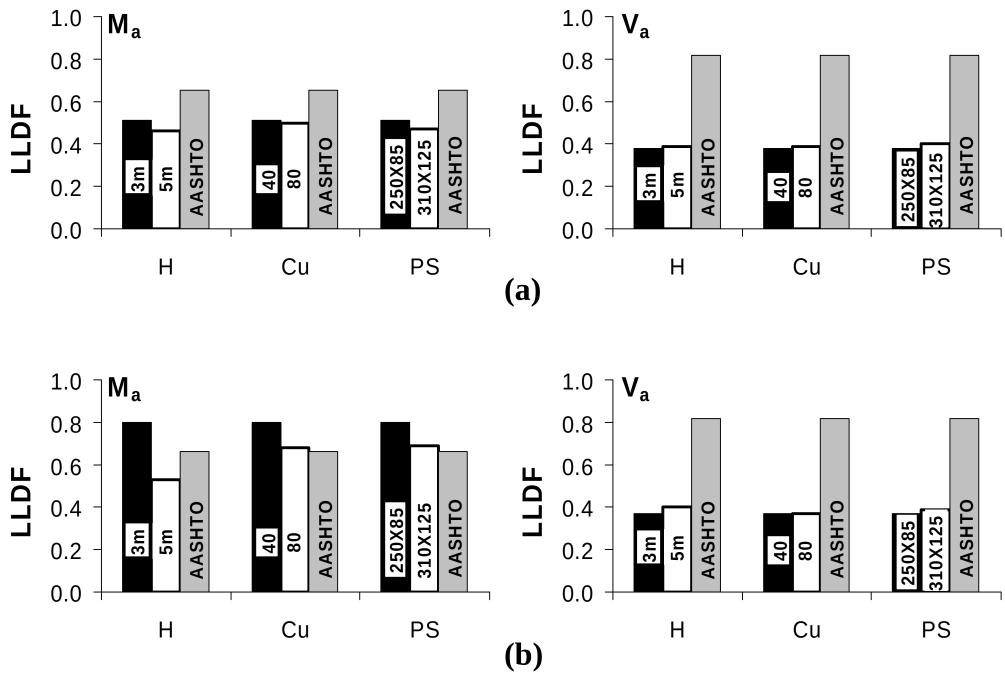

Figure 6.7 LLDFs in the abutment vs. various substructure properties for **(a)** 20 m IB **(b)** 40 m IB. (H= abutment height, C_u= undrained shear strength of foundation soil, PS= pile size)

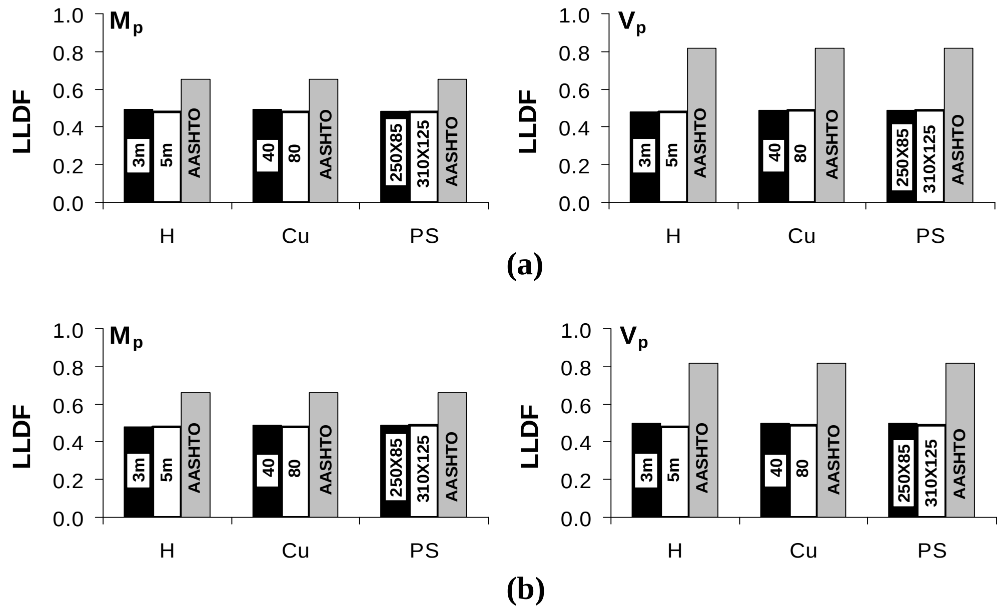

Figure 6.8 LLDFs in the pile vs. various substructure properties for (**a)** 20 m IB **(b)** 40 m IB (H= abutment height, C_u= undrained shear strength of foundation soil, PS= pile size)

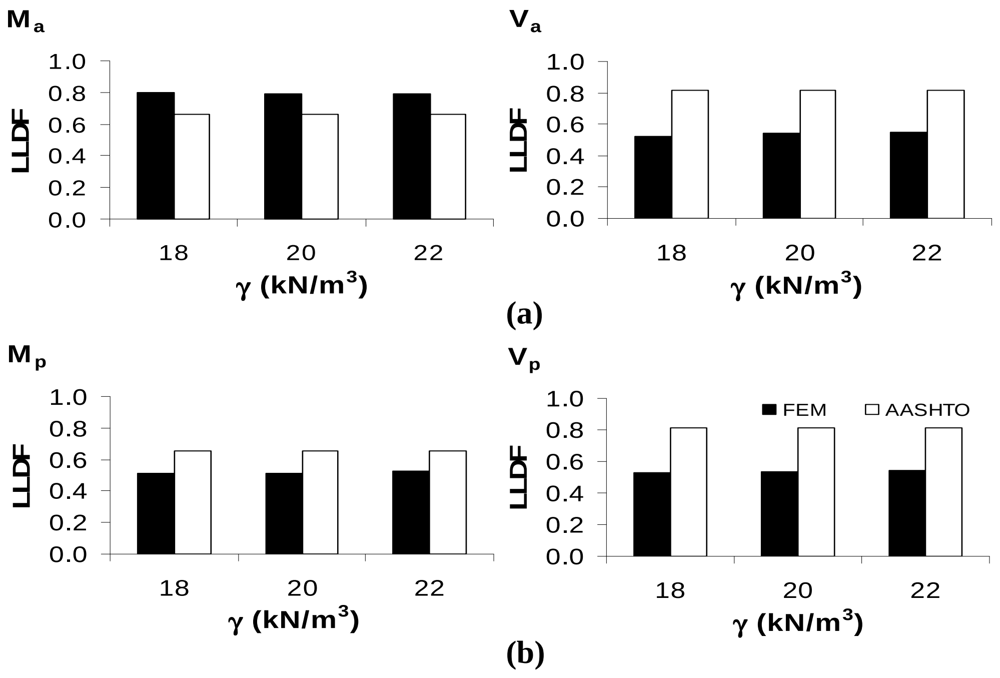

Figure 6.9 LLDFs vs. backfill unit weight (γ) for (**a)** abutment **(b)** pile

6.8 SUMMARY

In this chapter, a parametric study is conducted to investigate the applicability of the AASHTO LRFD LLDEs for IBs abutments and piles. For this purpose, The LLDFs obtained for IBs are compared with those calculated using AASHTO LRFD LLDEs to assess the applicability of AASHTO LRFD LLDEs to the design of IB abutments and piles under live load effects. Followings are the conclusions deduced from this study.

1. The parametric study reveals that AASHTO LRFD girder LLDEs are generally not applicable to the abutments and piles of IBs. AASHTO LRFD LLDEs lead to extremely conservative estimates of the live load shear in the abutments and live load moment and shear in the piles. However, the AASHTO LRFD LLDEs generally lead to unconservative estimates of live load moment in the abutments.

2. The analyses results revealed that the live load moment and shear in the piles and the live load shear in the abutment are generally independent of the span length, girder type and slab thickness. The girder spacing is found to be the only parameter that affects the distribution of live load moment and shear to the piles and live load shear to the abutment.

3. In addition, it is found that the distribution of flexural live load effects is highly dependent on the superstructure properties of the bridge. The distribution of the flexural live load effects is improved for longer IBs with flexible superstructures. Moreover, it is also found that the distribution of flexural live load effects within the abutment is better predicted by AASHTO LRFD girder LLDEs for IBs with longer spans, smaller girder size and spacing as well as thicker slabs.

4. The above conclusions are also confirmed for IBs with various substructure properties with the exception that taller abutments produce a better distribution of flexural live load effects within the abutment.

CHAPTER 7

LIVE LOAD DISTRIBUTION FORMULAE FOR INTEGRAL BRIDGE GIRDERS

In this study, live load distribution formulae for the girders of single-span IBs are developed. For this purpose, two and three dimensional finite element models (FEMs) of several IBs are built and analyzed. In the analyses, the effects of various superstructure properties such as span length, number of design lanes, prestressed concrete girder size and spacing as well as slab thickness are considered. The results from the analyses of two and three dimensional FEMs are then used to calculate the live load distribution factors (LLDFs) for the girders of IBs as a function of the above mentioned parameters. LLDFs for the girders are also calculated using the AASHTO formulae developed for simply supported bridges (SSBs). Comparison of the analyses results revealed that LLDFs for girder moments and exterior girder shear of IBs are generally smaller than those calculated for SSBs using AASHTO formulae especially for short spans. However, AASHTO LLDFs for interior girder shear are found to be in good agreement with those obtained for IBs. Consequently, direct live load distribution formulae and correction factors to the current AASHTO live load distribution equations are developed to estimate the girder live load moments and exterior girder live load shear for IBs with prestressed concrete girders.

To obtain LLDEs for IB girders, two and three dimensional finite element models (FEMs) of several IBs are built and analyzed. In the analyses, the effects of various structural properties are considered. The results from the analyses of two and three dimensional FEMs are then used to calculate the live load distribution factors (LLDFs) for the girders of IBs as a function of the structural properties considered in the analyses. The analyses results revealed that AASHTO LLDFs for interior girder shear are in good agreement with those obtained from finite element analyses (FEAs) (Dicleli and Erhan 2010). However, for girder moment, and exterior girder shear AASHTO LLDFs are generally much more conservative (larger) than those obtained from FEAs for IBs especially for short spans (more than 80% for some cases). Consequently, using linear and nonlinear regression analysis techniques and the available analysis results, LLDEs are developed to estimate the girder live load moments and exterior girder live load shears in IBs with prestressed concrete girders. Two sets of equations are developed to calculate the LLDFs for the IB girders considering two truck loading cases where only one lane is loaded and two or more lanes are loaded (similar to AASHTO). The first set of equations are developed in the form of correction factors which are used to multiply the LLDEs present in AASHTO (2007) for slab-on-girder jointed bridges to accurately calculate the LLDFs for the girder moment and exterior girder shear of IBs. This is particularly done to propose a methodology completely compatible with AASHTO (2007) for calculating live load effects in the girders of IBs. Such an approach will facilitate the application of these research findings to IB design by practicing engineers more effectively since design engineers are already familiar with using LLDEs available in AASHTO. The second set of equations is developed to directly obtain the LLDFs for the girder moment and exterior girder shear of IBs independent of AASHTO. However, this second set of equations contains smaller number of parameters for the estimation of interior girder moments compared to those present in AASHTO (2007).

7.1 BRIDGES AND PARAMETERS CONSIDERED IN THE ANALYSES

To develop LLDFs for prestressed concrete IB girders, live load analyses of IBs with various properties are conducted. The abutments of the IBs considered in this study are assumed to be 3 m. tall and supported by 12 m. long end-bearing steel HP250x85 piles often used in IB construction. The number of piles is set equal to the number of girders (i.e. one pile is assumed underneath each girder). The strength of the concrete used for the prestressed concrete girders is assumed to be 50 MPa while those of the slab and abutments are assumed to be 30 MPa. The granular backfill behind the abutments is assumed to have a unit weight of 20 kN/m^3. The foundation soil surrounding the piles is assumed to be medium-stiff clay with an undrained shear strength of C_u=40 kPa. The assumed clay stiffness is typical for IB construction as in stiffer soils; pre-drilled oversize holes filled with loose sand is generally provided along the top portion of the pile to reduce the resistance of the surrounding stiff soil to the lateral movements of the pile. A parametric study is conducted to cover a broad range of bridge properties found in practice. Nevertheless, the parameters included in this study are limited to superstructure properties used in AASHTO (2007) LLDEs since as stated earlier, the variations in substructure (abutments and piles), backfill and foundation soil properties are found to have negligible effects on the distribution of live load effects among the girders of IBs. The superstructure properties considered in the analyses include the span length (L), girder type (GT) (or girder stiffness) and spacing (S), slab thickness (t_s), cantilever length measured from the centroid of the exterior girder up to the face of the barrier wall (d_e) as well as number of loaded design lanes (N_L). The parameter, d_e, is solely used when calculating the live load effects in the exterior girders. The range of values considered for each parameter is given in Table 7.1. Five sets of analyses are considered as shown in the first column of Table 7.1. In each analysis set one of the parameters is considered to be dominant. For instance, in Analysis Set 1 while the span length is the main parameter, in Analysis Set 2 the girder type is the main parameter. For the main parameter, the full range of values considered is included in the analyses while the remaining parameters assume more limited range of values. This resulted in a total of 248 different 3-D and corresponding 2-D structural models of IBs and more than 1500 analyses cases for various longitudinal (for girder shear and moment) and transverse positions of the design trucks. In all the IB models, the number of girders is assumed to be at least equal to four per AASHTO (2007). For studying the effect of the parameters L, GT, t_s and d_e, the width of the bridges between the exterior girders is taken as 7.2 and 10.8 m. However, for studying the effect of the girder spacing, S, the width of the bridges between the exterior girders is taken as 14.4 m to be able to accommodate at least four girders spaced at 4.8 m. It was found that the bridge width results in slight differences in LLDFs for the girders of IBs (this does not happen in the case of SSB) with the narrower bridges yielding slightly more conservative estimates of live load effects. Consequently, the wider bridges are used only when formulating the effect of the girder spacing in the equations, while the narrower bridges are used for all the other parameters in the equations. Thus, using bridges with different widths results in more conservative development of LLDEs for IB girders for design purposes and avoids having a complex form of LLDEs for IBs that include the bridge width as a parameter.

Table 7.1. Parameters considered in the analyses.

Analyses Sets	L (m)	GT	t_s (m)	S (m)	d_e (m)	N_L - Loaded
1	**10, 15, 20, 25, 30, 35, 40, 45**	II, IV, VI	0.20	1.2, 2.4, 3.6	0.3, 0.9	1 and 2 or more
2	15, 30, 45	**I, II, III, IV, V, VI**	0.20	1.2, 2.4, 3.6	0.3, 0.9	1 and 2 or more
3	15, 30, 45	IV	**0.15, 0.20, 0.25, 0.30**	1.2, 2.4, 3.6	0.3, 0.9	1 and 2 or more
4	15, 30, 40	II, IV, VI	0.20	**1.2, 2.4, 3.6, 4.8**	0.3	1 and 2 or more
5	20, 30, 40	III, IV, VI	0.15, 0.20, 0.30	1.2, 2.4, 3.6	**-0.3, 0.3, 0.9, 1.5**	1 and 2 or more

7.2 DISCUSSION OF THE ANALYSES RESULTS

The analysis results for the interior girders and for the case where two or more design lanes are loaded are presented in Tables 7.2–7.5. The analyses results for the case where only one design lane is loaded are similar. Each table presents the results for a main parameter where the full range of values is used in the analyses. For instance, Table 7.2 lists the analyses results for the case where the span length, *L*, is taken as the main parameter while Table 7.3 lists the analyses results for the case where the girder spacing, *S*, is taken as the main parameter. Only a sample of the analysis results for the exterior girders and for the case where two or more design lanes are loaded is presented in Table 7.6. In the table, d_e is taken as the main parameter. In all the tables, the values of the parameters used, LLDF's obtained from finite element analyses (FEA) and AASHTO as well as the ratio, *R*, of the LLDFs obtained from AASHTO to those obtained from FEA (*R*=AASHTO / FEA) are presented for the girder moment and shear. The combination of various parameters presented in the tables may not always be realistic (e.g. the combination of girder type VI and a span length of 15 m). However, this was done deliberately to have adequate data covering the full range of possible variation of the parameters for the development of the LLDEs for IBs using regression analyses techniques and to cover all possible cases of scenarios.

For the interior girders, the analyses results revealed that the ratio, *R*, for the girder shear ranges between 0.99 and 1.10. Close examination of the data presented in Tables 7.2-7.5 indicates that most of the *R* values for the interior girder shear are within the range 1.03-1.06. Thus, LLDFs obtained from FEA are generally in good agreement with those calculated using AASHTO LLDEs. However, for the interior girder moment, the ratio, *R*, ranges between 0.87 and 1.87 where most of the *R* values are larger than 1.0 (i.e AASHTO LLDEs generally yield conservative estimates of LLDFs for the girder moment). The data presented in the tables reveal that the difference between the FEA results for IBs and AASHTO for the interior girder moment is more pronounced for bridges with shorter spans, larger girder sizes, smaller girder spacings and smaller slab thickness. In an earlier research study (Dicleli and Erhan, 2008a), the AASHTO LLDFs were compared with those obtained from FEA of SSBs and a reasonably good agreement was found between the two. Consequently, although AASHTO LLDEs are able to predict the distribution of live load effects in the interior girders of SSBs with reasonable accuracy (within 10 %), they fail to do so in the case of IBs (as much as 87% difference). This mainly results from the better distribution of live load moment among the girders of IBs and lesser variation of the LLDFs for IBs as a function of the parameters *L*, *S*, t_s and *GT*. The better distribution of the live load moment in IBs may be primarily due to the torsional rotational rigidity provided by the monolithic abutments to the girders and the slab, which is more predominant for shorter span bridges. Furthermore, the overhanging portion of the slab, which is free over the supports in jointed bridges, is fixed to the abutments in the case of IBs. This may also enhance the distribution of live load moment among the girders of IBs. It is also observed that the distribution of the interior girder live load moment is better for wider IBs. This becomes obvious if one compares the *R* values for the interior girder moment corresponding to the same set of parameters (L, S, t_s, GT) in Tables 7.2 and 7.3 (e.g. L=15 m, S=2.4 m, t_s=0.20 m and GT=IV). As mentioned earlier, the data in Table 7.3 is produced for a wider bridge to be able to accommodate at least four girders spaced at 4.8 m. This was done to properly include the effect of the girder spacing, *S*, in LLDEs for IBs (i.e. to include the full range of *S* values considered; S = 1.2, 2.4, 3.6, 4.8 m.). Consequently the LLDFs for the girder moment of IBs in Table 7.3 are smaller than those in Table 7.2 for the same set of parameters. However, since the bridge width is not considered in AASHTO LLDEs, a similar approach is also followed in the development of LLDEs for IBs. The equations are simply developed for narrower bridges that yield more conservative (larger) LLDFs for wider bridges. However, in the development of the LLDEs for IBs, the data for the narrower and wider bridges are used consistently (i.e. they are not mixed up, wider bridges are used in the formulation of the effect of girder spacing). The analysis results for the wider bridge are solely used to include the effect of the girder spacing in the LLDEs for IBs.

For the exterior girders, the analyses results are similar to those of the interior girders for the girder moment. However, the large values of *R* for the exterior girder shear compared to those of the interior girder shear is mainly due to the fixity and vertical support provided by the abutments to the overhanging portion of the slab. In the case of the SSB, the edges of the overhanging portion of the slab are all free (not supported vertically). Therefore, the wheel loads on the overhanging portion of the slab are directly transferred to the exterior girder. However, in the case of the IB, a portion of the wheel loads (especially near the support) is also distributed to the fixed support over the abutments. This reduces the shear load taken directly by the girder and produces a smaller LLDF for shear.

In summary, based on the data presented in Tables 7.2-7.5, it may be concluded that AASHTO LLDEs for interior girder shear may be used to calculate the live load shear forces in the interior girders of IBs. However, because of the large scatter of the ratio *R* in Tables 7.2-7.6, the AASHTO LLDEs for girder moment and exterior girder shear are not suited for IBs. Thus, in the following sections using regression analysis techniques and the available analysis results, two sets of LLDEs are developed to estimate the live load moments for the interior and exterior girders and live load shear for the exterior girders of IBs considering two truck loading cases where only one lane is loaded and two or more lanes are loaded (similar to AASHTO). The first set of equations are developed in the form of correction factors, which are used to multiply the LLDEs present in AASHTO (2007) for slab-on-girder jointed bridges to accurately calculate the LLDFs for the girder moment and exterior girder shear of IBs. The second set of equations is developed to directly obtain the LLDFs for the girder moment and exterior girder shear of IBs independent of AASHTO.

Table 7.2. Comparison of LLDFs from FEA results and AASHTO equations for the cases where two or more design lanes are loaded and the span length (L) is taken as the main parameter.

PARAMETER				DISTRIBUTION FACTOR					
				MOMENT			SHEAR		
***L* (m)**	***S* (m)**	**t_s (m)**	***GT***	**FEA**	**AASHTO**	**R**	**FEA**	**AASHTO**	**R**
10	2.4	0.20	II	0.640	0.795	1.24	0.810	0.816	1.01
15	2.4	0.20	II	0.633	0.704	1.11	0.795	0.816	1.03
20	2.4	0.20	II	0.630	0.654	1.04	0.795	0.816	1.03
25	2.4	0.20	II	0.615	0.618	1.00	0.791	0.816	1.03
30	2.4	0.20	II	0.612	0.586	0.96	0.783	0.816	1.04
35	2.4	0.20	II	0.603	0.564	0.94	0.781	0.816	1.04
40	2.4	0.20	II	0.596	0.545	0.91	0.780	0.816	1.05
45	2.4	0.20	II	0.590	0.528	0.89	0.775	0.816	1.05
10	2.4	0.20	IV	0.640	0.907	1.42	0.810	0.816	1.01
15	2.4	0.20	IV	0.625	0.803	1.29	0.785	0.816	1.04
20	2.4	0.20	IV	0.625	0.744	1.19	0.784	0.816	1.04
25	2.4	0.20	IV	0.621	0.702	1.13	0.783	0.816	1.04
30	2.4	0.20	IV	0.615	0.666	1.08	0.779	0.816	1.05
35	2.4	0.20	IV	0.605	0.640	1.06	0.777	0.816	1.05
40	2.4	0.20	IV	0.597	0.619	1.04	0.775	0.816	1.05
45	2.4	0.20	IV	0.588	0.598	1.02	0.753	0.816	1.08
10	2.4	0.20	VI	0.638	0.973	1.53	0.781	0.816	1.04
15	2.4	0.20	VI	0.629	0.861	1.37	0.775	0.816	1.05
20	2.4	0.20	VI	0.628	0.798	1.27	0.786	0.816	1.04
25	2.4	0.20	VI	0.628	0.752	1.20	0.788	0.816	1.04
30	2.4	0.20	VI	0.624	0.713	1.14	0.789	0.816	1.03
35	2.4	0.20	VI	0.617	0.685	1.11	0.786	0.816	1.04
40	2.4	0.20	VI	0.617	0.662	1.07	0.784	0.816	1.04
45	2.4	0.20	VI	0.598	0.640	1.07	0.782	0.816	1.04
10	1.2	0.20	IV	0.366	0.553	1.51	0.510	0.512	1.00
15	1.2	0.20	IV	0.340	0.493	1.45	0.482	0.512	1.06
20	1.2	0.20	IV	0.341	0.460	1.35	0.479	0.512	1.07
25	1.2	0.20	IV	0.338	0.435	1.29	0.475	0.512	1.08
30	1.2	0.20	IV	0.333	0.414	1.24	0.469	0.512	1.09
35	1.2	0.20	IV	0.326	0.400	1.23	0.465	0.512	1.10
40	1.2	0.20	IV	0.320	0.387	1.21	0.467	0.512	1.10
45	1.2	0.20	IV	0.316	0.376	1.19	0.464	0.512	1.10
10	3.6	0.20	IV	0.920	1.226	1.33	1.080	1.087	1.01
15	3.6	0.20	IV	0.910	1.081	1.19	1.068	1.087	1.02
20	3.6	0.20	IV	0.900	1.001	1.11	1.088	1.087	1.00
25	3.6	0.20	IV	0.890	0.943	1.06	1.083	1.087	1.00
30	3.6	0.20	IV	0.860	0.892	1.04	1.080	1.087	1.01
35	3.6	0.20	IV	0.789	0.857	1.09	1.063	1.087	1.02
40	3.6	0.20	IV	0.806	0.827	1.03	1.069	1.087	1.02
45	3.6	0.20	IV	0.789	0.799	1.01	1.067	1.087	1.02

Table 7.3. Comparison of LLDFs from FEA results and AASHTO equations for the cases where two or more design lanes are loaded and the girder spacing (*S*) is taken as the main parameter.

PARAMETER				DISTRIBUTION FACTOR					
				MOMENT			SHEAR		
***L* (m)**	***S* (m)**	**t_s (m)**	***GT***	**FEA**	**AASHTO**	**R**	**FEA**	**AASHTO**	**R**
15	1.2	0.20	IV	0.263	0.493	1.87	0.492	0.512	1.04
15	2.4	0.20	IV	0.490	0.803	1.64	0.772	0.816	1.06
15	3.6	0.20	IV	0.682	1.081	1.59	1.079	1.087	1.01
15	4.8	0.20	IV	0.946	1.342	1.42	1.312	1.332	1.02
30	1.2	0.20	IV	0.272	0.414	1.52	0.48	0.512	1.07
30	2.4	0.20	IV	0.524	0.666	1.27	0.794	0.816	1.03
30	3.6	0.20	IV	0.774	0.892	1.15	1.09	1.087	1.00
30	4.8	0.20	IV	1.005	1.104	1.10	1.308	1.332	1.02
40	1.2	0.20	IV	0.277	0.387	1.40	0.474	0.512	1.08
40	2.4	0.20	IV	0.518	0.619	1.19	0.790	0.816	1.03
40	3.6	0.20	IV	0.763	0.827	1.08	1.079	1.087	1.01
40	4.8	0.20	IV	0.979	1.022	1.04	1.310	1.332	1.02
40	1.2	0.20	II	0.323	0.345	1.07	0.476	0.512	1.08
40	2.4	0.20	II	0.524	0.545	1.04	0.729	0.816	1.12
40	3.6	0.20	II	0.720	0.726	1.01	1.009	1.087	1.08
40	4.8	0.20	II	0.909	0.894	0.98	1.290	1.332	1.03
40	3.6	0.15	VI	0.281	0.412	1.47	0.473	0.512	1.08
40	3.6	0.20	VI	0.504	0.662	1.31	0.796	0.816	1.03
40	3.6	0.25	VI	0.751	0.887	1.18	1.101	1.087	0.99
40	3.6	0.30	VI	0.986	1.097	1.11	1.319	1.332	1.01

R = AASHTO / FEA

Table 7.4. Comparison of LLDFs from FEA results and AASHTO equations for the cases where two or more design lanes are loaded and the slab thickness (t_s) is taken as the main parameter.

PARAMETER				DISTRIBUTION FACTOR					
				MOMENT			SHEAR		
L **(m)**	***S*** **(m)**	t_s **(m)**	***GT***	**FEA**	**AASHTO**	**R**	**FEA**	**AASHTO**	**R**
15	2.4	0.15	IV	0.646	0.865	1.34	0.788	0.816	1.04
15	2.4	0.20	IV	0.621	0.803	1.29	0.774	0.816	1.05
15	2.4	0.25	IV	0.615	0.759	1.23	0.781	0.816	1.04
15	2.4	0.30	IV	0.608	0.725	1.19	0.787	0.816	1.04
30	2.4	0.15	IV	0.632	0.716	1.13	0.778	0.816	1.05
30	2.4	0.20	IV	0.615	0.666	1.08	0.779	0.816	1.05
30	2.4	0.25	IV	0.600	0.630	1.05	0.779	0.816	1.05
30	2.4	0.30	IV	0.591	0.603	1.02	0.780	0.816	1.05
45	2.4	0.15	IV	0.604	0.643	1.06	0.769	0.816	1.06
45	2.4	0.20	IV	0.587	0.598	1.02	0.770	0.816	1.06
45	2.4	0.25	IV	0.576	0.567	0.98	0.771	0.816	1.06
45	2.4	0.30	IV	0.567	0.543	0.96	0.774	0.816	1.05
30	1.2	0.15	IV	0.341	0.443	1.30	0.474	0.512	1.08
30	1.2	0.20	IV	0.333	0.414	1.24	0.465	0.512	1.10
30	1.2	0.25	IV	0.325	0.394	1.21	0.470	0.512	1.09
30	1.2	0.30	IV	0.318	0.378	1.19	0.471	0.512	1.09
30	3.6	0.15	IV	0.900	0.962	1.07	1.068	1.087	1.02
30	3.6	0.20	IV	0.860	0.892	1.04	1.080	1.087	1.01
30	3.6	0.25	IV	0.820	0.843	1.03	1.081	1.087	1.01
30	3.6	0.30	IV	0.788	0.805	1.02	1.080	1.087	1.01

R = AASHTO / FEA

Table 7.5. Comparison of interior girder LLDFs from FEA results and AASHTO equations for the cases where two or more design lanes are loaded and the girder type (*GT*) is taken as the main parameter.

PARAMETER				DISTRIBUTION FACTOR					
				MOMENT			SHEAR		
***L* (m)**	***S* (m)**	**t_s (m)**	***GT***	**FEA**	**AASHTO**	**R**	**FEA**	**AASHTO**	**R**
15	2.4	0.2	I	0.622	0.659	1.06	0.794	0.816	1.03
15	2.4	0.2	II	0.632	0.704	1.11	0.795	0.816	1.03
15	2.4	0.2	III	0.638	0.756	1.18	0.771	0.816	1.06
15	2.4	0.2	IV	0.621	0.803	1.29	0.774	0.816	1.05
15	2.4	0.2	V	0.625	0.836	1.34	0.791	0.816	1.03
15	2.4	0.2	VI	0.621	0.861	1.39	0.775	0.816	1.05
30	2.4	0.2	I	0.594	0.550	0.93	0.778	0.816	1.05
30	2.4	0.2	II	0.612	0.586	0.96	0.783	0.816	1.04
30	2.4	0.2	III	0.614	0.628	1.02	0.775	0.816	1.05
30	2.4	0.2	IV	0.615	0.666	1.08	0.779	0.816	1.05
30	2.4	0.2	V	0.620	0.693	1.12	0.786	0.816	1.04
30	2.4	0.2	VI	0.624	0.713	1.14	0.789	0.816	1.03
45	2.4	0.2	I	0.569	0.495	0.87	0.771	0.816	1.06
45	2.4	0.2	II	0.588	0.528	0.90	0.775	0.816	1.05
45	2.4	0.2	III	0.588	0.565	0.96	0.775	0.816	1.05
45	2.4	0.2	IV	0.588	0.598	1.02	0.753	0.816	1.08
45	2.4	0.2	V	0.572	0.622	1.09	0.775	0.816	1.05
45	2.4	0.2	VI	0.598	0.640	1.07	0.782	0.816	1.04
30	1.2	0.2	I	0.313	0.348	1.11	0.471	0.512	1.09
30	1.2	0.2	II	0.326	0.369	1.13	0.473	0.512	1.08
30	1.2	0.2	III	0.331	0.393	1.19	0.474	0.512	1.08
30	1.2	0.2	IV	0.333	0.414	1.24	0.471	0.512	1.09
30	1.2	0.2	V	0.338	0.430	1.27	0.475	0.512	1.08
30	1.2	0.2	VI	0.342	0.442	1.29	0.475	0.512	1.08
30	3.6	0.2	I	0.779	0.731	0.94	1.063	1.087	1.02
30	3.6	0.2	II	0.831	0.782	0.94	1.081	1.087	1.01
30	3.6	0.2	III	0.855	0.840	0.98	1.085	1.087	1.00
30	3.6	0.2	IV	0.860	0.892	1.04	1.080	1.087	1.01
30	3.6	0.2	V	0.894	0.930	1.04	1.083	1.087	1.00
30	3.6	0.2	VI	0.893	0.958	1.07	1.088	1.087	1.00

R = AASHTO / FEA

Table 7.6. Comparison of exterior girder LLDFs from FEA results and AASHTO equations for the cases where two or more design lanes are loaded, t_s=0.2 m and d_e is taken as the main parameter.

PARAMETER				DISTRIBUTION FACTOR					
				MOMENT			SHEAR		
L (m)	**S (m)**	**d_e (m)**	**GT**	**FEA**	**AASHTO**	**R**	**FEA**	**AASHTO**	**R**
30	2.4	-0.3	III	0.418	0.416	1.00	0.275	0.408	1.48
30	2.4	0.3	III	0.526	0.551	1.05	0.494	0.571	1.16
30	2.4	0.9	III	0.637	0.685	1.08	0.706	0.734	1.04
30	2.4	1.5	III	0.754	0.820	1.09	0.898	0.898	1.00
20	3.6	-0.3	IV	0.489	0.664	1.36	0.374	0.544	1.45
20	3.6	0.3	IV	0.574	0.878	1.53	0.599	0.761	1.27
20	3.6	0.9	IV	0.666	1.093	1.64	0.809	0.978	1.21
20	3.6	1.5	IV	0.764	1.307	1.71	0.980	1.196	1.22
20	2.4	-0.3	III	0.381	0.477	1.25	0.258	0.408	1.58
20	2.4	0.3	III	0.476	0.632	1.33	0.456	0.571	1.25
20	2.4	0.9	III	0.582	0.786	1.35	0.624	0.734	1.18
20	2.4	1.5	III	0.697	0.940	1.35	0.788	0.898	1.14
20	3.6	-0.3	III	0.477	0.624	1.31	0.357	0.544	1.52
20	3.6	0.3	III	0.565	0.826	1.46	0.571	0.761	1.33
20	3.6	0.9	III	0.658	1.028	1.56	0.773	0.978	1.27
20	3.6	1.5	III	0.756	1.230	1.63	0.932	1.196	1.28
20	2.4	-0.3	VI	0.394	0.529	1.34	0.220	0.408	1.85
20	2.4	0.3	VI	0.481	0.700	1.46	0.412	0.571	1.39
20	2.4	0.9	VI	0.582	0.871	1.50	0.576	0.734	1.27
20	2.4	1.5	VI	0.698	1.042	1.49	0.724	0.898	1.24
20	3.6	-0.3	VI	0.485	0.713	1.47	0.307	0.544	1.77
20	3.6	0.3	VI	0.567	0.943	1.66	0.515	0.761	1.48
20	3.6	0.9	VI	0.657	1.173	1.79	0.706	0.978	1.39
20	3.6	1.5	VI	0.753	1.404	1.86	0.863	1.196	1.38
40	2.4	-0.3	VI	0.418	0.439	1.05	0.245	0.408	1.67
40	2.4	0.3	VI	0.515	0.581	1.13	0.445	0.571	1.28
40	2.4	0.9	VI	0.616	0.723	1.17	0.628	0.734	1.17
40	2.4	1.5	VI	0.728	0.864	1.19	0.797	0.898	1.13
40	3.6	-0.3	VI	0.496	0.588	1.18	0.358	0.544	1.52
40	3.6	0.3	VI	0.588	0.778	1.32	0.571	0.761	1.33
40	3.6	0.9	VI	0.735	0.968	1.32	0.752	0.978	1.30
40	3.6	1.5	VI	0.794	1.158	1.46	0.909	1.196	1.32

R = AASHTO / FEA

7.3 CORRECTION FACTORS TO ESTIMATE LLDFs FOR INTEGRAL BRIDGE GIRDERS

In this section, correction factors are developed to multiply the LLDEs present in AASHTO (2007) for slab-on-girder jointed bridges to accurately calculate the LLDFs for the girder moment of IBs, for the cases where two or more design lanes are loaded and only one design lane is loaded. In the developed equations all the parameters are measured in mm.

7.3.1 CORRECTION FACTORS FOR THE INTERIOR GIRDERS

7.3.1.1 GIRDER MOMENT - TWO OR MORE DESIGN LANES LOADED

The AASHTO (2007) LLDE for the composite interior girders of slab-on-girder jointed bridges with two or more design lanes loaded is as follows;

$$LLDE_{AASHTO} = 0.075 + \left(\frac{S}{2900}\right)^{0.6} \left(\frac{S}{L}\right)^{0.2} \left(\frac{K_g}{Lt_s^3}\right)^{0.1} \tag{7.1}$$

where K_g = a parameter representing the longitudinal stiffness of the composite slab-on-girder section of the bridge expressed as (AASHTO 2007);

$$K_g = n\left(I + Ae_g^2\right) \tag{7.2}$$

In the above equation, n = the ratio of the modulus of elasticity of the girder material to that of the slab material, I = the moment of inertia of the girder, A = cross-sectional area of the girder and e_g = distance between the centers of gravity of the girder and the slab.

To calculate the LLDF for the girder moment of IBs, the AASHTO LLDF obtained from Eqn. (7.1) is simply multiplied by a correction factor, F_{C1}. Accordingly, the LLDE for the girder moment of IBs is expressed as;

$$LLDE_{IAB} = F_{C1} \times LLDE_{AASHTO} \tag{7.3}$$

The correction factor, F_{C1}, is assumed to have the following form;

$$F_{C1} = aL^{b1}S^{b2}t_s^{b3}K_g^{b4} \tag{7.4}$$

where a, $b1$, $b2$, $b3$ and $b4$ = constants to be determined via regression analyses using the data presented in Tables 7.2-7.5. To obtain these constants, first the ratio R_1, of the LLDFs obtained from FEA to those obtained using AASHTO LLDE are plotted as a function of the span length, L as shown in Fig. 7.1(a) using the data presented in Table 7.2. Then, the minimum least square fit of the logarithm of the L-R_1 data presented in Fig. 7.1(a) is performed to obtain the following equation;

$$R_1 = 0.10L^{0.21} \tag{7.5}$$

The above equation, which is plotted using a thick solid line in Fig. 7.1(a), gives the ratio of the LLDFs obtained from FEA to those obtained using AASHTO LLDE as a function of the span length. The term $L^{0.21}$ in Eqn. (7.5), represents the term L^{b1} in Eqn (7.4). Thus, $b1$=0.21. The scatter present in Fig.

7.1(a) with respect to the plot of Eqn. (7.5) is mainly due to the error introduced by the absence of other parameters, S, t_s and K_g in the equation. This error will be corrected by involving the effect of these remaining parameters in the equation. For this purpose, a new ratio, R_2, is first calculated as;

$$R_2 = \frac{FEA}{R_1 \times LLDE_{AASHTO}} \tag{7.6}$$

In the above equation, R_2 represents the ratio of the LLDFs obtained from FEA to those obtained using AASHTO LLDEs corrected with respect to L. Then, the ratio R_2 is plotted as a function of the girder spacing, S, in Fig. 7.1 (b) using the data presented in Table 7.3. Next, the minimum least square fit of the logarithm of the data presented in Fig. 7.1(b) is performed to obtain the following equation;

$$R_2 = 0.35 S^{0.13} \tag{7.7}$$

The above equation is plotted using a thick solid line in Fig. 7.1(b). The term $S^{0.13}$ in Eqn. (7.7), represents the term S^{b2} in Eqn (7.4). Thus, $b2$=0.13. To calculate the parameter, $b3$, in Eqn (7.4), a similar procedure is followed. First, a new ratio R_3 is calculated as;

$$R_3 = \frac{FEA}{R_1 \times R_2 \times LLDE_{AASHTO}} \tag{7.8}$$

where R_3 represents the ratio of the LLDFs obtained from FEA to those obtained using AASHTO LLDEs corrected with respect to L and S. Then, the ratio R_3 is plotted as a function of the slab thickness, t_s, in Fig. 7.1 (c) using the data presented in Table 7.4. Next, the minimum least square fit of the logarithm of the data presented in Fig. 7.1 (c) is performed to obtain the following equation;

$$R_3 = 0.48 t_s^{0.15} \tag{7.9}$$

The above equation is plotted using a thick solid line in Fig. 7.1 (c). Note that in the figure, most of the data overlap indicating a small scatter. The term $t_s^{0.15}$ in Eqn. (7.9) represents the term t_s^{b3} in Eqn (7.4). Thus, $b3$=0.15. Finally, to obtain the terms a and $b4$, a new ratio R_4 is calculated as;

$$R_4 = \frac{FEA}{R_1 \times R_2 \times R_3 \times LLDE_{AASHTO}} \tag{7.10}$$

where, R_4 represents the ratio of the LLDFs obtained from FEA to those obtained using AASHTO LLDE corrected with respect to L, S and t_s. Then, the ratio R_4 is plotted as a function of K_g, in Fig. 7.1(d) using the data presented in Table 7.5. Next, the minimum least square fit of the logarithm of the R_4-K_g data presented in Fig. 7.1(d) is performed to obtain the following equation;

$$R_4 = 6.47 K_g^{-0.07} \tag{7.11}$$

The above equation is plotted using a thick solid line in Fig. 7.1 (d). The term $K_g^{-0.07}$ in Eqn. (7.11), represents the term K_g^{b4} in Eqn (7.4). Thus, $b4$=-0.07. The LLDF for the girder moment of IBs can be obtained by solving for FEA in Eqn. (7.10) (i.e. $FEA=LLDE_{IB}=R_1 x R_2 x R_3 x R_4 x LLDE_{AASHTO}$) Accordingly, the constant, a in Eqn (7.4) is obtained by multiplying the coefficients in front of the variables, L, S, t_s and K_g in Eqns. (7.5), (7.7), (7.9) and (7.11) respectively. Thus, a=0.10x0.35x0.47x6.47 = 0.111 = 1/9. The final form of the correction factor becomes;

$$F_{C1} = \frac{L^{0.21} S^{0.13} t_s^{0.15}}{9 K_g^{0.07}} \tag{7.12}$$

7.3.1.2 GIRDER MOMENT - ONE DESIGN LANE LOADED

The AASHTO (2007) LLDE for the composite interior girders of slab-on-girder jointed bridges with only one design lane loaded is as follows;

$$LLDE_{AASHTO} = 0.06 + \left(\frac{S}{4300}\right)^{0.4} \left(\frac{S}{L}\right)^{0.3} \left(\frac{K_g}{L t_s^3}\right)^{0.1} \tag{7.13}$$

To calculate the LLDF for the girder moment of IBs, the AASHTO LLDF calculated from Eqn. (7.13) is simply multiplied by a correction factor, F_{C2}. This correction factor is also assumed to have a form similar to that presented in Eqn. (7.4). Accordingly, following a procedure similar to that described in the previous section, the correction factor, F_{C2}, is obtained as;

$$F_{C2} = \frac{L^{0.22} S^{0.09} t_s^{0.06}}{6 K_g^{0.06}} \tag{7.14}$$

7.3.2. CORRECTION FACTORS FOR THE EXTERIOR GIRDERS

7.3.2.1 GIRDER MOMENT - TWO OR MORE DESIGN LANES LOADED

AASHTO (2007) does not have a separate LLDE for the exterior girder moment. Instead, to obtain the live load moments in the exterior girders, the LLDE for the interior girders (Eqn. (7.1)) is multiplied by an adjustment factor, *e*. The adjustment factor is a linear function of the cantilever length, d_e, measured from the centroid of the exterior girder up to the face of the barrier wall and it is given as;

$$e = 0.77 + \frac{d_e}{2800} \tag{7.15}$$

Although this approach gives reasonable estimates of the live load effects in exterior girders of jointed bridges where the slab is a simple cantilever over the exterior girder, a similar approach can not be used for IBs. The main reason for this is that in the case of IBs the slab overhanging over the exterior girder is not a simple cantilever. It is also fixed to the abutments at the bridge ends. Consequently, the ratio of the exterior and interior girder moments is not a simple linear function of d_e especially for short span bridges. Consequently, a correction factor, F_{C3}, which is a function of all the parameters considered, is developed to multiply the AASHTO LLDE for interior girders (Eqn (7.1)) of slab-on-girder jointed bridges to obtain the LLDF for IBs. For this purpose, the correction factor, F_{C3}, is assumed to have the following form;

$$F_{C3} = aL^{b1}S^{b2}t_s^{b3}K_g^{b4}\left(c + \frac{d_e}{f}\right) \tag{7.16}$$

where a, $b1$, $b2$, $b3$, $b4$, c, and f = constants to be determined via regression analyses. In the above equation, the correction factor is assumed to be a linear function of d_e since using a power function of the form used for the other parameters renders the equation ineffective for d_e=0 (-0.3 ≤ d_e ≤ 1.5). To obtain the constants c and f, first the ratio R_1, of the LLDFs obtained from FEA to those obtained using AASHTO LLDEs for interior girders are plotted as a function of the parameter, d_e in Fig. 7.1 (e) using the available analyses results for exterior girders of IBs. Then, the minimum least square fit of the d_e-R_1 data is performed to obtain the following linear equation;

$$R_1 = 0.7 + \frac{d_e}{3000} \tag{7.17}$$

The above equation gives the ratio of the LLDFs obtained from FEA to those obtained using AASHTO LLDE for interior girders as a function of the parameter d_e. From the above equation c=0.7 and f=3000. As observed from Fig. 7.1 (e), the obtained linear function depicted using a thick solid line closely matches the variation of the FEA data. A procedure similar to that described in the previous sections is followed to obtain the remainder of the unknown constants in Eqn (7.16). The final form of the correction factor becomes;

$$F_{C3} = \frac{2L^{0.30}t_s^{0.25}}{3S^{0.10}K_g^{0.12}}\left(0.7 + \frac{d_e}{3000}\right) \tag{7.18}$$

7.3.2.2 GIRDER MOMENT - ONE DESIGN LANE LOADED

In this section, a correction factor, F_{C4}, is developed to multiply the AASHTO LLDE for interior girders (Eqn (7.13)) of slab-on-girder jointed bridges to obtain the LLDF for IBs where only one design lane is loaded. Following a procedure similar to that described in the previous sections, the correction factor, F_{C4}, is obtained as;

$$F_{C4} = \frac{2\,L^{0.37} t_s^{0.18}}{5\,S^{0.07} K_g^{0.12}} \left(0.8 + \frac{d_e}{3000} \right) \qquad (7.19)$$

7.3.2.3 GIRDER SHEAR - TWO OR MORE DESIGN LANES LOADED

AASHTO (2007) does not have a separate LLDE for the exterior girder shear. Instead, to obtain the live load shear in the exterior girders, the LLDE for the interior girders is multiplied by an adjustment factor, e, which is a linear function of d_e The LLDE for the interior girder shear and the adjustment factor, e, are given as; (AASHTO 2007);

$$LLDE_{AASHTO} = 0.2 + \frac{S}{3600} - \left(\frac{S}{10700} \right)^{2.0} \qquad (7.20)$$

$$e = 0.6 + \frac{d_e}{3000} \qquad (7.21)$$

As explained earlier, such an approach can not be used for IBs as the slab overhanging over the exterior girder is not a simple cantilever. Consequently, a correction factor, F_{C5}, which is a function of all the parameters considered, is developed to multiply the AASHTO LLDE for interior girder shear (Eqn (7.20)) of slab-on-girder jointed bridges to obtain the LLDF for IBs. Following a procedure similar to that described in the previous sections, the correction factor, F_{C5}, is obtained as;

$$F_{C5} = \frac{14L^{0.10}t_s^{0.03}}{S^{0.25}K_g^{0.07}}\left(0.5 + \frac{d_e}{2500}\right) \tag{7.22}$$

7.3.2.4 GIRDER SHEAR - ONE DESIGN LANE LOADED

For cases where only one design lane is loaded, AASHTO (2007) suggests the use of the lever rule to calculate the live load shear effects in the exterior girders of regular jointed bridges. However, the lever rule can not be applied to IBs as the slab overhanging over the exterior girder is not a simple cantilever. Consequently, a correction factor, F_{C6}, which is a function of all the parameters considered, is developed to multiply the AASHTO LLDE for interior girder shear (Eqn (7.23)) of slab-on-girder jointed bridges to obtain the LLDF for IBs. The AASHTO LLDE for the interior girder shear for the case where only one design lane is loaded and the correction factor, F_{C6} (developed following a procedure similar to that described in the previous sections) are given as;

$$LLDE_{AASHTO} = 0.36 + \frac{S}{7600} \tag{7.23}$$

$$F_{C6} = \frac{4\,L^{0.05} t_s^{0.01}}{S^{0.09} K_g^{0.045}} \left(0.7 + \frac{d_e}{2100} \right) \quad (7.24)$$

7.4 LLDEs FOR INTEGRAL BRIDGE GIRDERS INDEPENDENT OF AASHTO

In this section, a second set of equations are developed to directly obtain the LLDFs for the girders of IBs independent of AASHTO (2007).

7.4.1 LLDES FOR THE INTERIOR GIRDERS

7.4.1.1. GIRDER MOMENT - TWO OR MORE DESIGN LANES LOADED

The FEA results presented in Tables 7.2-7.5 reveal that the variation of the LLDFs for the interior girders of IBs as a function of the girder type (*GT*) and t_s is modest. Accordingly, the LLDE for the interior girders of IBs is developed considering only the span length, *L*, and girder the spacing, *S*. Accordingly the LLDE is assumed to have the following form;

$$LLDE_{IB} = aS^{b1}L^{b2} \quad (7.25)$$

where *a*, *b1* and *b2* = constants to be determined via regression analyses using the data presented in Tables 7.2-7.5. To obtain these constants, first the FEA results are plotted as a function of the girder spacing, *S* as shown in Fig. 7.1

(f). Then, the minimum least square fit of the logarithm of the data presented in Fig. 7.1 (f) is performed to obtain the following equation;

$$D_s = 0.00106\, S^{0.82} \tag{7.26}$$

The above equation, which is plotted using a thick solid line in Fig. 7.1(f), gives the variation of the LLDFs obtained from FEA for IBs as a function of the girder spacing. The term $S^{0.82}$ in Eqn. (7.26), represents the term S^{b1} in Eqn (7.25). Thus, $b1$=0.82. The scatter present in Fig. 7.1(f) with respect to the plot of Eqn. (7.26) is mainly due to the error introduced by the absence of the parameter, L, in the equation. This error will be corrected by involving the effect of L in the equation. For this purpose, the FEA results are first divided by D_s and then the results are plotted as a function of the span length, L in Fig. 7.1 (g). This is done to decouple the FEA results from the effect of the girder spacing, S. Accordingly the ensuing ratio, D_L, is expressed as;

$$D_L = \frac{FEA}{D_s} \tag{7.27}$$

Then, the minimum least square fit of the logarithm of the data presented in Fig. 7.1 (g) is performed to obtain the following equation;

$$D_L = 1.887\, L^{-0.06} \tag{7.28}$$

The term $L^{-0.06}$ in Eqn. (7.28), represents the term L^{b2} in Eqn (7.25). Thus, $b2$=-0.06. From Eqn. (7.25), the LLDE for IBs is obtained by multiplying D_s by D_L. Thus, a=0.00106x 1.887=0.002=1/500. Substituting the values of a, $b1$ and $b2$ in Eqn. (7.25), the LLDE for the interior girder moment of IBs for the case where two or more design lanes are loaded is given as.

$$LLDE_{IAB} = \frac{S^{0.82}}{500\,L^{0.06}} \tag{7.29}$$

7.4.1.2. GIRDER MOMENT - ONE DESIGN LANE LOADED

A procedure similar to that described above is followed to obtain a LLDE for the interior girder moments of IBs for the case where only one design lane is loaded. The developed equation is as follows;

$$LLDE_{IAB} = \frac{3\,S^{0.72}}{500\,L^{0.13}} \tag{7.30}$$

7.4.2 LLDES FOR THE EXTERIOR GIRDERS

Following a procedure similar to that described in the previous sections a second set of equations are developed to directly obtain the LLDFs for the exterior girders of IBs independent of AASHTO (2007).

7.4.2.1 GIRDER MOMENT - TWO OR MORE DESIGN LANES LOADED

$$LLDE_{IAB} = \frac{L^{0.09} S^{0.53} t_s^{0.06}}{80 K_g^{0.04}} \left(0.5 + \frac{d_e}{5000} \right) \tag{7.31}$$

7.4.2.2 GIRDER MOMENT - ONE DESIGN LANE LOADED

$$LLDE_{IAB} = \frac{L^{0.06} S^{0.45}}{18 t_s^{0.02} K_g^{0.04}} \left(0.4 + \frac{d_e}{6000} \right) \tag{7.32}$$

7.4.2.3 GIRDER SHEAR - TWO OR MORE DESIGN LANES LOADED

$$LLDE_{IAB} = \frac{L^{0.10} S^{0.43} t_s^{0.03}}{14 K_g^{0.07}} \left(0.4 + \frac{d_e}{3000} \right) \tag{7.33}$$

7.4.2.4 GIRDER SHEAR - ONE DESIGN LANE LOADED

$$LLDE_{IAB} = \frac{2 L^{0.05} S^{0.34}}{15 t_s^{0.01} K_g^{0.04}} \left(0.5 + \frac{d_e}{3000} \right) \tag{7.34}$$

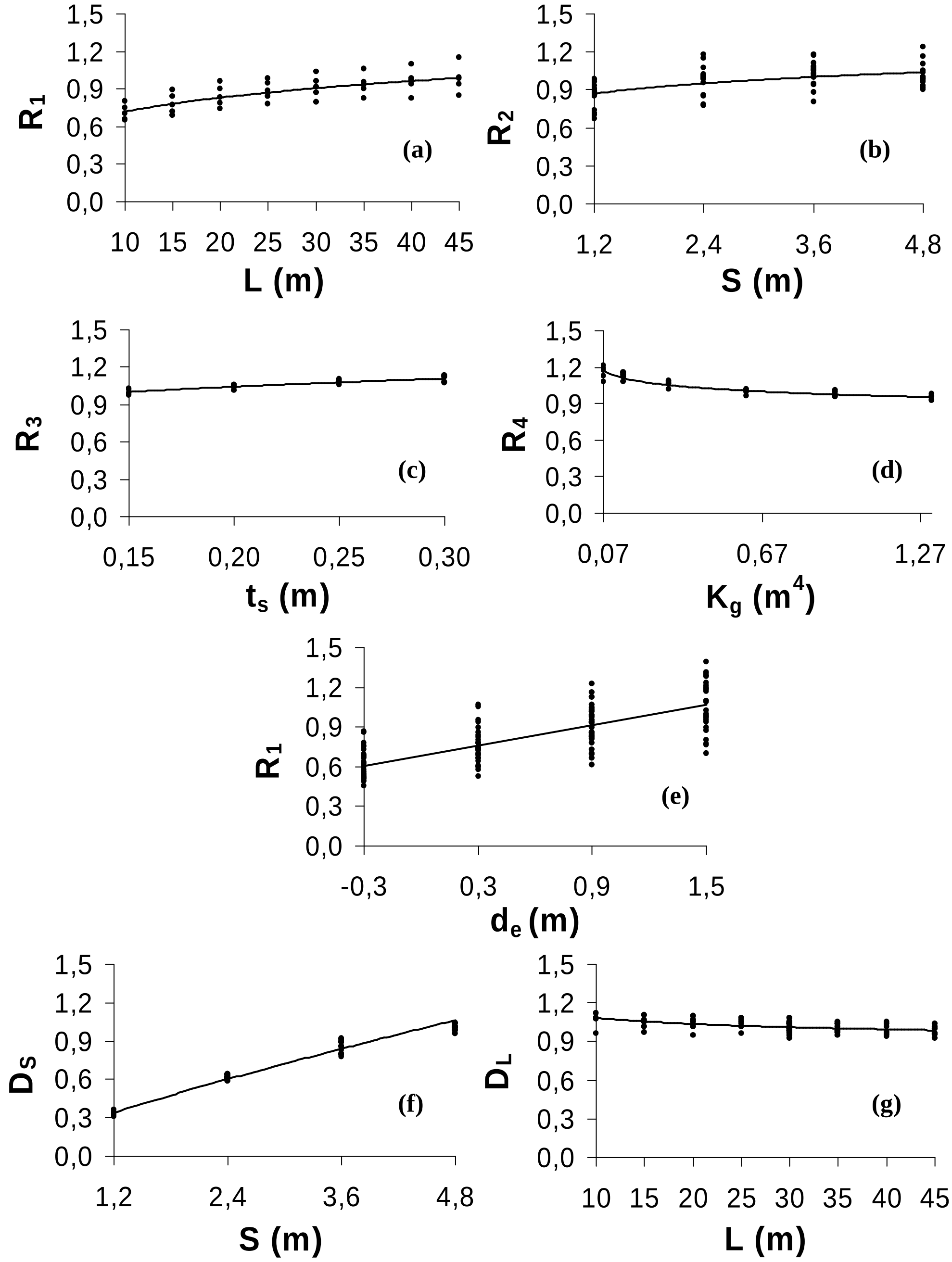

Figure 7.1 (a) R_1 versus L plot and minimum least square fit, (b) R_2 versus S plot and minimum least square fit, (c) R_3 versus t_s plot and minimum least square fit, (d) R_4 versus K_g plot and minimum least square fit, (e) R_1 versus d_e plot and minimum least square fit for exterior girders, (f) D_S versus S plot and minimum least square fit, (g) D_L versus L plot and minimum least square fit.

CHAPTER 8

LIVE LOAD DISTRIBUTION EQUATIONS FOR INTEGRAL BRIDGE SUBSTRUCTURES

In this study, live load distribution equations (LLDEs) for IB substructures are developed. For this purpose, numerous 3-D and corresponding 2-D structural models of typical IBs are built and analyzed under AASHTO live load. In the analyses, the effect of various superstructure and substructure properties such as span length, girder spacing, girder stiffness, abutment height, pile size, pile spacing and foundation soil stiffness are considered. The results from the 2-D and 3-D analyses are then used to calculate the live load distribution factors (LLDFs) for the abutments and piles of IBs as a function of the above mentioned properties. LLDEs are then developed to estimate the live load moments and shear in the abutments and piles of IBs using these LLDFs and nonlinear regression analysis methods.

To obtain LLDEs for IB abutments and piles, two (2-D) and three (3-D) dimensional FEMs of numerous IBs are built and analyzed. In the analyses, the effects of various geometric, structural and geotechnical properties are considered. The results from the analyses of 2-D and 3-D FEMs are then used to calculate the live load distribution factors (LLDFs) for the abutments and piles of IBs as a function of these geometric, structural and geotechnical properties considered in the analyses. Next, the behavior of the abutments and piles under live load effects is studied in detail using the available analyses results. Subsequently, using nonlinear regression analysis techniques and the available analysis results, LLDEs are developed to estimate the live load moments and shears in the abutments and piles of single-span IBs. Finally, the obtained LLDE's are verified using the results from finite element analyses (FEAs).

8.1 BRIDGES AND PARAMETERS CONSIDERED

In an earlier research study (Dicleli and Erhan 2010) the IB superstructure and substructure properties that affect the distribution of live load moment and shear in the abutments and piles are identified. These parameters are; span length, girder size and spacing for the superstructure and abutment height, pile size, pile spacing and foundation soil stiffness for the substructure. Using these superstructure and substructure parameters, a number of IB models are built and analyzed to develop LLDEs for IB abutments and piles. For the superstructure, the span lengths of the IBs considered in the analyses are assumed as 15, 20, 25, 35, 40, 45 m. Furthermore, AASHTO prestressed concrete girder types; II, III, V and VI spaced at 1.2, 2.4, 3.6 and 4.8 m. are considered in the analyses. A typical, 0.2 m thickness is assumed for the slab. The strength of the concrete used for the prestressed concrete girders is assumed to be 50 MPa while those of the slab and abutments are assumed to be 30 MPa. For the substructure, the abutments are assumed to be 2.5, 3, 4 and 5 m. tall and supported by 12 m. long end-bearing steel HP piles. The analyses are repeated for HP piles with the following sizes; 200x54, 250x85, 310x110 and 310x125. The assumed range of pile sizes is typical for IB construction. The spacing of these piles is assumed to be 1.2, 1.8, 2.4 and 3 m. In addition, the foundation soil surrounding the piles is assumed to be soft, medium,

medium-stiff and stiff clay with an undrained shear strength of C_u=20, 40, 80 and 120 kPa, respectively. The granular backfill behind the abutments is assumed to have a unit weight of 20 kN/m^3. The range of values considered for each parameter is given in Table 8.1. Seven sets of analyses are conducted as shown in the first column of Table 8.1. In each analysis set one of the parameters is considered to be dominant. For instance, in Analysis Set 1 while the span length is the main parameter, in Analysis Set 2 the girder spacing is the main parameter. For the main parameter, the full range of values considered is included in the analyses while the remaining parameters assume more limited range of values. In addition, the width of the IBs are considered as 12 m in Set 1 but 15.6 m in all the other sets to assess the effect of the bridge width (number of girder) on the distribution of live load in the abutments and piles. This resulted in more than 1200 different 3-D and corresponding 2-D structural models of IBs and more than 10,000 analyses for one design lane loaded case, two or more design lanes loaded case and for multiple truck positions in the transverse direction of the bridge.

Table 8.1. Parameters considered in the analyses.

PARAMETER	L (m)	S (m)	GT	H_a (m)	C_u (kPa)	HP	PS (m)
L (m)	15, 25, 35, 45	2.4, 3.6	II, VI	3, 5	40, 80	250x85, 310x125	1.2, 2.4
S (m)	20, 40	1.2, 2.4, 3.6, 4.8	II, VI	3, 5	40, 80	250x85, 310x125	1.2, 2.4
GT	20, 40	2.4, 3.6	II, III, IV, VI	3, 5	40, 80	250x85, 310x125	1.2, 2.4
H_a (m)	20, 40	2.4, 3.6	II, VI	2.5, 3, 4, 5	40, 80	250x85, 310x125	1.2, 2.4
C_u (kPa)	20, 40	2.4, 3.6	II, VI	3, 5	20 40, 80, 120	250x85, 310x125	1.2, 2.4
HP	20, 40	2.4, 3.6	II, VI	3, 5	40, 80	200x54, 250x85, 310x110 310x125	1.2, 2.4
PS (m)	20, 40	2.4, 3.6	II, VI	3, 5	40, 80	250x85, 310x125	1.2, 1.8, 2.4, 3.0

L: Span Length, S: Girder Spacing, GT: Girder Type, H_a: Abutment Height, C_u: Undrained shear strength of soil, HP: Pile size, PS: Pile spacing

8.2 BEHAVIOUR OF ABUTMENTS AND PILES OF IBs UNDER LIVE LOAD EFFECTS

8.2.1 BEHAVIOR OF ABUTMENTS AND PILES AS A FUNCTION OF THE SUPERSTRUCTURE PROPERTIES

In this section, the distribution of live load effects within the abutment and piles of IBs is studied in detail as a function of the superstructure parameters. This is done to identify those parameters that most influence the distribution of live load effects within the abutment and piles. For this purpose, first, a short and a long IB, with span lengths of 15 m. and 45 m. are considered to study the effect of the span length. Both bridges have seven AASHTO Type IV girders spaced at 2.4 m. Although AASHTO Type IV girders may not be suitable for both the 15 m and 45 m long IBs, this average girder size is deliberately considered to decouple the effect of the span length from the girder size. The slab is assumed to be 0.2 m thick. For both bridges, their 3 m tall and 1 m thick abutments are supported by seven HP250x85 piles. Both bridges are then analyzed under AASHTO truck loading. The analysis results are depicted in Figs. 8.1 (a) and (b). These figures display the variation of the LLDFs for the abutment and pile moments *(M)* and shears *(V)* across the width of the 15 m and 45 m long IBs, respectively. In the horizontal axis, the girder numbers (note that the piles are also aligned with the girder locations and hence the girder number refers to the position of each pile as well) are used to determine the position across the width of the bridge. Such an illustration will enable the reader to assess the concentrated effects transferred from specific girders to the abutments and piles. For both bridges, the influence line analyses revealed a truck position in the vicinity of the mid-span to produce the maximum moment and shear within the abutment and piles. Consequently, in the case of the longer span IB, the larger distance of the truck axles to the abutment produces a flared, the distribution of live load moment changes more gradually across the width of the abutment. The live load moment distribution within the abutment shown in Fig. 8.3(a) also confirms this statement. However, in the case of the shorter span IB, because of the shorter distance of the truck axles to the abutment, the distribution of the live load effects are relatively more concentrated. This obviously results in larger LLDFs for the abutments of shorter IBs as observed from the live load moment distribution within the abutment shown in Fig. 8.3(b). For instance, for the 15 m long IB, the LLDF for the abutment moment (M_a) obtained from FEAs is 0.95. However, for the longer, 45 m span IB, the LLDF for the abutment moment is obtained as 0.61. This clearly indicates that the effect of the span length on the distribution of live load moment is significant and must be considered as a dominant parameter in the development of LLDE for the abutment moment.

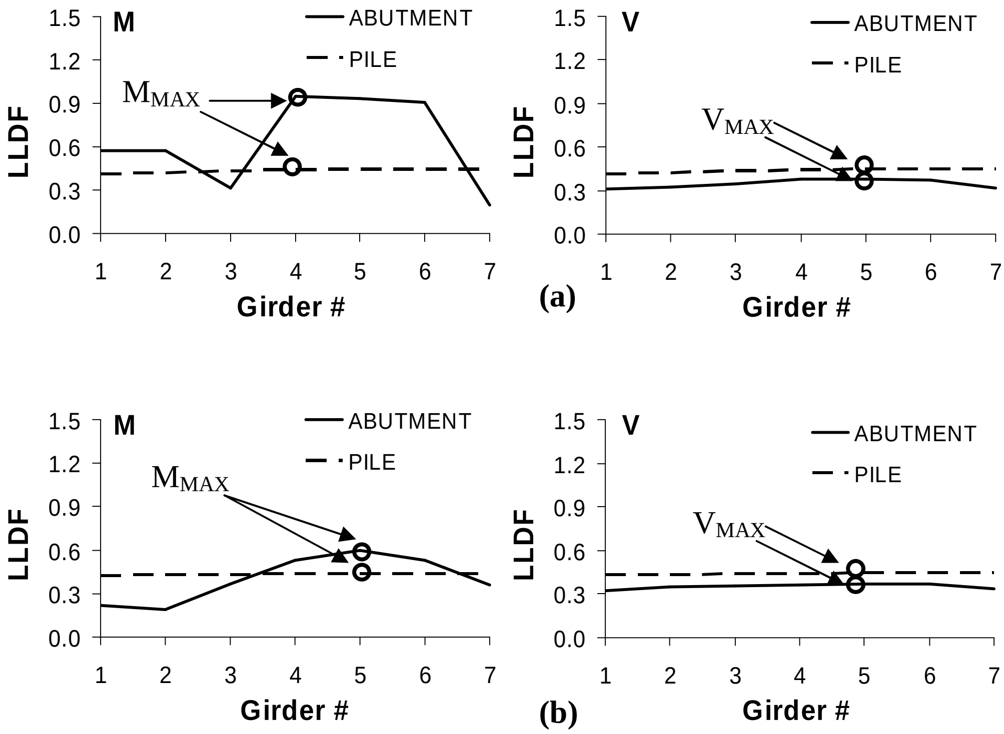

Figure 8.1 Distribution of live load effects among the piles and abutment for the IBs with span lengths of (a) 15 m (b) 45 m

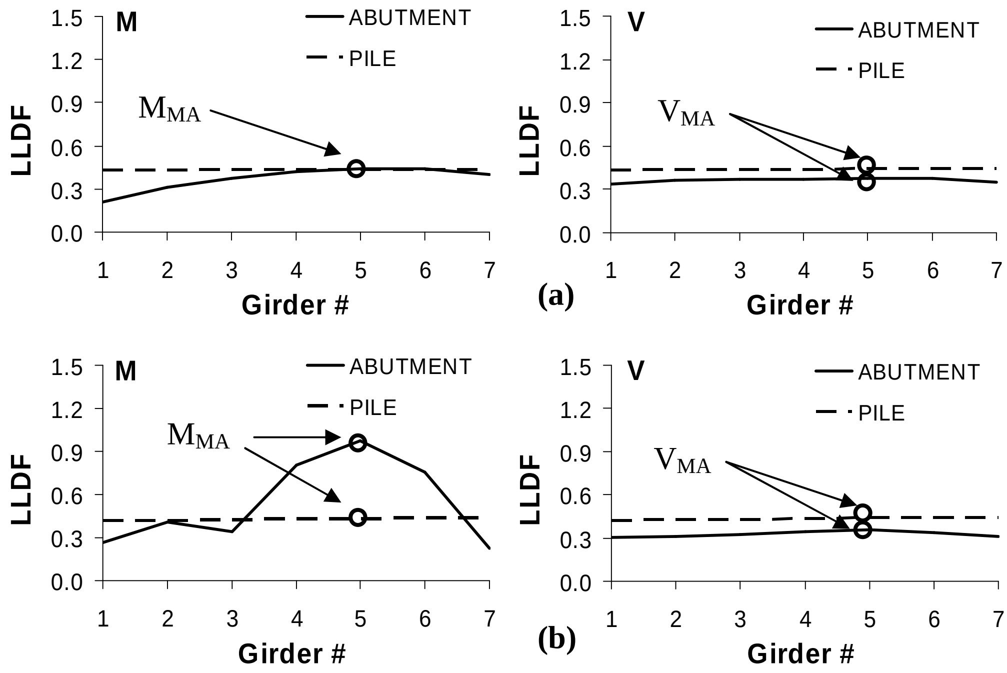

Figure 8.2 Distribution of live load effects among the piles and abutment for the IBs with AASHTO Type girders of (a) II (b) VI

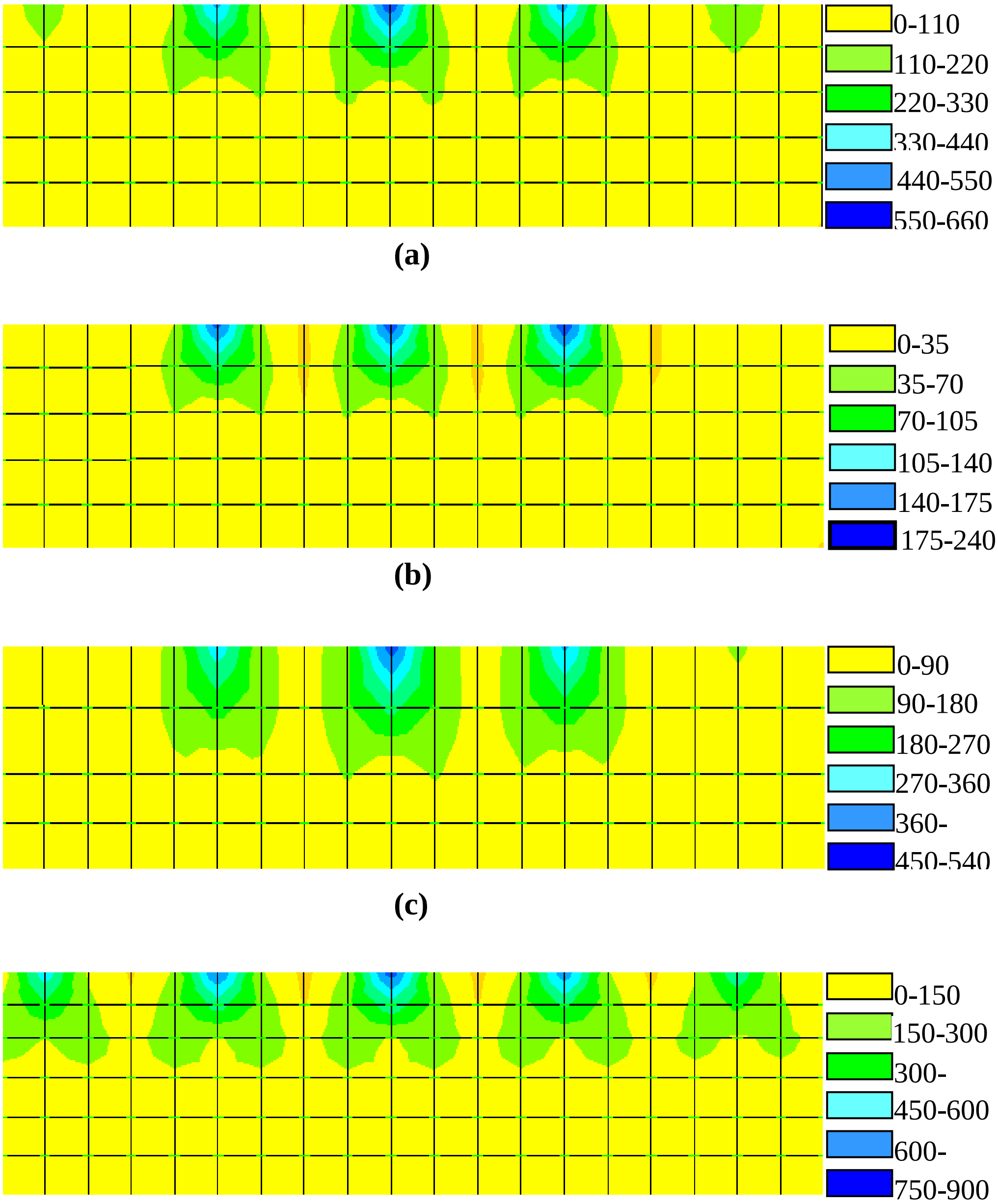

(a)

(b)

(c)

(d)

Figure 8.3 Moment distribution due to live load effects in the abutment for the IBs with (a) span lengths of 45 m (b) span lengths of 15 m (c) AASHTO Type VI girder (d) AASHTO Type II girder

It is noteworthy that as observed from Figs. 8.3 (a) and (b), the flexural live load distribution becomes more uniform away from the girders (closer to the bottom of the abutment). This leads to a more uniform distribution of live load effects among the piles as observed from Figs. 8.1(a) and (b). In the case of the abutment shear (*V*) (Fig. 8.1 (a) and (b)), the live load distribution is also more uniform. This is because; the shear effects within the abutment are largely produced by the horizontal resistance of the piles supporting the abutment, which also have a uniform distribution of live load shear. Accordingly, it may be concluded that the span length has only a negligible effect on the distribution of live load shear in the abutment and live load shear and moment in the piles. Thus, it need not be considered in the development of LLDEs for the abutment shear and pile moment and shear.

Next, the effect of the girder size on live load distribution within the abutment and piles is investigated. For this purpose, two IBs with AASHTO Type II and VI girders are considered. Both bridges are assumed to have 40 m. span length and 0.2 m thick slab supported by seven girders spaced at 2.4 m. Although a 40 m span can not be crossed with AASHTO Type II girders, the same span length as that of the AASHTO Type VI girders is deliberately considered to decouple the effect of the girder size from the span length. For both bridges, their 3 m tall and 1 m thick abutments are supported by seven HP250x85 piles. Both bridges are then analyzed under AASHTO truck loading. The analysis results are depicted in Figs. 8.2 (a) and (b). The figures show the variation of the LLDFs for the abutment and pile moments *(M)* and shears *(V)* across the width of the IBs with AASHTO Type II and VI girders, respectively. In the case of the IBs supported by larger girders, because of the higher flexural stiffness relative to the abutment, the distribution of the live load effects are relatively more concentrated (less uniform) as observed from Figs 8.3 (c) and (d). This obviously results in larger LLDFs for the abutments of IBs supported by stiffer girders as observed from Figs. 8.2 (a) and (b). For instance, for the IB supported by type VI girder, the LLDF for the abutment moment (M_a) obtained from FEAs is 0. 98. However, for the IB supported by type II girder, the LLDF for the abutment moment is obtained as 0.44. This clearly indicates that the effect of the girder size (stiffness) on the distribution of live load moment is significant and must be considered as a dominant parameter in the development of LLDE for the abutment moment. However, as observed from Figs. 8.2, the girder size (stiffness) has only a negligible effect on the distribution of live load shear in the abutment and live load shear and moment in the piles. Thus, it need not be considered in the development of LLDEs for the abutment shear and pile moment and shear.

The effect of the number of girders and girder spacing on live load distribution within the abutment and piles is also investigated. The ratio of the girder spacing (S) to the number of girders (N_b) (or bridge width), S/N_b, is found to represent the effect of both the number of girders and girder spacing. Accordingly, two narrow and two wide IBs, with girder spacings of 2.4 m and 3.6 m are considered. The IBs have 45 m span length and 0.2 m thick slab supported by AASHTO Type VI girders. The widths of the narrower IBs are 12 m. and have five and four girders for the cases of 2.4 and 3.6 m. girder spacings, respectively. The widths of the wider IBs are 15.6 m. and have seven and five girders for the cases of 2.4 and 3.6 m. girder spacings, respectively. The bridges are assumed to have 3 m tall and 1 m thick abutments supported by HP250x85 piles. The bridges are analyzed under AASHTO truck loading. The analyses results reveal that in the case of the wider IB with smaller girder spacing (or larger number of girders), the better distribution of the live effects among the girders produces a more uniform distribution of the live load effects within the abutments and piles as well. This obviously results in smaller LLDFs for the abutments and piles of wider (or bridges with larger number of girders) IBs with smaller girder spacings. For instance, for the narrower IBs, with girder spacings of 2.4 m. (S/N_b = 480 mm) and 3.6 m. (S/N_b = 900 mm), the LLDFs for the abutment moment (M_a) are 0.61 and 1.02, respectively. Nevertheless, for the wider IBs, with girder spacings of 2.4 m. (S/N_b i= 342 mm) and 3.6 m. (S/N_b = 720 mm), the LLDFs for the abutment moment (M_a) are 0.53 and 0.83, respectively. In the case of the abutment shear, for the narrower IBs, with girder spacings of 2.4 m. (S/N_b = 480 mm) and 3.6 m. (S/N_b = 900 mm), the LLDFs (V_a) are 0.47 and 0.66, respectively. On the other hand, for the wider IBs, with girder spacings of 2.4 m. (S/N_b = 342 mm) and 3.6 m. (S/N_b = 720 mm), the LLDFs for the abutment shear (V_a) are 0.37 and 0.61, respectively. Similar results are also obtained for the pile LLDFs. Accordingly, it may be concluded that the effect of the ratio of the girder spacing to number of girders (S/N_b) on the distribution of live load moment and shear is significant and must be considered as a dominant parameter in the development of LLDEs for the abutments and piles of IBs.

The earlier study (Erhan and Dicleli 2010) also reveals that the slab thickness has only a negligible effect on the distribution of live load moment and shear in the abutments and piles. Thus, it need not be considered in the development of LLDEs for the abutment and pile shear and moment.

8.2.2 BEHAVIOR OF ABUTMENTS AND PILES AS A FUNCTION OF SUBSTRUCTURE PARAMETERS

The earlier research study by Dicleli and Erhan (2008) revealed that the abutment height measured from the deck soffit (H_c) have considerable effects on the distribution of live load moment and shear within the abutments and piles. Accordingly, the effect of H_c on the distribution of live load moment and shear in the abutment and pile must be considered as a dominant parameter in the development of LLDEs for the abutment and pile. Furthermore, moment of inertia (I_p) and number of piles (N_p) as well as the undrained shear strength of the foundation soil (C_u) were also found to have significant effects on the distribution of live load moment in the abutments. However, the effect of I_p, N_p and C_u on the distribution of live load shear in the abutment as well as moment and shear in the pile were found to be negligible. Thus, while the effect of I_p, N_p and C_u on the distribution of live load within the abutment must be considered in the development of LLDEs for the abutment moment, the same parameters need not be considered in the development of LLDEs for the abutment shear as well as pile moment and shear.

8.3 LIVE LOAD DISTRIBUTION EQUATIONS FOR THE PILES

In this section, LLDEs are developed for the piles of IBs for the cases where one design lane and two or more design lanes are loaded. In the developed equations all the parameters are measured in mm.

The analyses results revealed that the number of girders (N_b) (or bridge width) and their spacing (S) and the abutment height measured from the deck soffit (H_c) have considerable effects on the distribution of live load moment and shear in the piles. However, the effects of the other substructure and superstructure parameters considered in the analyses are found to be negligible. Therefore, LLDEs for the piles are developed as a function of the three parameters mentioned above. Details about the development of LLDEs for the IB piles for two or more design lane and one design lane loaded cases are given in the following subsections.

8.3.1 LLDE FOR PILE MOMENT - TWO OR MORE DESIGN LANES LOADED CASE

Based on the trend of the data obtained from the analyses, the LLDE for the pile moment ($LLDE^{P}_{M-2L}$) is assumed to have the following form;

$$LLDE^{P}_{M-2L} = a.(S/N_b)^{b1}.H_c^{b2} \tag{8.1}$$

where a, $b1$, $b2$ = constants to be determined via regression analyses using the available data. A sample of data representing the LLDFs for the pile moment is given in Table 8.2. To obtain the constants in Eqn. (8.1), first, LLDFs obtained from FEAs for the two or more design lanes loaded case are plotted as a function of, S/N_b as shown in Fig. 8.4(a). Then, the minimum least square fit of the logarithm of the S/N_b- *LLDF* data is performed to obtain the following equation;

$$R_1 = 0.022\left(\frac{S}{N_b}\right)^{0.49} \tag{8.2}$$

The above equation, which is plotted using a thick solid line in Fig. 8.4 (a), gives the LLDFs for the pile moment obtained from FEA as a function of S/N_b. The term $(S/N_b)^{0.49}$ in Eqn. (8.2), represents the term $(S/N_b)^{b1}$ in Eqn (8.1). Thus, $b1$=0.49. The scatter present in Fig. 8.4 (a) with respect to the plot of Eqn. (8.2) is mainly due to the error introduced by the absence of the other parameter, H_c, in the equation. This error will be corrected by involving the effect of the remaining parameter in the equation. For this purpose, first, the ratio, R_2, of the FEA results to those obtained from Eqn (8.2) is calculated as;

$$R_2 = \frac{FEA}{R_1} \tag{8.3}$$

This is done to decouple the FEA results from the effect of the S/N_b ratio. Then, the ratio R_2 is plotted as a function of H_c, in Fig. 8.4(b). Next, the minimum least square fit of the logarithm of the data presented in Fig. 8.4(b) is performed to obtain the following equation;

$$R_2 = 0.68\,H_c^{\;0.07} \tag{8.4}$$

Finally, The LLDE for the pile moment for two or more design lane loaded case is obtained by multiplying R_1 by R_2. The final form of the LLDE is as follows;

$$LLDE_{M-2L}^{P} = \frac{1}{66}\left(\frac{S}{N_b}\right)^{0.5} H_c^{\;0.05} \tag{8.5}$$

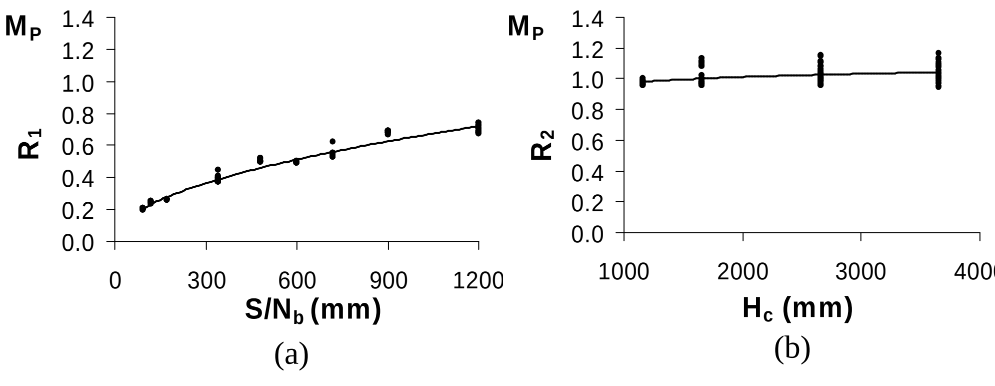

Figure 8.4 (a) R_1 versus S/N_b plot and minimum least square fit, (b) R_2 versus H_c plot and minimum least square fit for the pile moment LLDEs in the case of two or more loaded design lanes

Table 8.2. Pile live load distribution factors

PARAMETER							LLDF			
							MOMENT		SHEAR	
S (m)	L (m)	GT	H (m)	C_u (m)	d_p (m)	N_p	One design lane loaded	Two or more design lane loaded	One design lane loaded	Two or more design lane loaded
1.2	20	2	3	40	0.25	13	0.10	0.20	0.10	0.20
2.4	20	2	3	40	0.25	13	0.19	0.37	0.19	0.38
3.6	20	2	3	40	0.25	13	0.26	0.53	0.27	0.54
4.8	20	2	3	40	0.25	13	0.34	0.68	0.34	0.69
1.2	20	2	3	40	0.25	7	0.10	0.20	0.10	0.20
2.4	20	2	3	40	0.25	7	0.18	0.37	0.19	0.38
3.6	20	2	3	40	0.25	7	0.26	0.53	0.26	0.53
4.8	20	2	3	40	0.25	7	0.33	0.68	0.33	0.69
1.2	20	2	5	40	0.25	13	0.10	0.21	0.10	0.21
2.4	20	2	5	40	0.25	13	0.20	0.39	0.20	0.39
3.6	20	2	5	40	0.25	13	0.28	0.55	0.29	0.55
4.8	20	2	5	40	0.25	13	0.36	0.72	0.37	0.73
1.2	20	2	5	40	0.25	7	0.10	0.20	0.10	0.21
2.4	20	2	5	40	0.25	7	0.19	0.38	0.20	0.39
3.6	20	2	5	40	0.25	7	0.28	0.55	0.29	0.56
4.8	20	2	5	40	0.25	7	0.36	0.73	0.37	0.74
2.4	20	2	4	40	0.25	13	0.20	0.41	0.20	0.41
3.6	20	2	4	40	0.25	13	0.28	0.55	0.27	0.53
2.4	20	2	4	40	0.25	7	0.20	0.40	0.20	0.40
3.6	20	2	4	40	0.25	7	0.27	0.54	0.28	0.55
2.4	20	2	2.5	40	0.25	13	0.18	0.37	0.19	0.38
3.6	20	2	2.5	40	0.25	13	0.26	0.53	0.26	0.53
2.4	20	2	2.5	40	0.25	7	0.19	0.38	0.19	0.38
3.6	20	2	2.5	40	0.25	7	0.26	0.54	0.27	0.54
2.4	20	2	3	40	0.25	10	0.20	0.37	0.20	0.39
3.6	20	2	3	40	0.25	10	0.27	0.53	0.28	0.53
2.4	20	2	3	40	0.25	5	0.19	0.38	0.19	0.38
3.6	20	2	3	40	0.25	5	0.26	0.53	0.26	0.53
2.4	20	2	5	40	0.25	10	0.20	0.39	0.20	0.39
3.6	20	2	5	40	0.25	10	0.29	0.55	0.29	0.57
2.4	20	2	5	40	0.25	5	0.22	0.45	0.20	0.41
3.6	20	2	5	40	0.25	5	0.30	0.62	0.29	0.60

8.3.2. LLDE FOR PILE MOMENT – ONE DESIGN LANE LOADED CASE

Following a procedure similar to that described above, the LLDE for the pile moment for the one design lane loaded case is obtained as;

$$LLDE^{P}_{M-1L} = \frac{1}{160}\left(\frac{S}{N_b}\right)^{0.5} H_c^{\ 0.07} \tag{8.6}$$

8.3.3. LLDES FOR PILE SHEAR - TWO OR MORE DESIGN LANES LOADED CASE

Based on the trend of the data obtained from the analyses, the LLDE for the pile shear ($LLDE^{P}_{V-2L}$) is assumed to have the following form;

$$LLDE^{P}_{V-2L} = a.(S/N_b)^{b1}.H_c^{b2} \tag{8.7}$$

Following a procedure similar to that described for the derivation of the LLDE for the pile moment, the LLDE for the pile shear for the two or more design lanes loaded case is obtained as;

$$LLDE^{P}_{V-2L} = \frac{1}{60}\left(\frac{S}{N_b}\right)^{0.5} H_c^{\ 0.04} \tag{8.8}$$

8.3.4. LLDES FOR PILE SHEAR - ONE DESIGN LANE LOADED CASE

Following a procedure similar to that described above, the LLDE for the abutment shear for the one design lane loaded case is obtained as;

$$LLDE^{P}_{V-1L} = \frac{1}{145}\left(\frac{S}{N_b}\right)^{0.5} H_c^{\,0.06} \tag{8.9}$$

8.4 LIVE LOAD DISTRIBUTION EQUATIONS FOR THE ABUTMENTS

In this section, LLDEs are developed for the abutments of IBs for the cases where one design lane and two or more design lanes are loaded. In the developed equations, C_u is measured in kPa. However, all the other parameters are measured in mm.

The analyses results revealed that the girder spacing (S), number of girders (N_b) (or bridge width), girder stiffness parameter (K_g), span length (L), abutment height (H_c), moment of inertia (I_p) and number of piles (N_p) as well as the undrained shear strength of the foundation soil (C_u) have considerable effects on the distribution of live load moment in the abutment. Therefore, the LLDEs for the abutment moment are developed as a function of these parameters. However, the distribution of live load shear in the abutment is only affected by the girder spacing, number of girders and abutment height. Accordingly, the abutment shear LLDEs are developed as a function of these three parameters only. The details about the development of abutment LLDEs for two or more design lane and one design lane loaded cases are given in the following subsections.

8.4.1 LLDES FOR ABUTMENT MOMENT - TWO OR MORE DESIGN LANES LOADED CASE

Based on the trend of the data obtained from FEAs, the LLDEs for the abutment moment ($LLDE^{A}_{M-2L}$) is assumed to have the following form;

$$LLDE^{A}_{M-2L} = a.\left(\frac{S}{N_b}\right)^{b1}.K_g^{\;b2}.H_c^{b3}.L^{b4}.I_p^{b5}.\mu^{b6}.\left(\frac{N_p}{N_b}\right)^{b7} \tag{8.10}$$

In the above equation; μ is a parameter that represents the stiffness of the foundation soil surrounding the piles. It is expressed as follows (Haliburton 1971);

$$\mu = \frac{C_u.d_P}{\varepsilon_{50}} \tag{8.11}$$

where, C_u is the undrained shear strength of the foundation soil, d_p is the pile width and ε_{50} is the soil strain at 50% of the ultimate soil resistance. The term K_g in Eqn. (8.10) is a parameter representing the longitudinal stiffness of the composite slab-on-girder section of the bridge expressed as (AASHTO 2007);

$$K_g = n\left(I + Ae_g^2\right) \tag{8.12}$$

where, n is the ratio of the modulus of elasticity of the girder material to that of the slab material, I is the moment of inertia of the girder, A is the cross-sectional area of the girder and e_g is the distance between the centers of gravity of the girder and the slab. In Eqn.(8.10), a, *b1*, *b2, b3*, *b4, b5, b6 and b7* are constants that need to be determined via regression analyses using the available FEA data partially presented in Table 4. To obtain these constants, first, LLDFs obtained from FEAs are plotted as a function of S/N_b as shown in Fig. 8.5 (a). Then, the minimum least square fit of the logarithm of the S/N_b-*LLDF* data is performed to obtain the following equation;

$$R_1 = 0.034\left(\frac{S}{N_b}\right)^{0.49} \tag{8.13}$$

The above equation, which is plotted using a thick solid line in Fig. 8.5 (a), gives the LLDFs for the abutment moment obtained from FEA as a function of S/N_b. The term $(S/N_b)^{0.49}$ in Eqn. (8.13), represents the term $(S/N_b)^{b1}$ in Eqn (8.10). Thus, $b1$=0.49. The scatter present in Fig. 8.5 (a) with respect to the plot of Eqn. (8.13) is mainly due to the error introduced by the absence of the other parameters in the equation. This error will be corrected by involving the effect of the remaining parameters in the equation. For this purpose, first, the ratio, R_2, of the FEA results to those obtained from Eqn. (8.13) is calculated as;

$$R_2 = \frac{FEA}{R_1} \tag{8.14}$$

This is done to decouple the FEA results from the effect of the term, S/N_b. Then, the ratio R_2 is plotted as a function of the longitudinal stiffness parameter of the composite slab-on-girder section of the bridge (K_g), in Fig.

8.5(b). Next, the minimum least square fit of the logarithm of the data presented in Fig. 8.5 (b) is performed to obtain the following equation;

$$R_2 = 0.0061 K_g^{\ 0.19} \tag{8.15}$$

The above equation is plotted using a thick solid line in Fig. 8.5 (b). The term $K_g^{0.19}$ in Eqn. (8.15), represents the term K_g^{b2} in Eqn (8.10). Thus, $b2$=0.19. To calculate the parameter, $b3$, in Eqn (8.10), a similar procedure is followed. First, a new ratio R_3 is calculated as;

$$R_3 = \frac{FEA}{R_1 \times R_2} \tag{8.16}$$

Then, the ratio R_3 is plotted as a function of (H_c), in Fig. 8.5(c). Next, the minimum least square fit of the logarithm of the data presented in Fig. 8.5(c) is performed to obtain the following equation;

$$R_3 = 6.93 H_c^{-0.25} \tag{8.17}$$

The above equation is plotted using a thick solid line in Fig. 8.5(c). The term $H_c^{-0.25}$ in Eqn. (8.17) represents the term H_c^{b3} in Eqn.(8.10). Thus, $b3$=-0.25. Next, to obtain the term $b4$, a new ratio R_4 is calculated as;

$$R_4 = \frac{FEA}{R_1 \times R_2 \times R_3} \tag{8.18}$$

Then, the ratio, R_4, is plotted as a function of the span length (L), in Fig. 8.5(d). Next, the minimum least square fit of the logarithm of the data presented in Fig. 8.5 (d) is performed to obtain the following equation;

$$R_4 = 11.31L^{-0.24} \tag{8.19}$$

The above equation is plotted using a thick solid line in Fig. 8.5 (d). The term $L^{-0.24}$ in Eqn. (8.19) represents the term L^{b4} in Eqn (8.10). Thus, $b4$=-0.24. To obtain the term $b5$, a new ratio R_5 is calculated as;

$$R_5 = \frac{FEA}{R_1 \times R_2 \times R_3 \times R_4} \tag{8.20}$$

Then, the ratio R_5 is plotted as a function of moment of inertia of the piles (I_p), in Fig. 8.5(e). Next, the minimum least square fit of the logarithm of the data presented in Fig. 8.5(e) is performed to obtain the following equation;

$$R_5 = 4.28I_p^{-0.08} \tag{8.21}$$

The above equation is plotted using a thick solid line in Fig. 8.5(e). The term $I_p^{-0.08}$ in Eqn. (8.21) represents the term I_p^{b5} in Eqn (8.10). Thus, $b5$=-0.08. Subsequently, to obtain the term $b6$, a new ratio R_6 is calculated as;

$$R_6 = \frac{FEA}{R_1 \times R_2 \times R_3 \times R_4 \times R_5} \tag{8.22}$$

Then, the ratio R_6 is plotted as a function of (μ), in Fig. 8.5(f). Next, the minimum least square fit of the logarithm of the data presented in Fig. 8.5(f) is performed to obtain the following equation;

$$R_6 = 2.16\mu^{-0.06} \tag{8.23}$$

The above equation is plotted using a thick solid line in Fig. 8.5(f). The term

$\mu^{-0.06}$ in Eqn. (8.23) represents the term μ^{b6} in Eqn (8.10). Thus, $b6$=-0.06. Finally, to obtain the terms a and $b7$, a new ratio R_7 is calculated as;

$$R_7 = \frac{FEA}{R_1 \times R_2 \times R_3 \times R_4 \times R_5 \times R_6} \tag{8.24}$$

Then, the ratio R_7 is plotted as a function of (N_p/N_b), in Fig. 8.5(g). Next, the minimum least square fit of the logarithm of the data presented in Fig. 8.5(g) is performed to obtain the following equation;

$$R_7 = 1.03\left(\frac{N_p}{N_b}\right)^{-0.06} \tag{8.25}$$

The above equation is plotted using a thick solid line in Fig. 8.5(g). The term $(N_p/N_b)^{-0.06}$ in Eqn. (8.25), represents the term $(N_p/N_b)^{b7}$ in Eqn (8.10). Thus, $b7$=-0.06. The LLDE for the abutment moment of IBs is obtained by solving for FEA in Eqn. (8.24) (i.e. $FEA=LLDE^{ABUTMENT}=R_1 x R_2 x R_3 x R_4 x R_5 x R_6 x R_7$). Accordingly, the constant, a in Eqn (8.10) is obtained by multiplying the coefficients in front of the variables, S/N_b, K_g, H_c, L, I_p, μ, N_p/N_b in Eqns. (8.13), (8.15), (8.17), (8.19), (8.21), (8.23) and (8.25), respectively. Thus, a= $0.034 x 0.061 x 6.93 x 11.31 x 4.28 x 2.16 x 1.03$=1/7. The final form of the LLDE becomes;

$$LLDE^{A}_{M-2L} = \frac{S^{0.5}.K_g^{\,0.2}}{7.N_b^{\,0.44}.H_c^{\,0.25}.L^{0.25}.I_p^{\,0.08}.\mu^{0.06}.N_p^{\,0.06}} \tag{8.26}$$

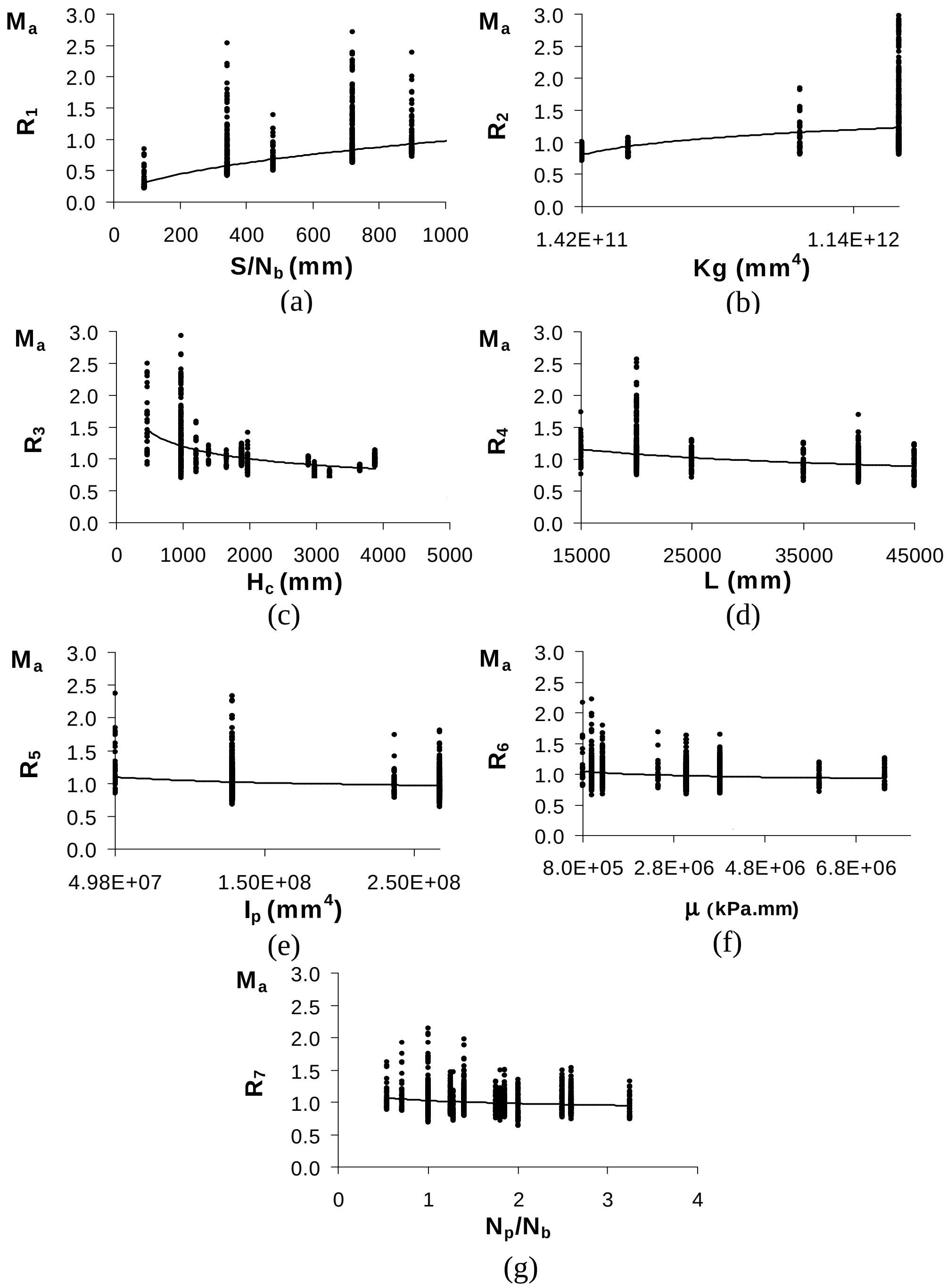

Figure 8.5 (a) R_1 versus S/N_b plot and minimum least square fit, (b) R_2 versus K_g plot and minimum least square fit (c) R_3 versus H_c plot and minimum least square fit (d) R_4 versus L plot and minimum least square fit (e) R_5 versus I_p plot and minimum least square fit (f) R_6 versus μ plot and minimum least square fit (d) R_7 versus N_p/N_b plot and minimum least square fit for the abutment moment LLDEs in the case of two or more loaded design lanes

Table 8.3. Abutment live load distribution factors

PARAMETER							LLDF			
							MOMENT		SHEAR	
S (m)	L (m)	GT	H (m)	C_u (m)	d_p (m)	N_p	One design lane loaded	Two or more design lane loaded	One design lane loaded	Two or more design lane loaded
1.2	20	2	3	40	0.25	13	0.21	0.27	0.10	0.20
1.2	20	2	3	80	0.25	13	0.19	0.26	0.10	0.20
1.2	20	2	3	40	0.31	13	0.19	0.26	0.10	0.20
1.2	20	2	3	80	0.31	13	0.19	0.26	0.09	0.20
2.4	20	2	3	40	0.25	13	0.36	0.51	0.17	0.38
2.4	20	2	3	80	0.25	13	0.33	0.50	0.18	0.39
2.4	20	2	3	40	0.31	13	0.32	0.47	0.18	0.38
2.4	20	2	3	80	0.31	13	0.32	0.48	0.18	0.39
3.6	20	2	3	40	0.25	13	0.49	0.78	0.29	0.60
3.6	20	2	3	80	0.25	13	0.47	0.68	0.27	0.60
3.6	20	2	3	40	0.31	13	0.47	0.77	0.29	0.60
3.6	20	2	3	80	0.31	13	0.45	0.75	0.30	0.61
4.8	20	2	3	40	0.25	13	0.56	0.90	0.35	0.72
4.8	20	2	3	80	0.25	13	0.54	0.89	0.35	0.73
4.8	20	2	3	40	0.31	13	0.54	0.89	0.35	0.72
4.8	20	2	3	80	0.31	13	0.52	0.89	0.36	0.74
1.2	40	6	3	40	0.25	13	0.52	0.47	0.10	0.19
1.2	40	6	3	80	0.25	13	0.39	0.39	0.10	0.19
1.2	40	6	3	40	0.31	13	0.39	0.37	0.10	0.19
1.2	40	6	3	80	0.31	13	0.31	0.34	0.10	0.19
2.4	40	6	3	40	0.25	13	0.59	0.80	0.18	0.37
2.4	40	6	3	80	0.25	13	0.48	0.68	0.19	0.37
2.4	40	6	3	40	0.31	13	0.48	0.69	0.18	0.37
2.4	40	6	3	80	0.31	13	0.41	0.61	0.19	0.38
3.6	40	6	3	40	0.25	13	0.80	1.15	0.28	0.57
3.6	40	6	3	80	0.25	13	0.65	1.01	0.29	0.59
3.6	40	6	3	40	0.31	13	0.64	1.01	0.29	0.58
3.6	40	6	3	80	0.31	13	0.56	0.92	0.30	0.61
4.8	40	6	3	40	0.25	13	0.89	1.23	0.33	0.73
4.8	40	6	3	80	0.25	13	0.74	1.11	0.34	0.73
4.8	40	6	3	40	0.31	13	0.74	1.12	0.34	0.74
4.8	40	6	3	80	0.31	13	0.65	1.04	0.35	0.72

8.4.2 LLDES FOR ABUTMENT MOMENT – ONE DESIGN LANE LOADED CASE

Following a procedure similar to that described above, the LLDE for the abutment moment for the one design lane loaded case is obtained as;

$$LLDE^{A}_{M-1L} = \frac{S^{0.33}.K_g^{\ 0.3}}{2.N_b^{\ 0.25}.H_c^{\ 0.3}.L^{0.53}.I_p^{\ 0.08}.\mu^{0.06}.N_p^{\ 0.08}} \qquad (8.27)$$

8.4.3 LLDES FOR ABUTMENT SHEAR - TWO OR MORE DESIGN LANES LOADED CASE

Based on the trend of the data obtained from the analyses, the LLDE for the abutment shear ($LLDE^{A}_{V-2L}$) is assumed to have the following form;

$$LLDE^{A}_{V-2L} = a.(S / N_b)^{b1}.H_c^{b2} \qquad (8.28)$$

Following a procedure similar to that described for the derivation of the LLDE for the abutment moment, the LLDE for the abutment shear for the two or more design lanes loaded case is obtained as;

$$LLDE^{A}_{V-2L} = \frac{S^{0.54}}{44.N_b^{\ 0.54}.H_c^{\ 0.04}} \qquad (8.29)$$

8.4.4 LLDES FOR ABUTMENT SHEAR– ONE DESIGN LANE LOADED CASE

Following a procedure similar to that described in the previous sections, the LLDE for the abutment shear for the one design lane loaded case is obtained as;

$$LLDE_{V-1L}^{A} = \frac{S^{0.52}}{90.N_b^{\ 0.52}.H_c^{\ 0.02}} \qquad (8.28)$$

CHAPTER 9

VERIFICATION OF THE DEVELOPED CORRECTION FACTORS AND LLDEs FOR INTEGRAL BRIDGES

9.1 VERIFICATION OF THE CORRECTION FACTORS AND LLDEs FOR INTEGRAL BRIDGES

In this section, the LLDEs derived for the girder moments of IBs are verified against the available FEA results. For this purpose, first, the LLDFs for the girder moments of IBs are calculated using (i) AASHTO LLDEs, (ii) AASHTO LLDEs multiplied by the developed correction factors (F_cxAASHTO) and (iii) the LLDEs developed for IBs independent of AASHTO (2007). The calculated LLDFs and FEA results are then plotted as a function of L, S, t_s and K_g in Figs. 9.1 and 9.2 for the interior girders and as a function of L, S, d_e and K_g in Figs. 9.3 and 9.4 for the exterior girders . Fig 9.1 (a), (b), (c) and (d) compare the calculated LLDFs and the FEA results as a function of L, S, t_s and K_g for the interior girder moments and for the case where two or more design lanes are loaded. Fig. 9.2 is similar but the comparison is performed for the case where only one design lane is loaded. In Fig. 9.3, similar comparisons are performed for the exterior girder moment considering the case where only two or more design lanes are loaded. Fig. 9.4 is similar but the comparison is performed for the exterior girder shear. As observed from the figures, the AASHTO LLDEs generally produce conservative estimates of live load girder moments and exterior girder shears in IBs for the range of values of L, S, t_s and K_g and d_e considered in this study. However, both the proposed correction factors multiplied by the AASHTO LLDEs (F_cxAASHTO) and the LLDEs proposed for IBs independent of AASHTO (2007), produce reasonable estimates of live load moments in the girders of single span, short to medium length IBs. To further verify the applicability of the proposed equations to IBs, the averages and standard deviations of the ratios of the LLDFs obtained from the proposed and AASHTO LLDEs to FEA results are presented in Table 9.1 for the entire data obtained from the analyses. The proposed correction factors and equations produce averages ranging between 1.01 and 1.07 and standard deviations ranging between 0.07 and 0.10. Nevertheless, AASHTO LLDEs produce averages ranging between 0.93 and 1.33 and standard deviations ranging between 0.17 and 0.32. This clearly indicates that the proposed correction factors and LLDEs produce more reasonable and less scattered estimates of live load effects in IB girders compared to AASHTO LLDEs.

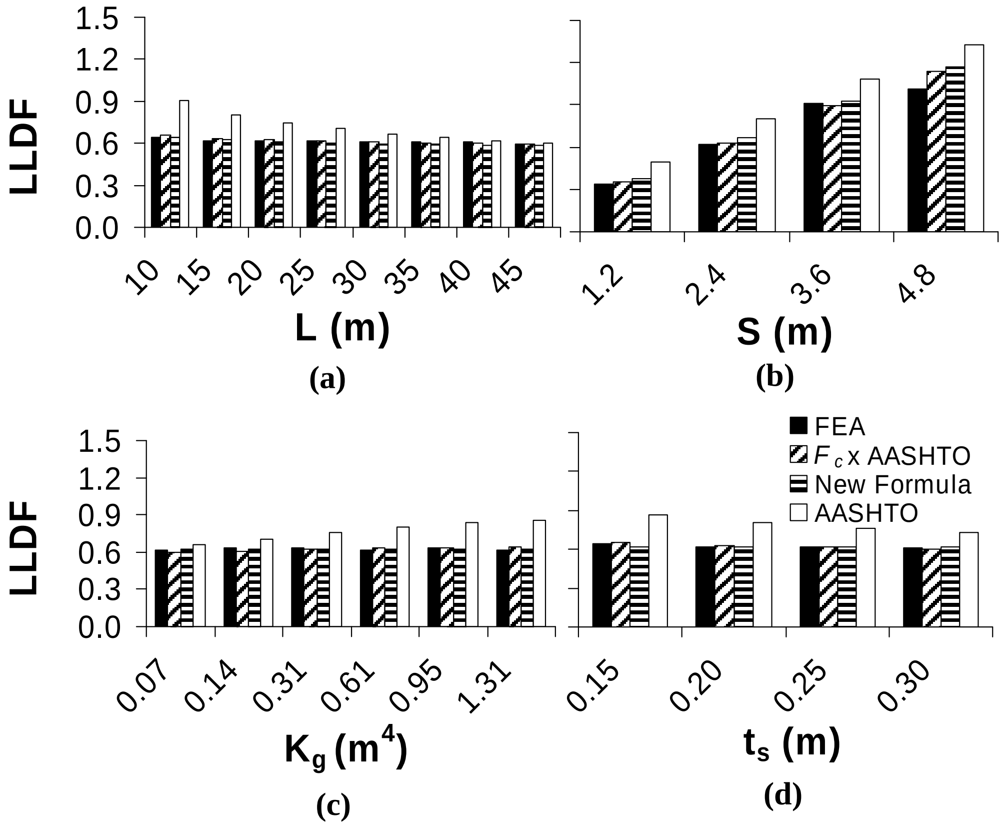

Figure 9.1 Comparison of the calculated LLDFs and FEA results for the interior girder moment of IBs and for the case where two or more design lanes are loaded as a function of (a) L, (S=2.4 m. t_s= 0.2 m, GT= IV) (b) S (L=15 m. t_s= 0.2 m, GT= IV), (c) K_g (L=15 m, S=2.4 m, t_s= 0.2 m), (d) t_s (L=15 m, S=2.4 m, GT=IV).

Table 9.1. Average and standard deviation of the ratio of the LLDFs obtained from the proposed and AASHTO LLDEs to FEA results.

		***F$_c$* x AASHTO**		**New Formula**		**AASHTO**	
	Loaded design lane	**AVG**	**STD**	**AVG**	**STD**	**AVG**	**STD**
M_{int}	**one**	1.01	0.09	1.06	0.09	1.17	0.18
	two or more	1.07	0.09	1.01	0.07	1.15	0.17
M_{ext}	**one**	1.06	0.09	1.05	0.08	1.33	0.32
	two or more	1.04	0.10	1.02	0.07	1.16	0.24
V_{ext}	**one**	1.03	0.09	1.04	0.09	0.93	0.14
	two or more	1.05	0.08	1.05	0.08	1.22	0.22

M_{int}: Interior girder moment, M_{ext}: Exterior girder moment, V_{ext}: Exterior girder shear, AVG: Average, STD: Standard deviation

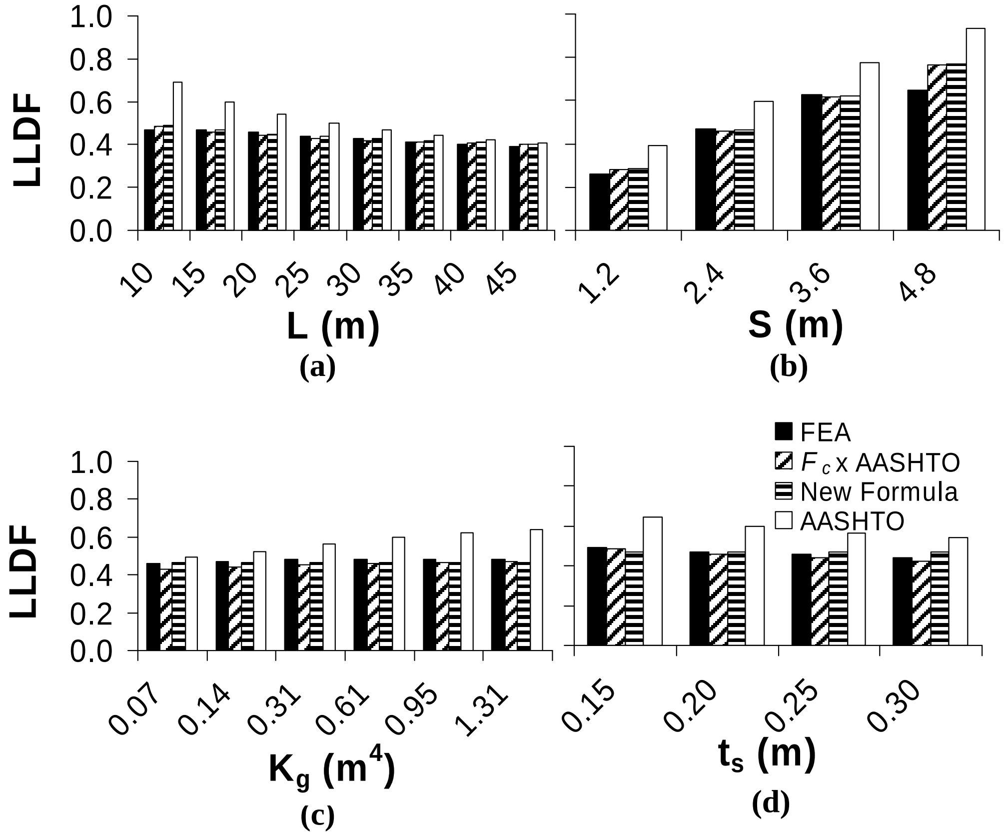

Figure 9.2 Comparison of the calculated LLDFs and FEA results for the interior girder moment of IBs and for the case where only one design lane is loaded as a function of (a) L, (S=2.4 m. t_s= 0.2 m, GT= IV) (b) S (L=15 m. t_s= 0.2 m, GT= IV), (c) K_g (L=15 m, S=2.4 m, t_s= 0.2 m), (d) t_s (L=15 m, S=2.4 m, GT=IV).

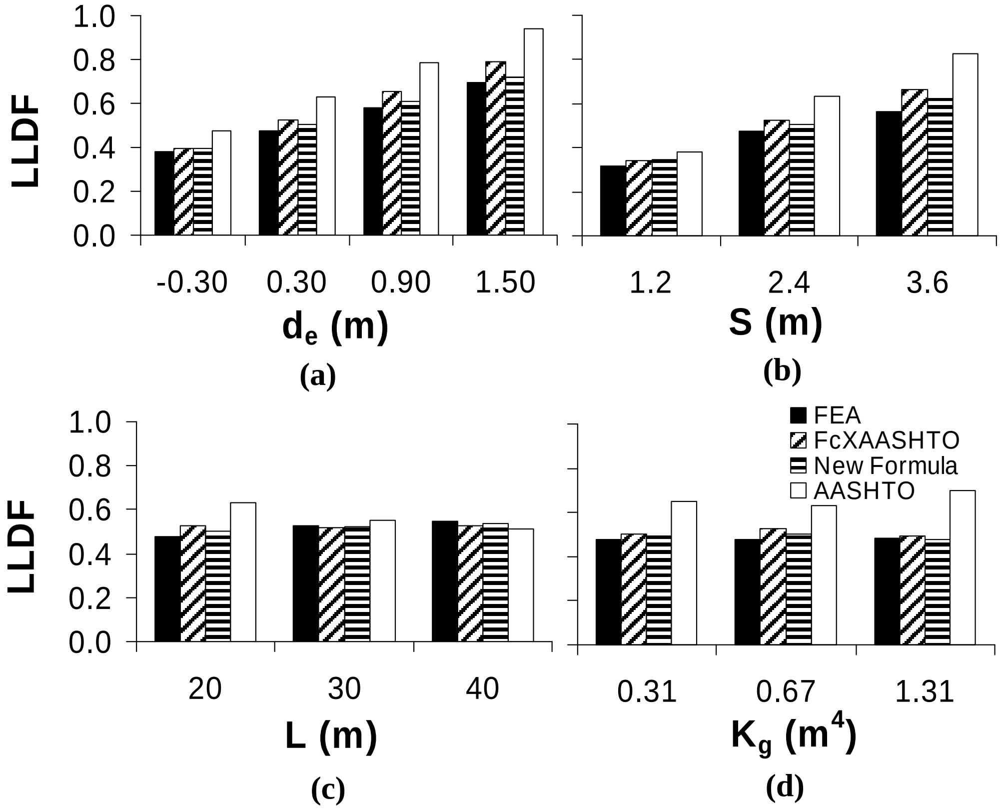

Figure 9.3 Comparison of the calculated LLDFs and FEA results for the exterior girder moment of IBs and for the case where two or more design lanes are loaded as a function of (a) *L*, (*S*=2.4 m. t_s= 0.2 m, *GT*= III, d_e=0.3) (b) *S* (*L*=20 m. t_s= 0.2 m, *GT*= III, d_e=0.3), (c) d_e (*L*=20 m, *S*=2.4 m, t_s= 0.2 m, *GT*= III), (d) K_g (*L*=20 m, *S*=2.4 m, t_s= 0.2 m, d_e=0.3).

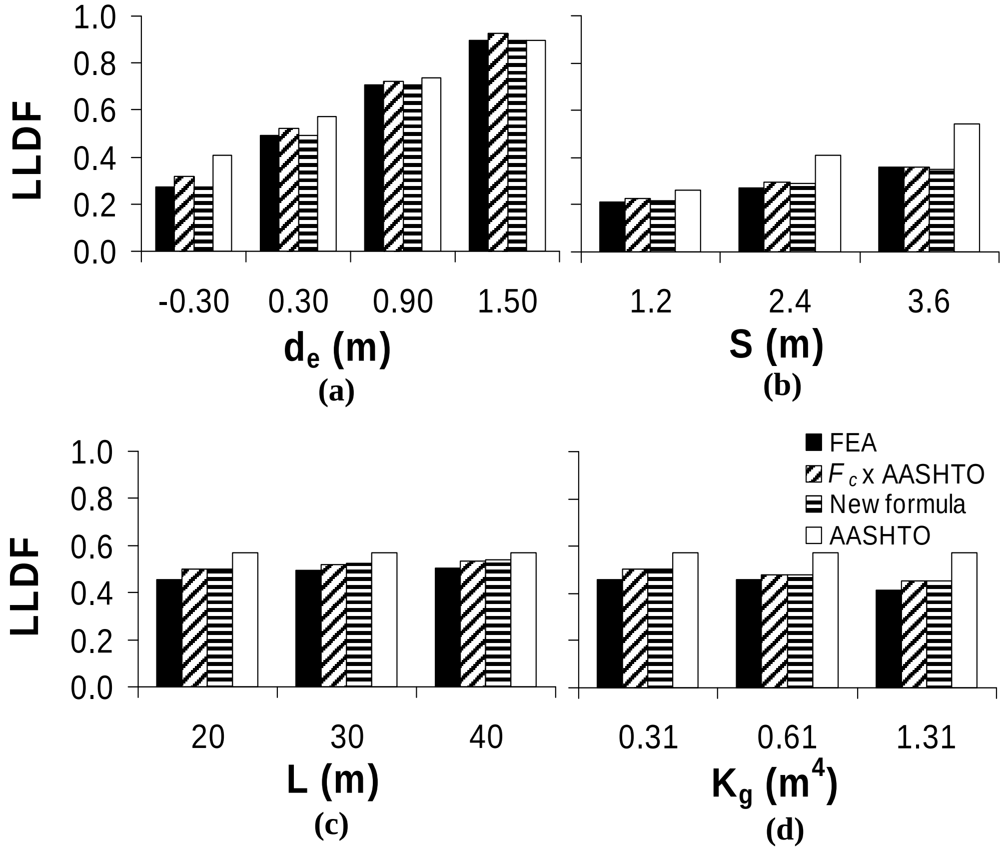

Figure 9.4 Comparison of the calculated LLDFs and FEA results for the exterior girder shear of IBs and for the case where two or more design lanes are loaded as a function of (a) *L*, (*S*=2.4 m. t_s= 0.2 m, *GT*= III, d_e=0.3) (b) *S* (*L*=20 m. t_s= 0.2 m, *GT*= VI, d_e=0.3), (c) d_e (*L*=20 m, *S*=2.4 m, t_s= 0.2 m, *GT*= III), (d) K_g (*L*=20 m, *S*=2.4 m, t_s= 0.2 m, d_e=0.3).

9.2 VERIFICATION OF THE DERIVED LLDEs FOR THE PILES

In this section, the LLDEs derived for the piles of IBs are verified against the available FEA results. For this purpose, the LLDFs for the piles of IBs are calculated using the developed equations. Then, the calculated LLDFs and FEA results are plotted as a function of the more dominant parameter, S in Figs. 9.5 and 9.6 for various abutment heights, H_c, measured from the deck soffit for the one design lane and two or more design lanes loaded cases, respectively. As observed from the Figures, the derived LLDEs produce reasonable estimates of LLDFs for the moments and shear in the piles. Furthermore, for the entire data used in the development of the LLDEs, the averages and standard deviations of the ratios of the LLDFs obtained from the derived equations to those from FEA are calculated for the pile moment and shear and presented in Table 9.2. As observed from the table, the calculated average values of the ratios range between 1.01 and 1.05 while the standard deviations are around 0.05. The small deviations of the values of the calculated average ratios from 1.0 and relatively small standard deviations also indicate that the derived equations produce reasonably good estimates of live load effects in IB piles for the range of parameters considered in this study.

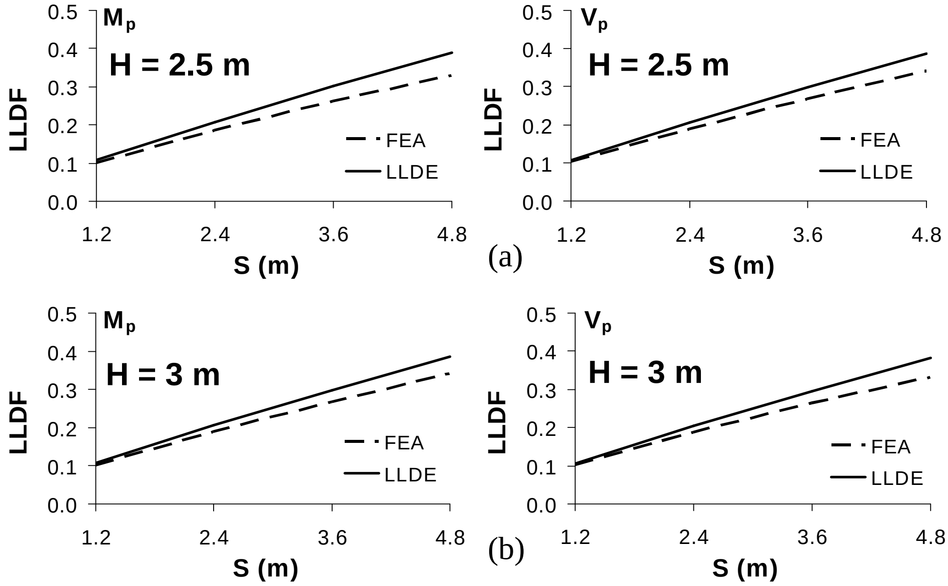

Figure 9.5 Comparison of the calculated LLDFs and FEA results for the piles of IBs where one design lane is loaded (a) 2.5 m. abutment height (b) 3 m. abutment height

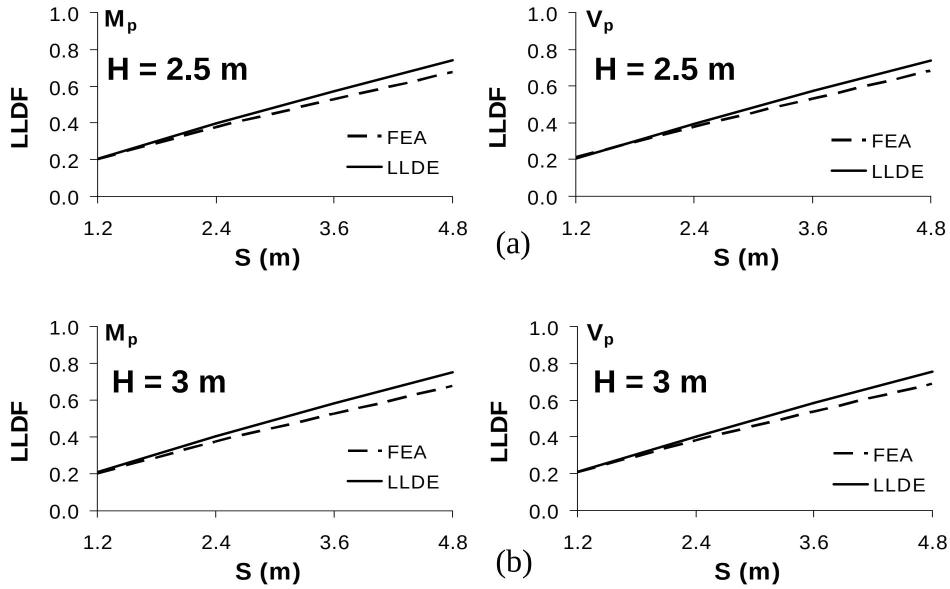

Figure 9.6 Comparison of the calculated LLDFs and FEA results for the piles of IBs where two or more design lanes are loaded (a) 2.5 m. abutment height (b) 3 m. abutment height

9.3 VERIFICATION OF THE DERIVED LLDEs FOR THE ABUTMENTS

In this section, the LLDEs derived for the abutments of IBs are verified against the available FEA results. For this purpose, the LLDFs for the abutments of IBs are calculated using the developed equations. Then, the calculated LLDFs and FEA results are plotted in Figs. 9.7-9.8 as functions of various dominant parameters used in the derivation of the LLDEs for the abutments. Figs. 9.7 and 9.8 compare the calculated LLDFs and the FEA results as a function of S, L, H_c and GT for the abutment moment of IBs for the one design lane and two or more design lanes loaded cases, respectively. For the abutment shear, Figs. 9.9 (a) and (b) compare the calculated LLDFs and the FEA results as a function of the more dominant parameter, S for various abutment heights, H_c, measured from the deck soffit for the one design lane and two or more design lanes loaded cases, respectively. As observed from the figures, the derived LLDEs produce reasonably good estimates of LLDFs for the live load moments and shear in the abutments. In addition, for the entire data used in the development of the LLDEs, the averages and standard deviations of the ratios of the LLDFs obtained from the derived equations to those from FEA are calculated for the abutment moment and shear and presented in Table 9.2. As observed from the table, the calculated average values of the ratios range between 1.00 and 1.07 while the standard deviations range between 0.07 and 0.19. The small deviations of the values of the calculated average ratios from 1.0 and relatively small standard deviations also indicate that the derived equations produce a reasonably good estimate of live load effects in IB abutments for the range of parameters considered in this study.

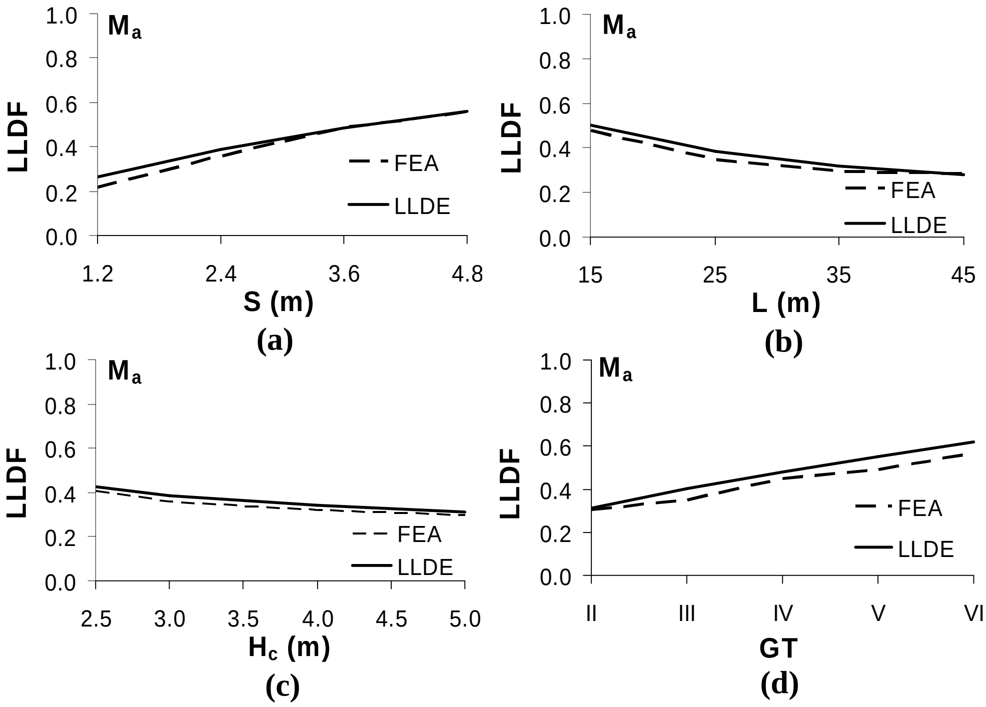

Figure 9.7 Comparison of the calculated LLDFs and FEA results for the abutment moment of IBs where two or more design lanes are loaded as a function of (a) *S*, (b) *L*, (c) H_c, (d) *GT*.

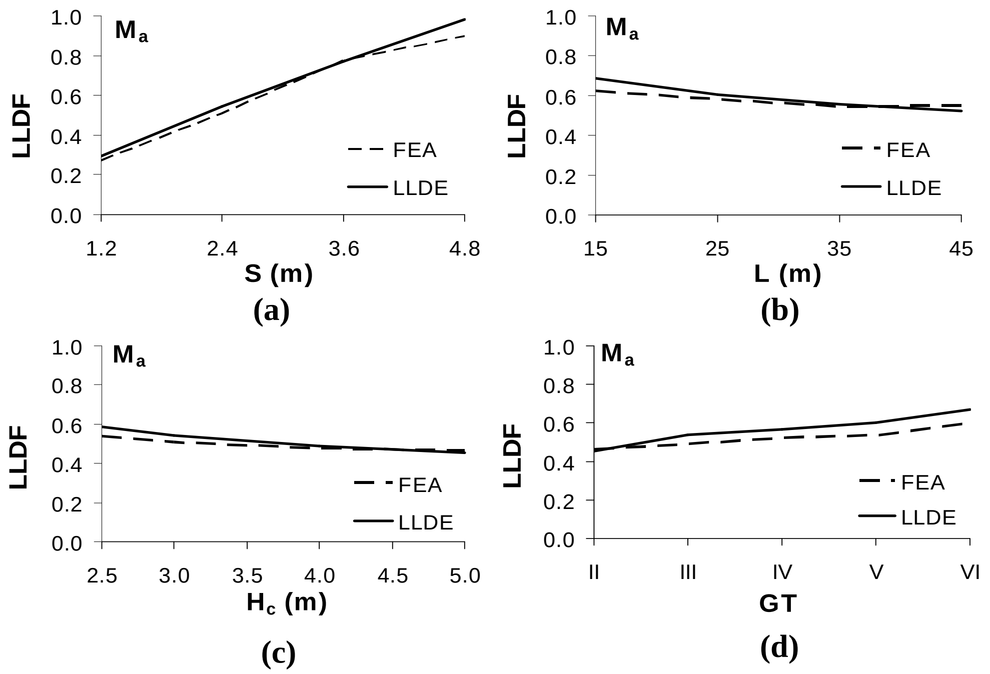

Figure 9.8 Comparison of the calculated LLDFs and FEA results for the abutment moment of IBs where one design lane is loaded as a function of (a) *S*, (b) *L*, (c) H_c, (d) *GT*.

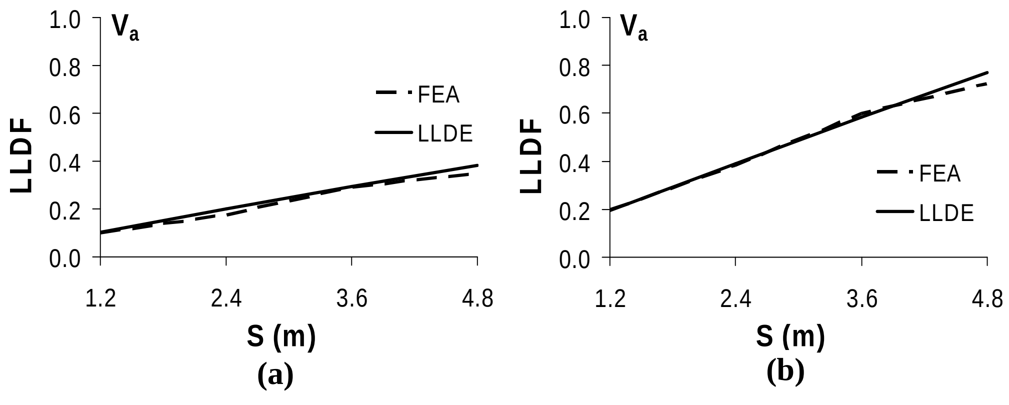

Figure 9.9 Comparison of the calculated LLDFs and FEA results for the abutment shear of IBs for the cases of (a) one design lane is loaded (b) two or more design lanes are loaded

Table 9.2. Average and Standard deviation values for the ratio of the proposed LLDE to the FEA results

			LLDE/FEA	
	Number of Loaded Design Lane		**AVG**	**STD**
Moment	**Two or more design lanes**	**Abutment**	1.03	0.17
		Pile	1.05	0.05
	One design lane	**Abutment**	1.07	0.19
		Pile	1.03	0.05
Shear	**Two or more design lanes**	**Abutment**	1.00	0.07
		Pile	1.04	0.05
	One design lane	**Abutment**	1.02	0.07
		Pile	1.05	0.05

CHAPTER 10

PART II: SEISMIC PERFORMANCE OF INTEGRAL BRIDGES

10.1. PROPERTIES OF INTEGRAL BRIDGES USED FOR SEISMIC ANALYSES

Three different existing IBs with one, two and three spans will be considered to investigate the seismic performance of IBs. The single span IB illustrated in Fig. 10.1 is located in Illinois, USA (IL. Route 4 Over Sugar Creek Bridge). The two span IB illustrated in Fig. 10.2 is located in Ontario, Canada (Hwy 400 Underpass at Major Mackenzie Drive) while the three span IB illustrated in Fig. 10.3 is located in Illinois, USA (IL. 4/13 Over Illinois Central Railroads). The single span IB has a span length of 34 m, a width of 13 m. The bridge superstructure is composed of a 195 mm thick slab supported by steel plate girders spaced at 2.24 m. The two spans IB has span lengths of 41 m each, a width of 35 m. The bridge superstructure is composed of a 225 mm thick slab supported by AASHTO Type VI prestressed concrete girders spaced at 2.38 m. The three span IB has span lengths of 15.7, 20.7 and 15.7 m., a width of 13 m and its 190 mm thick slab is supported by W760x173 steel girders spaced at 2.26 m. More details about these bridges are given in Table 10.1.

For the IBs considered in this study, a range of various geotechnical and substructure properties are considered to investigate the effect of soil–structure interaction and substructure properties at the abutments on the seismic performance of IBs. The details of these parameters are presented in Table 10.2. In addition, the properties of the foundation soil including its depth to the bedrock are chosen considering the seismic site soil types given in AASHTO LRFD Bridge Design Specification (AASHTO, 2007). Table 1.3 gives the details of the soil types and associated pile lengths considered in this study. Bedrock is assumed at the bottom of the considered soil profile.

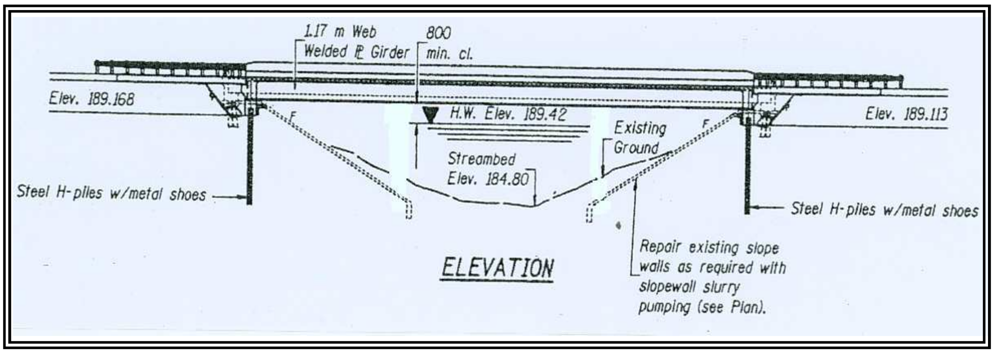

Figure 10.1. IL. Route 4 Over Sugar Creek Illinois /USA

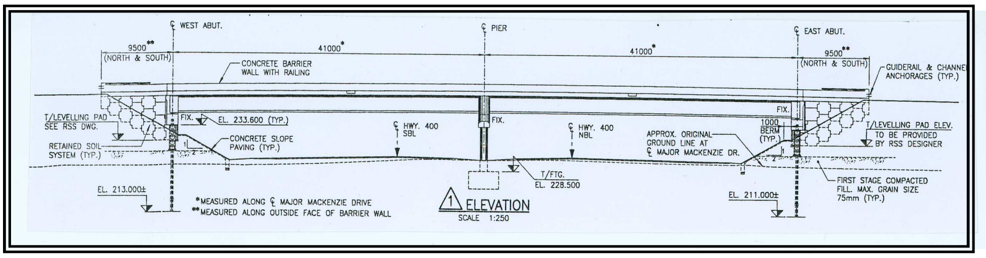

Figure 10.2. Hwy 400 Under Pass at Major Mackenzie Drive Ontario/Canada

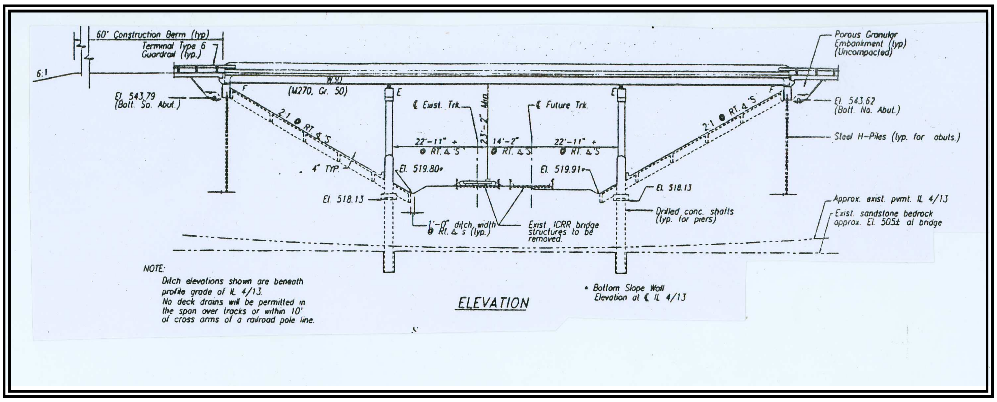

Fig. 10.3. IL. 4/13 Over Illinois Central Railroad Illinois /USA

Table 10.1. Properties of existing IBs considered

Bridge Properties	**Bridge 1**	**Bridge 2**	**Bridge 3**
Number of Span	1	2	3
Span Length (m)	34.25	41, 41	15.7, 20.7, 15.7
Width (m)	13	1	13
Girder Type	Steel (I) Plate Girder (Flanges: 408x51 mm, Web: 1170x12 mm)	Prestress Concrete AASHTO VI	Steel (I) W 760x173
Girder Spacing (m)	2.24	2.38	2.26
Pile Type	HP 310x125	HP 310x110	HP 250x63
Number of Piles	7	12	6
Abutment Height (m)	2.67	4	2.12
Abutment Thickness (m)	0.76	1.5	0.76
Pier Type	N/A	Multiple Column bent	Multiple Column bent
Pier Foundation	N/A	Pile	Pile

Table 10.2. Parameters of IBs considered in this study

Property	Parameter
Number of span length	1, 2 and 3
Abutment height (m)	3, 4 and 5
Abutment thickness (m)	1, 1.5 and 2
Pile size	250X85 and 310x174
Soil stiffness (sand)	Loose, Medium, Dense
Backfill compaction level	Compacted and uncompacted
Pile orientation	Strong and weak axis

Table 10.3. Soil types and related pile lengths

AASHTO Soil Types	Soil Types and Pile Lengths
Soil Type I	Dense sand , 15 m.
Soil Type II	Dense sand , 15 m.
Soil Type III	Medium sand , 15 m.
Soil Type IV	Loose sand, 15 m.

10.2 DESIGN OF THE INTEGRAL AND CONVENTIONAL BRIDGES

The IBs described above are redesigned as conventional and IBs in compliance with AASHTO LRFD Bridge Design Specifications (2007). This is done to study the relative performance of IBs in relation to conventional bridges and to allow for a realistic assessment of their seismic performance as a function of various structural and geotechnical parameters. In the design, the superstructures of the bridges are considered as similar to those of IBs described earlier. However the bearings and substructures of the bridges (abutments, piers and piles) are redesigned. The main difference between the conventional and IBs comes from the way the abutments are designed and built. Therefore, the same pier and associated pile sizes obtained for conventional bridges are also used for IBs to enable a fair comparison of the seismic performance of conventional and IBs. It is expected that such a comparison will clearly demonstrate the effect of the integral abutment design concept on the seismic performance.

In the design of the bridges, the site coefficient and peak ground acceleration are assumed as 1.2 and 0.35g respectively. The calculated seismically induced forces in the pier components are divided by appropriate response modification factors (R) recommended by AASHTO LRFD Bridge Design Specifications (2007). Accordingly, the response modification (R) is taken as 2 for the pier columns in the longitudinal and 3.5 in the transverse directions of the IB (in the transverse direction, the pier columns form a multi-column frame). In the design of a bridge, damage to the pile foundation is an undesirable situation. Therefore, flexural capacity of the piles is taken as 30% larger than that of the pier columns (AASHTO 2007) to prevent a potential damage. The details about the redesigned integral and conventional bridges are given in following subsection.

10.2.1 DESCRIPTION OF THE CONVENTIONAL BRIDGES

10.2.1.1 SINGLE SPAN BRIDGE

The elevation and plan view of the bridge is illustrated in Fig. 10.4 and 10.5 The length of the bridge is 34 m and the width is 13 m.

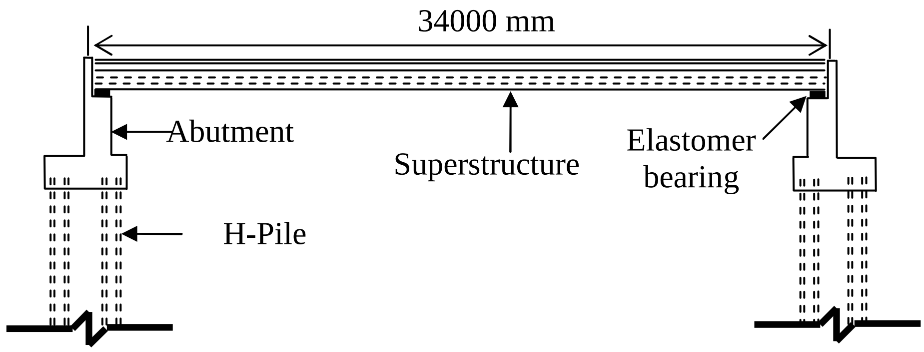

Figure 10.4. Elevation of single span bridge

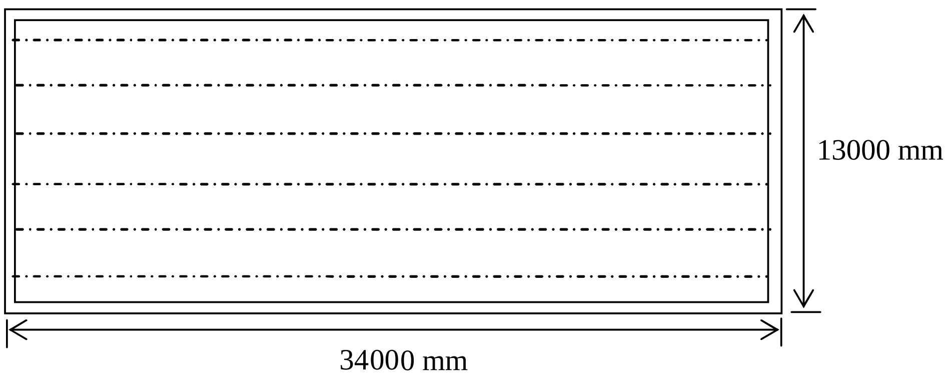

Figure 10.5. Plan view of single span bridge

The bridge has a slab-on-steel-girder deck. Fig. 10.6 displays the deck cross section. There are six steel girders supporting a 195 mm thick reinforced concrete slab and are spaced at 2240 mm. A 75 mm thick asphalt pavement is provided on the deck surface.

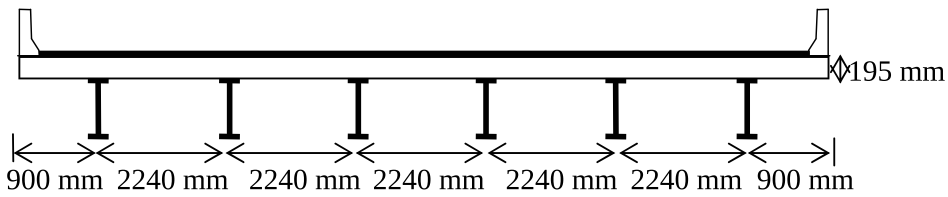

Figure 10.6. Deck cross section of single span bridge

Both abutments are seat type and are identical in geometry. The details of the abutments are illustrated in Fig 10.7. The abutments are supported on HP 200x54 steel HP piles. The details about the design of the abutments and steel HP piles are given in the subsequent sections.

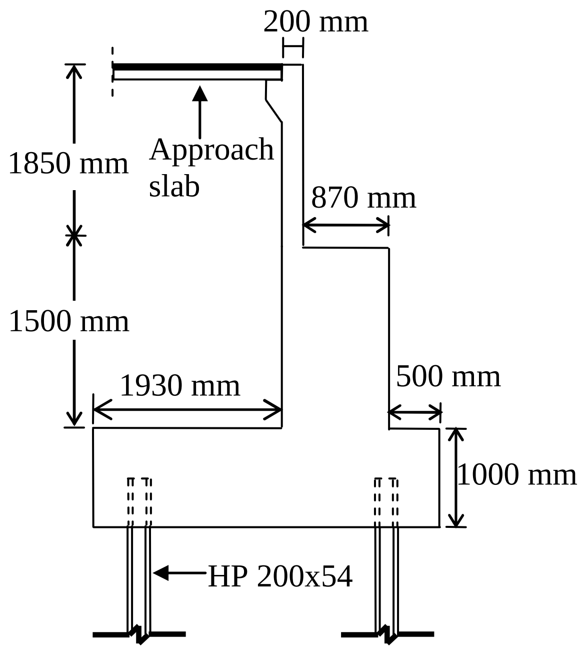

Figure 10.7. Abutment detail of single span bridge

10.2.1.2 TWO SPAN BRIDGE

The elevation and plan view of the bridge are illustrated in Figs. 10.8 and 10.9. The total length of the bridge is 82 m and the width is 16 m. The bridge has two spans with the lengths of 41 m each.

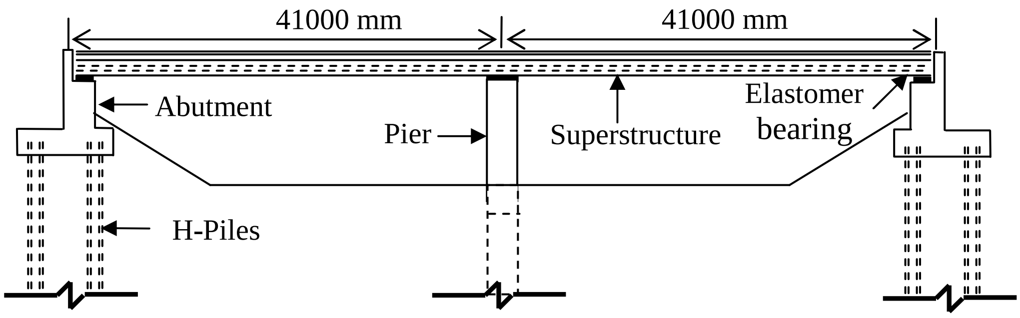

Figure 10.8. Elevation of two span bridge

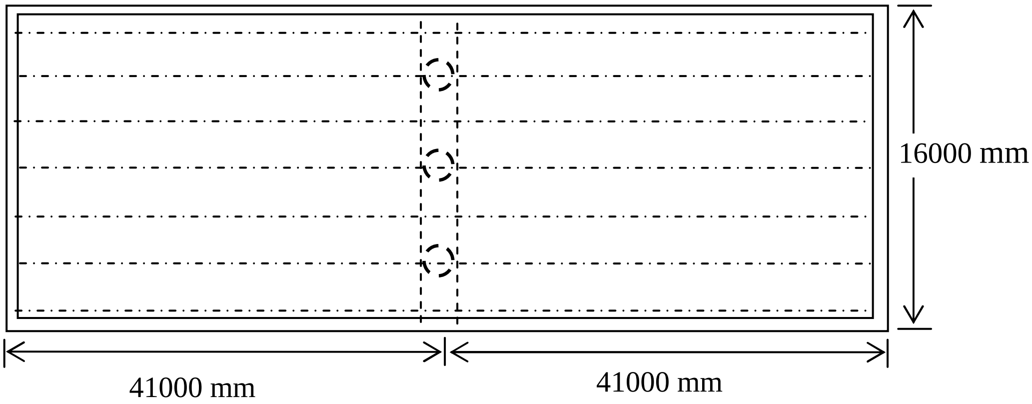

Figure 10.9. Plan view of two span bridge

The bridge has slab-on- prestessed concrete girder deck. Fig. 10.10 displays the deck cross section of the bridge. There are seven AASHTO type VI girders supporting a 225 mm thick reinforced concrete slab and are spaced at 2380 mm. A 75 mm thick asphalt pavement is provided on the deck surface.

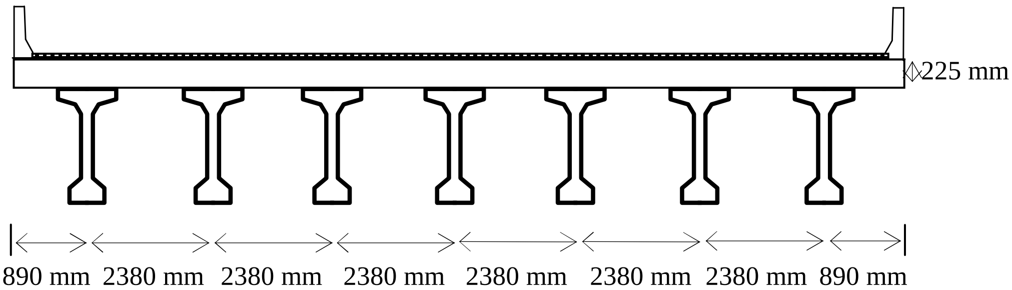

Figure 10.10. Deck cross section of two span bridge

The bridge pier is composed of three reinforced concrete columns supporting a cap beam. The geometry and dimensions of the pier are illustrated in Fig. 10.11.

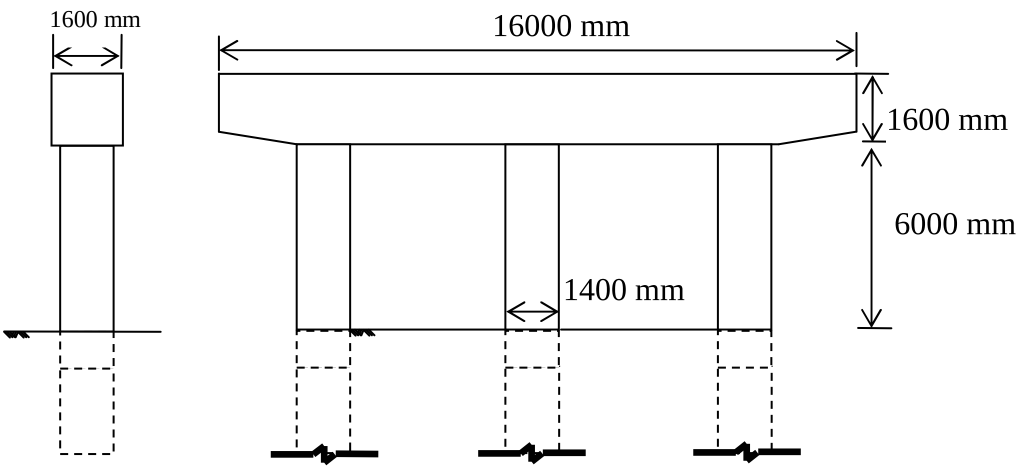

Figure 10.11. Cross section of pier, pier cap and reinforced concrete pile of two span bridge

Both abutments are seat type and are identical in geometry. The details of the abutments are illustrated in Fig 10.12. The abutments are supported on steel HP 250x85 piles.

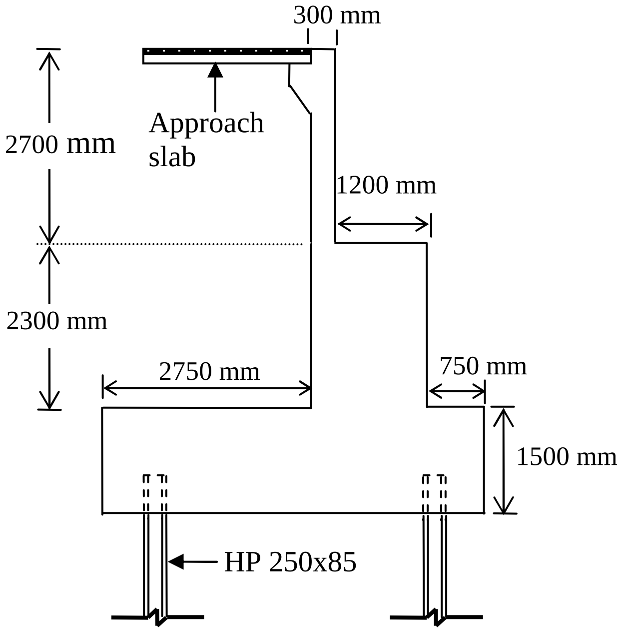

Figure 10.12. Abutment detail of two span bridge

10.2.1.3 THREE SPAN BRIDGE

The elevation and plan view of the bridges are illustrated in Fig. 10.13 and 10.14. The total length of the bridge is 52.1 m and the width is 13 m. The spans at the north and south ends are 15.7 m. The center span is 20.7 m.

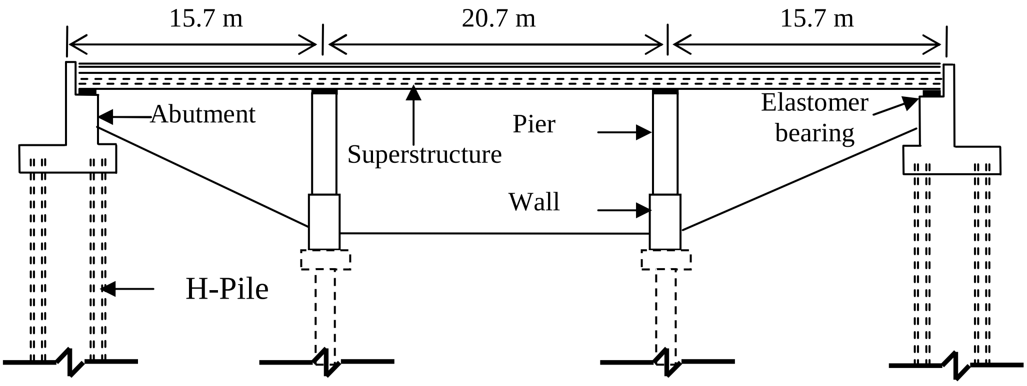

Figure 10.13. Elevation of three span bridge

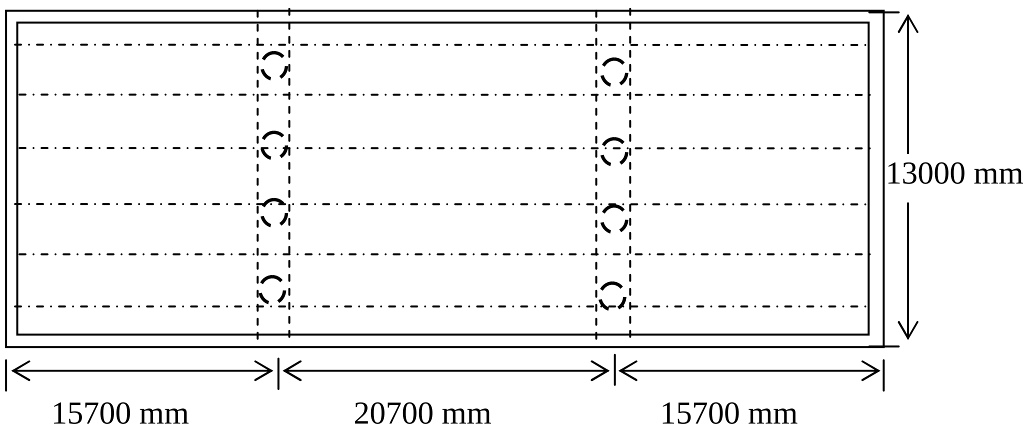

Figure 10.14. Plan view of three span bridge

The bridge has a slab-on-steel-girder deck. Fig. 10.15 displays the deck cross section of the bridge. There are six steel girders supporting a 190 mm thick reinforced concrete slab and are spaced at 2260 mm. A 75 mm thick asphalt pavement is provided on the deck surface.

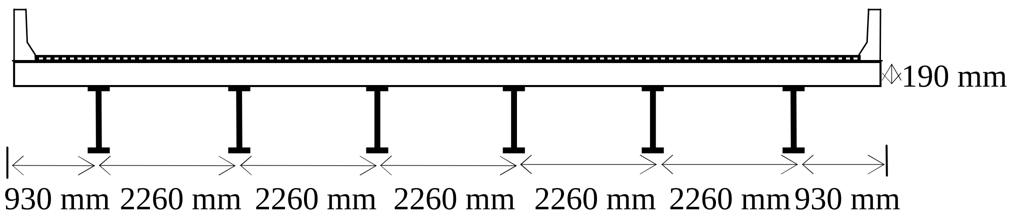

Figure 10.15. Deck cross section of three span bridge

The bridge piers are composed of four reinforced concrete columns and a cap beam. The geometry and dimensions of the pier are illustrated in Fig. 10.16.

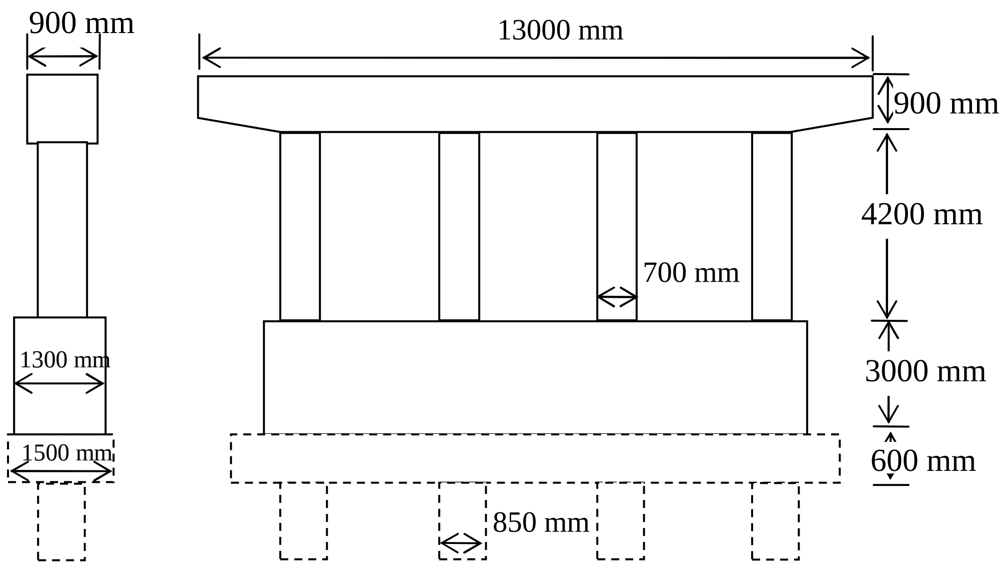

Figure 10.16. Cross section of pier, pier cap and reinforced concrete pile of three span bridge

The bridge has two identical seat type abutments. The dimensions and geometry of the abutments are illustrated in Fig 10.17. The abutments are supported on steel HP 200x54 piles.

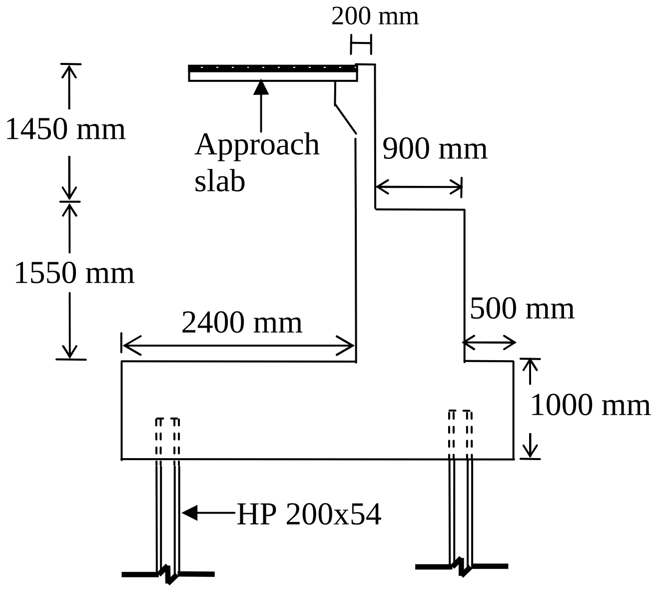

Figure 10.17. Abutment detail of three span bridge

10.2.2 DESCRIPTION OF THE INTEGRAL BRIDGES

The details about the redesigned IBs are given in this section. In the following subsections, abutment details and elevation of the IBs are illustrated.

10.2.2.1 SINGLE SPAN BRIDGE

10.2.2.1.1 General

The elevation of the single span bridge is illustrated in Fig. 10.18. The length of the bridge is 34 m and the width is 13 m.

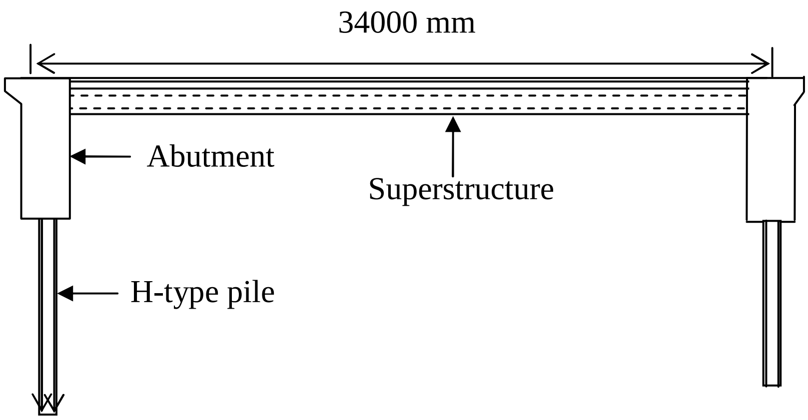

Figure 10.18. Elevation of single span IB

10.2.2.1.2 Abutment and Pile Details

The abutment and steel H-piles of single span IB are illustrated in Fig. 10.19. The abutment of the single span IB has a height of 2670 mm and a width of 760 mm. The abutment is supported by a single row of seven HP 310x125 piles.

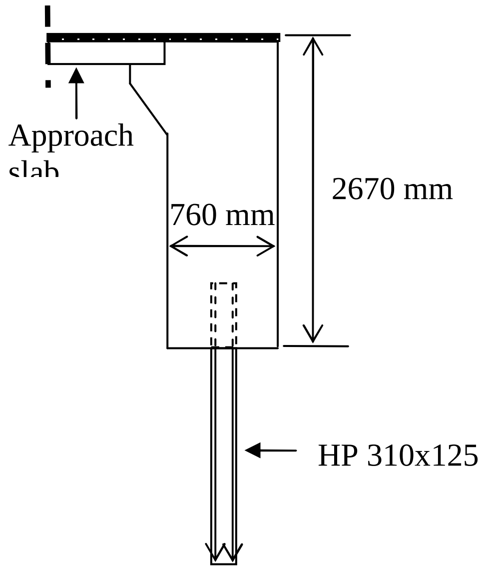

Figure 10.19. The abutment of single span bridge

10.2.2.2 TWO SPAN BRIDGE

10.2.2.2.1 General

The elevation of the two span bridge is illustrated in Fig. 10.20. The total length of the bridge is 82 m and the width is 16 m. The bridge has two spans with equal lengths of 41 m.

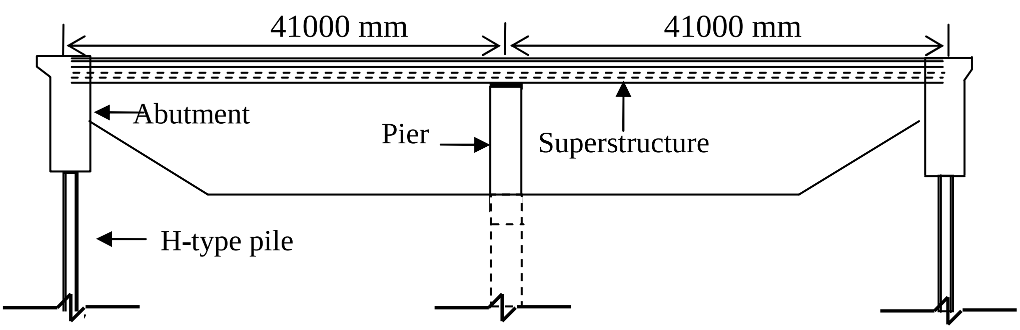

Figure 10.20. Elevation of two span IB

10.2.2.2.2 Abutment and Pile Details

The abutment and steel HP piles of the two spans IB are illustrated in Fig. 10.21. The abutment has a height of 4000 mm and a width of 1500 mm and it is supported by a single row of twelve HP 310x174 piles.

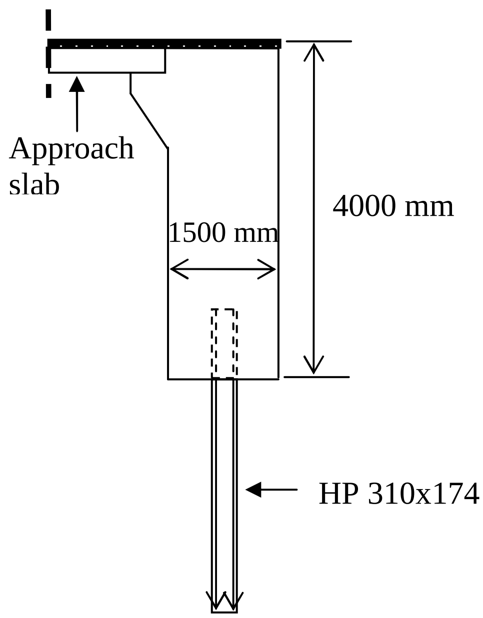

Figure 10.21. The abutment of two span bridge

10.2.2.3 THREE SPAN BRIDGE

10.2.2.3.1 General

The elevation of the bridge is illustrated in Fig. 10.22. The total length of the bridge is 52.1 m and the width is 13 m. The spans at the north and south ends of the bridge are 15.7 m. The middle span is 20.7 m. The width of the bridge is 13 m.

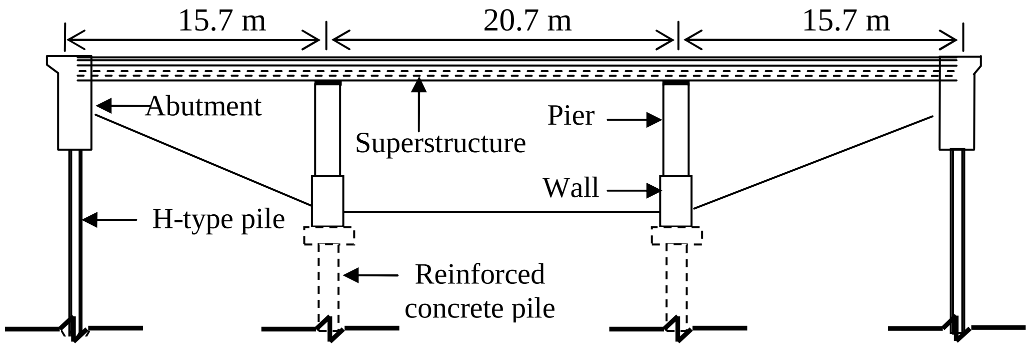

Figure 10.22. Elevation of three span IB

10.2.2.3.2 Abutment and Pile Details

The abutment and steel HP piles of the three spans IB are illustrated in Fig. 10.23. The abutment has a height of 2670 mm and a width of 760 mm and it is supported by a single row of six HP 250x85 piles.

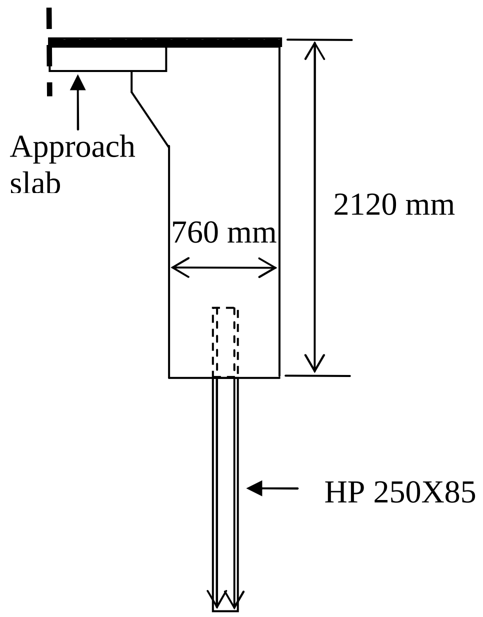

Figure 10.23. The abutment of three span bridge

CHAPTER 11

NONLINEAR MODELLING OF THE BRIDGES CONSIDERED IN THE ANALYSES

A detailed finite element model including nonlinear soil bridge interaction effects is needed for a realistic representation of the behavior of the bridge and load distribution among its various components when it is subjected to seismic loads. Accordingly, detailed 3-D nonlinear finite element models of the bridges considered in this study are built for nonlinear time history analyses. Details about the 3-D structural model of the bridges are presented in the following subsections.

11.1 MODELLING OF SUPERSTRUCTURE

The bridge superstructure is modeled using beam elements as shown in Fig. 11.1. Full composite action between the slab and the girders is assumed. The moment of inertia of the superstructure about the Y-axis is obtained by first calculating the moment of inertia of each composite girder using an effective slab width and multiplying the result by the number of girders. The moment of inertia of the superstructure about the Z-axis is also calculated assuming full composite action between slab and the girders. The superstructure is divided into a number of segments and its mass is lumped at each nodal point connecting the segments. Each mass is assigned four dynamic degrees of freedom; translations in the X and Y directions and rotations about the X and Z axes as shown in Fig. 11.1. The remaining two dynamic degrees of freedom are ignored deliberately to avoid triggering unwanted modes of vibration, which are not useful in the analysis. All six static degrees of freedom were used in the analysis. The in-plane translational stiffness of the deck is relatively much higher than that of the other members of the bridge. Accordingly, at the abutment and pier locations, the bridge deck is modeled as a transverse rigid bar of length equal to the center-to-center distance between the two exterior girders supporting the deck slab.

The transverse rigid bar is used to simulate the interaction between the axial deformation of the columns and torsional rotation of the bridge deck as well as the interaction between the in-plane rotations of the deck and displacements of the bearings. The transverse rigid bar is elevated to the level of the center of gravity of the bridge deck using a set of vertical rigid elements attached to it. This is done to accurately define the vertical location of the mass of the bridge deck. The rigid vertical elements are then connected to the bearings.

11.2 MODELING OF BEARINGS

The bridge superstructure is supported by elastomeric bearings on the pier and abutments. The shear stiffness of the elastomeric bearing depends partly on the hardness of the elastomer but mainly on the ambient temperature. The shear stiffness is fairly constant for all temperatures above freezing, but increases rapidly with decreasing temperatures. At -40 ^{o}C, the shear stiffness can be two and a half times the stiffness at construction temperature. Accordingly, the manufacturer's bearing catalogues now provide a minimum shear rate K_{min}, (at 20 ^{o}C) and maximum shear rate, K_{max}, (at -40 ^{o}C) for all laminated and plain elastomeric bearings available. Combining the appropriate shear rates for the corresponding temperature variations throughout the year may result in a combined effective shear force, which neither underestimates nor overestimates the bearing's behavior. This then produces the seismic force that is transferred to the substructure for which it must be designed. For the purpose of seismic analysis, an effective shear stiffness of $K_b=1.35x\ K_{min}$ is used for the elastromeric bearings.

$$K_{b\min} = \frac{G_b . A_b}{h_r} \tag{11.1}$$

Where, G_b is the shear modulus of the bearing material, A_b is the plan area of the bearings and h_r is the bearing thickness.

The elastomeric bearings are idealized as 3-D beam elements connected between the superstructure and the substructures at girder locations. The height of the beam elements is set equal to the thickness of the bearings. Pin connection is assumed at the joints linking the bearings to the substructures as shown in Fig. 11.1. To obtain the stiffness properties of these beam elements at the abutments and piers, first the calculated effective shear stiffness is set equal to the stiffness of a cantilever beam element with the same height, h_b, as the bearing thickness. The product of elastic modulus, E_b, and moment of inertia, I_b, of the beam element is then calculated as;

$$E_b . I_b = \frac{K_b . h_b^{\ 3}}{3} \tag{11.2}$$

In the model, E_b, is arbitrarily set equal to that of the concrete used in the construction of the bridge and, I_b, is calculated from the above equation to define the stiffness properties of the beam elements.

11.3 MODELING OF PIERS

The detailed structural model of the pier is illustrated in Fig. 11.1. The cap beam and the columns are modeled as beam elements. The parts of the beam elements within the joint connecting the cap beam to the columns are modeled as rigid elements. The tributary masses of the cap beam and the columns are lumped at the joints connecting them. The reinforced concrete piles are modeled using beam elements as well. The computer program X-TRACT (2007) is used to obtain the moment-curvature relationship and interaction diagrams of the pier columns and piles of IB considered in this study. The variation of the axial load effects on the pier columns due to seismic loads is also considered in the analyses. For this purpose, the moment curvature relationships of the piers and piles are obtained for several axial load levels. These diagrams are used to simulate the nonlinear behavior of the piers and piles of the multi-span bridges in the structural models. The details of the moment curvature relationships obtained for the reinforced concrete piers and piles of the multi span bridges considered in this study are given in following subsections.

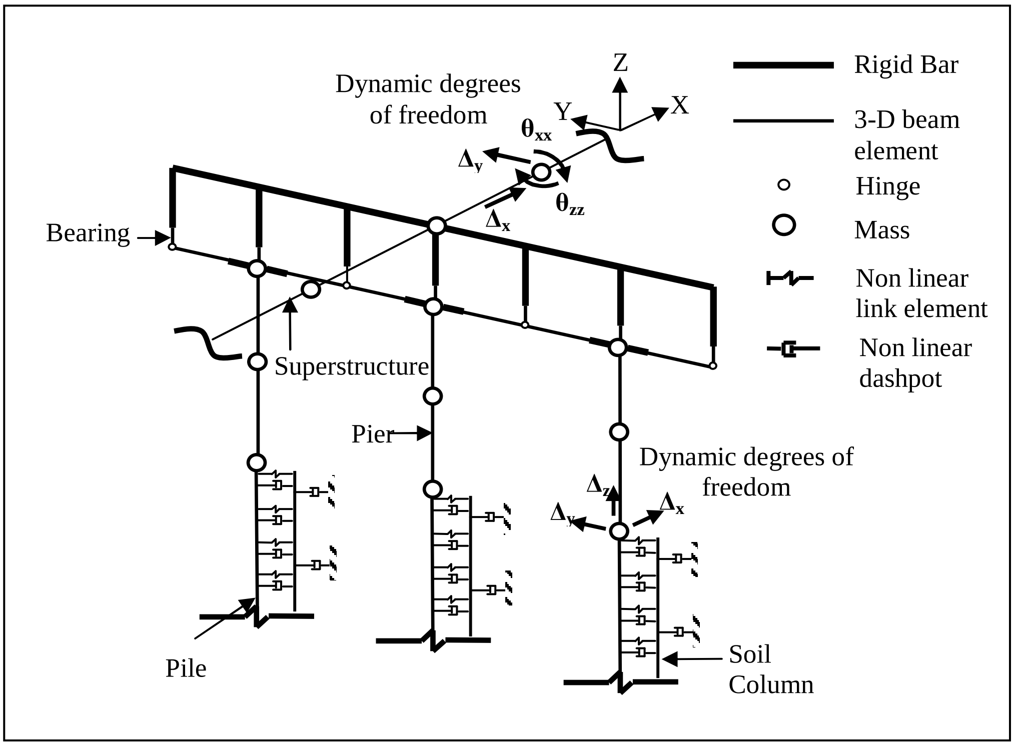

Figure 11.1. Structural modeling details at piers of two span IB

11.3.1 MOMENT CURVATURE RELATIONSHIPS FOR PIERS AND REINFORCED CONCRETE PILES OF THE BRIDGES

The multi-span bridges considered in this study have multiple column pier bents. The reinforced concrete columns at the piers have circular cross-section. Moment curvature relationships and interaction diagrams of these members are needed to build a nonlinear structural model of the multi-span bridges considered in this study. For these purpose, moment curvature relationships and interaction diagrams are obtained using the program X-TRACT (2009). Further details are given in the following subsections.

11.3.1.1 MATERIAL PROPERTIES OF REINFORCED CONCRETE PIERS AND PILES

11.3.1.1.1 Unconfined Concrete

The 28-Day compressive strength *(f'_c)* of the unconfined concrete is assumed as 30 Mpa. Crushing strain ***(ε_{cu})*** for the unconfined concrete is assumed to be 0.004 (Mander et.al 1988). This correlates well for bending failures of reinforced concrete columns with some inherent conservatism. Strain at completion of material spalling ***(ε_{sp})*** is 0.006. To define the stress-strain behavior of the cover concrete (Figs 11.2-11.3), the part of the falling branch in the region where $\varepsilon_c > 2\varepsilon_{co}$ is assumed to be a straight line which reaches a zero stress at the spalling strain, ε_{sp} (Mander et.al 1988) where f'_{co} and ε_{co} are the unconfined concrete strength and corresponding strain, respectively (ε_{co} is assumed as 0.002).

.

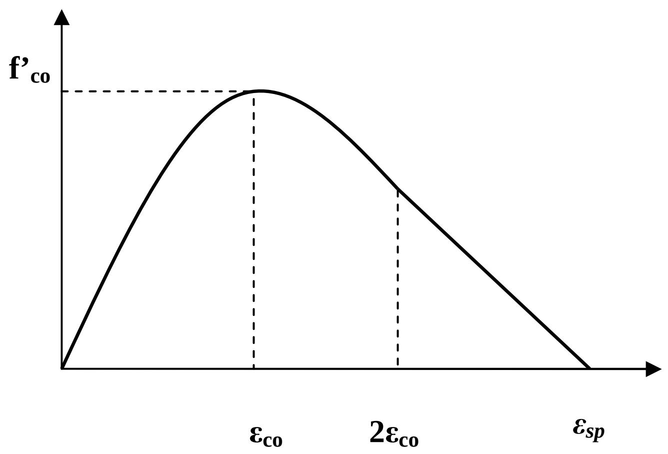

Figure 11.2. Stress-strain relationship of unconfined concrete

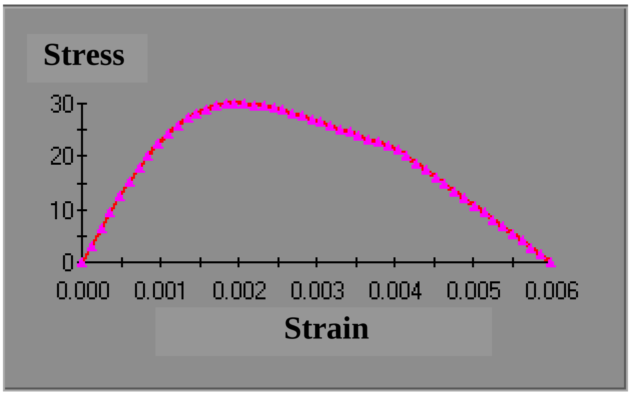

Figure 11.3. Stress-strain relationship of unconfined concrete (X-TRACT)

The elastic modulus of unconfined concrete is calculated as follows (Mander et.al 1988);

$$E_c = 5000\sqrt{f'_c} \tag{11.3}$$

11.3.1.1.2 Confined Concrete

The stress-strain relationship of confined concrete is illustrated in Fig. 11.4. Confined concrete core strength is determined by considering the effective confinement for the section. The following formula is used to calculate the confined concrete strength (Mander et.al 1988):

$$f'_{cc} = f'_{co}\left(-1.254 + 2.254\sqrt{1 + \frac{7.94 f'_l}{f'_{co}}} - 2\frac{f'_l}{f'_{co}}\right) \tag{11.4}$$

where; ***f'****$_l$* is given by following equation:

$$f_l' = \frac{1}{2} k_e \rho_s f_{yh} \qquad (11.5)$$

f_{yh}= yield strength of the transverse reinforcement

ρ_s = ratio of the volume of transverse confining steel to the volume of confined concrete core

k_e = a coefficient calculated from the ratio of area of effectively confined concrete core and area of core within center lines of perimeter spiral or hoops excluding area of longitudinal steel.

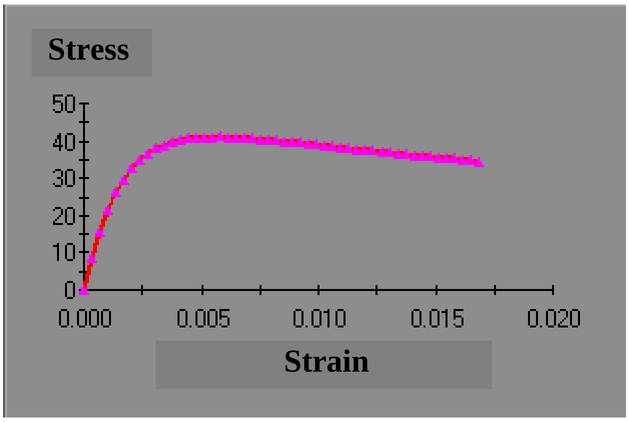

Figure 11.4. Stress-strain relationship of confined concrete (X-TRACT)

11.3.1.1.3 Crushing Strain (ε_{cu})

Crushing strain is associated with the concrete strain that occurs at the same time as hoop or transverse reinforcing fracture. The following formula is used to calculate the crushing strain (Mander et.al 1988).

$$\varepsilon_{cu} = 0.004 + 0.14\rho \frac{f_y}{f'cc} \qquad (11.6)$$

where;

ε_{cu}=The confined concrete strain capacity

ρ= Volumetric reinforcing ratio

f_y= Yield stress of the transverse confining steel.

f'_{cc}= The confined core strength.

11.3.1.2 GEOMETRIC PROPERTIES OF REINFORCED CONCRETE PIERS AND PILES

The pier of the two-span-bridge considered in this study has circular columns with 1.4 m diameter. The pier is also supported by reinforced concrete piles with a diameter of 1.4 m. The piers have 29 longitudinal reinforcing bars with a diameter of 28.65 mm and. spiral reinforcement with a diameter of 15.88 mm. The spacing of these spiral reinforcements is 68 mm. The piles also have 29 longitudinal reinforcing bars but with a diameter 35.8 mm and spiral reinforcement identical to that of the columns. The cross sections of the pier columns and piles of the two-span-bridge are illustrated in Fig. 11.5.

The pier of the three-span-bridge considered in this study has circular columns with 0.7 m diameter. The piers are also supported by reinforced concrete piles with a diameter of 0.85 m. The pier columns have 16 longitudinal reinforcing bars with a diameter of 19.05 mm and spiral reinforcement with a diameter of 12.70 mm. The spacing of these spiral reinforcements is 72 mm. The piles also have 16 longitudinal reinforcing bars but with a diameter 28.65 mm and spiral reinforcement with a diameter of 15.88. The spacing of these spiral reinforcements is 111 mm. The cross sections of the pier columns and piles of the two-span-bridge are illustrated in Fig. 11.6.

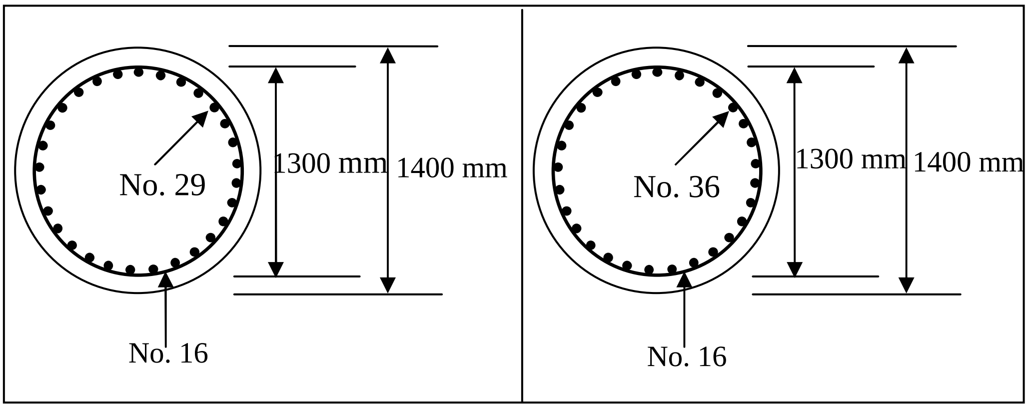

Figure 11.5. Cross section of **(a)** piers and **(b)** piles of two span bridge

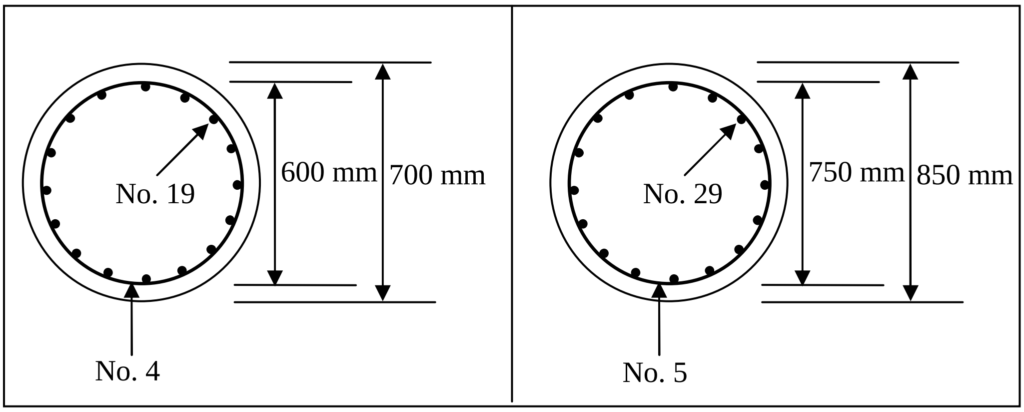

Figure 11.6. Cross section of **(a)** piers and **(b)** piles of three span bridge

11.3.1.3 MOMENT CURVATURE RELATIONSHIPS AND INTERACTION DIAGRAMS

The program X-TRACT is used to obtain the moment curvature relationship and interaction diagrams of the piers and piles of multi-span bridges considered in this study. The moment curvature and interaction diagrams for the reinforced concrete members whose properties are given in the previous section are displayed in Figs. 11.7-10. The moment curvature relationships are given only under an axial load due to dead load effects. However, the effects of the variation of the axial load in the pier columns due to seismic loads are also considered. For this purpose, the moment curvature relationships of the piers and piles are obtained at several axial load levels. The moment curvature relationships together with interaction diagrams are used to develop the envelope moment-curvature curves in the hysteretic models of the piers and piles to accurately simulate their nonlinear behavior in the structural models. The hysteretic behavior of the pier columns is simulated using the Takeda model (2009) which is available in SAP2000. Details about the Takeda Hysteretic Model are given in the following subsection.

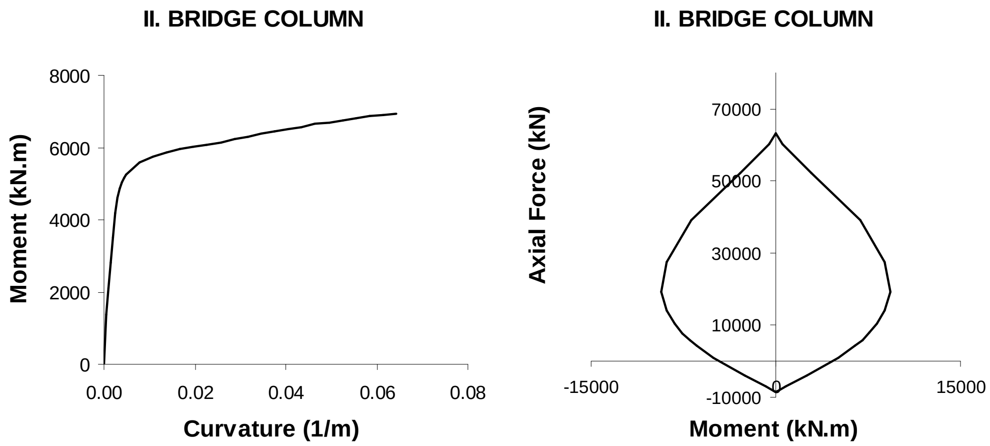

Figure 11.7. The moment curvature relationship and interaction diagram for the pier of two span bridge

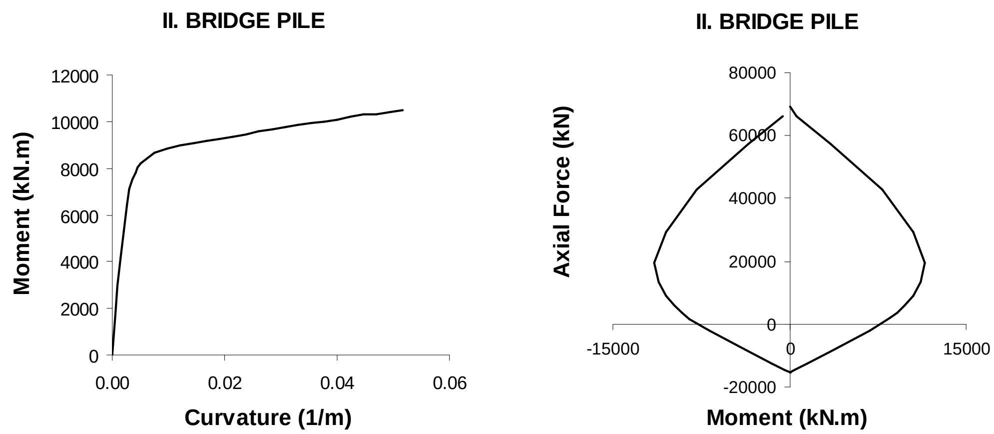

Figure 11.8. The moment curvature relationship and interaction diagram for the piles of two span bridge

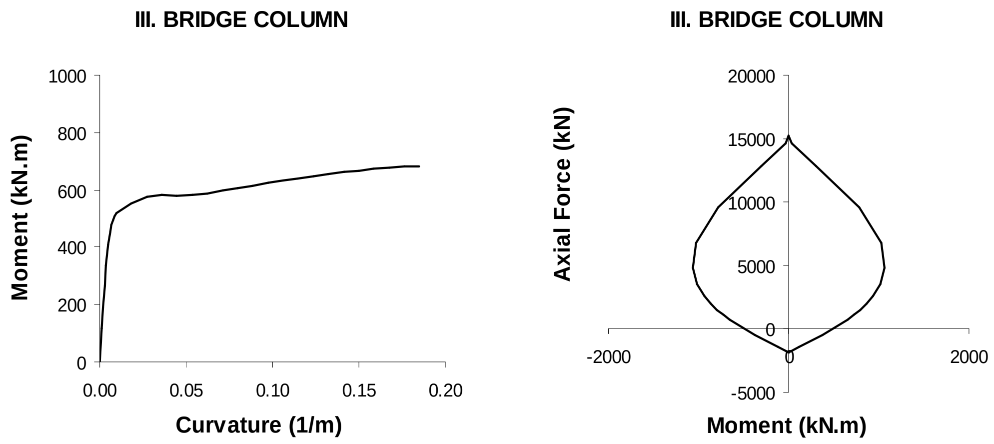

Figure 11.9. The moment curvature relationship and interaction diagram for the piles of three span bridge

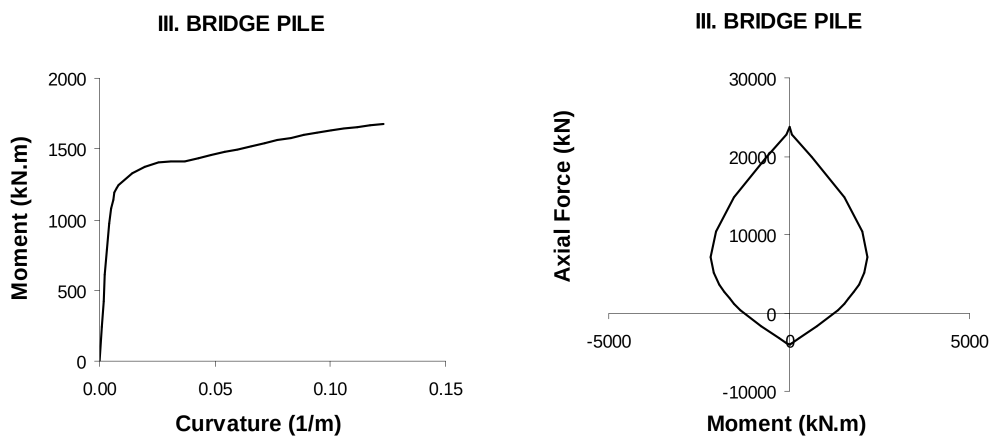

Figure 11.10. The moment curvature relationship and interaction diagram for the piles of three span bridge

11.3.1.4 TAKEDA MODEL

The nonlinear behavior of the reinforced concrete columns and piles of the bridges considered in this study are defined in the structural model by using nonlinear flexural link elements at the ends of the structural members. The nonlinear behavior of these link elements is defined by various hysteresis models. A variety of hysteresis models defining the nonlinear behavior of reinforced concrete members are available in the literature (Takeda et al. 1970; Jirsa et al.1999). Among these hysteresis models, Takeda et al.'s (1970) hysteresis model is the most commonly accepted one for defining the nonlinear flexural behavior of reinforced concrete members (İlki and Kumbasar, 2000). Moreover, Takeda et al.'s (1970) hysteresis model is a realistic theoretical model which recognizes the continually varying stiffness and energy absorbing characteristics of reinforced concrete members (Takeda et al. 1970) under moment reversal. Therefore, the hysteresis model proposed by Takeda et al. (1970) was used to model the nonlinear cyclic flexural behavior of the reinforced concrete column and pile elements of the bridges considered in this study. Fig. 11.11 shows Takeda et al.'s (1970) hysteretic model. The Takeda et al.'s (1970) model uses the monotonic moment curvature (or rotation) relationship of the reinforced concrete section. Therefore, the moment curvature relationships obtained in previous section are used as envelope curves in Takeda model.

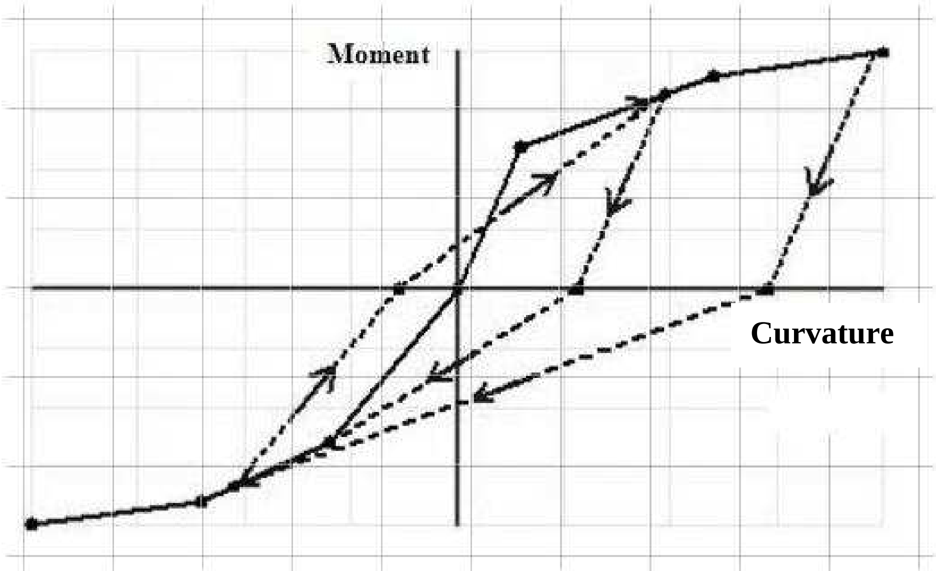

Figure 11.11. Takeda hysteresis model

11.4 MODELING OF ABUTMENTS AND STEEL PILES

The abutments are modeled using frame elements. X-TRACT (2007) program is used to obtain the moment curvature relationship of the abutments of the bridges considered in this study. These diagrams are used to simulate the nonlinear behavior of the abutments in the structural models. The steel H piles are also modeled using frame elements. The current state of design practice does not use capacity design approach to prevent plastic hinging and hence damage to the steel H piles at the abutments under seismic excitations. This is mainly due to the much larger size and hence much larger flexural capacity of the abutments compared to that of the piles. Therefore, the cyclic behavior of steel H-piles is modeled using an elasto-plastic hysteretic behavior. The Plastic-Wen model is used to simulate the nonlinear behavior of the piles

(Dicleli 2007). Accordingly, a nonlinear link (hinge) element is placed at the top of the piles to allow for plastic hinging during seismic excitations.

11.5. NONLINEAR MODEL OF THE ABUTMENT-BACKFILL INTERACTION

11.5.1 MONOTONIC ABUTMENT-BACKFILL INTERACTION MODEL

To model the cyclic abutment backfill behavior under seismic load, a monotonic load-deflection (p-y) envelope curve is required. Literature review conducted on monotonic load deflection envelope curves to simulate abutment-backfill behavior under lateral load revealed several research studies on the topic (Shamsabadi and et. al. 2007, Lemnitzer and et. al. 2009, Duncan and Mokwa 2001). The monotonic load deflection envelope curve proposed by Duncan and Mokwa (2001) is more commonly used to simulate the nonlinear abutment -backfill behavior (Lemitzer et.al 2009, Cole and Rollins 2006, Basha and Babu 2009). Thus, it is used also in this study. Duncan and Mokwa (2001) proposed the following equation to define the monotonic load-deflection (p-y) curve for the backfill behind the abutments.

$$P = \frac{y}{\dfrac{1}{K_{\max}} + R_f \dfrac{y}{P_{ult}}} \qquad (11.7)$$

where, P is passive resistance (units of force), P_{ult} is ultimate (maximum) passive resistance (units of force), y is deflection (units of length), K_{max} is the initial slope of the load-deflection curve (units of force/length). R_f can be defined as follows;

$$R_f = 1 - \frac{P_{ult}}{K_{\max} . y_{\max}} \tag{11.8}$$

Duncan and Chang (1970) found that values of R_f ranging from 0.75 to 0.95 were appropriate for hyperbolic representations of abutment-backfill interaction. Duncan and Mokwa (2001) have used a value of R_f = 0.85 for hyperbolic load-deflection curves. Accordingly, in this study, a value of R_f = 0.85 for hyperbolic load-deflection curves will be used. A typical hyperbolic p-y curve defined by Duncan and Mokwa (2001) is illustrated in Fig. 11.12.

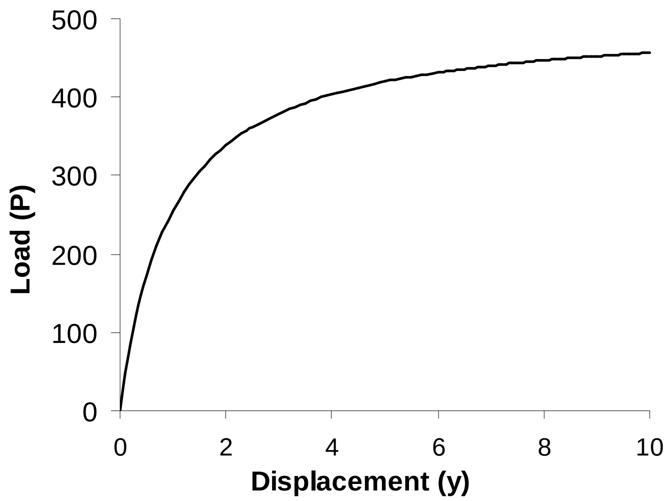

Figure 11.12. Hyperbolic P (Load)-Y (Displacement) curve

Ultimate passive resistance (P_{ult}) and initial slope of the p-y curve *(K_{max})* is needed to define the hyperbolic load-deflection curve for the backfill. Details about estimation of P_{ult} and K_{max} are given in the following subsection.

11.5.1.1 ULTIMATE PASSIVE RESISTANCE *(P_{ult})* OF BACKFILL

A triangular earth pressure distribution is generally assumed for the backfill soil as illustrated in Fig. 11.13 (Lemitzer et.al 2009, Duncan and Mokwa 2001). Accordingly, the passive soil resistance behind the wall type structures can be computed using the following equation.

$$E_{ph} = \frac{1}{2}.H^2.w.K_p.\gamma \qquad (11.9)$$

where, H is the wall height, w is the wall width, γ is the unit weight of backfill and K_p is the passive earth pressure coefficient.

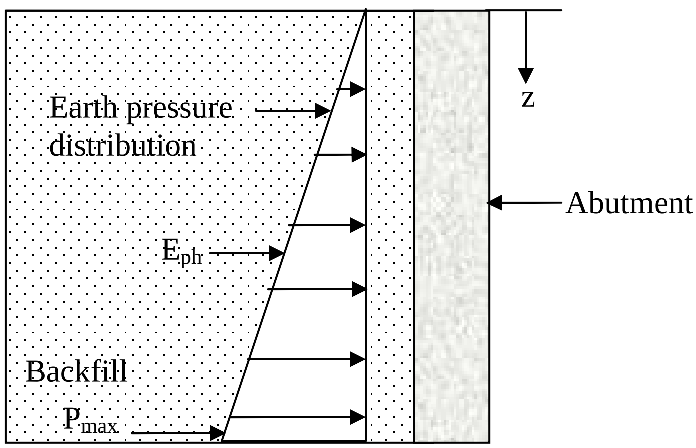

Figure 11.13. Earth pressure distribution for backfill

However, Caltrans (2006) recommends the following equation to calculate the passive soil resistance behind wall type structures based on full scale test results on typical Caltrans bridge abutments (Maroney 1995).

$$E_{ph} = A_e .239.\frac{H}{1.7} \qquad (11.10)$$

where, H is the wall height in meters and $A_e = w \times H$ (w is the wall width in meters) is the effective wall area in meters square.

Setting Eq. 11.9 equal to Eq. 11.10 and assuming γ =20 kN/m^3 for the backfill, K_p is calculated as 14. The obtained value of 14 for the passive earth pressure coefficient seems very high compared to those calculated using Rankine's earth pressure theory (Coduto 2001). However, this high value of passive earth pressure coefficient has already been confirmed by the full scale experimental tests of Lemitzer et. al. (2009) on abutments. This research study reveals that the passive earth pressure coefficient for the peak level of resistance can be approximated between 15.1 and 16.3. In this research study, passive earth pressure coefficient K_p is assumed as 14 per Caltrans' recommendation to define the hyperbolic load-deflection curve for abutment-backfill interaction.

The linear distribution of backfill pressure along the height of the abutment is taken into account to obtain the ultimate (maximum) passive resistance of backfill pressure at a particular location along the height of the abutment. Accordingly, the ultimate passive resistance, P_{ult} of backfill needs to be calculated as a function of the depth, z, from the abutment top. For this purpose, referring to Fig. 11.13, first the maximum earth pressure (P_{max}) at the bottom of the abutment is calculated as;

$$P_{\max} = \frac{2.E_{ph}}{H.w} \tag{11.11}$$

Then, the ultimate earth pressure at any point along to abutment height *(P_{pz})* is calculated as follows;

$$P_{ult-z} = \frac{P_{\max}}{H}.z \tag{11.12}$$

11.5.2 HYSTERETIC ABUTMENT-BACKFILL INTERACTION MODEL

In this research, the hysteretic behavior of abutment-backfill system under cyclic loads is simulated using the analytical relationships proposed by Cole and Rollins (2006). Cole and Rollins (2006) have conducted an experimental research study to define the hysteretic behavior of abutment-backfill system under cyclic loads. Full scale tests were performed to study the hysteretic behavior of abutment-backfill and pile cap-backfill interactions. Then, an analytical method has been developed to define the hysteretic behavior of abutment-backfill system using experimental data. In their research study, Cole and Rollins (2006) used the p-y curve purposed by Duncan and Mokwa (2001) as an envelope curve to model the hysteretic behavior of abutment-backfill interaction.

In the hysteresis model of Cole and Rollins (2006), first the hyperbolic load *(P)*-deflection *(Y)* envelope curve for the abutment-backfill system must be defined (Fig 11.12). The initial slope of the load-deflection curve (K_{max}) as well as the ultimate passive resistance *(P_{ult})* are the main parameters, which are used to define the hysteretic behavior of the abutment-backfill system. The initial slope *(K_{max})* of the p-y curve is estimated as 246 kN/mm for clean sand. This value is used for K_{max} to define the envelope curve of nonlinear cyclic abutment-backfill interaction. The ultimate passive resistance, P_{ult}, along the height of the abutment is obtained from Eq. 11.12.

In the hysteretic relationship proposed by Cole and Rollins (2006), a linear approximation of the stiffness of the reloaded force-deflection curve is defined as K_r and the horizontal offset for the linear load versus deflection approximation is called the apparent soil movement *(Δ_s)* as shown in Fig. 72,. The apparent soil movement is somewhat less than the maximum previous backfill deflection *(Δ_p)*, due to the rebound and relaxation of the backfill when the load is removed. For deflections less than Δ_s , the passive resistance is assumed to be zero. The intercept between the linear reloaded force-deflection curve and the hyperbolic load-deflection curve is defined by the coordinate *(Δ_{int}, P_{int})* as shown in Fig. 11.14. For deflections beyond Δ_{int}, the passive load-deflection follows the hyperbolic curve until the load is released.

Accordingly, the hysteretic behavior of the abutment-backfill system is defined by several normalized parameters. The first parameter is obtained by normalizing the apparent soil movement by the previous deflection (Δ_s / Δ_p).

$$\frac{\Delta_s}{\Delta_p} = \frac{(\Delta_p / H)}{0.0095 + 1.23(\Delta_p / H)} \tag{11.13}$$

The second parameter expresses the reloaded soil stiffness normalized by the maximum (initial) soil stiffness ($K_r / K_{\max}$) as a function of the apparent soil movement normalized by the abutment height (Δ_s / H).

$$\frac{K_r}{K_{\max}} = \frac{(\Delta_s / H)}{0.0013 + 1.40(\Delta_s / H)} \qquad (11.14)$$

In the hysteretic relationship shown in Fig. 11.14, the remaining inflection point of the proposed model *(Δ_{int}, P_{int})* defines where the reduced stiffness *(K_r)* intercepts the predefined hyperbolic shape (Fig. 11.14). This point is found by setting the equation of the reloaded soil stiffness and hyperbolic equation equal to one another and solving for Δ_{int} using the positive solution of the quadratic equation.

$$\Delta_{\text{int}} = \frac{-B + \sqrt{B^2 - 4AC}}{2A} \qquad (11.15)$$

where, $A = K_r.R_f / P_{ult}$, $B = K_r / K_m - K_r.R_f. \Delta_s / P_{ult} - 1$ and $C = -K_r \Delta_s / K_m$.

Then, P_{int} can be computed using the following equation, which is obtained by substituting Δ_{int} into Eq. 11.14.

$$P_{\text{int}} = (\Delta_{\text{int}} - \Delta_s).K_r \qquad (11.16)$$

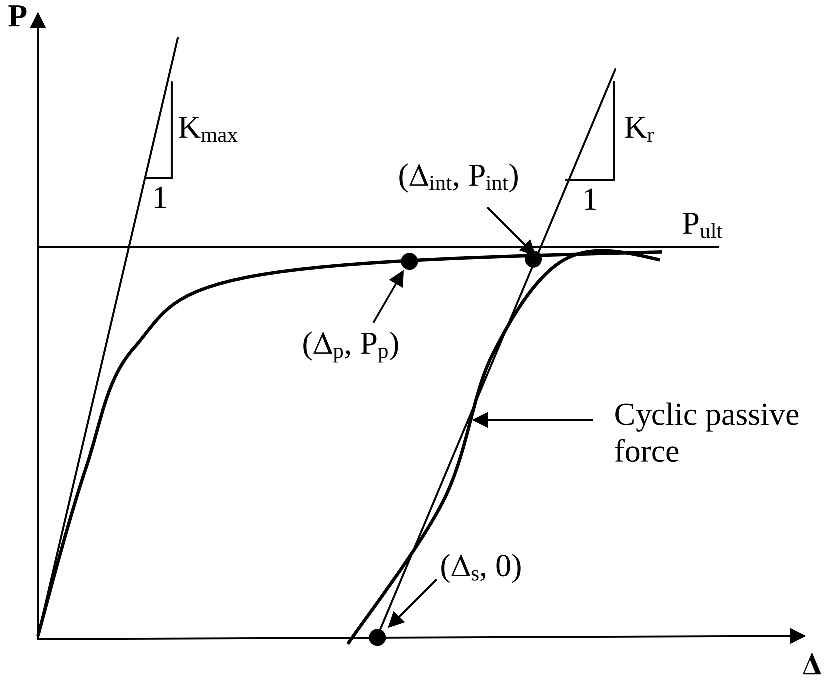

Δ_p= Previous peak deflection
P_p= Previous peak passive resistance
K_{max}= Initial soil stiffness of the load-deflection curve
K_r= Reloaded soil stiffness
Δ_s= Apparent soil movement
Δ_{int}= The deflection intercept of K_r and hyperbolic relationship
P_{int}= Passive load intercept of K_r and hyperbolic relationship

Figure 11.14. Cyclic-hyperbolic terminology (Cole and Rollins 2006)

The nonlinear behavior of the abutment-backfill system of the bridges considered in this study is simulated in the structural model by using nonlinear link elements. These link elements are attached at the nodal points along of the abutment. The load-displacement envelope relationship of the link elements are defined using the hyperbolic p-y curves. In these p-y curves, ultimate passive resistance of backfill is obtained at each nodal point (where the links are attached) along the height of the abutment using Eq. 11.12. The nonlinear cyclic behavior of these link elements is defined by various hysteresis models which is available in SAP2000. Pivot hysteresis model is found to be the most appropriate one to model the hysteretic behavior of abutment-backfill system under seismic loads. Information about the pivot hysteresis model is given in the following section.

11.5.2.1 PIVOT HYSTERETIC MODEL

In this study, the hysteretic behavior of abutment-backfill system was simulated with the pivot hysteresis model (Dowell et al. 1998) available in SAP2000 (2006) (Fig. 11.15 and 11.16). In this model, the unloading curves are guided toward a single point (pivot point) in the load-displacement plane (Dowell et al. 1998). The analytical hysteresis model proposed by Cole and Rollins (2006) for the simulation of abutment-backfill interaction behavior shows characteristics similar to those of the pivot hysteresis model. As observed from Fig. 11.17, the unloading curves are guided toward a single point in the hysteretic load-displacement relationship of abutment-backfill system as well. Accordingly, the pivot hysteresis model is used to simulate the hysteretic behavior of the abutment-backfill system in the structural model.

The pivot hysteresis model (Dowell et al. 1998) requires the force-deformation envelope as well as two additional parameters for capturing the pinching and stiffness degradation properties of reinforced concrete members. In Fig. 11.16, the term "$\boldsymbol{\alpha}$" refers to the stiffness degradation parameter and the term "$\boldsymbol{\beta}$" corresponds to pinching parameter. However, in the full scale tests performed by Cole and Rollins (2006) on abutment-backfill systems, no pinching is observed. Accordingly pinching effects is excluded from the model by setting $\boldsymbol{\beta=1}$. The parameter $\boldsymbol{\alpha}$ is calculated from the intersections of the two consecutive unloading lines K_{r1} and K_{r2} as shown in Fig. 11.18. Thus;

$$\alpha = \frac{K_{r_2} . K_{r_1}}{K_{r_2} - K_{r_1}} . (\Delta_{s_1} - \Delta_{s_2}) . \frac{1}{F_y} \tag{11.17}$$

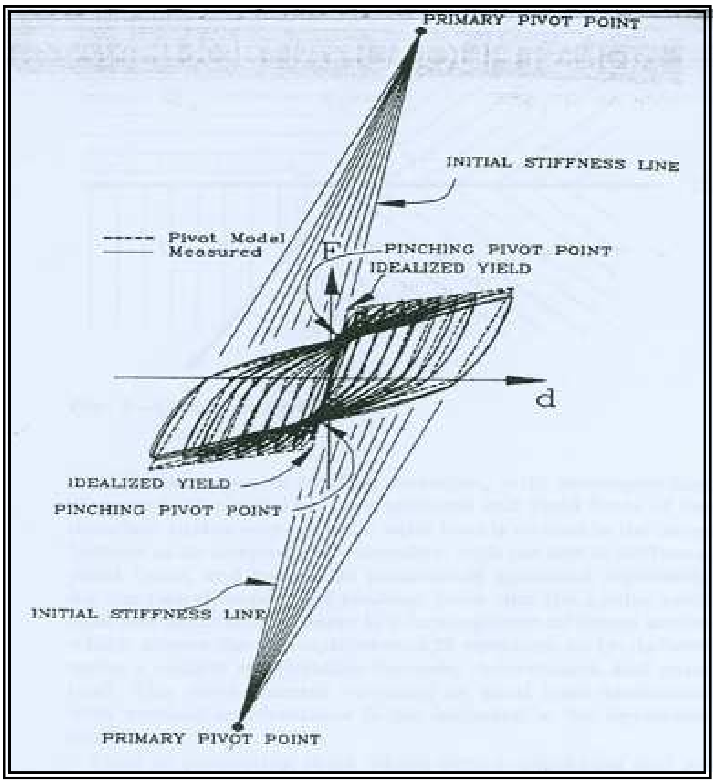

Figure 11.15. Pivot Hysteretic Model (Dowell et. al 1998)

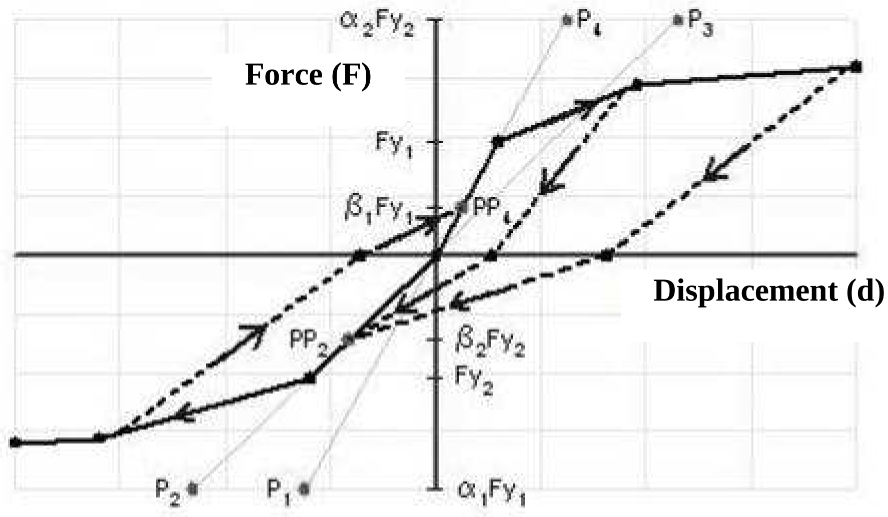

Figure 11.16. Pivot Hysteretic Model (SAP2000)

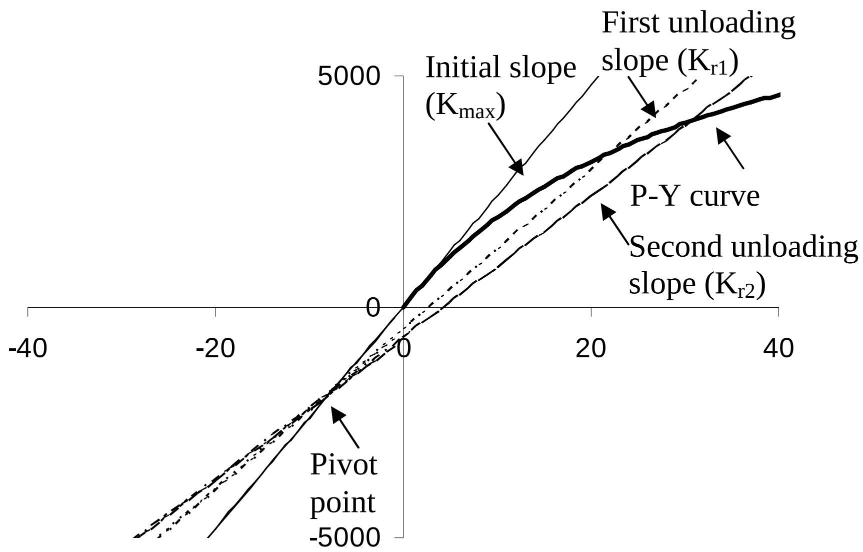

Figure 11.17. Hysteretic abutment-backfill interaction diagram for two-span bridge

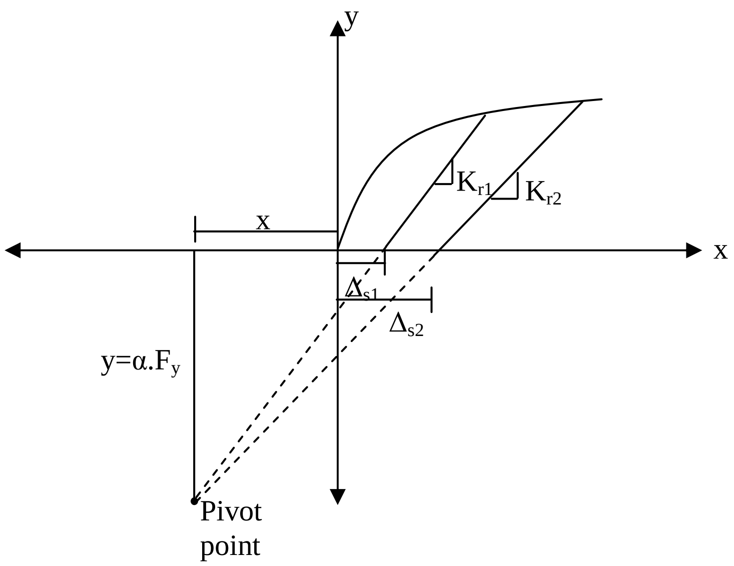

Figure 11.18. Calculation of the parameter of α

11.5.3 RADIATION DAMPING COEFFICIENT FOR ABUTMENT BACKFILL INTERACTION

When wall type structures interact the backfill under dynamic loads, some of the energy is dissipated due to radiation damping. The bridge abutments are typical example to this phenomenon. Accordingly, this radiation damping effects at the abutments must be incorporated in the structural models of bridges under dynamic loads. Scott (1973) and Jain and Scott (1993) purposed a radiation damping coefficient *(c)* to simulate the radiation damping effects as follows;

$$c = \sqrt{\frac{2}{1-v}.G.\rho} \tag{11.18}$$

where, ν is the Poisson's ratio, G is the shear modulus and ρ is the mass density of the backfill. The radiation damping coefficient is obtained for per unit area (m^2) of the abutment from the equation given above. In the structural model, dashpots are connected to the nodal points along the abutment height and the damping coefficients of these dashpots are calculated from Eq. 11.18 to simulate radiation damping.

11.5.4. IMPLEMENTATION OF ABUTMENT-BACKFILL INTERACTION IN THE STRUCTURAL MODEL

In the structural model, the hysteretic behavior of the abutment backfill system is simulated by using nonlinear link elements with pivot hysteresis model available in SAP2000 connected to the nodes along the length of the abutment (Fig. 11.19). The radiation damping effects for the abutment-backfill system are simulated in the structural model using dashpots (Fig. 11.19). In addition, during seismic excitation, there is a compression-only interaction between the abutment and backfill. Accordingly, gap elements with a zero gap connected in series with the nonlinear links and dashpots are incorporated in the structural model to simulate this behavior (Fig. 11.19).

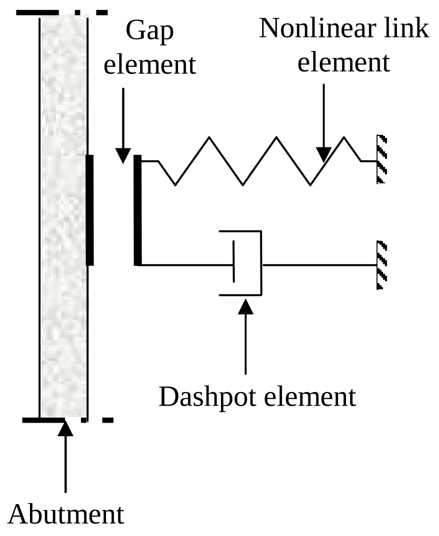

Figure 11.19. Implementation of abutment-backfill interaction in the structural model

11.6. NONLINEAR MODEL OF SOIL PILE INTERACTION

11.6.1 P-Y CURVES

The soil-pile interaction for a particular point along the pile is defined by a nonlinear load (*P*)-deformation (*Y*) curve, where *P* is the lateral soil resistance per unit length of pile and *Y* is the lateral deflection. This p-y relationship for sand may be approximated at any specific depth H, by the following equation (API 2000);

$$P = A.P_u.\tanh\left[\frac{k.H}{A.P_u}.y\right] \qquad (11.19)$$

where;

A= a factor to account for cyclic or static loading condition such that:

A=0.9 for cyclic loading, $A = \left[3 - 0.8\frac{H}{D}\right] \geq 0.9$ for static loading

P_u= Ultimate bearing capacity at the depth H, (kN/m)

k= initial modulus of subgrade reaction, (kN/m^3). It is obtained from Fig. 11.20 as a function of the angle of inertial friction (φ)

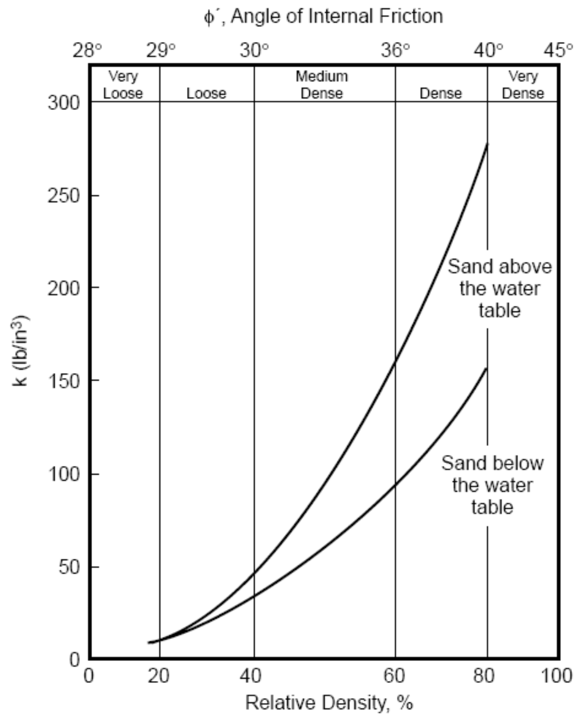

Figure 11.20. Subgrade modulus for sand as a function of angle of inertial friction (φ)

11.6.1.1. LATERAL BEARING CAPACITY FOR SAND

The ultimate lateral bearing capacity for sand has been found to vary from a value at shallow depths *(P_{us})* determined by Eq.11.20 to a value at deep depths *(P_{ud})* determined by Eq. 11.21. At a given depth the equation giving the smallest value of P_u should be used as the ultimate bearing capacity API (2000).

$$P_{us} = (C_1.H + C_2.D).\gamma.H \tag{11.20}$$

$$P_{ud} = C_3.D.\gamma.H \tag{11.21}$$

where;

P_u=Ultimate resistance (kN/m) (s=shallow, d=deep)

γ=effective soil weight (kN/m^3)

H= depth, (m)

C_1, C_2, C_3= Coefficient determined from Fig. 11.21 as a function of the angle of inertial friction (φ).

D= average pile diameter from surface to depth (m).

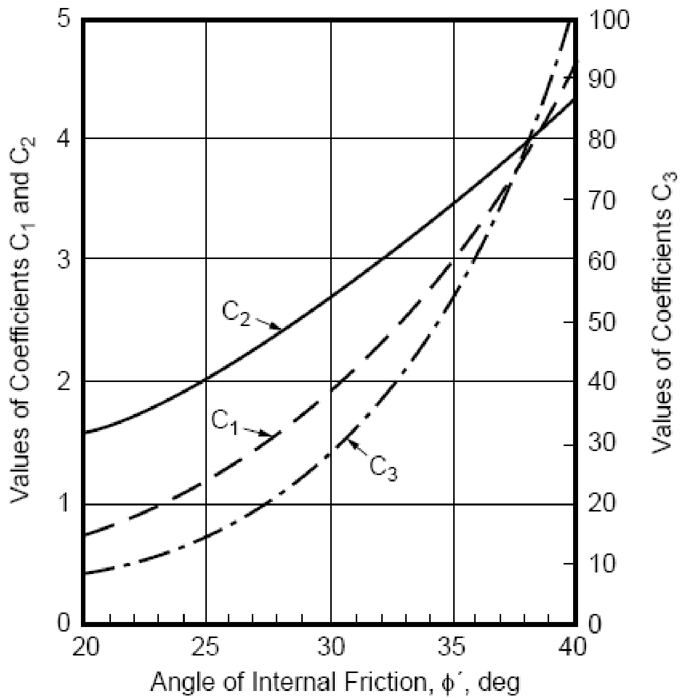

Figure 11.21. Values of coefficients as a function of angle of inertial friction (φ)

11.6.2 HYSTERETIC SOIL-PILE INTERACTION MODEL

Literature review conducted on the simulation of the soil-pile load deflection hysteretic behavior under lateral load reversals revealed several research studies on the topic (Nagomi et. al. 1992, Boulanger et. al. 1999, Shirato et. al. 2006, Rovithis et. al 2009). The soil-pile load deflection hysteresis model proposed by Shirato et. al (2006) is found to be more practical to employ in commercially available structural analysis software such as SAP2000. Thus, the hysteresis model proposed by Shirato et. al (2006) is used in this study for the simulation of hysteretic soil-pile interaction behavior. Shirato et. al (2006) have conducted an experimental research study to obtain analytical hysteretic p-y curves for soil-pile interaction modeling. In these models, envelope p-y curves for the hysteresis model are assumed as elasto-plastic (Fig. 11.22). The p-y curves obtained from the API (2000) recommendation as part of this research study are also nearly elasto-plastic and hence, suited well for the model proposed by Shirato et. al (2006) as shown in Fig. 11.23. Furthermore, the experimental research study conducted by Shirato et. al (2006) reveals that unloading curves are parallel to the initial slope of elasto-plastic p-y curves (Fig. 11.24). This hysteretic behavior of the soil-pile system is simulated in the structural model by using nonlinear link elements in SAP2000. These link elements are attached at the nodal points along the length of the pile. The load-displacement envelope relationship of the link elements are defined using the p-y curves recommended by API (2000) and their nonlinear cyclic behavior is defined by the Takeda hysteresis model available in SAP2000 as in this model unloading curves are also parallel to the initial slope of elasto-plastic p-y curves

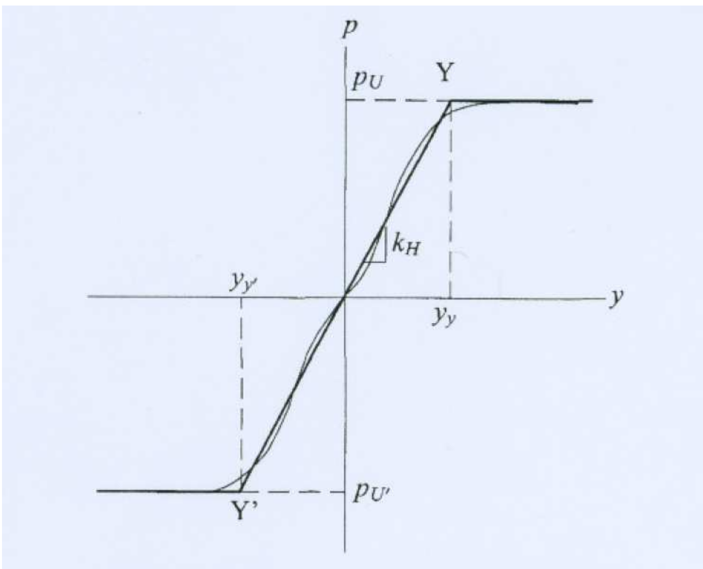

Figure 11.22. Elasto-plastic p-y curve (Shirato et. al. (2006))

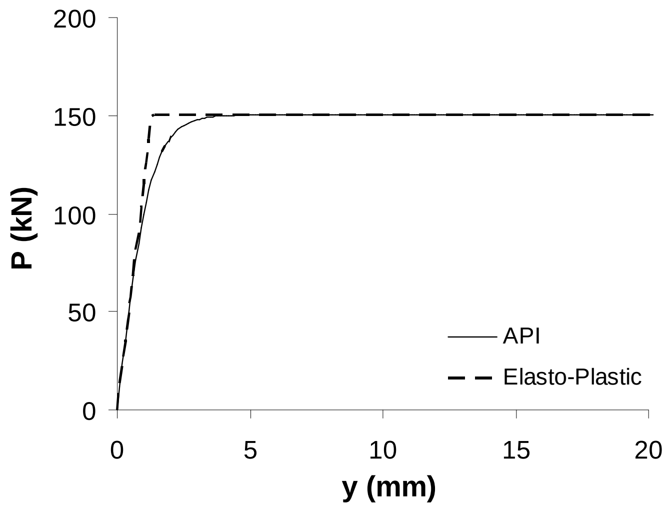

Figure 11.23. A typical P-Y curve and its elasto-plastic idealization

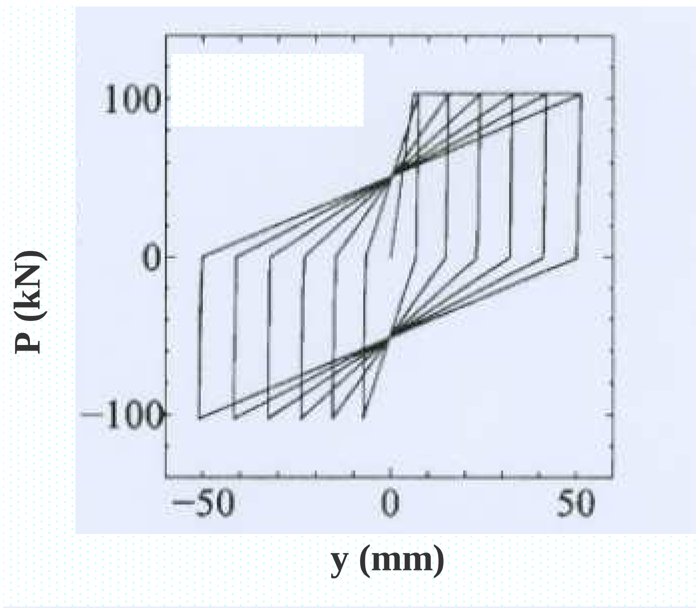

Figure 11.24. Hysteretic p-y curve (Shirato et. al. 2006)

11.6.3 RADIATION DAMPING COEFFICIENT FOR SOIL-PILE INTERACTION

The piles interact with the surrounding soil under seismic loads. This interaction leads to dissipation of the energy due to radiation damping. Accordingly, the effect of radiation damping at the piles must be incorporated in the structural models of the bridges. Anandarajah (2005) purposed a radiation damping coefficient *(c)* to simulate the radiation damping effects as follows;

$$c = A.\rho.V_s \tag{11.22}$$

where, A is the tributary area between the points along the pile, ρ unit weight of the soil, V_s shear wave velocity. The radiation damping coefficient is obtained for per unit area (m^2) of the pile from the equation given above. In the structural model, dashpots are attached at the nodal points along the pile to simulate the radiation damping effects and the damping coefficients of these dashpots are calculated from Eq. 11.22 to simulate radiation damping. The densities and shear wave velocities for various foundation soils employed in this research study are listed in Table 11.3.

11.6.4. IMPLEMENTATION OF SOIL-PILE INTERACTION HYSTERETIC BEHAVIOR IN THE STRUCTURAL MODEL

To implement nonlinear soil pile interaction behavior in the structural model, nonlinear link elements and dashpots are attached at each node along to the pile as shown in Fig.11.25. The hysteretic behavior of the soil-pile system is simulated by using nonlinear link elements with Takeda's hysteresis model available in SAP2000 connected to the nodes along the length of the pile (Fig 11.25). The envelope relationship for the Takeda's model is defined using the p-y curves recommended by API (2000). To simulate radiation damping, dashpots are placed at the nodal points along the pile (Fig. 11.25). The nonlinear link elements and dashpots are then connected to the nodes along the soil column simulating free field motion of the foundation soil. The details about modeling of the soil column are given in following section.

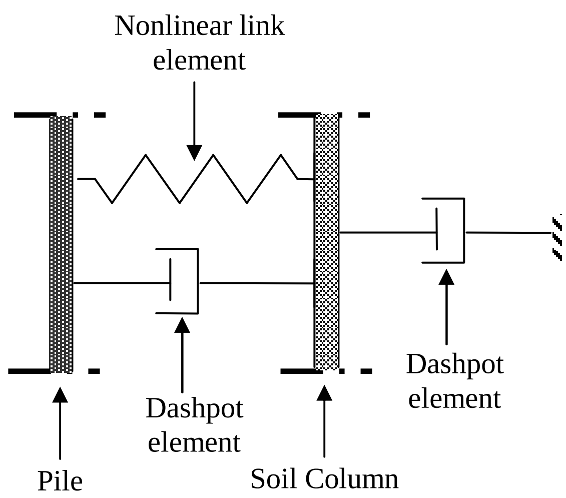

Figure 11.25. Implementation of soil-pile interaction in the structural model

11.7. SOIL COLUMN MODELS

In bridge design, generally the relative movement of the surrounding soil (free-field motion) during the earthquake is not considered. However, this may result in an incorrect simulation of the overall behavior of the bridges during a potential earthquake especially for soft soil conditions where free field movements may be considerable. For this purpose, in this study, a soil-column model is used to simulate the relative movement of the surrounding soil (free-field soil) in the structural model. The foundation soil is first modeled using the program PROSHAKE (2009). In the soil column models, the 15 m depth soil is divided into five three meter long segments. Then, time history analyses of the soil column (free-field soil) are performed using the seven earthquake records used in the analyses. The analyses are repeated for four different levels of peak ground accelerations (0.2g, 0.35g, 0.5g and 0.8g) for each earthquake. The equivalent shear modulus and damping ratios for the soil column are then obtained from the analyses results for each earthquake and the levels of peak ground accelerations considered in the analyses. These parameters are then used to build soil column models in SAP2000 integrated with the bridge model. In the following subsections, first the details about the selected earthquakes are given. Then the Proshake analyses results are presented.

11.7.1 SELECTED EARTHQUAKES

Seven earthquake ground motions whose response spectra are compatible with the AASHTO spectrum for soil type I (Rock) are selected from the PEER (Pacific Earthquake Engineering Research) strong motion database of the University of California, Berkeley. The reason for considering rock as the type of soil is that the ground motions are applied at the base of the piles at the bedrock level and the free-field effect of the foundation soil above the bedrock is considered separately in the structural model using an equivalent soil column for various soil types. Details of the selected ground motions are given in Table 11.1.

Table 11.1. Properties of the selected ground motions

Earthquake	Station/ Component	Magnitude	Distance (km)	A_p (g)	V_p (cm/s)	A_p/V_p (1/s)
Loma Prieta, 1989	58222SF-Presidio	6.9	83.1	0.20	32.4	6.05
Loma Prieta, 1989	1601 Palo Alto-SLAC Lab	6.9	36.3	0.28	29.3	9.2
Mammoth Lakes, 1980	54214 Long Valley Dam	6.0	20.0	0.41	33.9	11.8
San Fernando, 1971	266 Pasadena-Old Seismo Lab	6.6	19.1	0.20	10.9	18.2
Northridge, 1994	24592 LA, City Terrace	6.7	37.0	0.26	12.8	20.2
Northridge, 1994	24592 LA, City Terrace	6.7	37.0	0.32	14.1	23.4
Whitter, 1987	108 Carbon Canyon Dam	6.0	26.8	0.20	6.5	30

The comparison of the AASHTO design spectrum for soil type I and the acceleration response spectra of the selected earthquakes are given in Figure 11.26. The acceleration time histories of the ground motions are illustrated in Figure 11.27.

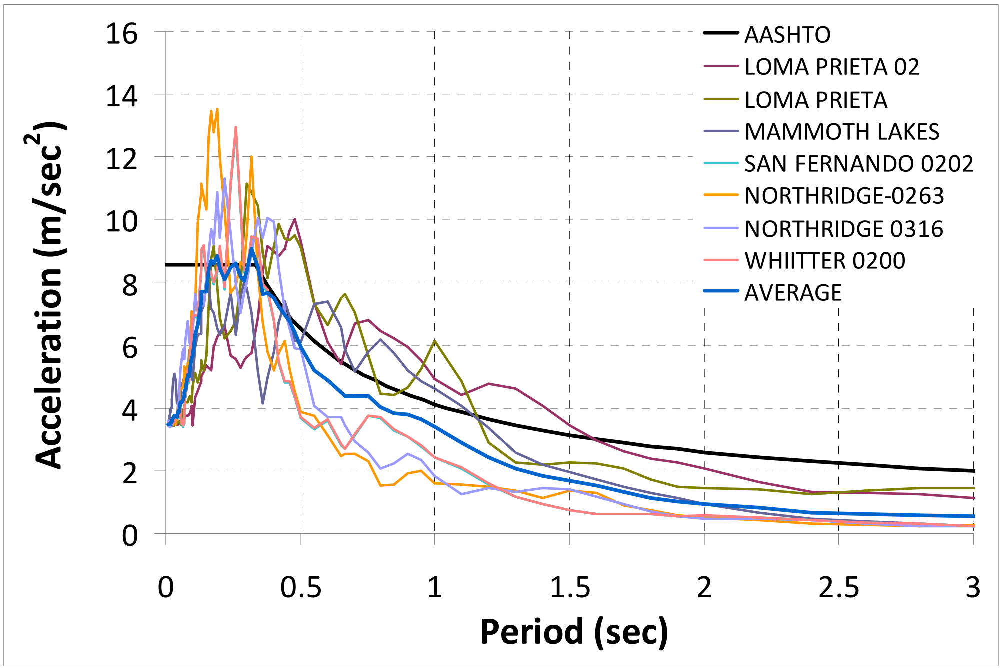

Figure 11.26. The comparison of the AASHTO design spectrum and acceleration spectrums of selected earthquakes

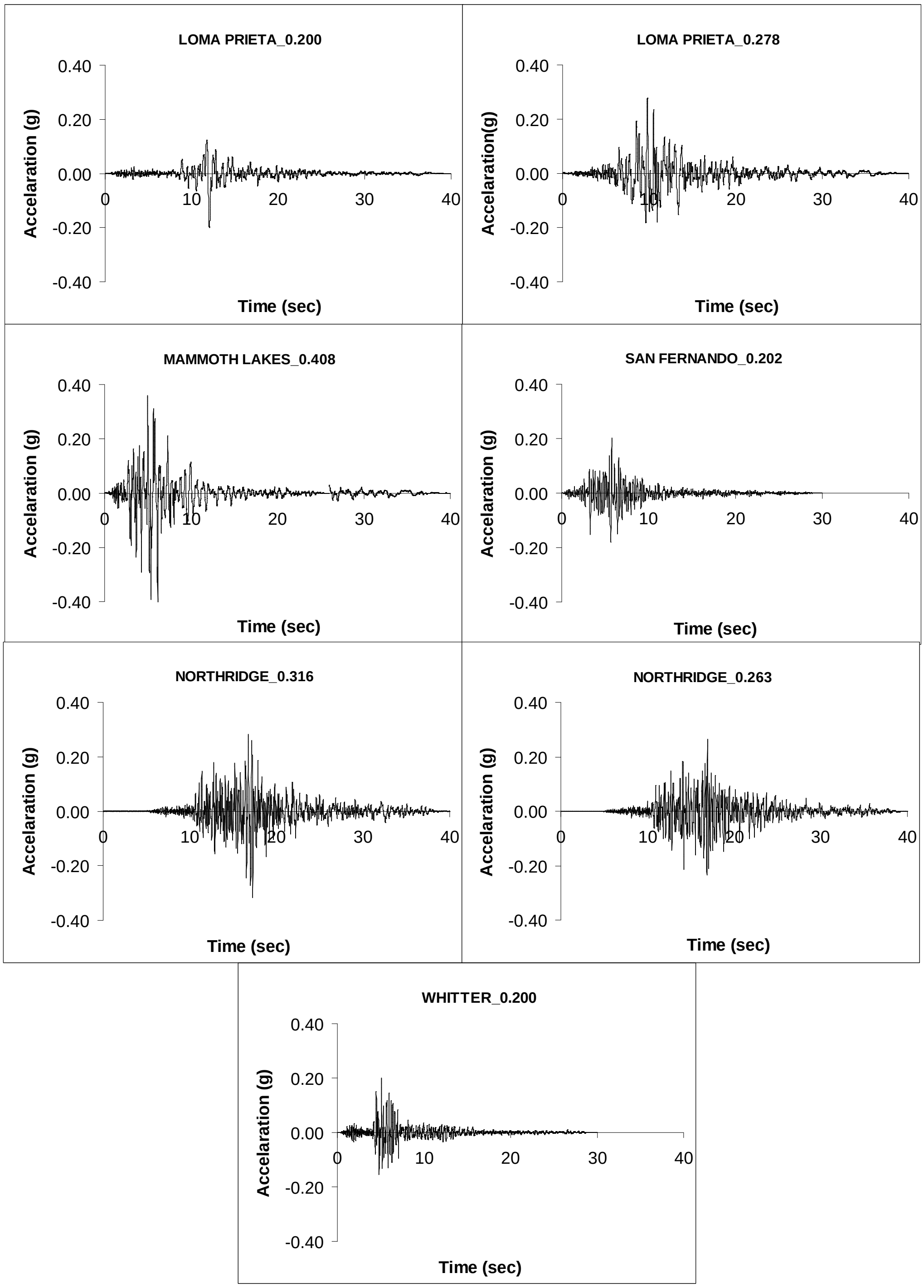

Figure 11.27. Time vs. acceleration graphs of selected earthquakes

11.7.2. PROSHAKE ANALYSES

The properties of the foundation soil and the related pile lengths used in the analyses are chosen considering the seismic site soil types given in AASHTO LRFD Bridge Design Specifications (AASHTO, 2007). Table 11.2 gives the details of the soil types and associated pile lengths considered in this study. Bedrock is assumed at the bottom of the considered soil profile.

Table 11.2. Soil types and related pile lengths

AASHTO Soil Types	Soil Types and Pile Lengths
Soil Type I	Dense sand , 15 m.
Soil Type II	Medium-dense sand , 15 m.
Soil Type III	Medium sand , 15 m.
Soil Type IV	Loose sand, 15 m.

Each soil type is defined by two properties; the maximum shear modulus**,** G_{max} and the shear wave velocity ν_s The maximum shear modules **(**G_{max}**)** is defined as (FHWA 1997);

$$G_{\max} = 11700 N^{0.8} \tag{11.23}$$

where N represents the standard penetration test blows per foot and G_{max} is expressed in kN/m^2. The shear wave velocity ν_s for the soil types considered is calculated as follows.

$$\nu_s = \sqrt{\frac{G_{\max} . g}{\gamma}} \tag{11.24}$$

where; g is the gravitational acceleration and γ is the unit weight of soil.

Table 11.3 gives the recommended N and γ values obtained from FHWA (1997) and corresponding G_{max} and v_s values calculated from Eqs. 11.23 and 11.24 for the AASHTO soil types considered in the analyses.

Table 11.3. The properties of soil types considered in this study

AASHTO Soil Types	**γ (kN/m^3)**	**N**	**G_{max} (kPa)**	**v_s (m/sec)**
Soil Type I	20	40	224.000	330
Soil Type II	19	27	163.400	290
Soil Type III	18	18	118.000	250
Soil Type IV	16	7	55.000	150

The soil types whose properties given above are modeled using the program PROSHAKE to obtain their free field response and to determine their equivalent shear modulus and damping properties for modeling purposes in SAP2000. In the models, the soil is divided into five segments with three meters lengths. Then, time history analyses are performed for each soil type using the selected earthquake records. The analyses are repeated for four different peak ground acceleration levels (0.2g, 0.35g, 0.5g and 0.8g) of each earthquake. The shear modulus and damping ratios of each segment of the soil types are obtained from the analyses results. The obtained shear modulus and damping ratios are presented in Tables 11.4-11. These parameters are then used to build soil column models in SAP2000 to simulate the effect of free field motion of the foundation soil on the seismic response of the bridge.

To test the accuracy of the soil column models built in SAP2000, the nonlinear time history analyses of the soil columns alone (without the bridge) are performed using the program SAP2000 and compared with those obtained from PROSHAKE. It is found that the displacement and velocity time histories obtained from SAP2000 analyses are generally in good agreement with those obtained from PROSHAKE analyses (Figs. 11.28-32). Thus, the soil column model is used together with the bridge model to simulate free-field effects.

Table 11.4. The equivalent shear modulus (G) (kN/m^2) for soil type I

Earthquakes	A_p	(m)	Peak Ground Accelerations (g)			
			0.20	**0.35**	**0.50**	**0.80**
Sanfernando	0.20	**-1.50**	190277	175608	169049	162628
		-4.50	146710	118327	107043	89675
		-7.50	119217	87842	72496	49766
		-10.50	102993	71147	53332	34139
		-13.50	94878	63554	43785	28592
		-15.00	1397984	1375868	1364266	1349922
Northridge	0.26	**-1.50**	185122	172628	168152	163384
		-4.50	131260	110703	104400	92986
		-7.50	98836	77437	70829	52839
		-10.50	80802	61908	52892	35778
		-13.50	73777	57729	42515	31160
		-15.00	1387021	1375951	1361608	1346497
Northridge	0.32	**-1.50**	189677	170686	164498	153895
		-4.50	145350	106189	94514	77570
		-7.50	116058	67421	56294	39658
		-10.50	97169	48742	37822	27639
		-13.50	84197	41138	31963	23677
		-15.00	1390690	1360727	1350217	1346202
Loma Prieta	0.20	**-1.50**	193075	168877	158613	143706
		-4.50	152491	104783	85338	61780
		-7.50	123433	64646	43097	26443
		-10.50	103306	40716	25650	13141
		-13.50	89287	30244	17304	9739
		-15.00	1390174	1341416	1326455	1301874
Loma Prieta	0.28	**-1.50**	184785	170063	160459	152086
		-4.50	131155	105228	86655	73228
		-7.50	97581	64106	43841	34576
		-10.50	75525	41659	27976	18006
		-13.50	61311	33235	19519	13059
		-15.00	1374279	1350444	1339613	1332802

Table 11.5. The equivalent damping ratio (ζ) (%) for soil type I

Earthquakes	A_p	(m)	Peak Ground Accelerations (g)			
			0.20	**0.35**	**0.50**	**0.80**
Sanfernando	0.20	**-1.50**	3.35	4.34	4.80	5.25
		-4.50	6.57	9.31	10.54	12.44
		-7.50	9.22	12.65	14.40	17.51
		-10.50	10.97	14.55	16.98	20.19
		-13.50	11.85	15.46	18.40	21.27
		-15.00	1.08	1.21	1.29	1.38
Northridge	0.26	**-1.50**	3.68	4.55	4.86	5.20
		-4.50	7.92	10.14	10.82	12.06
		-7.50	11.42	13.84	14.59	17.05
		-10.50	13.45	15.70	17.04	19.87
		-13.50	14.25	16.33	18.59	20.77
		-15.00	1.15	1.21	1.31	1.41
Northridge	0.32	**-1.50**	3.39	4.69	5.12	5.97
		-4.50	6.69	10.63	11.89	13.82
		-7.50	9.56	14.98	16.54	19.11
		-10.50	11.6	17.66	19.47	21.45
		-13.50	13.06	18.82	20.61	22.23
		-15.00	1.13	1.31	1.38	1.41
Loma Prieta	0.20	**-1.50**	3.17	4.81	5.58	6.82
		-4.50	6.09	10.78	12.93	15.72
		-7.50	8.76	15.3	18.5	21.69
		-10.50	10.94	18.9	21.84	24.45
		-13.50	12.48	20.95	23.55	25.41
		-15.00	1.13	1.44	1.53	1.66
Loma Prieta	0.28	**-1.50**	3.7	4.73	5.42	6.12
		-4.50	7.93	10.73	12.78	14.32
		-7.50	11.56	15.38	18.39	20.1
		-10.50	14.05	18.72	21.39	23.4
		-13.50	15.79	20.36	23.08	24.47
		-15.00	1.22	1.38	1.45	1.5

Table 11.6. The equivalent shear modulus (G) (kN/m^2) for soil type II

Earthquakes	A_p	(m)	Peak Ground Accelerations (g)			
			0.20	**0.35**	**0.50**	**0.80**
Sanfernando	0.20	**-1.50**	134703	127650	123383	116615
		-4.50	96756	84306	73615	60465
		-7.50	76242	59120	45762	31622
		-10.50	65421	44846	33454	23112
		-13.50	61077	39529	28550	19968
		-15.00	1409101	1391673	1382102	1373231
Northridge	0.26	**-1.50**	130324	126587	124298	119403
		-4.50	89085	83872	77433	66230
		-7.50	67977	61050	48329	37489
		-10.50	58324	45174	34020	25200
		-13.50	56012	37034	29300	19534
		-15.00	1404524	1386136	1378841	1366049
Northridge	0.32	**-1.50**	130813	123995	116624	114418
		-4.50	87776	75436	63087	59872
		-7.50	62227	46521	35959	31987
		-10.50	46811	33315	26401	21462
		-13.50	42379	28378	25078	15445
		-15.00	1392652	1380699	1376471	1363377
Loma Prieta	0.20	**-1.50**	131816	120295	112315	104414
		-4.50	90586	68600	56089	44356
		-7.50	64751	38292	27189	16450
		-10.50	46120	23690	14182	8796
		-13.50	35650	15327	10199	5286
		-15.00	1380645	1358645	1346519	1333477
Loma Prieta	0.28	**-1.50**	132382	120196	115652	111922
		-4.50	90326	68123	60269	54620
		-7.50	65279	38403	29995	26095
		-10.50	49346	24883	18184	13822
		-13.50	41246	18798	13774	9480
		-15.00	1389787	1367539	1362570	1351939

Table 11.7. The equivalent damping ratio (ζ) (%) for soil type II

Earthquakes	A_p	(m)	Peak Ground Accelerations (g)			
			0.20	0.35	0.50	0.80
Sanfernando	0.20	-1.50	3.78	4.45	4.86	5.55
		-4.50	7.85	9.68	11.26	13.27
		-7.50	10.87	13.48	15.63	18.5
		-10.50	12.49	15.82	18.13	20.7
		-13.50	13.17	16.9	19.25	21.54
		-15.00	1.02	1.12	1.18	1.23
Northridge	0.26	-1.50	4.20	4.56	4.77	5.24
		-4.50	8.98	9.75	10.7	12.37
		-7.50	12.10	13.18	15.16	17.31
		-10.50	13.60	15.75	18.01	20.14
		-13.50	13.96	17.4	19.05	21.65
		-15.00	1.05	1.15	1.2	1.28
Northridge	0.32	-1.50	4.15	4.8	5.55	5.8
		-4.50	9.17	10.99	12.86	13.36
		-7.50	12.99	15.48	17.62	18.43
		-10.50	15.42	18.16	19.83	21.14
		-13.50	16.32	19.3	20.18	22.75
		-15.00	1.12	1.18	1.21	1.3
Loma Prieta	0.20	-1.50	4.06	5.16	6.04	6.94
		-4.50	8.76	12	13.95	15.92
		-7.50	12.6	17.15	19.62	22.47
		-10.50	15.56	20.55	23.12	24.78
		-13.50	17.68	22.79	24.28	26.15
		-15.00	1.19	1.33	1.41	1.49
Loma Prieta	0.28	-1.50	4	5.17	5.66	6.08
		-4.50	8.8	12.07	13.3	14.18
		-7.50	12.52	17.13	18.87	19.91
		-10.50	15	20.23	22.01	23.22
		-13.50	16.55	21.85	23.24	24.51
		-15.00	1.13	1.27	1.3	1.37

Table 11.8. The equivalent shear modulus (G) (kN/m^2) for soil type III

Earthquakes	A_p	(m)	Peak Ground Accelerations (g)			
			0.20	0.35	0.50	0.80
Sanfernando	0.20	-1.50	93363	88330	85643	78775
		-4.50	66057	54870	49396	38094
		-7.50	50437	36725	29740	19552
		-10.50	42227	28379	20840	13567
		-13.50	38234	24978	19652	10637
		-15.00	1425614	1409806	1405157	1384499
Northridge	0.26	-1.50	92287	89208	86614	82966
		-4.50	64334	58042	52386	46078
		-7.50	51507	39331	32629	28511
		-10.50	42113	29706	21792	18580
		-13.50	33792	24418	18844	14085
		-15.00	1417712	1405831	1398359	1390423
Northridge	0.32	-1.50	90235	83033	81654	78008
		-4.50	58724	46751	44434	36526
		-7.50	41045	29037	27590	18560
		-10.50	31483	22608	19201	11956
		-13.50	28446	23259	16821	12312
		-15.00	1412612	1407730	1393772	1385200
Loma Prieta	0.20	-1.50	88131	80410	76346	72599
		-4.50	54839	41715	35124	30995
		-7.50	34096	20753	16610	10556
		-10.50	22653	12441	8505	4957
		-13.50	17854	9101	5609	2929
		-15.00	1392629	1375963	1366434	1351407
Loma Prieta	0.28	-1.50	87986	83404	81106	74060
		-4.50	54532	45998	42358	33796
		-7.50	34402	24510	21218	16442
		-10.50	24164	16453	13053	8014
		-13.50	19639	12453	9841	5522
		-15.00	1400198	1391349	1384417	1366833

Table 11.9. The equivalent damping ratio (ζ) (%) for soil type III

Earthquakes	A_p	(m)	Peak Ground Accelerations (g)			
			0.20	0.35	0.50	0.80
Sanfernando	0.20	-1.50	3.98	4.66	5.03	6.09
		-4.50	8.28	10.62	11.77	14.26
		-7.50	11.55	14.56	16.35	19.46
		-10.50	13.34	16.74	18.97	21.72
		-13.50	14.23	17.72	19.42	22.85
		-15.00	0.92	1.02	1.04	1.16
Northridge	0.26	-1.50	4.13	4.54	4.9	5.41
		-4.50	8.64	9.96	11.14	12.43
		-7.50	11.33	13.98	15.52	18.22
		-10.50	13.37	16.36	18.64	21.16
		-13.50	15.21	17.88	19.73	22.89
		-15.00	0.97	1.04	1.08	1.15
Northridge	0.32	-1.50	4.41	5.4	5.62	5.94
		-4.50	9.82	12.34	12.85	14.38
		-7.50	13.6	16.55	16.97	19.85
		-10.50	15.85	18.4	19.59	22.24
		-13.50	16.72	18.21	20.49	21.99
		-15.00	1	1.03	1.11	1.15
Loma Prieta	0.20	-1.50	4.69	5.82	6.48	7.09
		-4.50	10.63	13.46	14.91	15.99
		-7.50	15.14	19.01	20.57	22.88
		-10.50	18.39	22.15	23.73	25.45
		-13.50	20.1	23.48	25.09	26.63
		-15.00	1.12	1.21	1.28	1.37
Loma Prieta	0.28	-1.50	4.71	5.34	5.71	6.85
		-4.50	10.69	12.51	13.31	15.21
		-7.50	15.07	17.85	18.83	20.64
		-10.50	17.95	20.63	21.92	23.93
		-13.50	19.43	22.14	23.18	25.14
		-15.00	1.07	1.12	1.16	1.27

Table 11.10. The equivalent shear modulus (G) (kN/m^2) for soil type IV

Earthquakes	A_p	(m)	Peak Ground Accelerations (g)			
			0.20	**0.35**	**0.50**	**0.80**
Sanfernando	0.20	**-1.50**	25798	22728	20499	17873
		-4.50	14321	9555	6864	5189
		-7.50	9650	5872	4631	3336
		-10.50	8411	5466	4289	3376
		-13.50	7200	4633	3534	2694
		-15.00	1457000	1445845	1440861	1435761
Northridge	0.26	**-1.50**	28386	25267	23095	20936
		-4.50	17958	13327	10600	7873
		-7.50	12710	7952	6804	5781
		-10.50	10119	6306	6072	3344
		-13.50	9531	6233	3241	2369
		-15.00	1464770	1453890	1441592	1433770
Northridge	0.32	**-1.50**	26921	23998	23122	20688
		-4.50	15814	11591	9943	6780
		-7.50	11109	7957	6713	4454
		-10.50	10061	6420	5508	3169
		-13.50	9713	5765	3663	2411
		-15.00	1467299	1451753	1443950	1434305
Loma Prieta	0.20	**-1.50**	26140	23443	22822	21658
		-4.50	14468	10613	8896	6398
		-7.50	7302	4969	3586	2054
		-10.50	3555	2128	1808	1469
		-13.50	2568	1781	1663	1011
		-15.00	1440486	1434329	1443950	1434305
Loma Prieta	0.28	**-1.50**	27149	24800	23290	21020
		-4.50	15925	11375	9223	6528
		-7.50	9118	5935	3998	2692
		-10.50	6115	3392	2548	1678
		-13.50	3589	2478	1933	1225
		-15.00	1445496	1436961	1432459	1426052

Table 11.11. The equivalent damping ratio (ζ) (%) for soil type IV

Earthquakes	A_p	(m)	Peak Ground Accelerations (g)			
			0.20	0.35	0.50	0.80
Sanfernando	0.20	-1.50	5.79	7.34	8.7	10.42
		-4.50	12.78	16.31	18.74	20.72
		-7.50	16.23	19.92	21.38	22.94
		-10.50	17.34	20.39	21.78	22.89
		-13.50	18.43	21.38	22.68	23.77
		-15.00	0.81	0.85	0.86	0.88
Northridge	0.26	-1.50	4.61	6.06	7.16	8.41
		-4.50	10.36	13.47	15.37	17.83
		-7.50	13.9	17.76	18.82	20.02
		-10.50	15.81	19.4	19.68	22.93
		-13.50	16.34	19.49	23.06	24.19
		-15.00	0.77	0.82	0.86	0.89
Northridge	0.32	-1.50	5.23	6.7	7.14	8.58
		-4.50	11.76	14.67	15.96	18.84
		-7.50	15.01	17.75	18.92	21.59
		-10.50	15.86	19.27	20.35	23.15
		-13.50	16.17	20.04	22.52	24.13
		-15.00	0.76	0.83	0.85	0.89
Loma Prieta	0.20	-1.50	5.61	6.98	7.14	8.97
		-4.50	12.68	15.36	17.06	20.53
		-7.50	18.34	21.69	23.92	25.85
		-10.50	22.66	24.53	25.35	27.71
		-13.50	23.93	25.12	27.52	28.98
		-15.00	0.86	0.88	0.92	0.98
Loma Prieta	0.28	-1.50	5.14	6.29	7.06	8.36
		-4.50	11.69	14.82	16.61	19.14
		-7.50	16.71	19.84	22.13	23.77
		-10.50	19.63	22.87	23.95	25.29
		-13.50	22.61	24.04	24.86	26.08
		-15.00	0.85	0.88	0.89	0.92

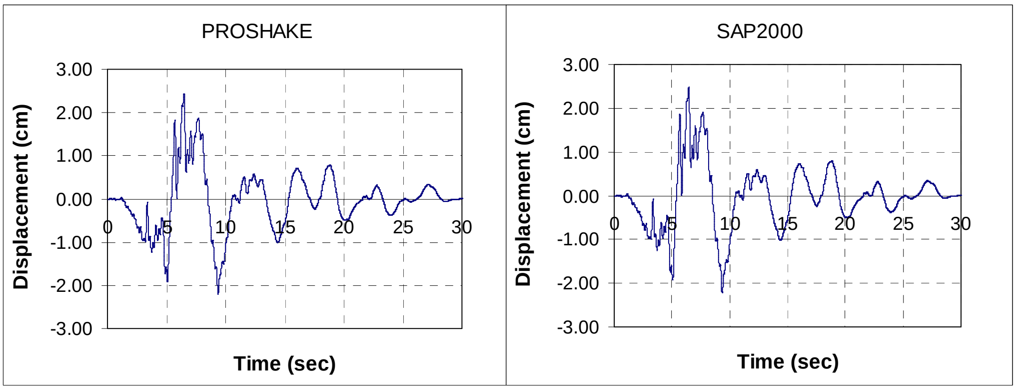

Figure 11.28. The displacement time histories obtained from PROSHAKE and SAP2000 analyses for San Fernando earthquake for A_p=0.2

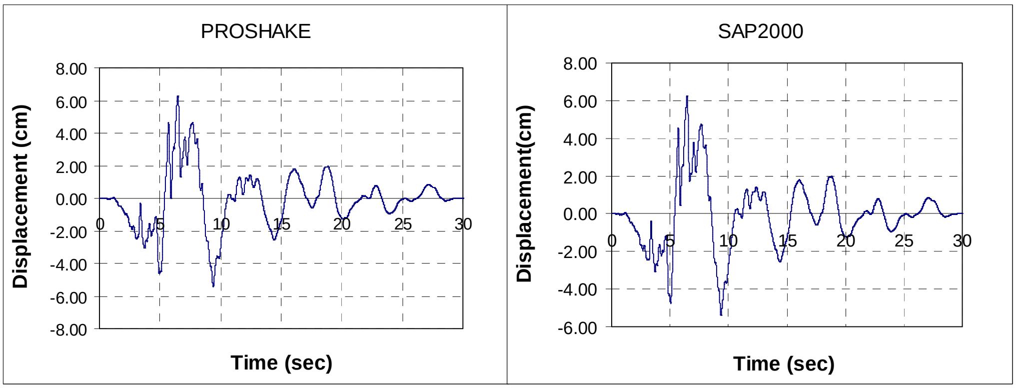

Figure 11.29. The displacement time histories obtained from PROSHAKE and SAP2000 analyses for San Fernando earthquake for A_p=0.5

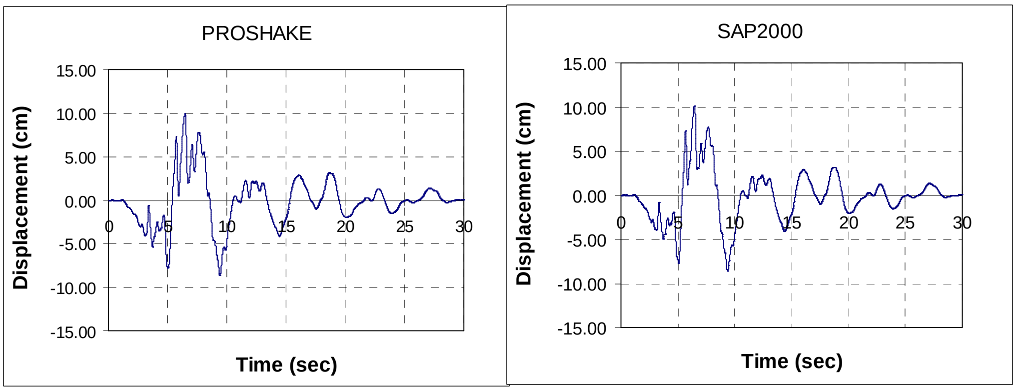

Figure 11.30. The displacement time histories obtained from PROSHAKE and SAP2000 analyses for San Fernando earthquake for A_p=0.8

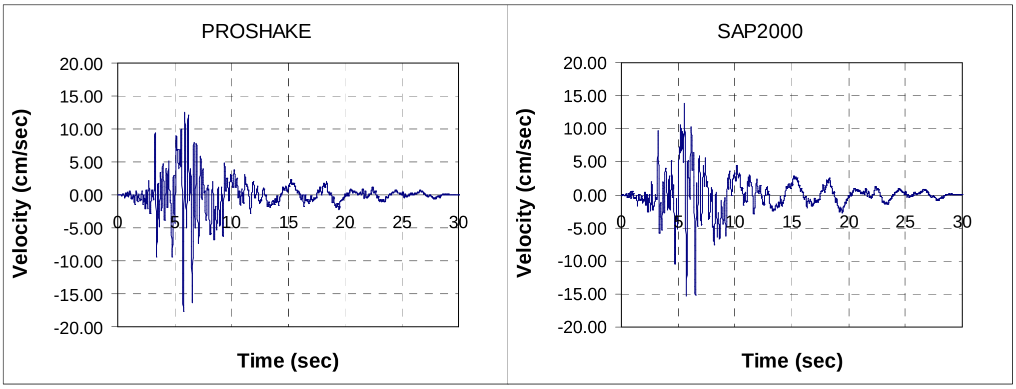

Figure 11.31. The velocity time histories obtained from PROSHAKE and SAP2000 analyses for San Fernando earthquake for A_p=0.2

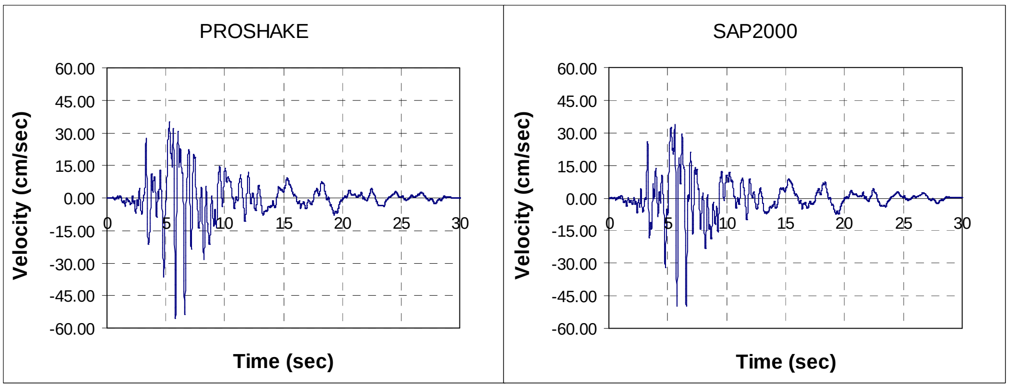

Figure 11.32. The velocity time histories obtained from PROSHAKE and SAP2000 analyses for San Fernando earthquake for A_p=0.8

11.7.3. IMPLEMENTATION OF SOIL COLUMN MODELS IN THE STRUCTURAL MODEL

The soil column models are built in SAP2000 using the parameters obtained from PROSHAKE analyses. Beam elements having a high flexural rigidity but a shear stiffness computed using the equivalent shear modulus obtained from PROSHAKE analyses is used to model the soil column (Fig. 11.33). The soil mass is lumped at each node along the soil column. Dashpots are used to simulate the equivalent damping effects in the soil. In the structural model, the free field motion of the foundation soil (e.g. displacements or accelerations of the soil layers) should not be affected by the response of the bridge due to the very large size of the soil field. This could be achieved by selecting a very large shear area for the soil column in the structural model. However, a too large shear area selected for the soil column may produce numerical instability during the nonlinear solution procedure as the stiffness of the soil column will be much larger than those of the structural members of the bridge. Accordingly, in the structural model, the size of the shear area of the soil column must be selected carefully to prevent such numerical instability during the nonlinear solution procedure. To define the optimum shear area of the soil columns used in the structural models, sensitivity analyses are conducted. For this purpose, nonlinear time history analyses of the soil column models having different shear area together with the bridge model are performed using the program SAP2000. Then the maximum displacements obtained from PROSHAKE analyses are compared to those obtained from SAP2000 analyses where the soil column and the bridge are modeled together (Fig 11.34). The maximum displacements are found to be almost same, when the shear area is chosen as larger than 600 m^2. Accordingly, the soil columns are modeled using frame elements having a shear area of 600 m^2 together with the bridge model.

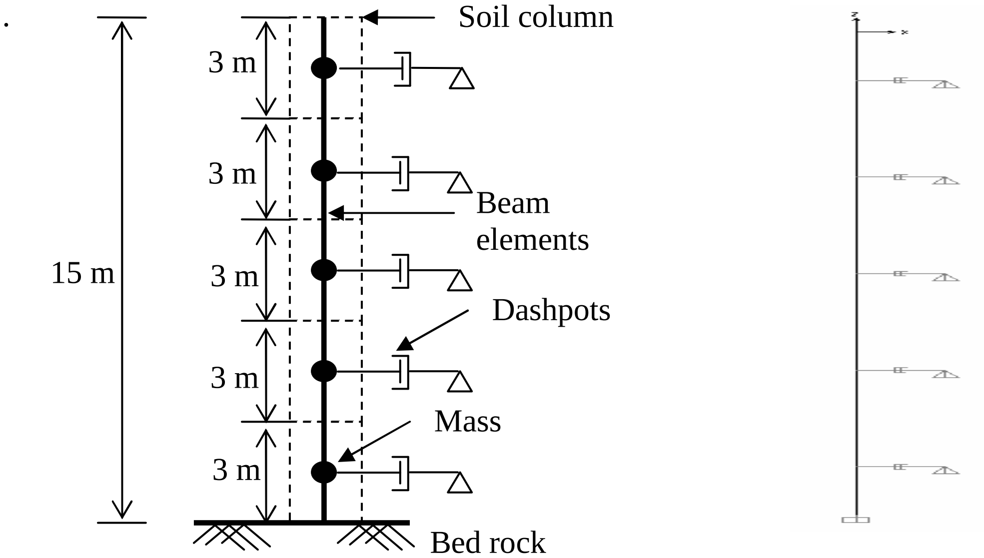

Figure 11.33. Soil column model

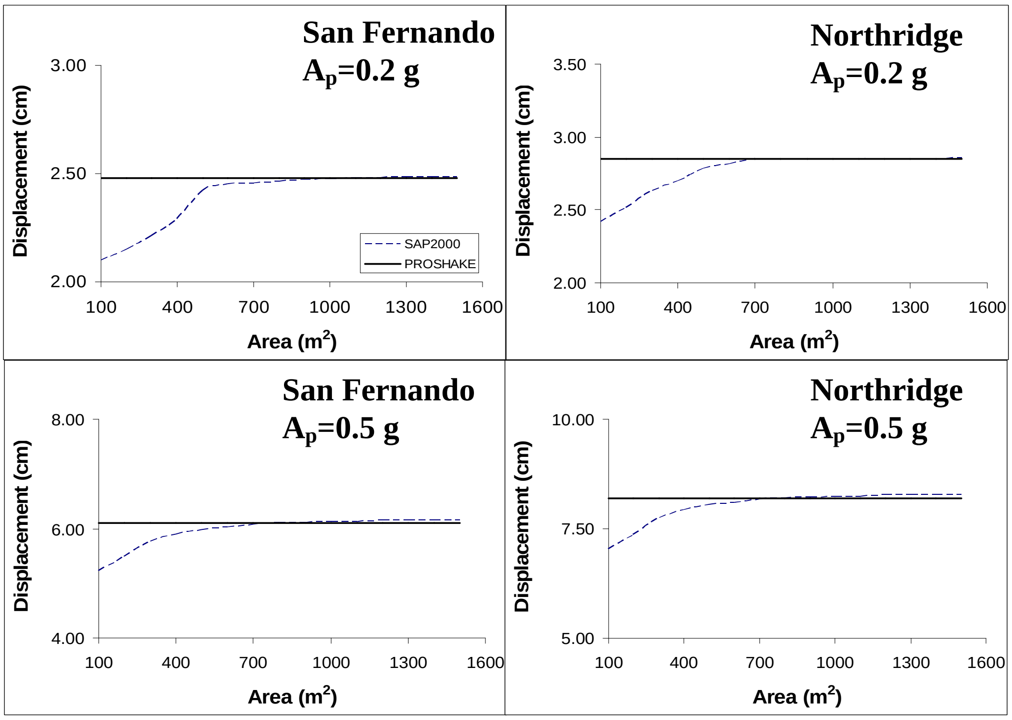

Figure 11.34. Sensitivity analyses results for shear area of soil column

CHAPTER 12

EFFECT OF MODELLING SIMPLIFICATONS ON SEISMIC ANALYSIS RESULTS OF INTEGRAL BRIDGES

In this part of the thesis study, the effect of modeling assumptions and simplifications on the seismic analyses results of IBs is investigated. This is mainly done to investigate the possibility of using a simpler model to facilitate the nonlinear time history analyses conducted as part of this research study. For this purpose, five structural models of two-span IB considered in this study are built in decreasing levels of complexity starting from a nonlinear structural model including the true behavior of the foundation and backfill soil and gradually simplifying the model to a level where the effect of backfill and foundation soil is totally excluded. In the most complicated nonlinear structural model (Model 1), the foundation soil is modeled in two parts (i) as a shear column with dashpots to simulate free field motion and (ii) dynamic p-y curves and dashpots connected between the piles and the shear column to simulate local soil-pile interaction effects and radiation damping. Moreover, the nonlinear dynamic interaction between the backfill and abutment is modeled using nonlinear springs and dashpots. The nonlinear model is simplified gradually where four additional models are built. First, the shear column is excluded from the structural model (Model 2). Then, the dashpots which are used to simulate radiation damping are excluded from the structural model (Model 3). Next, the soil-pile interaction is modeled using linear springs (Model 4). Finally, the piles are modeled without springs using an equivalent pile length concept (Model 5). On all the structural models considered, two sets of analyses are conducted by including and excluding the abutment-backfill interaction effects. Nonlinear time history analyses of the modeled IBs are then conducted using a set of ground motions with various intensities representing small, medium and large intensity earthquakes. The analyses results are then used to assess the effect of modeling complexity level on the seismic behavior of IBs.

12.1. NONLINEAR TIME-HISTORY ANALYSES OF THE BRIDGE MODELS

A total of 10 IB models are built and the nonlinear time history analyses of the IB models are conducted using the seven earthquake ground motions considered in this study. The nonlinear time history analyses are repeated for peak ground accelerations of 0.2g, 0.35g, 0.5g and 0.8g for each selected earthquake. This led to a total of 280 different analyses cases. The analyses results are given in the following sections.

12.1.1 ANALYSES RESULTS

In the following subsections, the effect of modeling simplification on seismic analysis of IBs is presented in terms of the maximum displacements of the deck and bearings as well as the maximum displacements and plastic end rotations of the steel piles and pier columns. The analyses results are presented in Figs 12.1-12.7 as the average of the results from the seven ground motions considered in this study.

12.1.1.1 EFFECT OF MODELLING SIMPLIFICATION ON THE DECK AND BEARING DISPLACEMENTS

Fig. 12.1 and 12.2 display the maximum absolute deck and bearing (bearings on the pier) displacements relative to the pier top in the longitudinal direction as a function of five structural modeling cases considered in this study and for the cases of including and excluding the abutment-backfill interaction behavior from the structural model. Figs. 12.3 and 12.4 display similar results in the transverse direction. It is observed from the figures that simplification of the structural model leads to significant discrepancies in the analyses results for the maximum deck and bearing displacements. The figures reveal that compared to simpler structural models, the most complicated structural model (Model 1) results in larger deck displacements especially for the case where the bridge is subjected to large intensity earthquakes. For instance, for structural Model 1 subjected to ground motions scaled to A_p=0,8g, the maximum deck displacement in the longitudinal direction is obtained as 109 mm for the case where the abutment-backfill interaction behavior is included in the structural model. However, for structural Models 2, 3, 4 and 5 analyzed using the same ground motions and scales and including the abutment-backfill behavior in the structural models, the maximum deck displacements are obtained as 87, 92, 101 and 98 mm respectively. The differences between the maximum average deck displacements obtained from Model 1 and Models 2, 3, 4 and 5 are 25%, 18%, 8% and 11% respectively. Similar results are also obtained in the transverse direction as observed from Fig. 12.3. For the maximum bearing displacements, the observations are similar to those of the deck displacements as observed from Fig. 12.2 and 12.4. Similar observations are also made for the cases where the abutment-backfill interaction behavior is excluded from the structural model. That is, Model 1 yields deck and bearing displacements larger than those obtained from the other simpler models. However, the figures also reveal that in general, larger maximum absolute deck and bearing displacements are obtained when the nonlinear abutment-backfill interaction behavior is excluded from the structural model, especially for the case where the bridge is subjected to large intensity earthquakes. These observations obviously indicate that a full soil column model (including radiation damping and p-y curves representing local soil-pile interaction) and the nonlinear abutment backfill interaction behavior must be included in the structural models of IBs for an accurate estimation of seismic deck and bearing displacements.

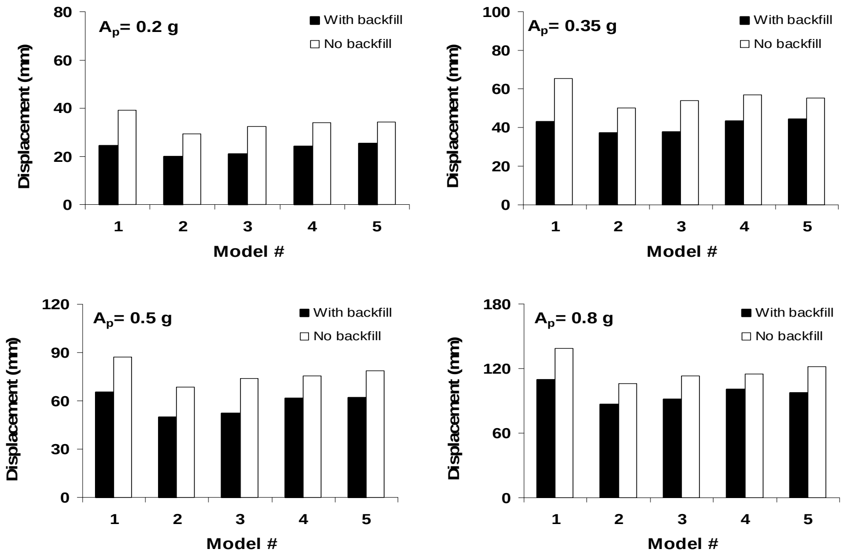

Figure 12.1. Deck displacements in longitudinal direction obtained from the analyses of Models 1-5 for including and excluding backfill in the structural model

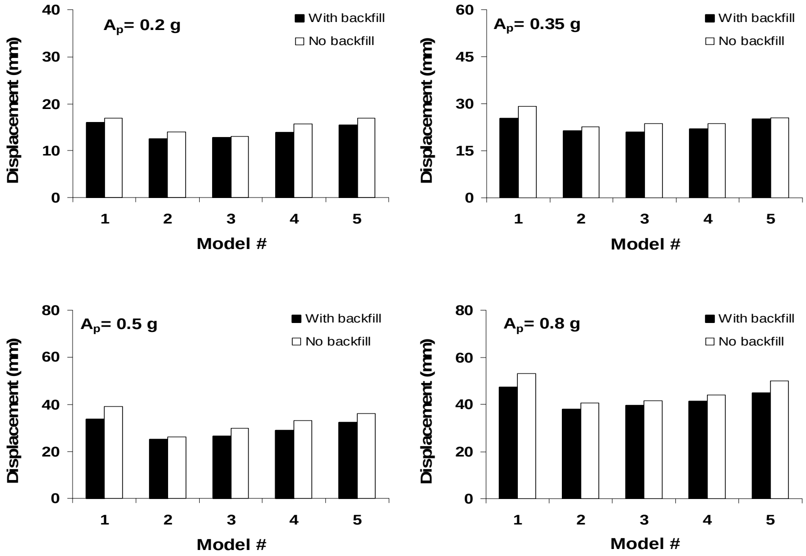

Figure 12.2. Bearing displacements in longitudinal direction obtained from the analyses of Models 1-5 for including and excluding backfill in the structural model

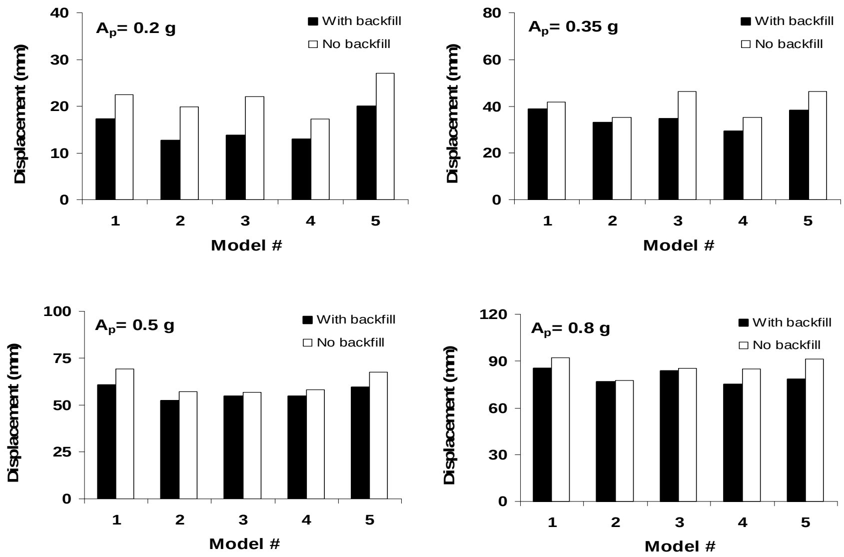

Figure 12-3. Deck displacements in transverse direction obtained from the analyses of Models 1-5 for including and excluding backfill in the structural model

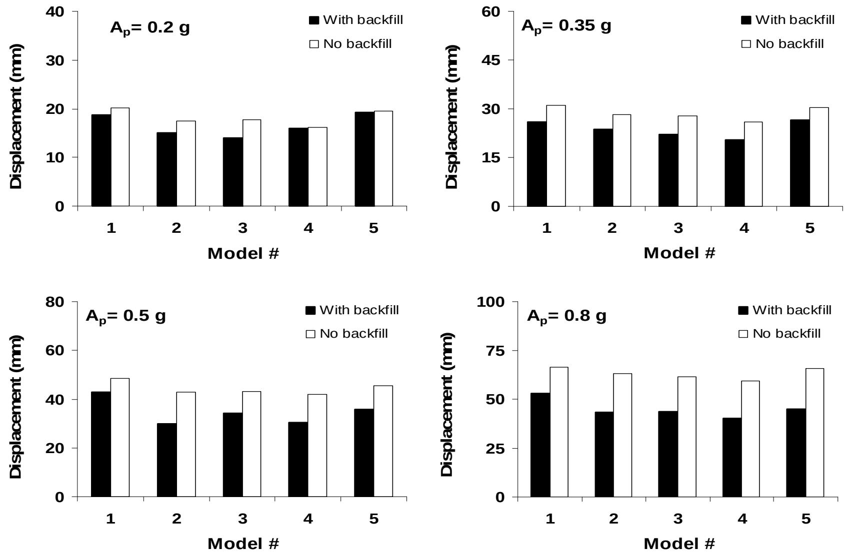

Figure 12.4 Bearing displacements in transverse direction obtained from the analyses of Models 1-5 for including and excluding backfill in the structural model

12.1.1.2 EFFECT OF MODELLING SIMPLIFICATION ON THE PIER COLUMN DRIFTS AND ROTATIONS

In this section, the effect of the model simplification on the pier column drifts (top displacement minus bottom displacement) and rotations is studied. Fig. 12.5-8 display the maximum absolute pier column drifts and rotations in the longitudinal and transverse direction as a function of five structural modeling cases considered in this study and for the cases of including and excluding the abutment-backfill interaction behavior from the structural model. It is observed from the figures that simplification of the structural model leads to significant discrepancies in the analyses results for the pier column drifts and rotations. The figures reveal that compared to simpler structural models, the most complicated structural model (Model 1) results in larger pier column drift especially for the case where the bridge is subjected to large intensity earthquakes. For instance, for structural Model 1 subjected to ground motions scaled to A_p=0,8g, the maximum pier column drift in the longitudinal direction is obtained as 55 mm for the case where the abutment-backfill interaction behavior is included in the structural model. However, for structural Models 2, 3, 4 and 5 analyzed using the same ground motions and scales and including the abutment-backfill behavior in the structural models, the maximum column drifts are obtained as 45, 47, 49 and 52 mm respectively. The differences between the maximum average pier column drifts obtained from Model 1 and Models 2, 3, 4 and 5 are 22%, 17%, 12% and 6% respectively. Similar results are also obtained in the transverse direction as observed from Fig. 12.7. For the maximum pier rotations, the observations are similar to those of the deck displacements as observed from Fig. 12.6 and 12.8. Similar observations are also made for the cases where the abutment-backfill interaction behavior is excluded from the structural model. That is, Model 1 yields pier column drifts and rotations larger than those obtained from the other simpler models. However, the figures also reveal that in general, larger maximum column drift and rotations are obtained when the nonlinear abutment-backfill interaction behavior is excluded from the structural model, especially for the case where the bridge is subjected to large intensity earthquakes. These observations obviously indicate that a full soil column model (including radiation damping and p-y curves representing local soil-pile interaction) and the nonlinear abutment backfill interaction behavior must be included in the structural models of IBs for an accurate estimation of seismic pier column drifts and rotations.

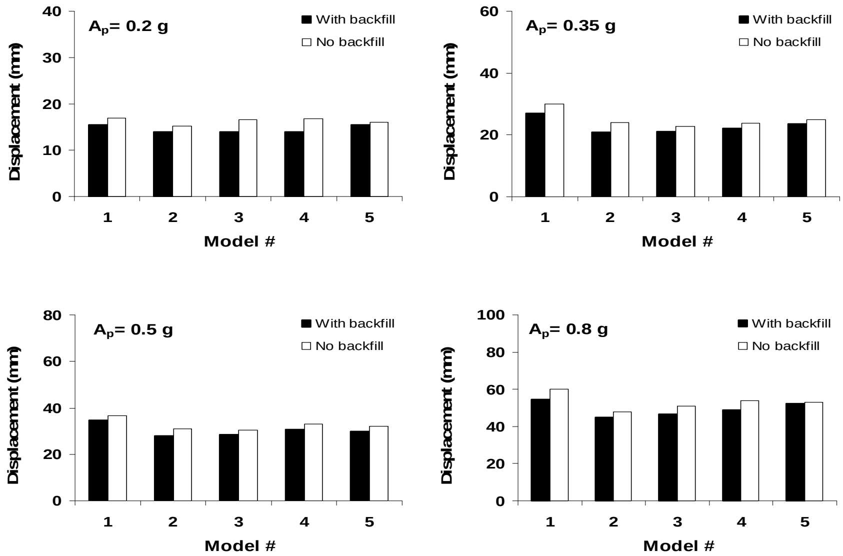

Figure 12.5. Pier column drifts in longitudinal direction obtained from the analyses of Models 1-5 for including and excluding backfill in the structural model

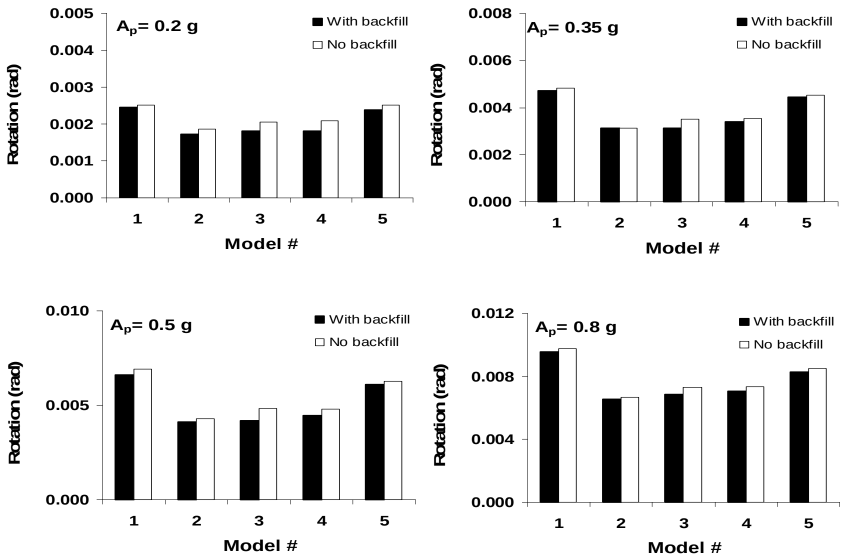

Figure 12.6. Pier column rotations in longidudinal direction obtained from the analyses of Models 1-5 for including and excluding backfill in the structural model

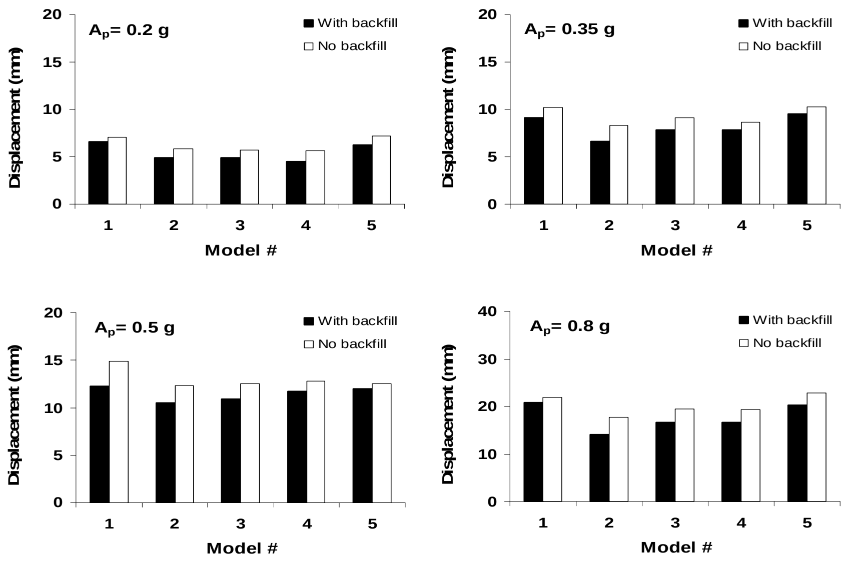

Figure 12.7. Pier column drifts obtained in transverse direction from the analyses of Models 1-5 for including and excluding backfill in the structural model

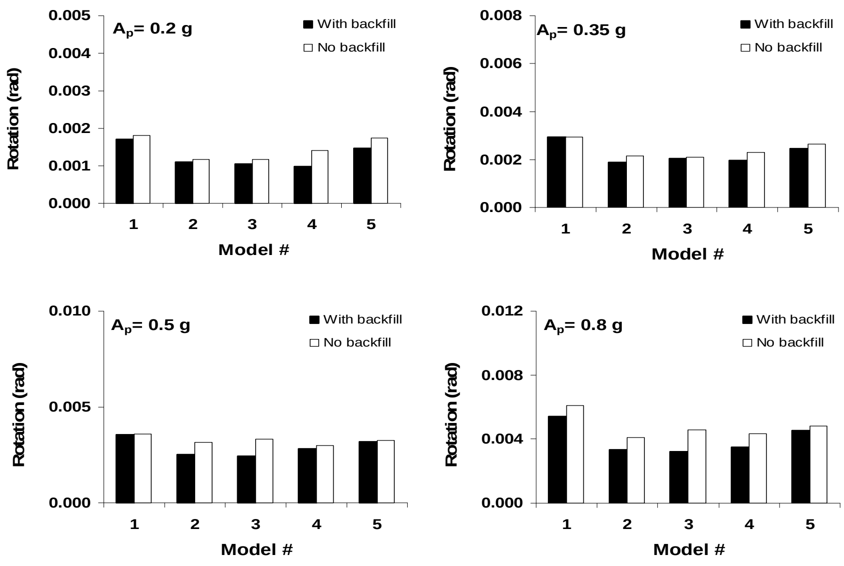

Figure 12.8. Pier column rotations in transverse direction obtained from the analyses of Models 1-5 for including and excluding backfill in the structural model

12.1.1.3 EFFECT OF MODELLING SIMPLIFICATION ON THE STEEL H-PILE DISPLACEMENTS AND ROTATIONS

In this section, the effect of the model simplification on the displacements and rotations of the steel H piles underneath the abutment in the transverse and longitudinal directions is studied. Fig. 12.9 and 12.10 display the maximum pile displacements and rotations in the longitudinal direction as a function of five structural modeling cases considered in this study and for the cases of including and excluding the abutment-backfill interaction behavior from the structural model. Figs. 12.11 and 12.12 display similar results in the transverse direction. It is observed from the figures that simplification of the structural model leads to significant discrepancies in the analyses results for the maximum pile displacements and rotations of IBs. The figures reveal that compared to simpler structural models, the most complicated structural model (Model 1) results in larger pile displacements especially for the case where the bridge is subjected to large intensity earthquakes. For instance, for structural Model 1 subjected to ground motions scaled to A_p=0,8g, the maximum pile displacement in the longitudinal direction is obtained as 95 mm for the case where the abutment-backfill interaction behavior is included in the structural model. However, for structural Models 2, 3, 4 and 5 analyzed using the same ground motions and scales and including the abutment-backfill behavior in the structural models, the maximum deck displacements are obtained as 72, 77, 87, and 84 mm respectively. The differences between the maximum average deck displacements obtained from Model 1 and Models 2, 3, 4 and 5 are 32%, 23%, 9% and 13%. respectively. Similar results are also obtained in the transverse direction as observed from Fig. 12.11. For the maximum pile rotations, the observations are similar to those of the pile displacements as observed from Fig. 12.10 and 12.12. Similar observations are also made for the cases where the abutment-backfill interaction behavior is excluded from the structural model. That is, Model 1 yields pile displacements and rotations larger than those obtained from the other simpler models. However, the figures also reveal that in general, larger maximum pile displacements and rotations are obtained when the nonlinear abutment-backfill interaction behavior is excluded from the structural model, especially for the case where the bridge is subjected to large intensity earthquakes. These observations obviously indicate that a full soil column model (including radiation damping and p-y curves representing local soil-pile interaction) and the nonlinear abutment backfill interaction behavior must be included in the structural models of IBs for an accurate estimation of seismic pile displacements and rotations.

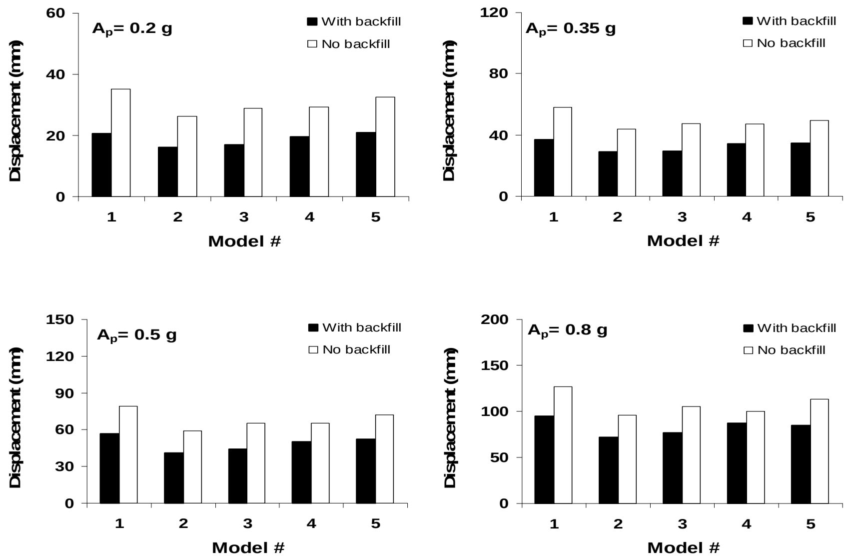

Figure 12.9. Pile underneath the abutment displacements in longitudinal direction obtained from the analyses of Models 1-5 for including and excluding backfill in the structural model

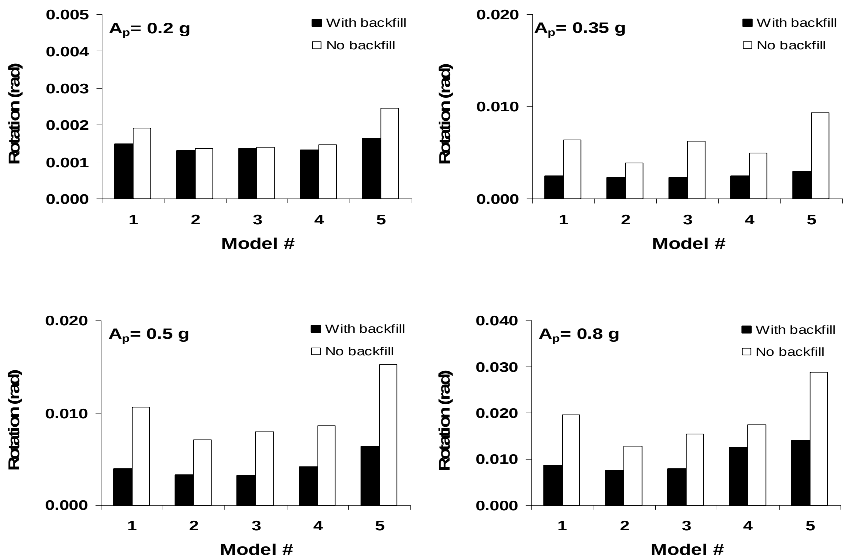

Figure 12.10. Pile underneath the abutment rotations in longitudinal direction obtained from the analyses of Models 1-5 for including and excluding backfill in the structural model

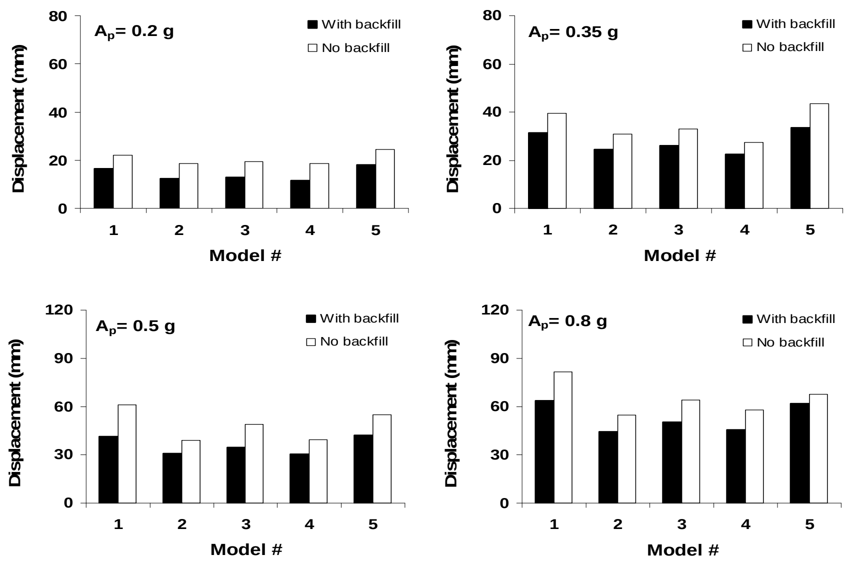

Figure 12-11. Pile underneath the abutment displacements in transverse direction obtained from the analyses of Models 1-5 for including and excluding backfill in the structural model

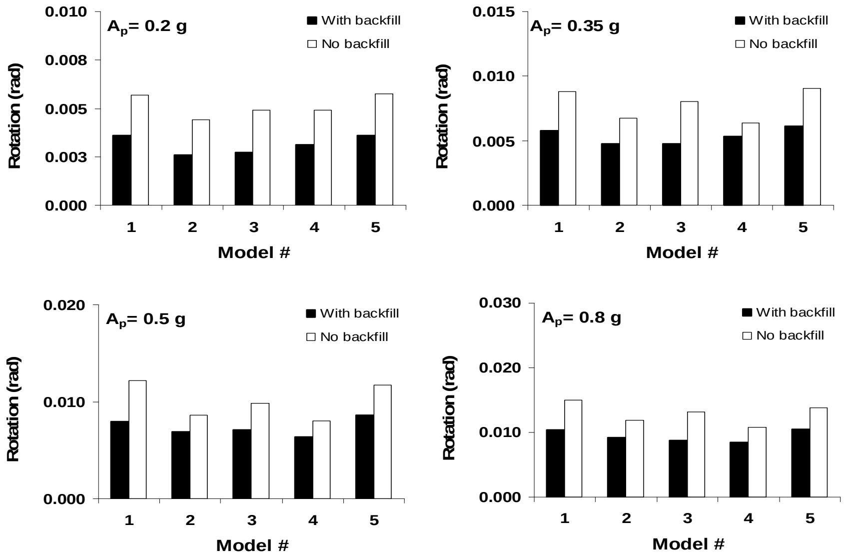

Figure 12.12. Pile underneath the abutment rotations obtained in transverse direction from the analyses of Models 1-5 for including and excluding backfill in the structural model

12.1.1.4 EFFECT OF MODELLING SIMPLIFICATION ON THE DISPLACEMENTS OF PILES UNDERNEATH THE PIER

In this section, the effect of the model simplification on the displacements of the piles underneath the pier is studied. Fig. 12.13 displays the maximum pile displacements in the longitudinal direction as a function of five structural modeling cases considered in this study and for the cases of including and excluding the abutment-backfill interaction behavior from the structural model. Fig. 12.14 displays similar results in the transverse direction. It is observed from the figures that simplification of the structural model leads to significant discrepancies in the analyses results for the maximum pile displacements and rotations of IBs. The figures reveal that compared to simpler structural models, the most complicated structural model (Model 5) results in larger pile displacements especially for the case where the bridge is subjected to large intensity earthquakes. For instance, for structural Model 5 subjected to ground motions scaled to A_p=0,8g, the maximum pile displacement in the longitudinal direction is obtained as 71 mm for the case where the abutment-backfill interaction behavior is included in the structural model. However, for structural Model 1, 2, 3 and 4 analyzed using the same ground motions and scales and including the abutment-backfill behavior in the structural models, the maximum pile displacements are obtained as 63, 36, 38, and 39 mm respectively. The differences between the maximum average pile displacements obtained from Model 5 and Model 1, 2, 3 and 4 are 13%, 97%, 87% and 82%. respectively. Similar results are also obtained in the transverse direction as observed from Fig. 12.14. That is, Model 5 yields pile displacements larger than those obtained from the other models. However, the figures also reveal that in general, the nonlinear abutment-backfill interaction behavior is found to have negligible effects on the pile displacements.

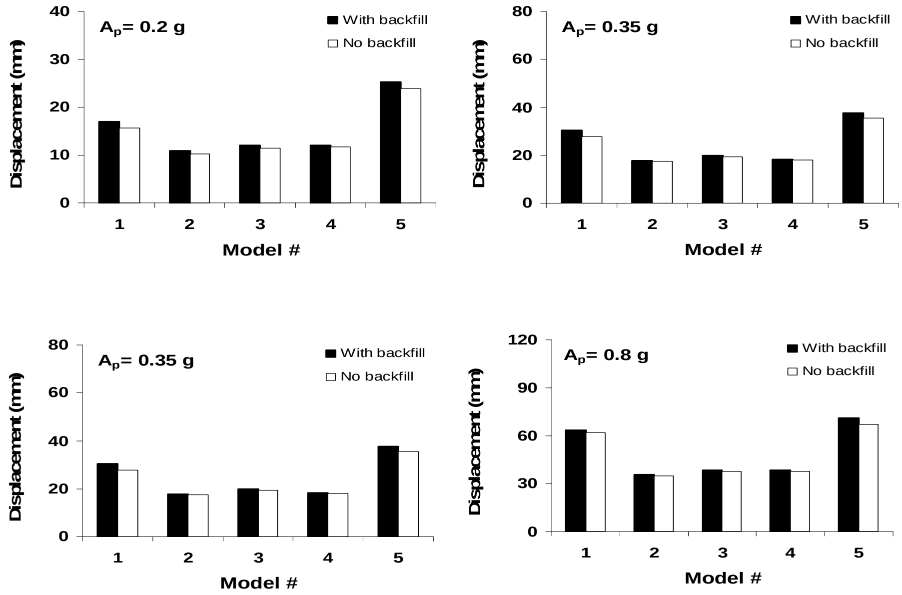

Figure 12.13. Pile underneath the pier displacements in longitudinal direction obtained from the analyses of Models 1-5 for including and excluding backfill in the structural model

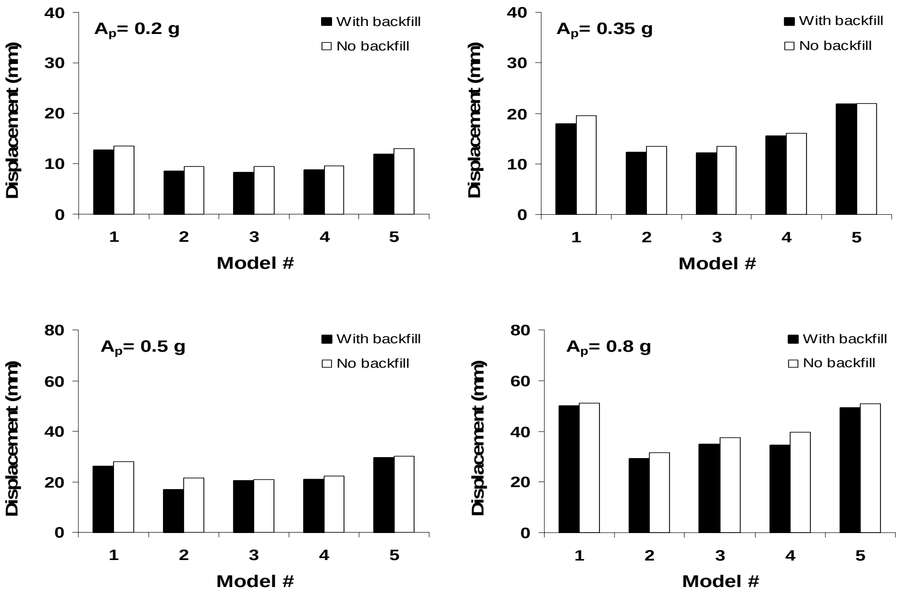

Figure 12.14. Pile underneath the pier displacements in transverse direction obtained from the analyses of Models 1-5 for including and excluding backfill in the structural model

CHAPTER 13

SEISMIC PERFORMANCE EVALUATION OF INTEGRAL BRIDGES AS A FUNCTION OF VARIOUS PARAMETERS

In this part of the thesis study, the effect of soil-structure interaction and substructure properties at the abutments on the seismic performance of IBs is investigated. For this purpose, numerous nonlinear structural models of a two-span IB including dynamic soil-bridge interaction effects are built. Then, nonlinear time history analyses of the IB models are conducted using a set of ground motions with various intensities. In the analyses, the effect of various substructure properties such as soil stiffness, backfill compaction level, pile size and orientation, abutment height and thickness are considered. The results of the nonlinear time history analyses are then used to assess the seismic performance of IBs as a function of the structural and geotechnical parameters considered in this study.

13.1 PARAMETERS CONSIDERED

A parametric study is conducted to investigate the effects of various structural and geotechnical parameters on the seismic performance of IBs. The stiffness of the foundation soil (sand) is anticipated to affect the seismic performance of IBs. Thus, four different soil stiffness (loose, medium, medium-dense and dense sands) are considered in the analyses. Furthermore, to cover a wide range of possible IB configurations, abutment height (3, 4 and 5 m) and thickness (1, 1.5 and 2 m) as well as pile size (HP250x85 and HP310x174) and orientation are varied. The details of these parameters are presented in Table 12.1.

Table 13.1. Parameters considered in the analyses.

PARAMETERS	DESCRIPTION
Pile sizes	HP 310x174 (LP), HP 250x85 (SP)
Pile orientation	Strong axis (SA) and weak axis (WA) bending
Abutment thickness (m)	1, 1.5, 2.
Abutment height (m)	3, 4, 5.
Soil type	Loose, medium, medium-dense and dense
Backfill compaction level	Compacted and uncompacted backfill

LP: Large Pile, SP: Small Pile, SA: Strong Axis, WA: Weak Axis

13.2 NONLINEAR TIME-HISTORY ANALYSES OF THE BRIDGE MODELS

A total of 16 IB models are built and the nonlinear time history analyses of the IB models are conducted using the seven earthquake ground motions considered in this study. The nonlinear time history analyses are repeated for peak ground accelerations of 0.2g, 0.35g, 0.5g and 0.8g for each selected earthquake. This led to a total of 448 different analyses cases. The analyses results are given in the following sections.

13.2.1 EFFECT OF FOUNDATION SOIL STIFFNESS ON THE SEISMIC PERFORMANCE OF INTEGRAL BRIDGES

In the following subsections, the effect of the foundation soil stiffness on the seismic performance of IBs is presented in terms of the maximum displacements of the deck and bearings as well as the maximum displacements and plastic end rotations of the steel piles and pier columns obtained in both longitudinal and transverse directions. The analyses results are presented in Figs 13.1-13.8 as the average of the results from the seven ground motions considered in this study.

13.2.1.1 THE EFFECT OF FOUNDATION SOIL STIFFNESS ON THE PERFORMANCE OF THE DECK AND BEARINGS

Figs. 13.1 and 13.2 display the maximum absolute deck and bearing (bearings on the pier) displacements relative to the pier top in longitudinal and transverse directions respectively, as a function of the peak ground acceleration for various foundation soil stiffnesses. It is observed from the figures that the foundation soil stiffness has a significant effect on the maximum deck displacements. The figures reveal that stiffer foundation soils produce smaller maximum absolute displacement in the deck of IBs especially in the case of large intensity earthquakes. This is mainly due to the larger foundation flexibility in the case of soft soil conditions producing larger absolute deck displacements. For instance, for A_p=0,8g, the maximum deck displacements in the longitudinal direction are 118 and 94 mm for loose and dense sands respectively. The differences between the maximum average deck displacements obtained for dense and loose sands are 25%. Consequently, for IBs built on stiff soils, smaller deck displacements are expected. However, in the case of bearing displacements relative to the pier top, stiffer foundation soil conditions results in larger bearing displacements. For stiff foundation soil conditions, the substructure displacement is small. This obviously produces higher displacement demand on the much more flexible bearings. However, because of the large flexibility of the bearings, the difference between the bearing displacements for various foundation soil stiffness conditions is negligible.

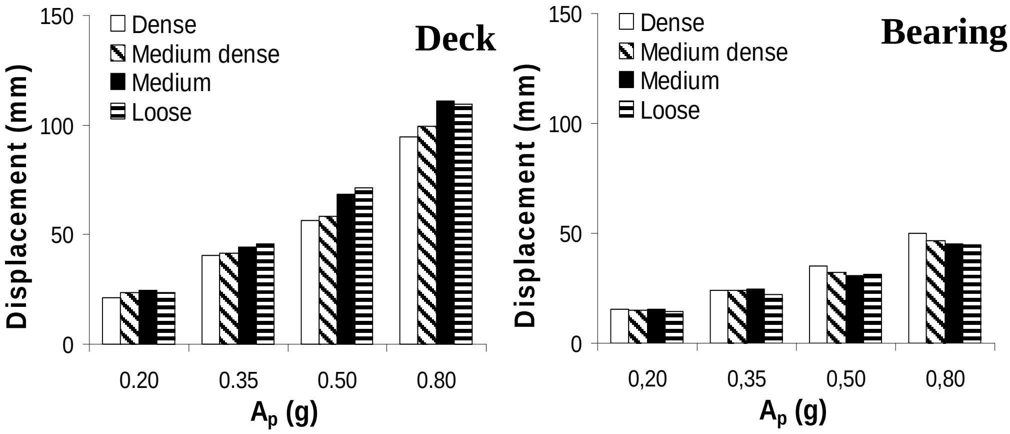

Figure 13.1. Deck and bearing displacements in longitudinal direction vs. peak ground acceleration for different soil stiffnesses.

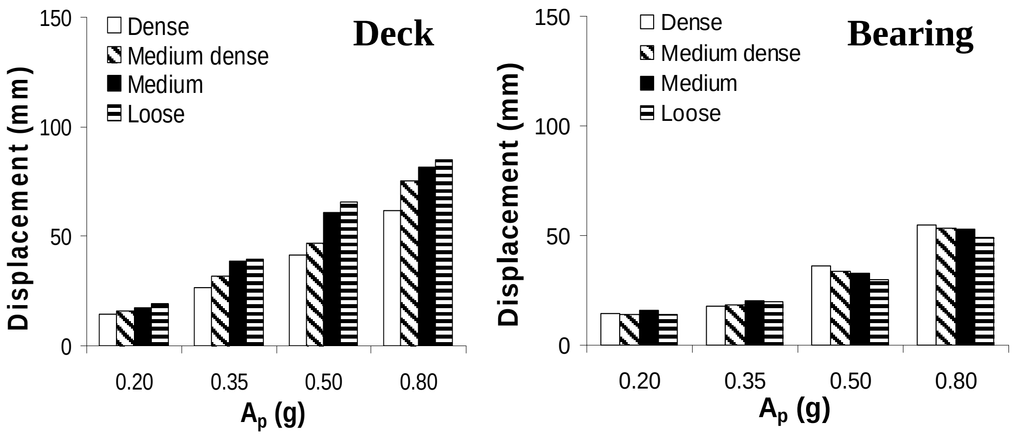

Figure 13.2. Deck and bearing displacements in transverse direction vs. peak ground acceleration for different soil stiffness.

13.2.1.2 THE EFFECT OF FOUNDATION SOIL STIFFNESS ON THE PERFORMANCE OF THE PIER COLUMNS

In this section, the effect of the foundation soil stiffness on the performance of the pier columns is studied in terms of the column drifts (top displacement minus bottom displacement) and rotations. Smaller plastic drifts and rotations are indicative of less structural damage and hence better seismic performance. The effect of the foundation soil stiffness on the pier column drifts and rotations in the longitudinal and transverse directions are illustrated in Figs. 13.3 and 13.4. It is observed from the figures that the foundation soil stiffness has a significant effect on the pier column drifts and rotations for IBs. The figures reveal that larger foundation soil stiffness values produce larger maximum column drifts and rotations especially in the case of large intensity earthquakes. This could be explained as follows; for stiff foundation soil conditions, the pile displacements are small. This obviously produces higher drift/rotation demands on the pier columns. For instance, for A_p=0,8g, the maximum pier column drifts in the longitudinal direction are 48 and 63 mm for loose and dense sands respectively. The difference between the maximum average drifts obtained for dense and loose sands is 31 %. Similar results are also obtained for column end rotations., For instance, for A_p=0.5g, the maximum column end rotations in the longitudinal direction for loose and dense sands are 0.0050 and 0.0063 rad. respectively. The differences between the maximum average column end rotations obtained for dense and loose sands is 26 %. In summary, the effect of foundation soil stiffness on the pier column drift and rotations is found to be significant. The piers of IBs built on soft soil conditions will experience less damage (better performance) in the case of a potential earthquake.

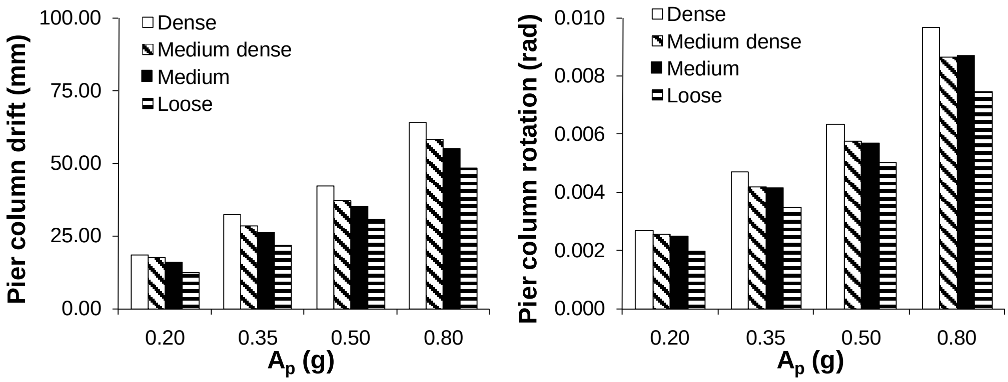

Figure 13.3. Pier column drifts and end rotations in longitudinal direction vs. peak ground acceleration for different soil stiffnesses.

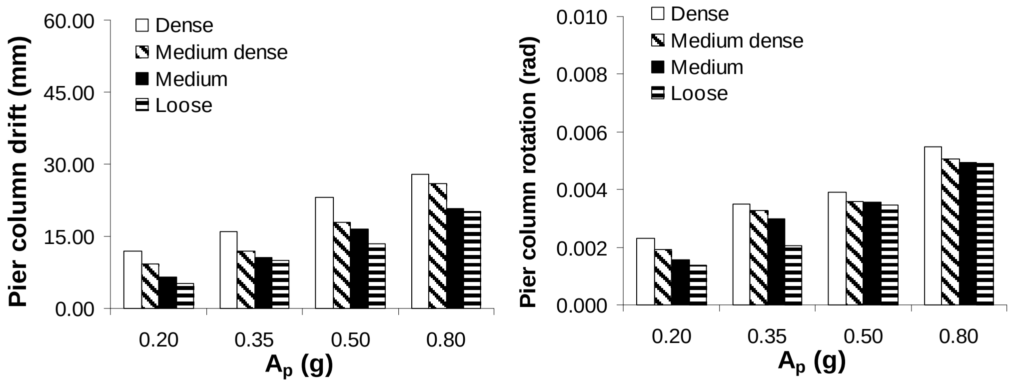

Figure 13.4. Pier column drifts and end rotations in transverse direction vs. peak ground acceleration for different soil stiffnesses

13.2.1.3 THE EFFECT OF FOUNDATION SOIL STIFFNESS ON PERFORMANCE OF STEEL H PILES

In this section, the effect of the foundation soil stiffness on the displacements and end rotations of the steel H piles underneath the abutments is studied. Fig. 13.5 and 13.6 display the variations in steel H pile displacements and end rotations in the longitudinal and transverse directions respectively, as a function of the range of peak ground accelerations considered in this study for various foundation soil stiffnesses. As observed from the figures, the foundation soil stiffness has remarkable effects on the pile displacements and end rotations for IBs. The analyses results reveal that larger sand stiffness values produce smaller maximum displacements in steel H piles of IBs especially in the case of large intensity earthquakes due to the large rigidity of the pile-soil system. For instance, for A_p=0,8g, the maximum pile displacements in the longitudinal direction are 98 and 77 mm for loose and dense sands respectively. The difference between the maximum pile displacements obtained for dense and loose sands is 28 %. For the steel H pile top rotations however, the opposite is true. That is, larger foundation soil stiffness values produce larger maximum plastic rotations in steel H piles of IBs. In the case of stiff foundation soil conditions, the equivalent pile length, which is the length of the pile to the point of fixity within the soil, becomes much smaller. This results in much larger plastic rotations since the cord rotations are calculated as the ratio of pile displacement to the equivalent pile length. The maximum difference between the maximum pile rotations obtained for dense and loose sands is 156%. Accordingly, the steel H piles of IBs built on soft soil conditions (smaller plastic rotations) will experience less damage (better performance) in the case of a potential earthquake.

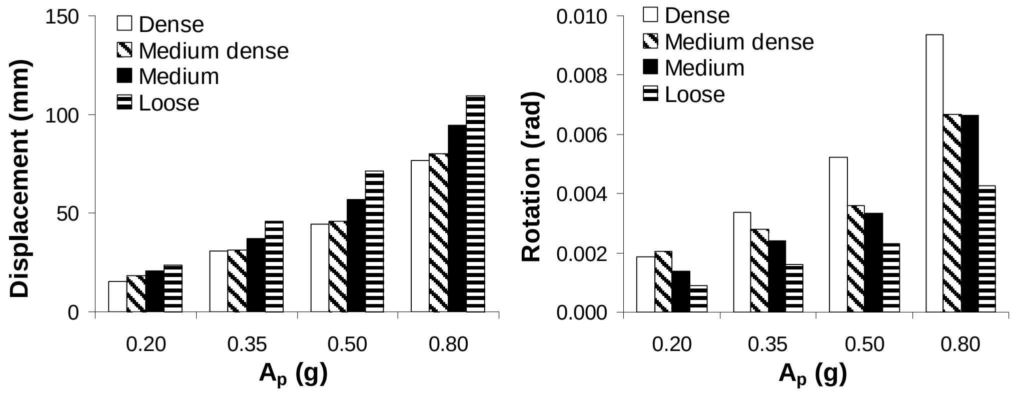

Figure 13.5. Steel H-Pile displacements and rotations in longitudinal direction vs. peak ground acceleration for different soil stiffnesses.

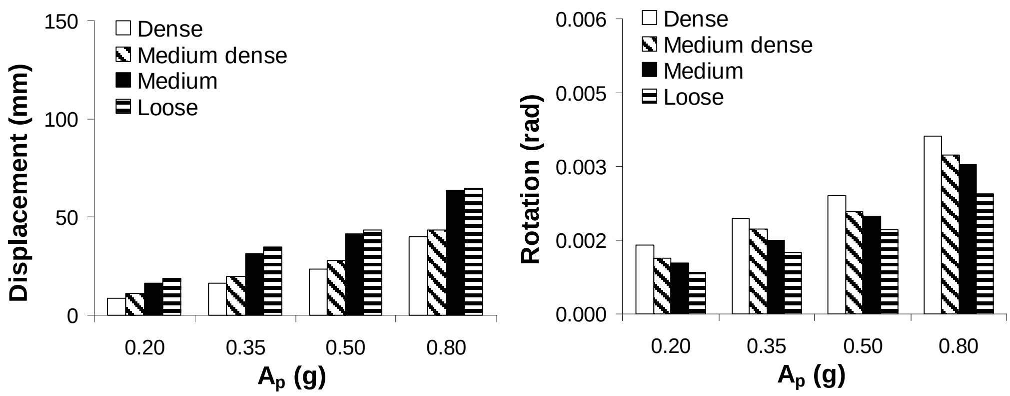

Figure 13.6. Steel H-Pile displacements and rotations in transverse direction vs. peak ground acceleration for different soil stiffnesses

13.2.1.4 THE EFFECT OF FOUNDATION SOIL STIFFNESS ON PERFORMANCE OF PILES UNDERNEATH THE PIER

In this section, the effect of the foundation soil stiffness on the displacements of the reinforced concrete piles underneath the piers is studied. It is noteworthy that due to the capacity protection design procedure, flexural yielding is allowed only at the pier column bases. Hence, the piles do not experience any plastic end rotations. Figs. 13.7 and 13.8 display the effect of the foundation soil stiffness on the pile displacements in the longitudinal and transverse directions respectively, as a function of the peak ground accelerations considered in this study for various foundation soil stiffnesses. The figures reveal that the foundation soil stiffness has remarkable effects on the displacements of the reinforced concrete piles in IBs. For instance, for A_p=0,8g, the maximum pile displacements in longitudinal direction are 42.6 and 34.1 mm for loose and dense sands respectively. The maximum difference between the maximum pile displacements obtained for dense and loose sands is 25%.

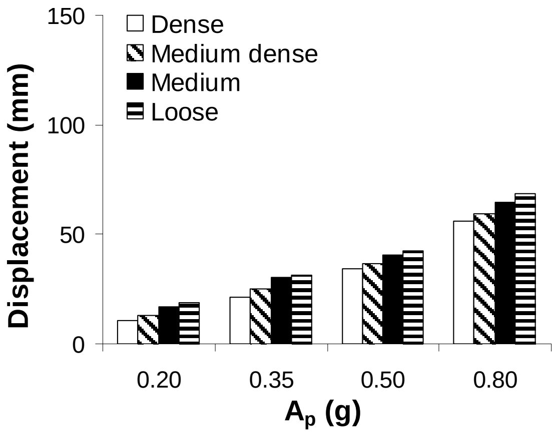

Figure 13.7. Pile (underneath the pier) displacements in longitudinal direction vs. peak ground acceleration for different soil stiffnesses.

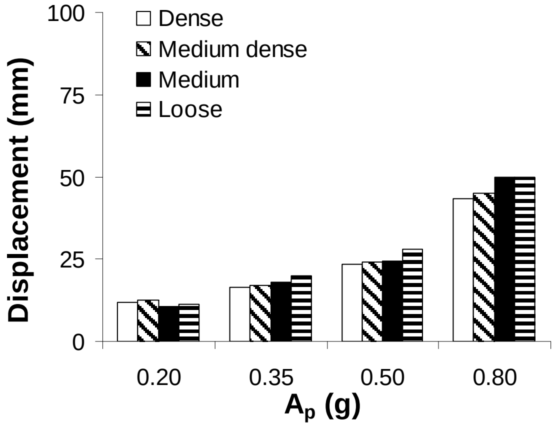

Figure 13.8. Pile (underneath the pier) displacements in transverse direction vs. peak ground acceleration for different soil stiffnesses.

13.2.2 EFFECT OF ABUTMENT HEIGHT AND THICKNESS ON THE SEISMIC PERFORMANCE OF INTEGRAL BRIDGES

In the following subsections, the effect of the abutment height and thickness on the seismic performance of IBs is presented in terms of the maximum displacements of the deck and bearings as well as the maximum displacements and plastic end rotations of the steel H piles and pier columns. The analyses results are presented in Figs 13.9-13.16 as the average of the results from the seven ground motions considered in this study.

13.2.2.1 ABUTMENT HEIGHT AND THICKNESS VERSUS DECK AND BEARING DISPLACEMENTS

Figs. 13.9-12 display the maximum absolute deck and bearing (bearings on the pier) displacements relative to the pier top in the longitudinal and transverse directions as a function of the peak ground acceleration for various abutment height and thickness. It is observed from the figures that the abutment height and thickness have significant effects on the maximum deck displacements. The figures reveal that taller and thicker abutments produce larger maximum absolute displacements in the deck of IBs especially in the case of large intensity earthquakes. This is mainly due to the larger mass of the abutment in the case of taller and thicker abutment producing larger overall period of the bridge. In addition, taller abutments produce larger overall structural flexibility resulting in longer fundamental periods. Accordingly, this results in larger deck and bearing displacements. For instance, for A_p=0,8g, the maximum deck displacement is 116 mm in the longitudinal direction for the IB with an abutment height of 5 m. However, for the same bridge, but with abutment heights of 3 and 4 m and subjected to an identical peak ground acceleration, the maximum deck displacements are obtained as 88 mm and 99 mm respectively. The differences between the maximum average deck displacements obtained for IB with abutment height of 5m and those with abutment heights of 3 and 4m are 32% and 17% respectively. Similar results for the maximum deck displacements are also obtained for various abutment thicknesses (Figs. 13.10 and 13.12). That is, larger abutment thicknesses produce larger deck displacements. In summary, IBs with smaller abutment height and thickness exhibit better performance due to smaller deck displacements especially under large intensity earthquakes.

However, as observed from Figs. 13.9-12 the abutment height is found to have only a negligible effect on the maximum bearing displacements in both longitudinal and transverse directions of IBs. For instance, for A_p=0.8g, the maximum bearing displacement in longitudinal direction is obtained as 49 mm for the IB with an abutment height of 5 m. However, for the same bridge, but with abutment heights of 3 and 4 m and subjected to an identical peak ground acceleration, the maximum bearing displacements are obtained as 45 mm and 47 mm respectively. The differences between the maximum average bearing displacements obtained for the IB with abutment height of 5m and those with abutment heights of 3 and 4m are 9% and 4% respectively. Similar results are also observed for the maximum bearing displacements for various abutment thicknesses (Figs. 13.10 and 13.12). That is the bearing displacements are similar regardless of the thickness of the abutment. This could be explained as follows: For IBs with taller and thicker abutments, the superstructure displacement is large. This obviously produces higher displacement demands on the much more flexible bearings. However, because of the large flexibility of the bearings, the difference between the bearing displacements for various abutment height and thickness conditions is negligible.

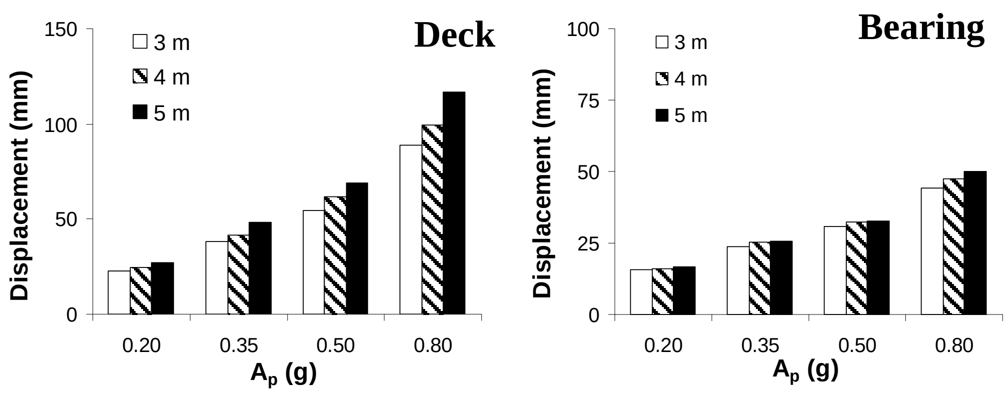

Figure 13.9. Deck and bearing displacements in longitudinal direction vs. peak ground acceleration for different abutment height

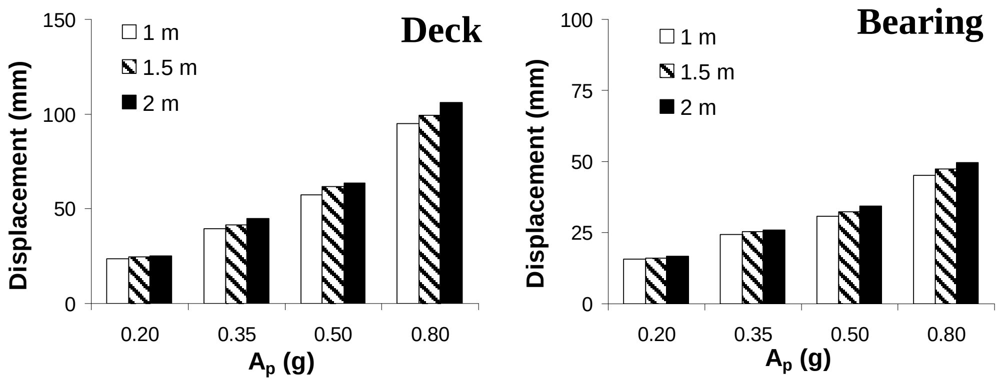

Figure 13.10. Deck and bearing displacements in longitudinal direction vs. peak ground acceleration for different abutment thickness

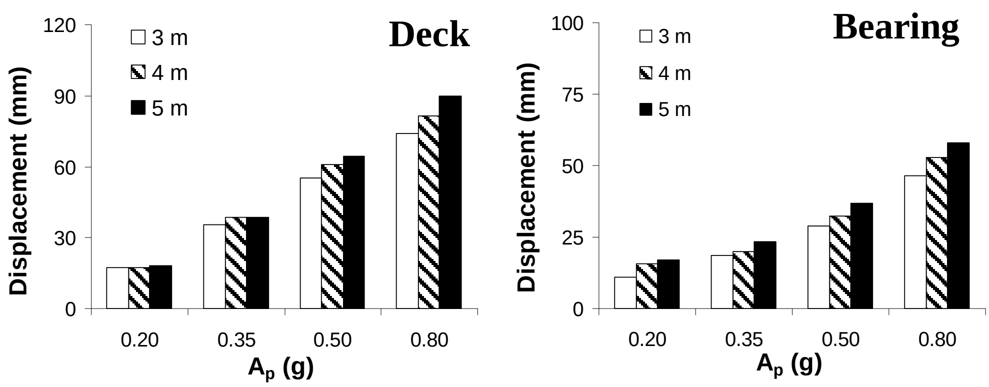

Figure 13.11. Deck and bearing displacements in transverse direction vs. peak ground acceleration for different abutment height

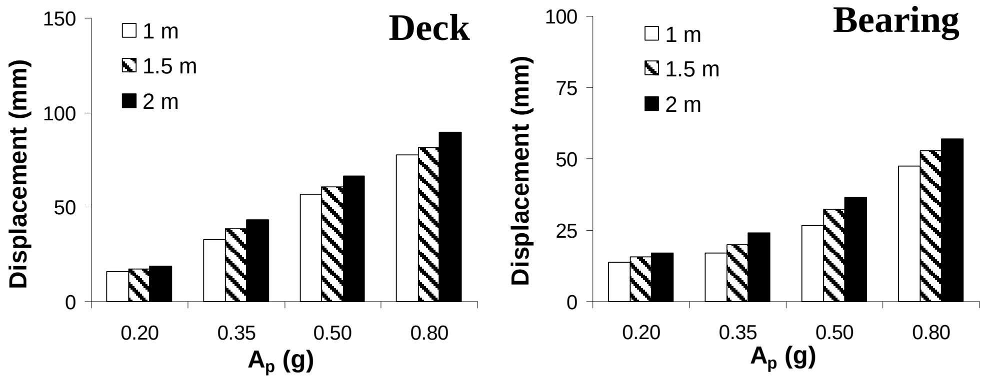

Figure 13.12. Deck and bearing displacements in transverse direction vs. peak ground acceleration for different abutment thickness

13.2.2.2 THE EFFECT OF ABUTMENT HEIGHT AND THICKNESS ON THE PERFORMANCE OF THE PIER COLUMNS

In this section, the effect of the abutment height and thicknesses on the performance of the pier columns is studied in terms of the column drifts (top displacement minus bottom displacement) and end rotations in both longitudinal and transverse directions. The effect of the abutment height and thickness on the pier column drifts and end rotations are illustrated in Figs. 13.13-16. It is observed from the figures that the abutment height and thickness have negligible effects on the pier column drifts and end rotations. For instance, for A_p=0,8g, the maximum pier column drifts in longitudinal direction are obtained as 53, 55 and 56 mm for IBs with abutment heights of 3, 4 and 5 m respectively. The difference between the maximum average pier column drifts for IBs with an abutment height of 5 m and abutment heights of 3 and 4 m are 6%, 2% respectively. In addition, for A_p=0,8g, the maximum column end rotations in the longitudinal direction are 0.0085, 0.0087 and 0.0088 rad. for the IBs with the abutment height of 3, 4 and 5 m respectively. The difference between the maximum average pier column rotations obtained for IBs with abutment heights of 5 m and abutment heights of 3 and 4 m are 3%, 1% respectively. Similar observations are also made for the maximum pier column drifts and end rotations in longitudinal and transverse directions for various abutment thicknesses (Figs. 13.14 and 13.16). In summary, the effect of abutment height and thickness on the pier column performance under seismic loads is found to be negligible. This is mainly due to the large flexibility of the rubber bearings over the piers negating the effect of the abutment geometric properties on the performance of the piers.

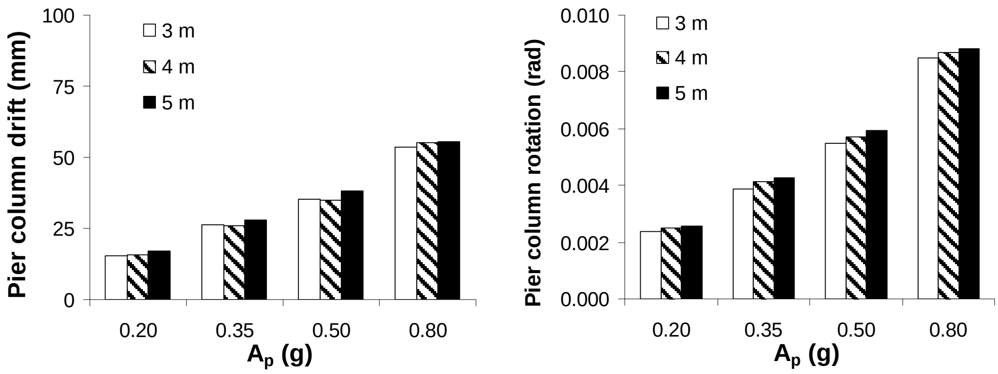

Figure 13.13. Pier column drifts and end rotations in longitudinal direction vs. peak ground acceleration for different abutment heights

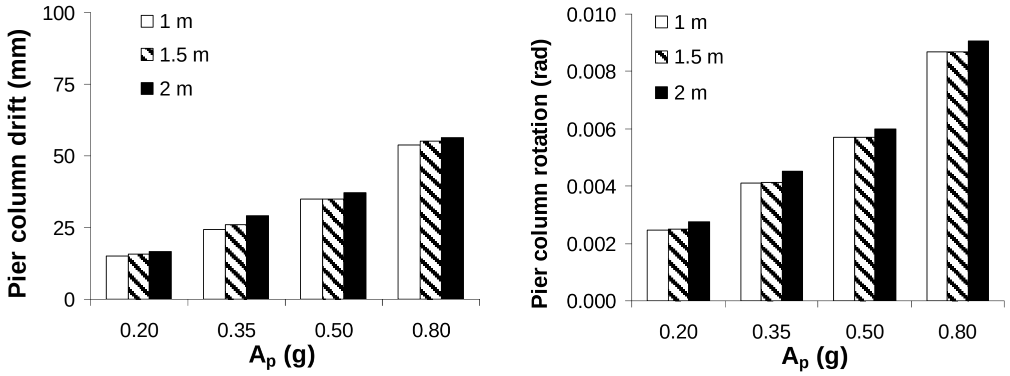

Figure 13.14. Pier column drifts and end rotations in longitudinal direction vs. peak ground acceleration for different abutment thicknesses

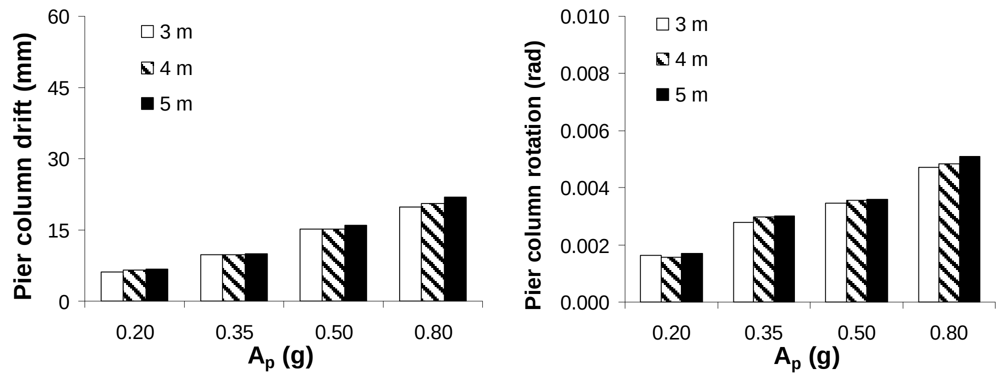

Figure 13.15. Pier column drifts and end rotations in transverse direction vs. Peak ground acceleration for different abutment heights

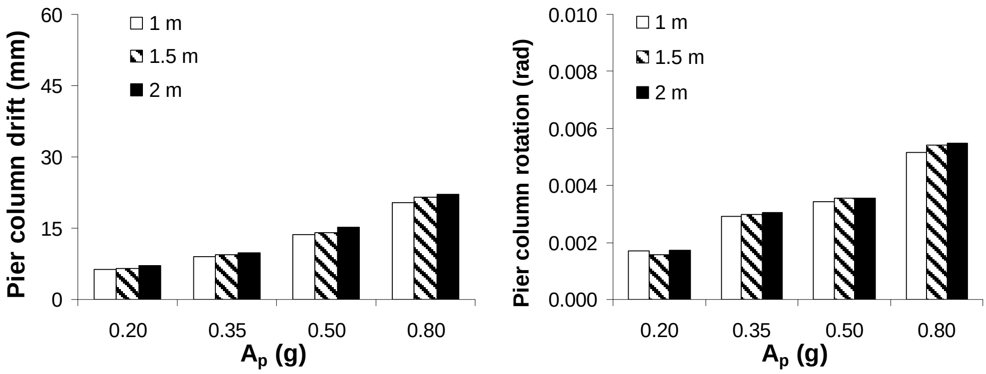

Figure 13.16. Pier column drifts and end rotations in transverse direction vs. peak ground acceleration for different abutment thicknesses

13.2.2.3 THE EFFECT OF ABUTMENT HEIGHT AND THICKNESS ON THE PERFORMANCE OF STEEL H PILES

In this section, the effect of the abutment height and thicknesses on the performance of the steel H piles underneath the abutment is studied in terms of the pile displacements and end rotations. The effect of the abutment height and thickness on the pile displacements and end rotations in longitudinal and transverse directions are illustrated in Figs. 13.17-20. It is observed from the figures that the abutment height and thickness have significant effects on the maximum pile displacements and end rotations. The figures reveal that taller and thicker abutments produce larger maximum displacement in the steel H piles of IBs especially in the case of large intensity earthquakes. This is mainly due to the larger mass of abutment in the case of taller and thicker abutment producing larger deck displacement. In addition, taller abutments produce larger overall structural flexibility resulting in longer fundamental periods. Accordingly, this results in larger displacements and end rotations in the steel

H piles underneath the abutments. For instance, for A_p=0,8g, the maximum pile displacement in the longitudinal direction is 108 mm for the IB with an abutment height 5 m. However, for the same bridge, but with abutment heights of 3 and 4 m and subjected to an identical peak ground acceleration, the maximum pile displacements are obtained as 73 mm and 85 mm respectively. The differences between the maximum average pile displacements obtained for IB with an abutment height of 5m and those with abutment heights of 3 and 4m are 48% and 27% respectively. Similar observations are also made for the maximum pile end rotations in the transverse and longitudinal directions for various abutment thicknesses (Figs. 13.18 and 13.20).

The abutment thickness is also found to have remarkable effects on the maximum pile displacements and rotations in the longitudinal and transverse directions as observed from Figs. 13.19 and 13.20. For instance, for A_p=0.8g, the maximum pile displacement in the longitudinal direction is obtained as 91 mm for the IB with an abutment thickness of 2 m. However, for the same bridge, but with abutment thicknesses of 1.0 and 1.5 m and subjected to an identical peak ground acceleration, the maximum pile displacements in the longitudinal direction are obtained as 81 mm and 85 mm respectively. The differences between the maximum average pile displacements obtained for the IB with an abutment thickness of 2m and those with abutment thicknesses of 1 and 1.5 m are 12 % and 7 % respectively. Similar observations are also made for the maximum pile end rotations in the transverse and longitudinal directions for various abutment thicknesses (Figs. 13.18 and 13.20).

In summary, for IBs having shorter and thinner abutments, an improvement in the seismic performance is expected due to smaller pile and deck displacements.

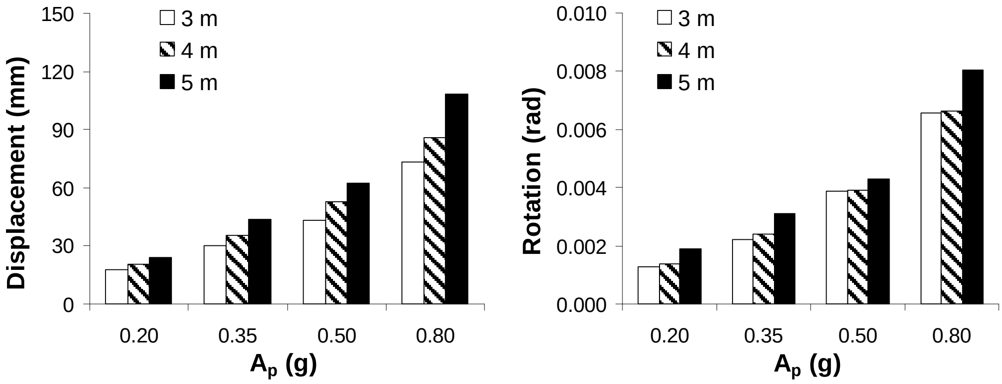

Figure 13.17. Steel H-Pile displacements and rotations in longitudinal direction vs. peak ground acceleration for different abutment heights.

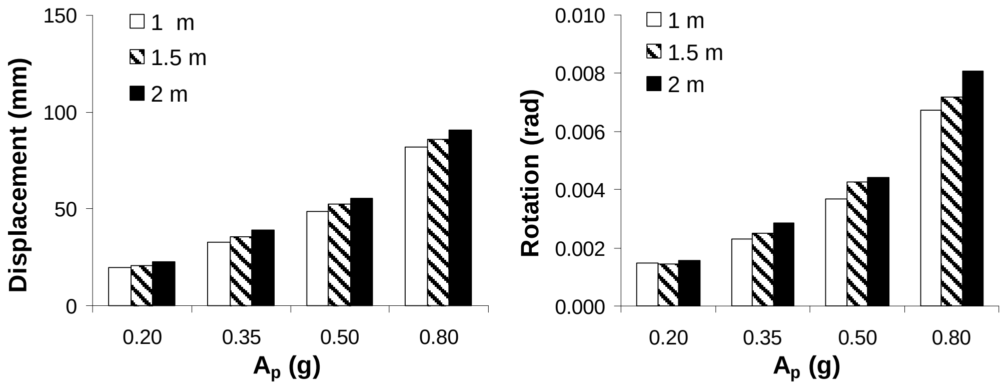

Figure 13.18. Steel H-Pile displacements and rotations in longitudinal direction vs. peak ground acceleration for different abutment thicknesses.

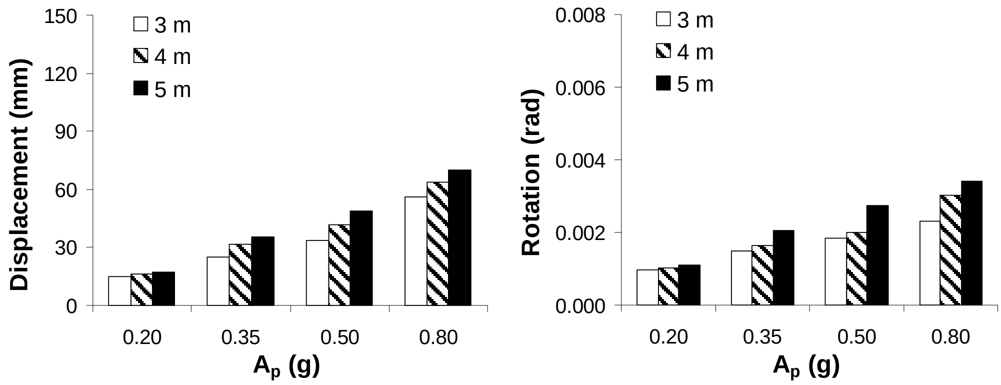

Figure 13.19. Steel H-Pile displacements and rotations in transverse direction vs. peak ground acceleration for different abutment heights.

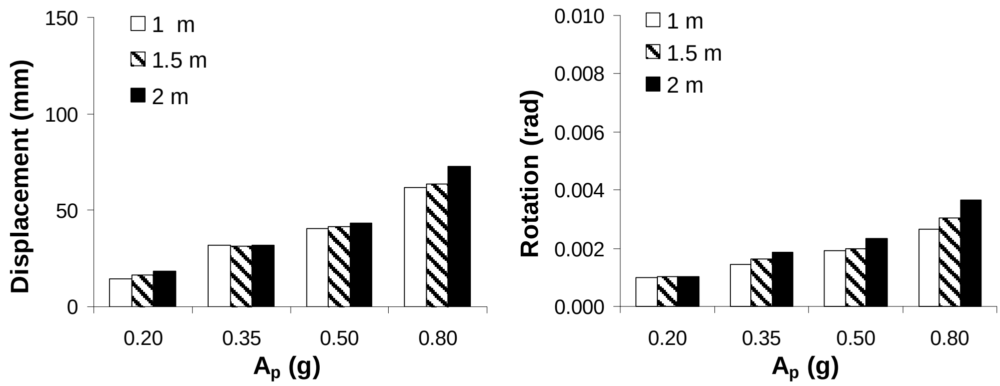

Figure 13.20. Steel H-Pile displacements and rotations in transverse direction vs. peak ground acceleration for different abutment thicknesses.

13.2.2.4 THE EFFECT OF ABUTMENT HEIGHT AND THICKNESS ON PERFORMANCE OF PILES UNDERNEATH THE PIER

In this section, the effect of the abutment height and thicknesses on the performance of piles underneath the pier is studied in terms of the pile displacements in the longitudinal and transverse directions. The effect of the abutment height and thickness on the pile displacements are illustrated in Figs. 13.21-24. It is observed from the figures that the abutment height and thickness have negligible effects on the maximum pile displacements. For instance, for A_p=0.8g, the maximum pile displacements in the longitudinal direction are obtained as 62, 63 and 64 mm for IBs with the abutment height of 3, 4 and 5 m respectively. The difference between the maximum average pile displacements obtained for the IB with an abutment height of 5 m and those with abutment heights of 3 and 4 m are 3 % and 2 % respectively. Similar results are also obtained for the maximum pile displacements for various abutment thicknesses (Figs. 13.22 and 13.24). In summary, the effect of abutment height and thickness on the performance of piles underneath the pier is found to be negligible, this is mainly due to the large flexibility of the rubber bearings over the piers negating the effect of the abutment geometric properties on the performance of the piers.

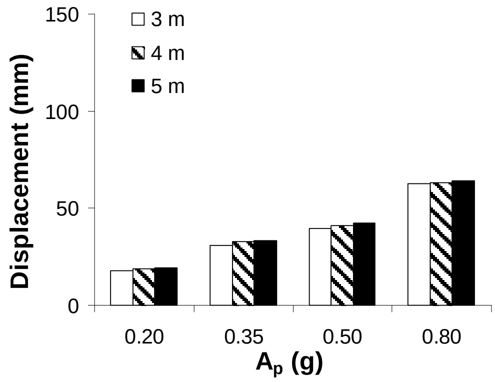

Figure 13.21. Pile (underneath the pier) displacements in longitudinal direction vs. peak ground acceleration for different abutment heights.

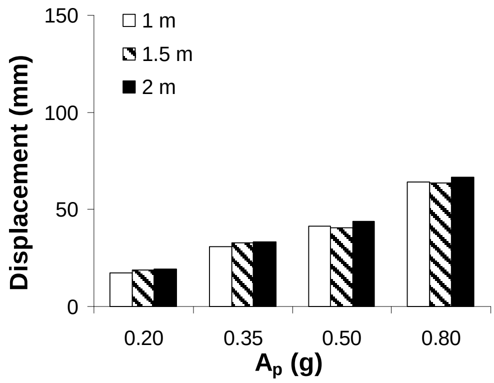

Figure 13.22. Pile (underneath the pier) displacements in longitudinal direction vs. peak ground acceleration for different abutment thicknesses.

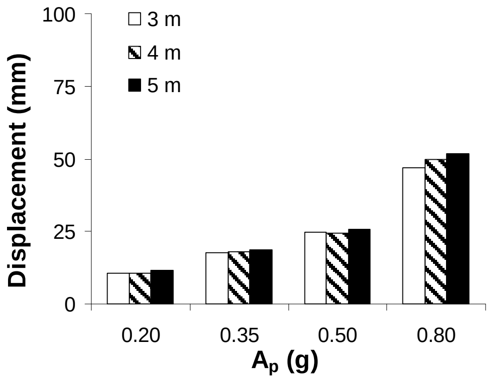

Figure 13.23. Pile (underneath the pier) displacements in transverse direction vs. peak ground acceleration for different abutment heights.

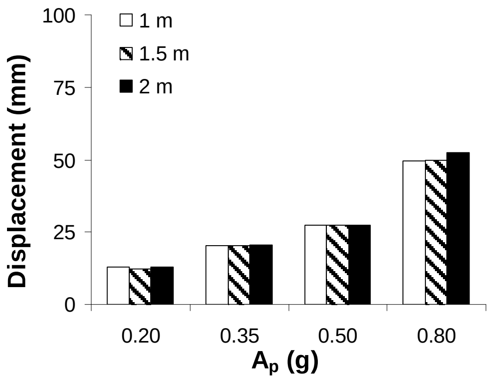

Figure 13.24. Pile (underneath the pier) displacements in transverse direction vs. peak ground acceleration for different abutment thicknesses.

13.2.3 EFFECT OF PILE SIZE AND ORIENTATION ON THE SEISMIC PERFORMANCE OF INTEGRAL BRIDGES

In the following subsections, the effect of the size and orientation of the piles at the abutments on the seismic performance of IBs is presented in terms of the maximum displacements of the deck and bearings as well as the maximum displacements and plastic end rotations of the pier columns and steel H piles at the abutments. The analyses results are presented in Figs. 13.25-13.40 as the average of the results from the seven ground motions considered in this study.

13.2.3.1 THE EFFECT OF PILE SIZES AND ORIENTATIONS ON DECK AND BEARING PERFORMANCES

Figs. 13.25-28 display the maximum absolute deck and bearing (bearings on the pier) displacements relative to the pier top as a function of the peak ground acceleration for various pile sizes and orientations in the longitudinal and transverse directions. It is observed from the figures that pile size and orientation have significant effects on the maximum deck displacements. The figures reveal that smaller piles oriented to bend about their weak axis produce larger maximum absolute displacements in the deck of IBs especially in the case of large intensity earthquakes. For instance, for A_p=0,8g, the maximum deck displacement in the longitudinal direction is 110 mm for the IB supported by HP250x85 (small pile) piles at the abutments.

However, for the same bridge, but supported by HP310x125 (large pile) piles at the abutments the maximum deck displacement is obtained as 99 mm. The difference between the maximum average deck displacements obtained for IBs with the small and large size piles is 11%. Similar observations are also made for the maximum deck displacements in the transverse and longitudinal directions for various pile orientations (Fig. 13.26 and 13.28).

However, in the case of bearing displacements, the pile size and orientation are found to have only negligible effects as observed from Figs. 13.25-28. For instance, for A_p=0.8g, the maximum bearing displacement in the longitudinal direction is obtained as 49 mm for the IB supported by HP 250x85 . HP250x85 (small pile) piles at the abutments. However, for the same bridge, but supported by HP310x125 (large pile) piles at the abutments the maximum bearing displacement is obtained as 47 mm. The difference between the maximum average bearing displacements obtained for IB with the small and large piles is only 4 %. Similar observations are also made for the maximum bearing displacements in the transverse and longitudinal directions for various pile orientations (Fig. 13.26 and 13.28). In summary, IBs with large piles oriented to bend about their strong axis exhibit better performance due to smaller deck displacements under large intensity earthquakes.

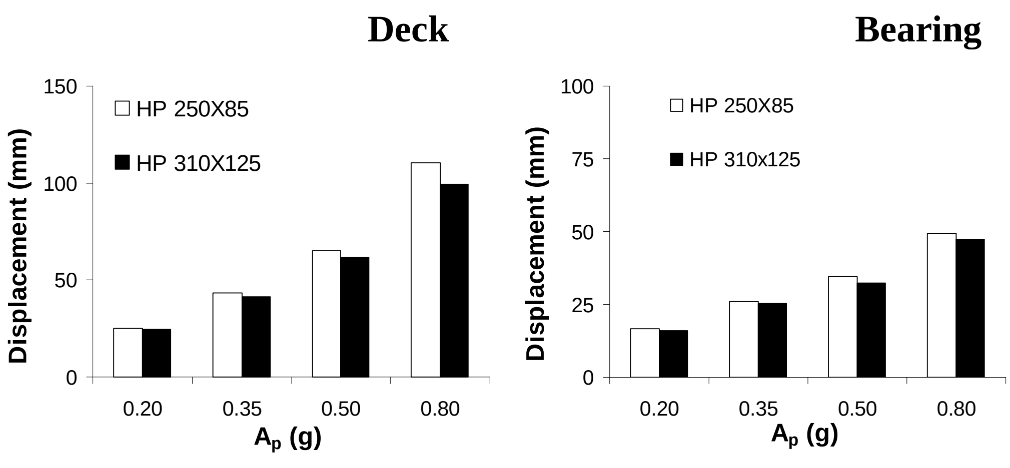

Figure 13.25. Deck and bearing displacements in longitudinal direction vs. peak ground acceleration for different pile sizes

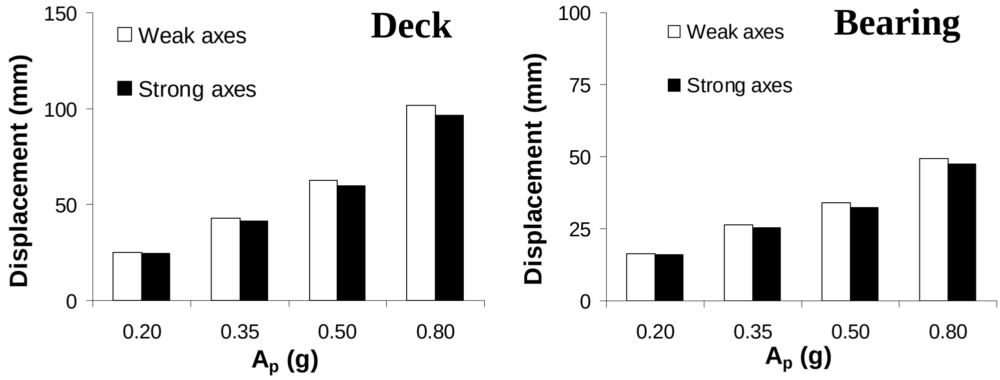

Figure 13.26. Deck and bearing displacements in longitudinal vs. peak ground acceleration for different pile orientations.

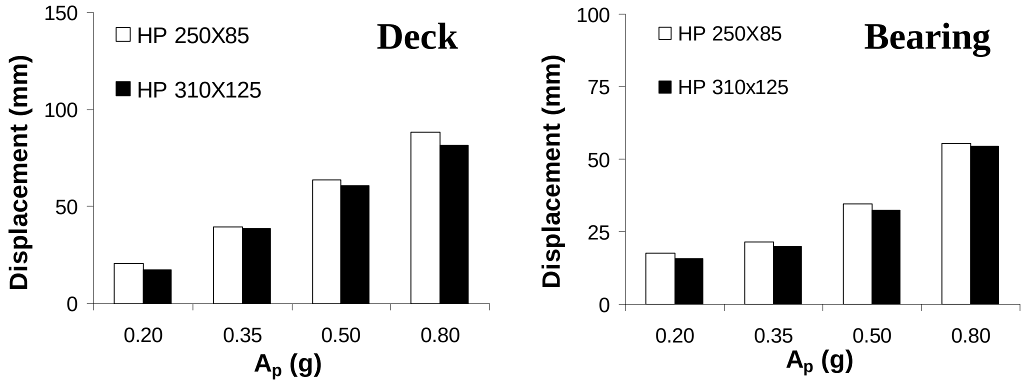

Figure 13.27. Deck and bearing displacements in transverse direction vs. peak ground acceleration for different pile sizes

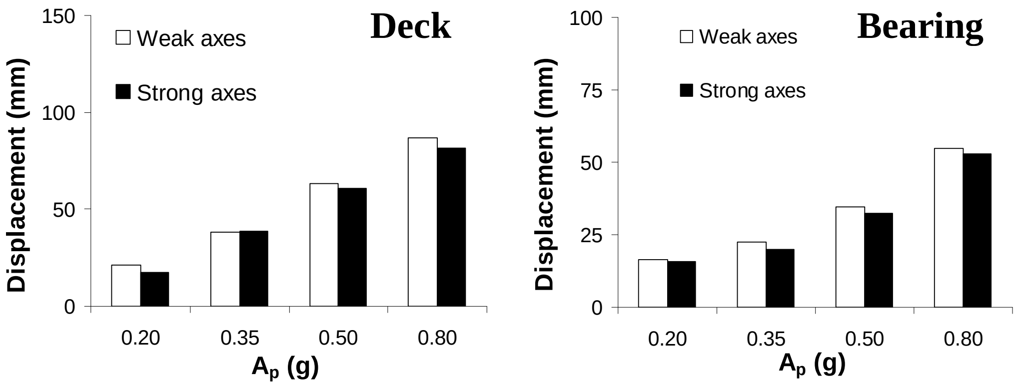

Figure 13.28. Deck and bearing displacements in transverse direction vs. peak ground acceleration for different pile orientations

13.2.3.2 THE EFFECT OF PILE SIZES AND ORIENTATIONS ON THE PERFORMANCE OF THE PIER COLUMNS

In this section, the effect of the pile sizes and orientations on the performance of the pier columns is studied in terms of the column drifts (top displacement minus bottom displacement) and end rotations. Smaller plastic rotations are indicative of less structural damage and hence better seismic performance. The effect of the pile sizes and orientations on the pier column drifts and end rotations are illustrated in Fig. 13.29-32. It is observed from the figures that the foundation soil stiffness has negligible effects on the pier column drifts and rotations. For instance, for A_p=0,8g, the maximum pier column end rotation is 0.0091 rad for the IB with the pile size of HP250x85 (small pile). However, for the same peak ground acceleration level, the maximum pier column rotation is obtained as 0.0086 rad for the IB with the pile size of HP310x174 (large pile). The difference between the maximum average pier column end rotation obtained for IB with the small and large piles is 6 %.

Consequently, the effect of pile sizes and orientations on the seismic performance of pier column is negligible.

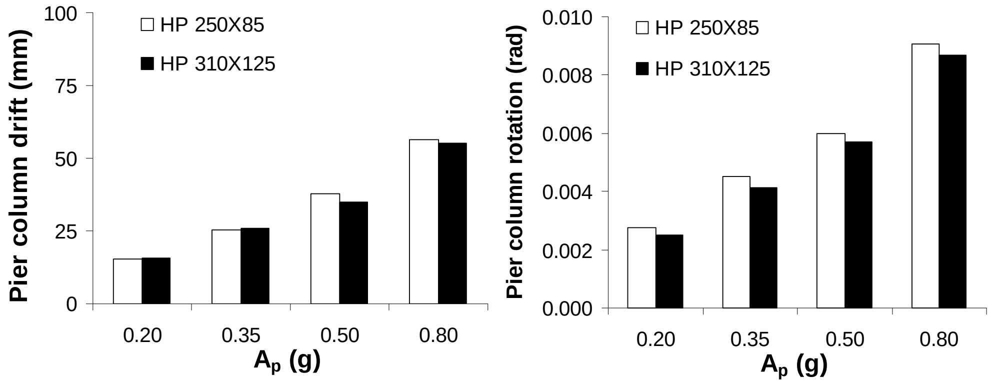

Figure 13.29. Pier column drifts and end rotations in longitudinal direction vs. peak ground acceleration for different pile sizes

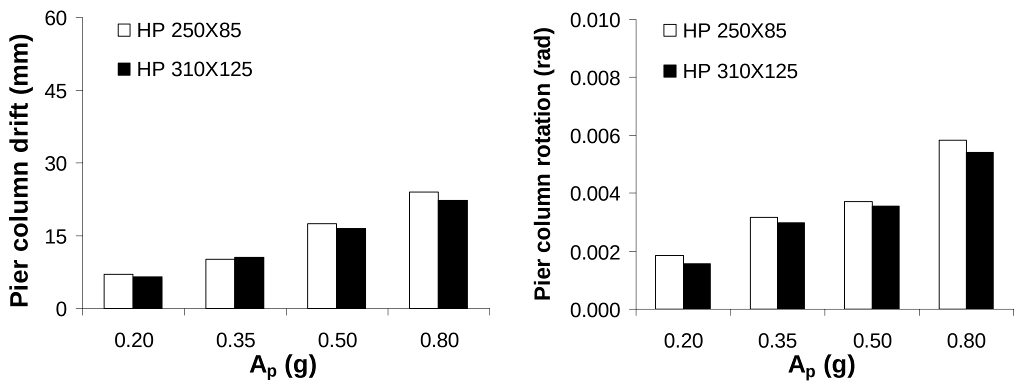

Figure 13.30. Pier column drifts and end rotations in longitudinal direction vs. peak ground acceleration for different pile orientations.

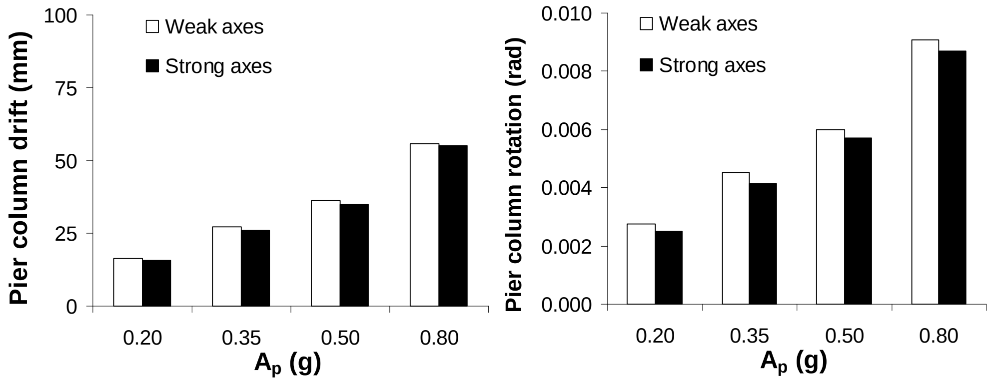

Figure 13.31. Pier column drifts and end rotations in transverse direction vs. peak ground acceleration for different pile sizes

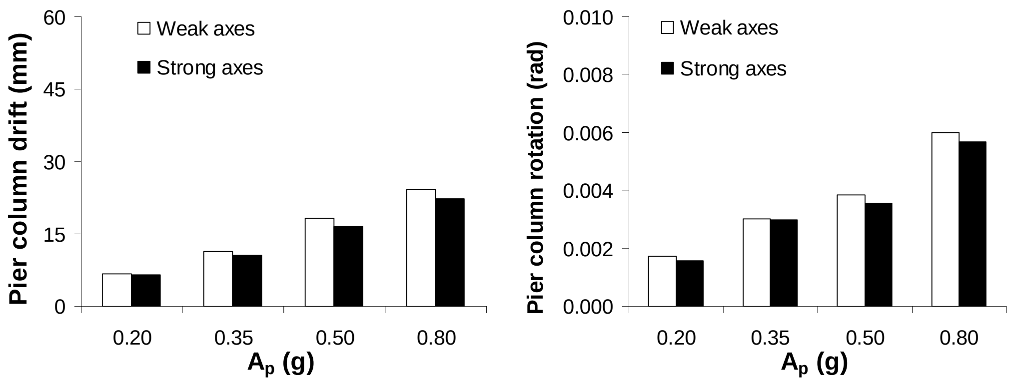

Figure 13.32. Pier column drifts and rotations in transverse direction vs.peak ground acceleration for different pile orientations.

13.2.3.3 THE EFFECT OF PILE SIZES AND ORIENTATIONS ON THE PERFORMANCE OF STEEL H PILES

In this section, the effect of the pile sizes and orientations on the performance of the steel H piles underneath the abutment is studied in terms of the pile displacements and end rotations. The effect of pile sizes and orientations on the pile displacements and end rotations in longitudinal and transverse directions are illustrated in Figs. 13.37-40. It is observed from the figures that the pile sizes and orientations have significant effects on the maximum pile displacements and end rotations. The figures reveal that smaller piles oriented in weak axis produce larger maximum displacement in the steel H piles of IBs especially in the case of large intensity earthquakes. This is mainly due to the flexible piles underneath the abutment producing larger deck displacement. Accordingly, this results in larger displacements and end rotations in the steel H piles underneath the abutments. For instance, for A_p=0,8g, the maximum pile end rotation in the longitudinal direction is 0.009 rad with the pile size of HP250x85. However, for the same bridge, but with pile size of HP310x174 and subjected to an identical peak ground acceleration, the maximum pile end rotation is obtained as 0.007 rad. The differences between the maximum average pile rotations obtained for IB with a pile size of HP250x85 and those with a pile size of HP310x174 is 28%. Similar observations are also made for the maximum pile end rotations in the transverse and longitudinal directions for various pile sizes and orientations (Figs. 13.34 and 13.36).

The pile orientation is also found to have remarkable effects on the maximum pile displacements and rotations in the longitudinal and transverse directions as observed from Figs. 13.35 and 13.36. For instance, for A_p=0.8g, the maximum pile end rotation in the longitudinal direction is obtained as 0.0072 mm for the IB with the piles oriented in strong axis. However, for the same bridge, but with pile oriented in weak axis and subjected to an identical peak ground acceleration, the maximum pile end rotation in the longitudinal direction is obtained 0.0098 rad. The differences between the maximum average pile end rotations obtained for IBs with piles oriented in strong and weak axis are 36 %.. Similar observations are also made for the maximum pile displacements in the transverse and longitudinal directions for various pile orientations (Figs. 13.18 and 13.20).

Consequently, for IBs having larger piles oriented in strong axis, smaller pile displacements and rotations are expected. Accordingly, the IBs having larger piles oriented in strong axis exhibit better performance due to smaller pile displacements and rotations during seismic excitation.

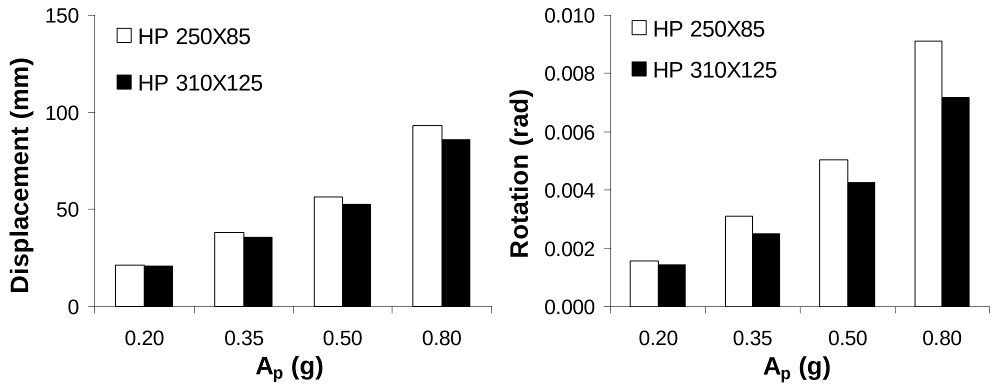

Figure 13.33. Steel H-Pile displacements and rotations in longitudinal direction vs. peak ground acceleration for different pile sizes.

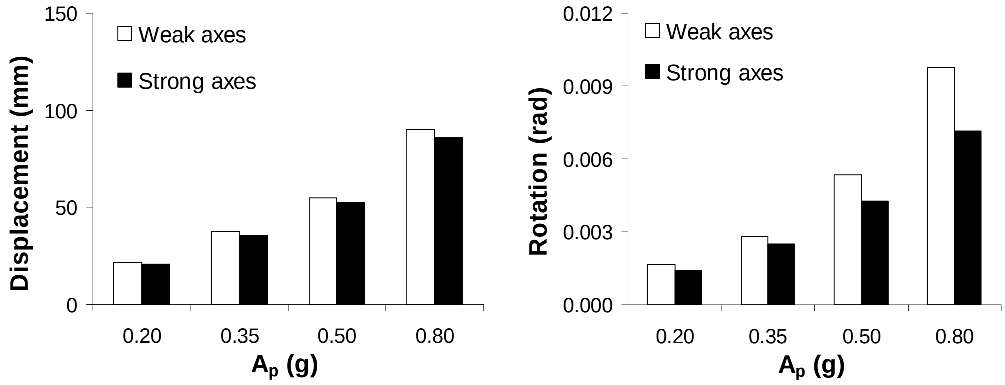

Figure 13.34. Steel H-Pile displacements and rotations in longitudinal direction vs. peak ground acceleration for different pile orientations.

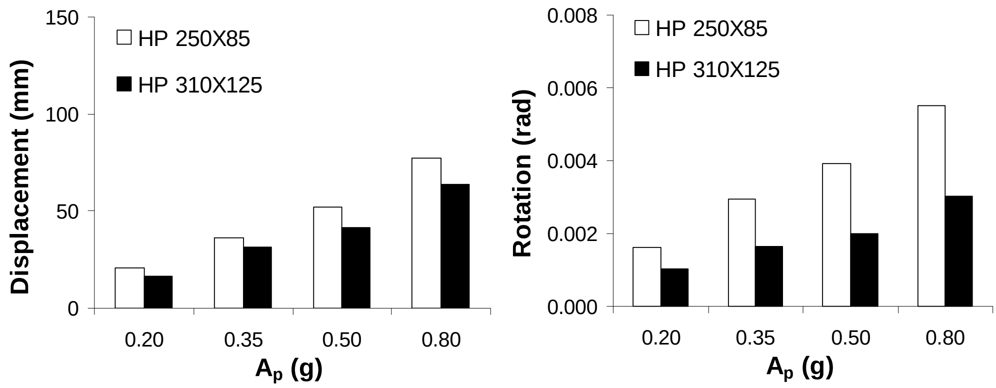

Figure 13.35. Steel H-Pile displacements and rotations in transverse direction vs. Peak ground acceleration for different pile sizes.

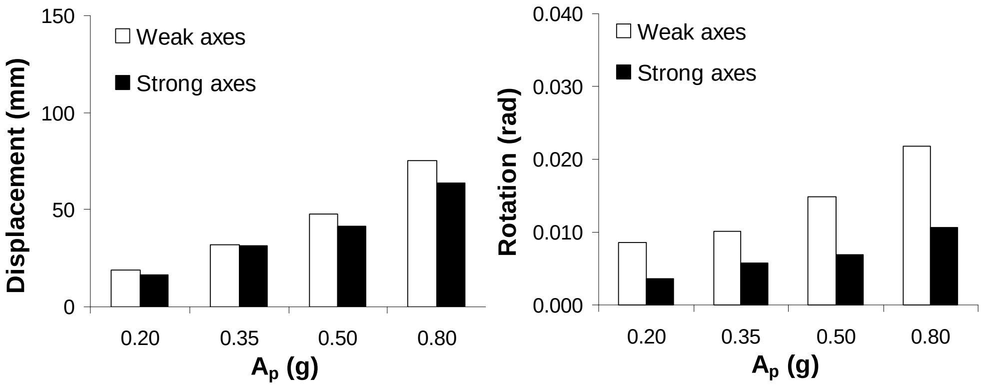

Figure 13.36. Steel H-Pile displacements and rotations in transverse direction vs. peak ground acceleration for different pile orientations.

13.2.3.4 THE EFFECT OF PILE SIZES AND ORIENTATIONS ON PERFORMANCE OF PILES UNDERNEATH THE PIER

In this section, the effect of the pile sizes and orientations on the performance of piles underneath the pier is studied in terms of the pile displacements in the longitudinal and transverse directions. The effect of the pile sizes and orientations on the pile displacements are illustrated in Figs. 13.37-40. It is observed from the figures that the pile sizes and orientations have negligible effects on the maximum pile displacements. For instance, for A_p=0.8g, the maximum pile displacements in the longitudinal direction are obtained as 64 and 67 mm mm for IBs with the pile size of HP250X85 and HP310X174 respectively. The difference between the maximum average pile displacements obtained for the IB with pile size of HP250X85 and those with pile size of HP310X174 is 5 %. Similar results are also obtained for the maximum pile displacements for various pile orientations (Figs. 13.38 and 13.40). In summary, the effect of pile sizes and orientations on the performance of piles underneath the pier is found to be negligible; this is mainly due to the large flexibility of the rubber bearings over the piers negating the effect of the steel H-piles properties on the performance of the piles underneath the pier.

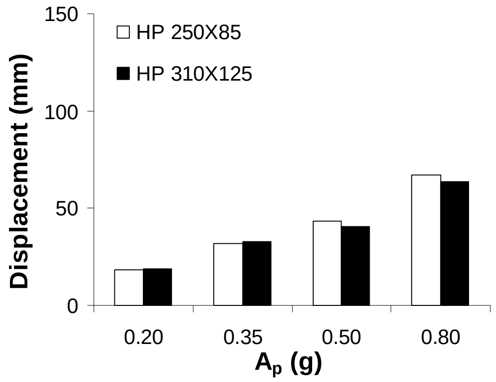

Figure 13.37. Pile (underneath the pier) displacements in longitudinal direction vs. peak ground acceleration for different pile sizes.

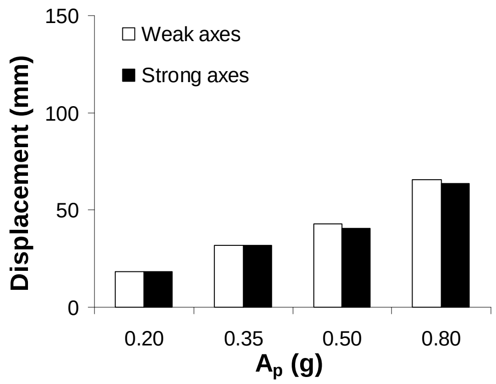

Figure 13.38. Pile (underneath the pier) displacements in longitudinal direction vs. peak ground acceleration for different pile orientations.

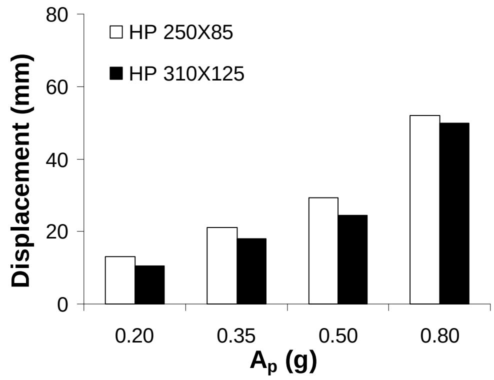

Figure 13.39. Pile (underneath the pier) displacements in transverse direction vs. peak ground acceleration for different pile sizes.

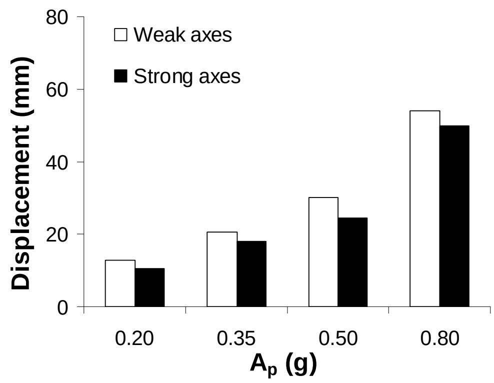

Figure 13.40. Pile (underneath the pier) displacements in transverse direction vs. peak ground acceleration for different pile orientations.

13.2.3 EFFECT OF BACKFILL COMPACTION LEVEL ON THE SEISMIC PERFORMANCE OF INTEGRAL BRIDGES

In the following subsections, the effect of the backfill compaction level on the seismic performance of IBs is presented in terms of the maximum displacements of the deck and bearings as well as the maximum displacements and plastic end rotations of the pier columns and steel H piles at the abutments. The analyses results are presented in Figs. 13.41-13.48 as the average of the results from the seven ground motions considered in this study.

13.2.3.1 THE EFFECT OF BACKFILL COMPACTION LEVEL ON THE PERFORMANCE OF THE DECK AND BEARINGS

Figs. 13.41-42 display the maximum absolute deck and bearing (bearings on the pier) displacements relative to the pier top as a function of the peak ground acceleration for backfill compaction level in the longitudinal and transverse directions. It is observed from the figures that backfill compaction level negligible effects on the maximum deck and bearing displacements in longitudinal and transverse directions. For instance, for A_p=0,8g, the maximum deck displacement in the longitudinal direction is 101 mm for uncompacted backfill (unit weight is 18 kN/m^3) and 99 m for compacted backfill (unit weight is 20 kN/m^3). The difference between the maximum average deck displacements obtained for IB with the compacted and uncompacted backfill is only 2 %. Similar observations are also made for the maximum bearing in longitudinal and the maximum deck and bearing displacements in transverse directions for various backfill compaction level (Figs. 13.41 and 13.42).

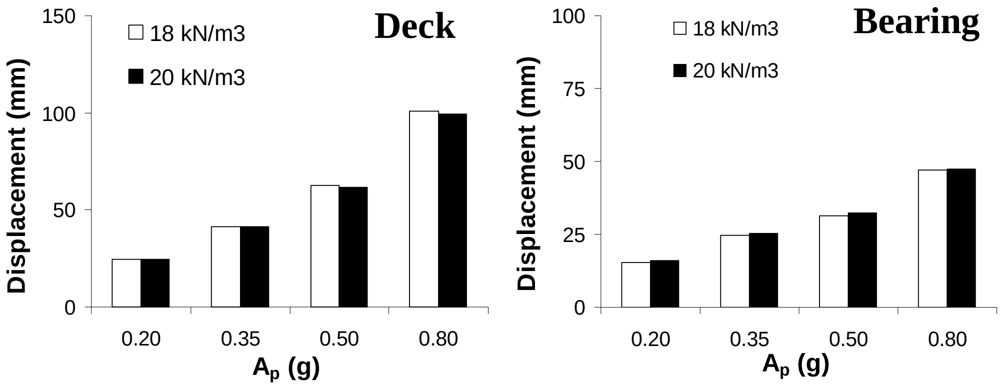

Figure 13.41. Deck and bearing displacements in longitudinal direction vs. peak ground acceleration for different backfill compaction level.

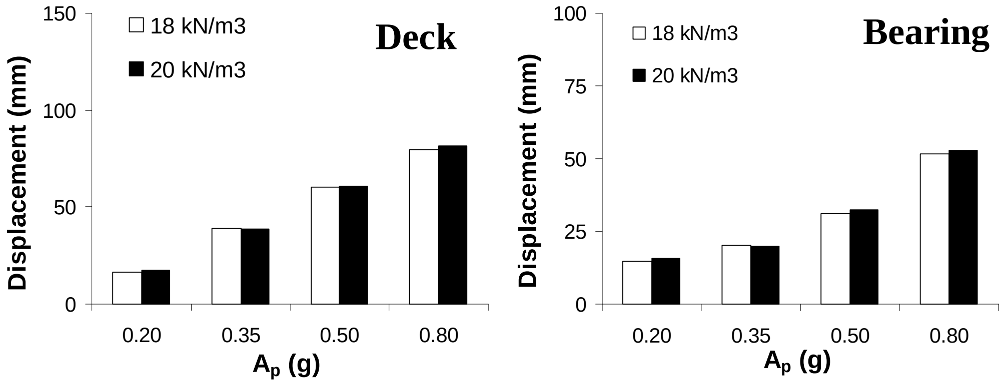

Figure 13.42. Deck and bearing displacements in transverse direction vs. peak ground acceleration for different backfill compaction level.

13.2.3.2 THE EFFECT OF BACKFILL COMPACTION LEVEL ON THE PERFORMANCE OF THE PIER COLUMNS

In this section, the effect of the backfill compaction level on the performance of the pier columns is studied in terms of the column drifts (top displacement minus bottom displacement) and rotations. The effect of the backfill compaction level on the pier column drifts and rotations in the longitudinal and transverse directions are illustrated in Figs. 13.43 and 13.44. It is observed from the figures that the backfill compaction level has a negligible effect on the pier column drifts and rotations for IBs. For instance, for A_p=0,8g, the maximum pier column rotations in longitudinal direction are obtained as 0.0086 rad for uncompacted backfill and 0.0087 for uncompacted backfill. The difference between the maximum average pier column rotation obtained for IB with uncompacted and compacted backfill is 1 %. For instance, for A_p=0,8g, the maximum pier column rotations in the longitudinal direction are 0.0087 and 0.0086 for compacted and uncompacted backfills respectively. The difference between the maximum average column rotations obtained for compacted and uncompacted backfills is 1 %. Similar observations are also made for the maximum pier column drifts and rotations in transverse directions for various backfill compaction level (Fig. 13.43).

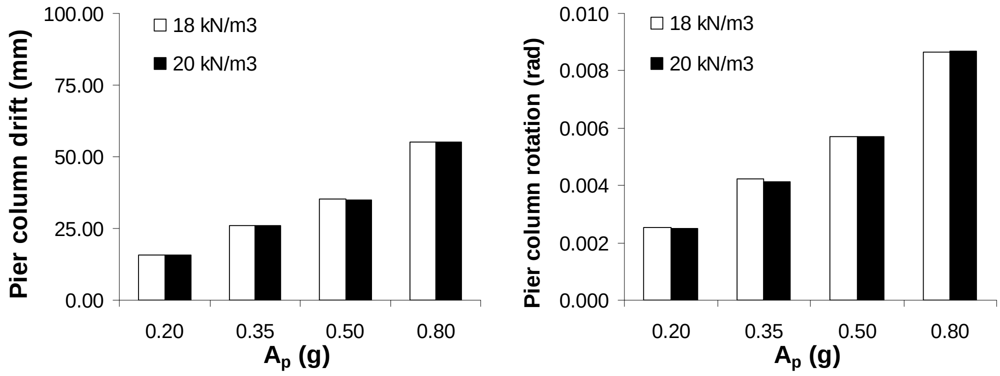

Figure 13.43. Pier column drifts and rotations in longitudinal direction vs. Peak ground acceleration for different backfill compaction level.

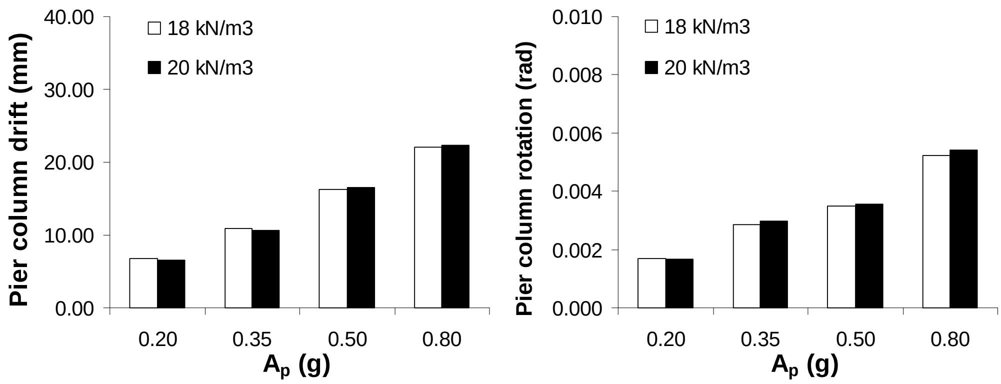

Figure 13.44. Pier column drifts and rotations in transverse direction vs. Peak ground acceleration for different backfill compaction level.

13.2.3.3 THE EFFECT OF BACKFILL COMPACTION LEVEL ON THE PERFORMANCE OF STEEL H PILES

In this section, the effect of the backfill compaction level on the performance of the steel H piles underneath the abutment is studied in terms of the pile displacements and end rotations. The effect of backfill compaction level on the pile displacements and end rotations in longitudinal and transverse directions are illustrated in Figs. 13.45 and 13.46. It is observed from the figures that the pile sizes and orientations have negligible effects on the maximum pile displacements and end rotations. For instance, for A_p=0,8g, the maximum pile end rotation in the longitudinal direction is 0.0075 rad and 0.0072 for compacted backfill rad for IBs with the uncompacted backfill and 0.0072 rad for IBs with compacted backfill. The differences between the maximum average pile rotations obtained for IBs with compacted and uncompacted backfill are 4 %. Similar results are also observed for the maximum pile displacements and rotations in transverse direction for various backfill compaction level (Fig. 13.46). This obviously indicates that the effect of backfill compaction level on the seismic performance of steel H piles underneath the abutment is negligible.

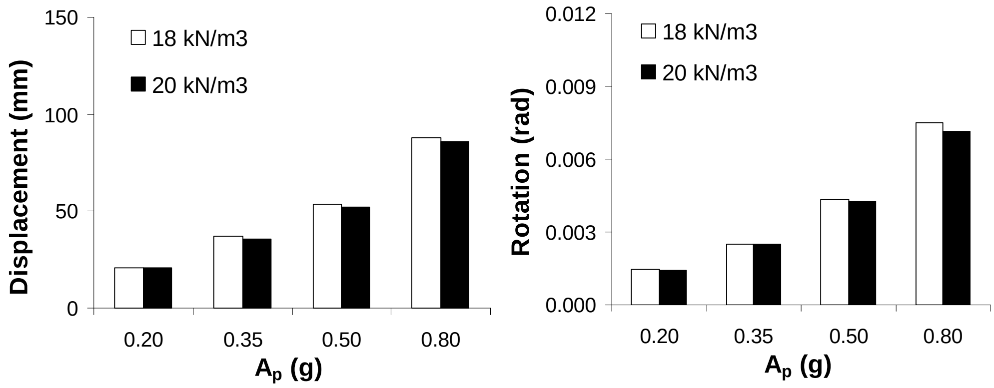

Figure 13.45. Steel H-Pile displacements and rotations in longitudinal direction vs. peak ground acceleration for different backfill compaction level.

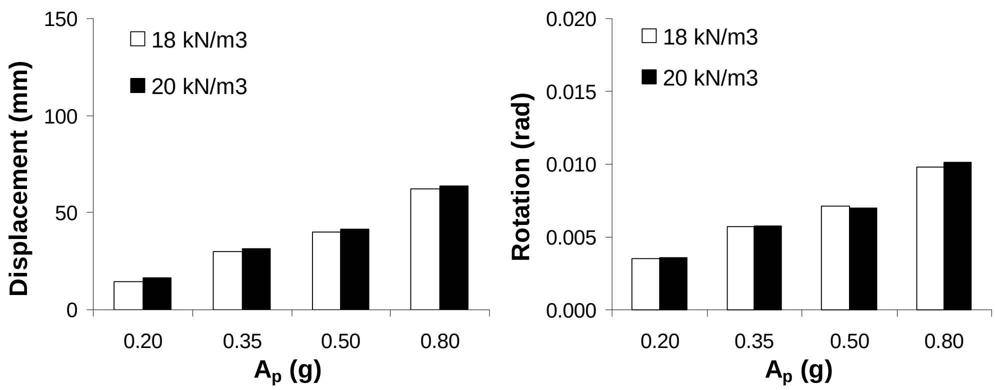

Figure 13.46. Steel H-Pile displacements and rotations in transverse direction vs. peak ground acceleration for different backfill compaction level.

13.2.3.4 THE EFFECT OF BACKFILL COMPACTION LEVEL ON PERFORMANCE OF PILES UNDERNEATH THE PIER

In this section, the effect of the backfill compaction level on the performance of piles underneath the pier is studied in terms of the pile displacements in the longitudinal and transverse directions. The effect of the backfill compaction level on the pile displacements are illustrated in Figs. 13.47 and 13-48. It is observed from the figures that the pile sizes and orientations have negligible effects on the maximum pile displacements. For instance, for A_p=0.8g, the maximum pile displacements in the longitudinal direction are obtained as 63 and 64 mm for IBs with uncompacted and compacted backfill respectively. The difference between the maximum average pile displacements obtained for the IB with uncompacted and compacted backfill is 2 %.. In summary, the effect of backfill compaction level on the performance of piles underneath the pier is found to be negligible.

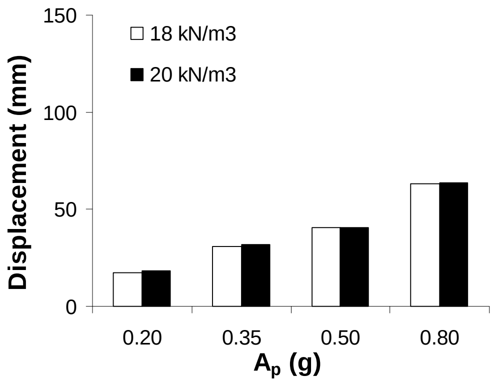

Figure 13.47. Pile (underneath the pier) displacements in longitudinal direction vs. Peak ground acceleration for different backfill compaction level.

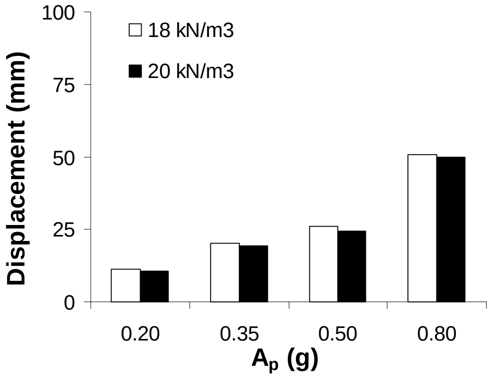

Figure 13.48. Pile (underneath the pier) displacements in transverse direction vs. Peak ground acceleration for different backfill compaction level.

CHAPTER 14

LOW CYCLE FATIGUE EFFECTS IN INTEGRAL BRIDGE PILES UNDER SEISMIC LOAD REVERSAL

The most common types of piles used at the abutments of IBs are steel H-piles. Under the effect of medium and large intensity ground motions, the seismically-induced lateral cyclic displacements in steel H-piles of IBs could be considerable. As a result, the piles may experience cyclic plastic deformations following a major earthquake. This may result in the reduction of their service life due to low-cycle fatigue effects. Accordingly, low cycle fatigue in IAB piles is investigated under seismic effects in this study. For this purpose, IBs with two spans are considered. Three dimensional (3-D) nonlinear structural models of these IBs including dynamic soil-bridge interaction effects are built. Then, nonlinear time history analyses of the IB models are conducted using a set of ground motions with various intensities representing small, medium and large intensity earthquakes. In the analyses, the effect of various properties such as soil stiffness, pile size (HP 310x174 (LP), HP 250x85 (SP)) and orientations (WA: Weak Axis, SA: Strong Axis) are considered. The magnitude of cyclic displacements of steel H piles are then determined from the analyses results. Then, a fatigue damage model is used together with the cyclic displacement obtained from seismic analyses to determine the remaining service life of IB piles under cyclic displacement due to thermal effects.

14.1 STRAIN-BASED LOW CYCLE FATIGUE

Low-cycle fatigue failure of structural components is caused by cyclic loads or displacements of relatively larger magnitude that may produce significant amounts of plastic strains in the structural component. Generally, the number of displacement cycles that leads to failure of a component is determined as a function of the plastic strains in the localized region of the component being analyzed. This is referred to as strain-based approach to fatigue life estimate of structural components. This approach is appropriate for determining the fatigue life of steel H-piles supporting the abutments as it considers the seismic-induced large plastic deformations that may occur in localized regions of the piles where fatigue cracks may begin.

Koh and Stephens (1991) proposed an equation to calculate the number of constant amplitude strain cycles to failure for steel sections under low cycle fatigue. This equation is based on the total strain amplitude, ε_a, and expressed as follows:

$$\varepsilon_a = M(2N_f)^m \tag{14.1}$$

where, M = 0.0795, m = -0.448 and N_f is the number of cycles to failure. The above equation is used for the estimation of the maximum strain amplitude steel H-piles can sustain before their failure takes place due to low-cycle fatigue effects within the service life of the bridge. For a bridge to serve its intended purpose, it must sustain the effect of seismic and thermal cyclic displacements throughout its service life. The seismically-induced and thermal strains in steel H-piles are assumed to have variable amplitudes consisting of large and small cycles. Therefore, Eq. (14.1), which is derived for constant amplitude cycles, cannot be used directly to obtain the maximum strain amplitude a pile may sustain. Conservatively assuming that both the large and small cycles due to seismic and thermal effects induce low cycle fatigue damage in the steel H-piles (a small cycle may occur following a large cycle where plastic deformations have already been induced), Miner's rule (Miner 1945) may be used in combination with Eq. (14.1) to obtain the maximum strain amplitude a pile may sustain. Miner (1945) defined the cumulative fatigue damage induced in a structural member by load or displacement cycles of different amplitudes as:

$$\sum_{i}^{n} \frac{n_i}{N_i} \leq 1 \tag{14.2}$$

where, n_i is the number of cycles associated with the i_{th} loading (or displacement) case and N_i is the number of cycles to failure for the same case. The above equation states that if a load or displacement is applied n_i times, only a fraction, n_i/N_i of the fatigue life has been consumed. The fatigue failure is then assumed to take place when n_i/N_i ratios of the cycles with different amplitudes add up to 1.

14.2. ANALYSES OF THE BRIDGE MODELS

A total of eight IB models are built considering two different pile sizes and orientations and four different soil stiffness. First, pushover analyses of these IB are conducted to obtain the cyclic strains in the piles due to thermal movements. Further details about modeling and analyses of IBs under thermal effects can be found elsewhere (Dicleli and Albhaisi 2003) The analyses results reveal that the steel H-piles remain within their elastic limits due to small thermal induced displacements resulting from estimates of the steel H piles for the IB considered in this study. Then, nonlinear time history analyses of the IB models are conducted using the seven earthquake ground motions considered in this study. The nonlinear time history analyses are repeated for peak ground accelerations of 0.2, 0.35, 0.5 and 0.8 g for each selected earthquake. This led to a total of 224 different analyses cases. The analyses results are given in the following sections. the small total length of the IB considered in this study. Consequently, low cycle fatigue effects under thermal loading are not expected for the particular bridge considered in this study. Hence, thermal-induced effects are not included for low cycle fatigue life

14.2.1. ANALYSES RESULTS

The hysteric (cyclic) moment-rotation relationships of the steel H-piles are obtained from the nonlinear time history analyses results. Then, a Matlab algorithm is developed to calculate the amplitude of positive *(ε_{ap})* and negative *(ε_{an})* strain cycles from these moment rotation relationships. In the Matlab algorithm the following equation is used to calculate the average strain amplitudes *(ε_a)* per cycle*;*

$$\varepsilon_a = \frac{|\varepsilon_{pa}| + |\varepsilon_{pa}|}{2} \qquad (14.3)$$

Next, the number of displacement / strain cycles *(N_f)* that leads to failure of ~~a~~ steel H-piles is determined using the method purposed by Koh and Stephens (1991) given earlier. Furthermore, cumulative fatigue damage index for the H-piles are obtained using the Miner's rule (Miner 1945). The number of cycles and cumulative fatigue damage index for the H-piles of IBs are tabulated in Table 14.1 for different pile sizes, in Table 14.2 for different pile orientations and in Table 14.3 for different soil stiffnesses. The analyses results are presented for peak ground accelerations of 0.35, 0.5 and 0.8 g. In the case of 0.2g peak ground acceleration, hysteretic (cyclic) behavior is not observed as the piles remain within their elastic limit under such a small amplitude of peak ground acceleration. In the following subsections, the effect of pile size, orientation~~s~~ and soil stiffness on the low cycle fatigue damage of Steel H-piles of IBs is studied.

14.2.1.1 EFFECT OF PILE SIZE ON LOW CYCLE FATIGUE PERFORMANCE OF STEEL H-PILES

In this section the effect of pile size on low cycle fatigue performance of steel H-piles is studied. The analyses results are tabulated in Table. 14.1 in terms of cumulative fatigue damage index ranging between 0 and 1.0 where 0 represents no damage, and 1 represents total failure) for various peak ground acceleration levels and earthquakes. The results presented in Table 1 clearly reveal that as the size of the pile increases, cumulative fatigue damage index decreases. For instance, in the case of the Northridge earthquake scaled to a peak ground acceleration of A_p=0.8g, cumulative fatigue damage index is calculated as 0.0013 for the larger pile. However, for the same bridge supported by smaller piles at the abutment and subjected to the same earthquake and peak ground acceleration level, the low cycle fatigue damage index is calculated as 0.0037. This obviously results from the greater bending capacity of larger piles that require larger displacements to reach their fatigue strain amplitude limit. However, in the case of the smaller piles, the piles may easily reach their fatigue strain amplitude limit at smaller displacements amplitudes.

Table 14.1. Number of cycles and fatigue damage index for different pile sizes.

Earthquake	Pile Size	A_p=0.35g		A_p=0.50g		A_p=0.80 g	
		Number of cycles	$\sum_i^n \frac{n_i}{N_i}$	**Number of cycles**	$\sum_i^n \frac{n_i}{N_i}$	**Number of cycles**	$\sum_i^n \frac{n_i}{N_i}$
Loma Prieta Ap=0.200 g	HP 310x174	85	0.0001	76	0.0003	59	0.0008
	HP 250x85	72	0.0003	79	0.0005	62	0.0011
Loma Prieta Ap=0.278 g	HP 310x174	80	0.0005	65	0.0007	62	0.0012
	HP 250x85	75	0.0008	72	0.0011	86	0.0021
Mammoth Lake	HP 310x174	55	0.0002	52	0.0005	42	0.0014
	HP 250x85	61	0.0006	63	0.0012	45	0.0019
Northridge Ap=0.263 g	HP 310x174	78	0.0007	52	0.0009	62	0.0013
	HP 250x85	74	0.0018	58	0.0030	61	0.0037
Northridge Ap=0.316 g	HP 310x174	93	0.0003	88	0.0006	79	0.0012
	HP 250x85	85	0.0011	86	0.0021	84	0.0026
San Fernando	HP 310x174	62	0.0004	42	0.0008	46	0.0010
	HP 250x85	56	0.0006	52	0.0009	62	0.0013
Whitter	HP 310x174	77	0.0001	72	0.0002	67	0.0006
	HP 250x85	80	0.0002	77	0.0005	81	0.0011

14.2.1.2 EFFECT OF PILE ORIENTATION ON LOW CYCLE FATIGUE PERFORMANCE OF STEEL H-PILES

In this section the effect of pile orientation on low cycle fatigue performance of steel H-piles at the abutments is studied. The analyses results are ~~is~~ tabulated in Table. 14.2 in terms of fatigue damage indices for various earthquakes and peak ground accelerations. As observed from the Table, larger cumulative fatigue damage indices are obtained when the H piles are oriented to bend about their weak axis. For instance, in the case of the Loma Prieta earthquake scaled to a peak ground acceleration of A_p=0.8g, the cumulative fatigue damage index is calculated as 0.0023 for piles oriented to bend about their weak axis. However, for the same earthquake and peak ground acceleration levels, the low cycle damage index is calculated as 0.0012 for piles oriented to bend about their strong axis. This obviously results ~~in~~ from the greater bending capacity of oriented to bend about their strong axis that require larger displacements to reach their fatigue strain amplitude limit.

Table 14.2. Number of cycles and fatigue damage index for different pile orientation.

Earthquake	Pile Orientation	A_p=0.35g		A_p=0.50g		A_p=0.80 g	
		Number of cycles	$\sum_i^n \frac{n_i}{N_i}$	Number of cycles	$\sum_i^n \frac{n_i}{N_i}$	Number of cycles	$\sum_i^n \frac{n_i}{N_i}$
Loma Prieta Ap=0.200 g	Strong	85	0.0001	76	0.0003	59	0.0008
	Weak	81	0.0002	87	0.0007	78	0.0011
Loma Prieta Ap=0.278 g	Strong	80	0.0005	65	0.0007	62	0.0012
	Weak	81	0.0009	68	0.0012	69	0.0023
Mammoth Lake	Strong	55	0.0002	52	0.0005	42	0.0014
	Weak	65	0.0004	67	0.0009	56	0.0018
Northridge Ap=0.263 g	Strong	78	0.0007	52	0.0009	62	0.0013
	Weak	81	0.0010	65	0.0015	69	0.0023
Northridge Ap=0.316 g	Strong	93	0.0003	88	0.0006	79	0.0012
	Weak	90	0.0006	96	0.0014	86	0.0019
San Fernando	Strong	62	0.0004	42	0.0008	46	0.0010
	Weak	61	0.0005	56	0.0009	58	0.0012
Whitter	Strong	77	0.0001	72	0.0002	67	0.0006
	Weak	81	0.0002	75	0.0004	75	0.0008

14.2.1.3 EFFECT OF FOUNDATION SOIL STIFFNESS ON LOW CYCLE FATIGUE PERFORMANCE OF STEEL H-PILES

In this section, the effect of soil stiffness on low cycle fatigue performance of steel H-piles at the abutments is studied. The stiffness of the foundation soil is observed to have a remarkable effect on the cumulative fatigue damage index of steel H-piles under seismic loading. As the soil stiffness increases, cumulative fatigue damage index of steel H-piles also increases, as observed from Table 14.3. For example, in the case of the Northridge earthquake scaled to a peak ground acceleration of A_p=0.5g, the cumulative fatigue damage index is calculated as 0.0006 for loose sand. However, for the same earthquake and peak ground acceleration levels, the low cycle damage index is calculated as 0.0018 for dense sand.

Table 14.3. Number of cycles and fatigue damage index for different soil stiffness.

Earthquake	Soil stiffness	A_p=0.35g		A_p=0.50g		A_p=0.80 g	
		Number of cycles	$\sum_i^n \frac{n_i}{N_i}$	Number of cycles	$\sum_i^n \frac{n_i}{N_i}$	Number of cycles	$\sum_i^n \frac{n_i}{N_i}$
Loma Prieta Ap=0.200 g	Dense	60	0.0006	68	0.0008	83	0.0009
	Medium dense	56	0.0005	52	0.0007	52	0.0008
	Medium	85	0.0001	76	0.0003	59	0.0008
	Loose	82	0.0001	72	0.0002	63	0.0006
Loma Prieta Ap=0.278 g	Dense	55	0.0008	61	0.0013	63	0.0014
	Medium dense	79	0.0006	75	0.0008	70	0.0013
	Medium	80	0.0005	65	0.0007	62	0.0012
	Loose	68	0.0004	72	0.0005	65	0.0008
Mammoth Lake	Dense	41	0.0010	45	0.0014	45	0.0015
	Medium dense	52	0.0007	46	0.0011	48	0.0015
	Medium	55	0.0002	52	0.0005	42	0.0014
	Loose	65	0.0001	51	0.0003	53	0.0008
Northridge Ap=0.263 g	Dense	78	0.0010	80	0.0018	80	0.0024
	Medium dense	80	0.0008	74	0.0014	77	0.0020
	Medium	78	0.0007	52	0.0009	62	0.0013
	Loose	82	0.0005	78	0.0006	59	0.0008
Northridge Ap=0.316 g	Dense	80	0.0009	80	0.0013	85	0.0021
	Medium dense	78	0.0007	76	0.0011	72	0.0017
	Medium	93	0.0003	88	0.0006	79	0.0012
	Loose	85	0.0002	89	0.0005	81	0.0008
San Fernando	Dense	54	0.0005	63	0.0009	60	0.0010
	Medium dense	59	0.0005	59	0.0008	54	0.0010
	Medium	62	0.0004	42	0.0008	46	0.0010
	Loose	65	0.0002	43	0.0006	45	0.0008
Whitter	Dense	72	0.0005	67	0.0007	73	0.0007
	Medium dense	72	0.0003	70	0.0006	71	0.0007
	Medium	77	0.0001	72	0.0002	67	0.0006
	Loose	67	0.0001	69	0.0002	68	0.0004

14.2.2. SUMMARY OF OBSERVATIONS ON CUMULATIVE FATIGUE DAMAGE OF STEEL H-PILES

This study reveals that cumulative fatigue damage in the steel H-piles induced by seismic loadings are negligible. As mentioned earlier, the fatigue failure is assumed to take place when the cumulative n_i/N_i ratios of the cycles with different amplitudes add up to 1 according to Miner's rule. However, the cumulative fatigue damage indices calculated from Miner's rule (Miner 1945) range between 0.0008 and 0.0037 as observed from Tables 14.1-3. Even in the case of earthquakes with very large peak ground accelerations (0.8 g), the cumulative fatigue damage indices are much small than 1. This obviously indicates that seismically induced low cycle damage~~s~~ is not of a concern for short to medium length IBs.

CHAPTER 15

COMPARISION OF SEISMIC PERFORMANCE OF INTEGRAL AND CONVENTIONAL BRIDGES

In this part of the thesis study, seismic performances of integral and conventional bridges are compared. For this purposes, three existing IBs with various properties are selected and then designed as conventional jointed bridges. The nonlinear structural models of the integral and conventional bridges are then built according to the modeling assumptions described earlier. Next, nonlinear time history analyses of the bridge models are conducted using the the set of ground motions selected earlier. In the analyses, the ground motions are scaled to peak ground accelerations ranging between 0.2g and 0.8g to assess the seismic performance of integral bridges in relation to that of conventional bridges at various performance levels.

15.1. NONLINEAR TIME-HISTORY ANALYSES OF THE BRIDGE MODELS

The integral and conventional bridge models are built and nonlinear time history analyses of the bridge models are conducted using the seven earthquake ground motions considered in this research study. The nonlinear time history analyses are repeated for peak ground accelerations of 0.2g, 0.35g, 0.5g and 0.8g for each selected earthquake. This led to more than 200 different analyses cases. The analyses results are presented in the following sections.

15.2 ANALYSES RESULTS

In the following subsections, seismic performance of integral and conventional bridges with one, two and three spans are compared in terms of the maximum displacements of the deck and bearings as well as the maximum displacements and plastic end rotations of the pier columns and steel H piles at the abutments. The analyses results are presented in Figs 15.1-15.20 as the average of the results from the seven ground motions for various peak ground accelerations considered in this study.

15.2.1 COMPARISION OF THE SEISMIC PERFORMANCE OF SINGLE SPAN INTEGRAL AND CONVENTIONAL BRIDGES

In this section, seismic performance assessment of the single span integral and conventional bridges is studied. To assess the seismic performance of integral bridges relative to that of conventional bridges, the maximum deck and pile displacements as well as plastic end rotations of the steel H piles at the abutments are compared. The comparison of maximum deck and pile displacements in the longitudinal and transverse directions as well as the plastic end rotations of the steel piles at the abutments are illustrated in Figs 15.1-4. The figures reveal that in the case of conventional bridges, larger deck and pile displacements as well as larger pile rotations are obtained. For instance, for the single span integral bridge subjected to earthquakes with a peak ground acceleration of, A_p=0,8g, the maximum deck displacement is obtained as 22 mm. However, for the conventional bridge subjected to earthquakes with the same level of peak ground acceleration, the maximum deck displacement in the longitudinal direction is obtained as 90 mm. The difference between the maximum deck displacements obtained for the integral and conventional bridges is about 400 %. Similar differences are also obtained for the end rotations of the piles at the abutments. For instance, for the single span integral and conventional bridges subjected to earthquakes with a peak ground acceleration of A_p=0.5g, the maximum pile end rotations in the longitudinal direction are obtained as 0.00109 and 0.00305 rad respectively.. The difference between the maximum pile end rotations obtained for the integral and conventional bridges is about 280 %. Similar results are also obtained for the maximum pile displacements in both orthogonal directions as observed from Fig. 15.3 and 15.4. The main reason for such large differences in the seismic response of integral and conventional bridges could be attributed to the monolithic construction of integral bridges. In the case of conventional bridges, the superstructure is supported by flexible, elastomeric bearings at the abutments where the superstructure is free to move due to the presence of expansion joints. This type of a structural configuration produces very large deck displacements compared to that of integral bridges where the abutment is rigidly connected to the superstructure preventing the free movement of the deck in combination with the resistance provided by the backfill. Furthermore, conventional bridge abutments tend to transfer larger forces to the pile foundations due to lack of lateral restraint provided by the superstructure, the effect of dynamic active backfill pressure and large inertial forces due to their heavier weight compared to that of integral bridge abutments. This obviously leads to larger pile end rotations and displacements at the abutments of conventional bridges. In summary, single span integral bridges exhibit superior performance compared to that of conventional bridges.

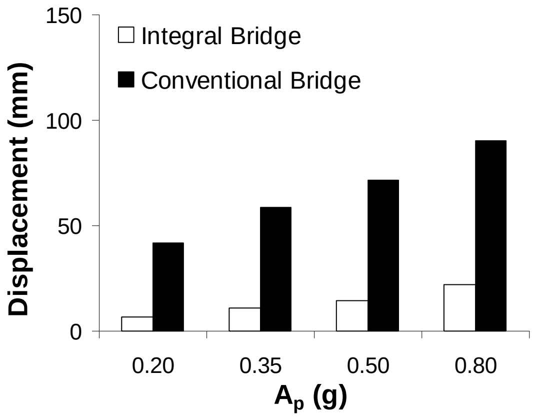

Figure 15.1. Deck displacements in the longitudinal direction vs. peak ground acceleration for single span integral and conventional bridges

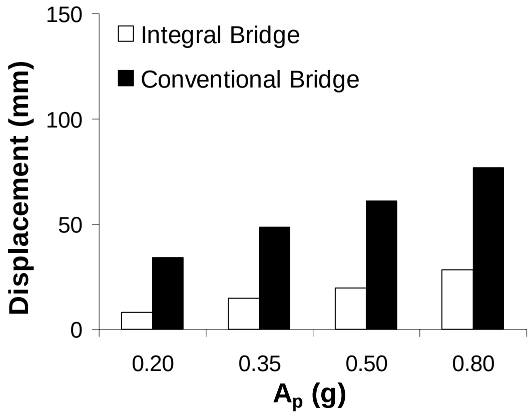

Figure 15.2. Deck displacements in the transverse direction vs. peak ground acceleration for single span integral and conventional bridges

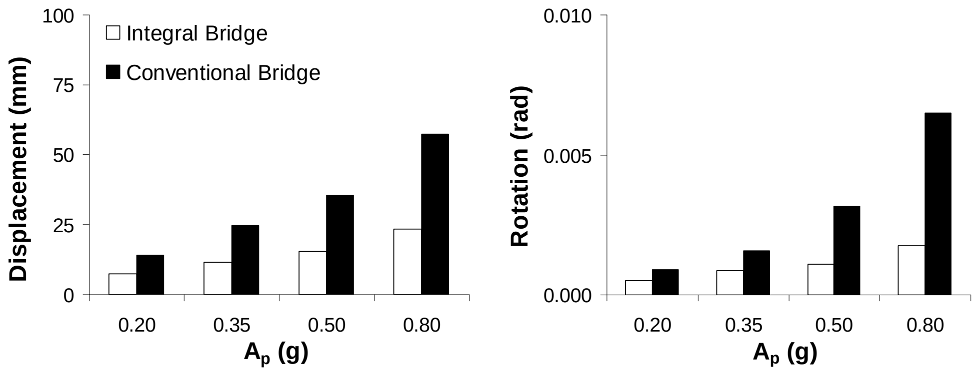

Figure 15.3. Pile displacements and end rotations in the longitudinal direction vs. peak ground acceleration for single span integral and conventional bridges

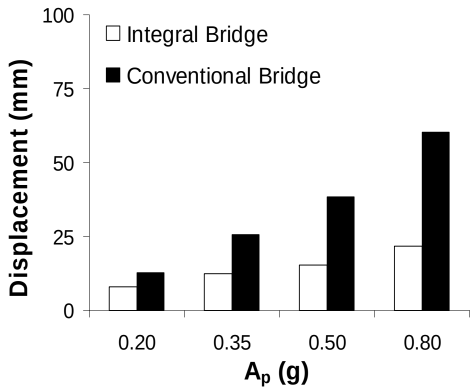

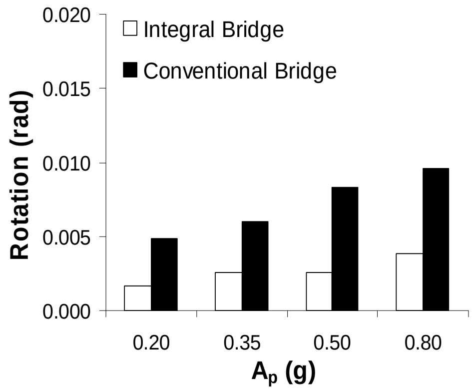

Figure 15.4. Pile displacements and end rotations in the transverse direction vs. peak ground acceleration for single span integral and conventional bridges

15.2.2 COMPARISION OF THE SEISMIC PERFORMANCE OF TWO SPAN INTEGRAL AND CONVENTIONAL BRIDGES

In this section, seismic performance assessment of two span integral and conventional bridges is studied. To assess the seismic performance of two span integral bridges in comparison to conventional bridges, the maximum deck, pier, bearing and pile displacements as well as plastic end rotations of the pier columns, steel H piles underneath the abutments and reinforced concrete piles underneath the piers are compared. The comparison of maximum displacements and rotations of the bridge members are illustrated in Figs 15.5-15.12. The figures reveal that larger deck displacements and pier column drifts and end rotations are obtained in the case of conventional bridges. For instance, for the two span integral bridge subjected to earthquakes with a peak ground acceleration of A_p=0,8g, the maximum pier column drift and end rotation in longitudinal direction are obtained as 55 mm and 0.0087 rad. respectively. However, for the two span conventional bridge subjected to the same level of peak ground acceleration, the maximum pier column drift and rotation are obtained as 70 mm and 0.0102 rad respectively. The differences between the maximum pier column drifts and end rotations of the integral and conventional bridges are 27 % and 17 % respectively. However, smaller displacements and plastic end rotations for the steel H piles are calculated in the case of the two span conventional bridge (Fig. 15.9 and 15.10). For instance, for the two span integral bridge subjected to earthquakes with a peak ground acceleration of A_p=0.5g, the maximum pile displacement and rotation are obtained as 53 mm and 0.00428 rad. respectively. However, for the two span conventional bridge subjected to the same level of peak ground acceleration, the maximum pile displacement and rotation are obtained as 36 mm and 0.00228 rad respectively. The differences between the maximum pile displacement and rotation obtained for the integral and conventional bridges are 68 % and 87 % respectively.

The smaller deck displacements in the case of integral bridges are mainly due to the monolithic construction of the abutments with the superstructure restraining the lateral movement of the deck in both orthogonal directions combined with the resistance of the backfill. In the case of integral bridge piers, the lateral displacements of the deck in integral bridges is mainly accommodated by the flexible bearings over the piers producing smaller pier column drifts and rotations but larger steel H pile displacements and rotations at the abutments. In the case of the two span conventional bridge however, the pier resists a greater share of the seismic load due to larger tributary superstructure mass supported by the piers. Consequently, in the case of integral bridges, while the deck displacements and pier column drifts and rotations are smaller, abutment pile displacements and rotations are larger than those of conventional bridges. However, in the design of especially long IBs inelastic displacement and rotations in steel H piles are already expected under thermal movement. Therefore, seismically induced inelastic displacements and rotations in steel H-piles do not pose a problem as long as they do not lead to low cycle fatigue failure of steel H piles at the abutments. As earlier analyses revealed that low cycle fatigue is not of concern in steel H-piles at the abutments, the larger inelastic displacements and rotations in the steel H-piles of IBs are not indicative of an inferior performance compared to that of conventional bridges. Enlighten of these observations and explanations, it may be concluded that IBs have superior seismic performance compared to conventional bridges for the bridges under considerations.

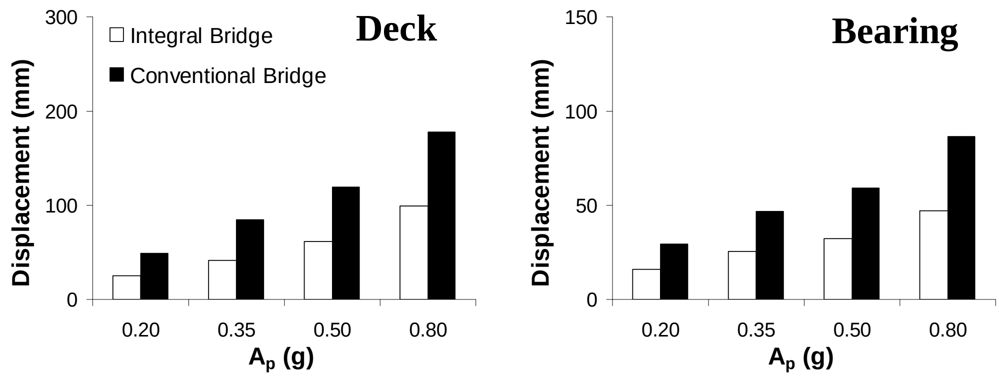

Figure 15.5. Deck and bearing displacements in longitudinal direction vs. peak ground acceleration for two span integral and conventional bridges

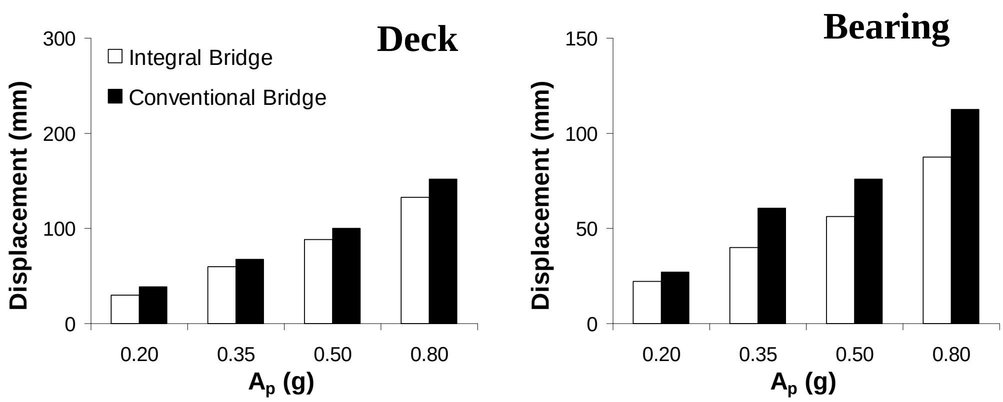

Figure 15.6. Deck and bearing displacements in transverse direction vs. peak ground acceleration for two span integral and conventional bridges

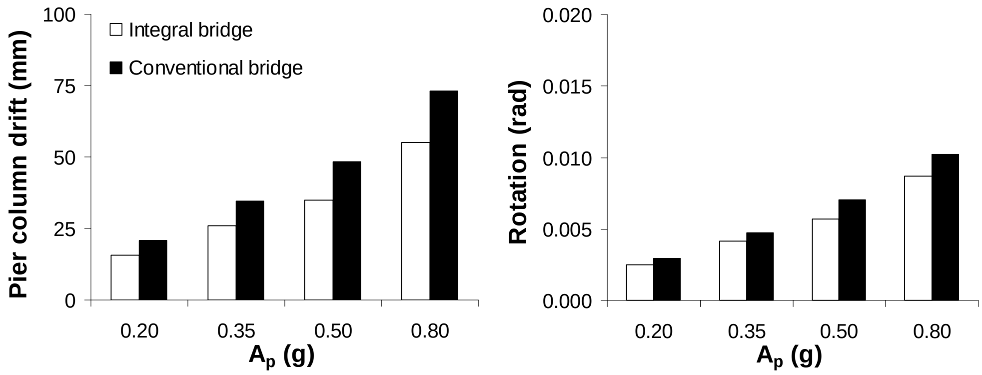

Figure 15.7. Pier column drifts and rotations in longitudinal direction vs. peak ground acceleration for two span integral and conventional bridges

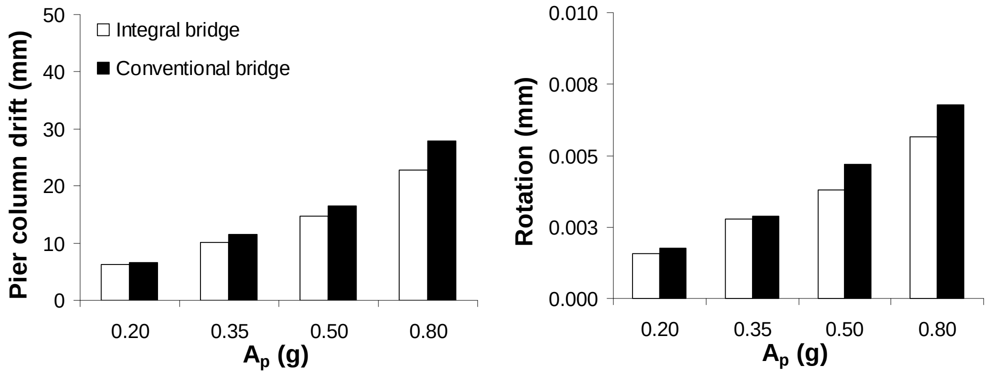

Figure 15.8. Pier column drifts and rotations in transverse direction vs. peak ground acceleration for two span integral and conventional bridges

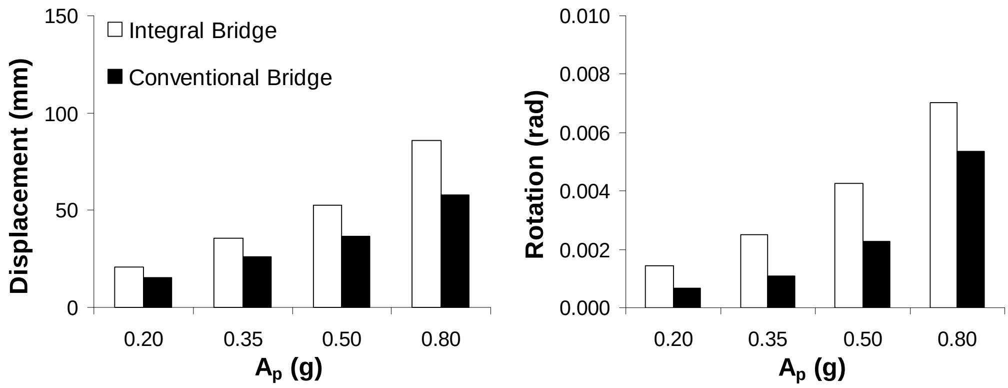

Figure 15.9. Steel H-piles displacements and rotations in longitudinal direction vs. peak ground acceleration for two span integral and conventional bridges

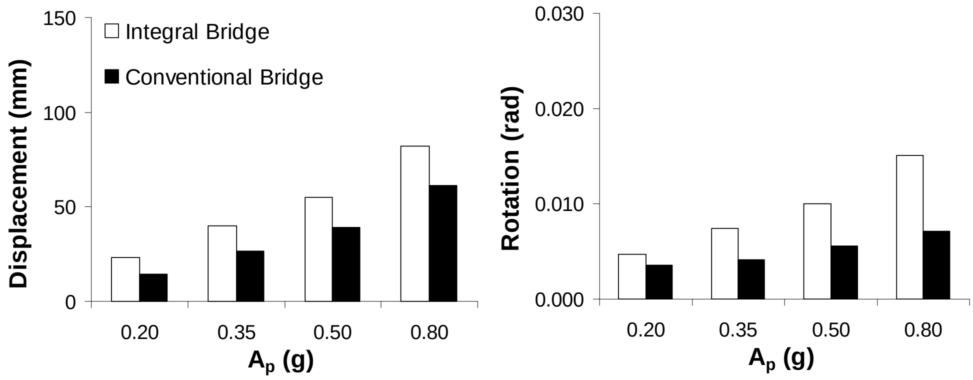

Figure 15.10. Steel H-piles displacements and rotations in transverse direction vs. peak ground acceleration for two span integral and conventional bridges

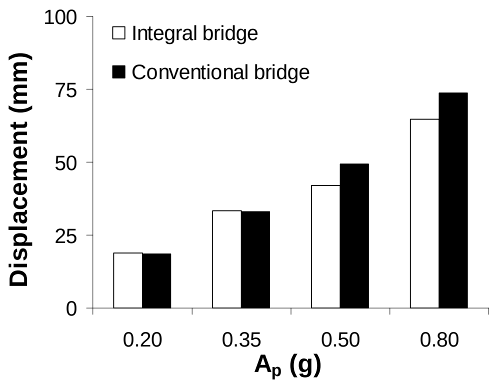

Figure 15.11. Reinforced concrete pile displacements and rotations in longitudinal direction vs. peak ground acceleration for two span integral and conventional bridges

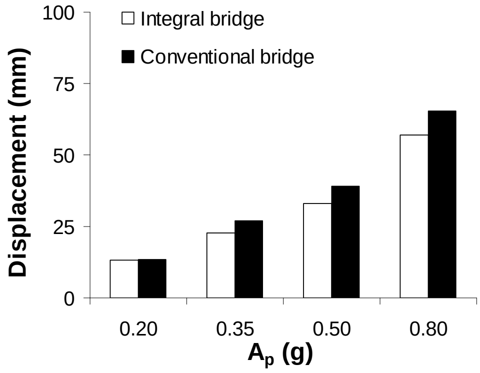

Figure 15.12. Reinforced concrete pile displacements and rotations in transverse direction vs. peak ground acceleration for two span integral and conventional bridges

15.2.3 COMPARISION THE SEISMIC PERFORMANCE OF THREE SPAN INTEGRAL AND CONVENTIONAL BRIDGES

In this section, seismic performance assessment of three span integral and conventional bridges is studied. To assess the seismic performance of three span integral in comparison to conventional bridges, the maximum deck, pier, bearing and pile displacements as well as plastic end rotations of the pier columns, steel H piles underneath the abutments and reinforced concrete piles underneath the piers are compared. The comparison of maximum displacements and end rotations of the bridge members are illustrated in Figs 15.13-15.20. The figures reveal that larger deck displacements and pier column drifts and end rotations are obtained in the case of conventional bridges. For instance, for the two span integral bridge subjected to earthquakes with a peak ground acceleration of A_p=0,8g, the maximum pier column drift and end rotation in longitudinal direction are obtained as 39 mm and 0.0160 rad. respectively. However, for the three span conventional bridge subjected to the same level of peak ground acceleration, the maximum pier column drifts and end rotation are obtained as 55 mm and 0.0176 rad respectively. The differences between the maximum pier column drifts and end rotations of the integral and conventional bridges are 41 % and 10 % respectively. However, smaller displacements and plastic rotations for the steel piles are calculated in the case of three span conventional bridge as observed from Figs. 15.15 and 15.16. For instance, for the three span integral bridge subjected to earthquakes with a peak ground acceleration of A_p=0.8g, the maximum pile displacement and rotation in longitudinal direction are obtained from the analyses of three span IB as 66 mm and 0.0109 rad. respectively. However, for the three span conventional bridge subjected to the same level of peak ground acceleration, the maximum pile displacement and rotation are obtained as 59 mm and 0.0094 rad respectively. The difference between the maximum pile displacement and rotation obtained for the integral and conventional bridges are 12 % and 16 % respectively.

The smaller deck displacements in the case of integral bridges are mainly due to the monolithic construction of the abutments with the superstructure restraining the lateral movement of the deck in both orthogonal directions combined with the resistance of the backfill. In the case of integral bridge piers, the lateral displacements of the deck in integral bridges is mainly accommodated by the flexible bearings over the piers producing smaller pier column drifts and rotations but larger steel H pile displacements and rotations at the abutments. In the case of the three span conventional bridges however, the pier resists a greater share of the seismic load due to larger tributary superstructure mass supported by the piers. Consequently, in the case of integral bridges, while the deck displacements and pier column drifts and rotations are smaller, abutment pile displacements and rotations are larger than those of conventional bridges. However, in the design of especially long IBs inelastic displacement and rotations in steel H piles are already expected under thermal movement. Therefore, seismically induced inelastic displacements and rotations in steel H-piles do not pose a problem as long as they do not lead to low cycle fatigue failure of steel H piles at the abutments. As earlier analyses revealed that low cycle fatigue is not of concern in steel H-piles at the abutments, the larger inelastic displacements and rotations in the steel H-piles of IBs are not indicative of an inferior performance compared to that of conventional bridges. Enlighten of these observations and explanations, it may be concluded that IBs have superior seismic performance compared to conventional bridges for the bridges under considerations.

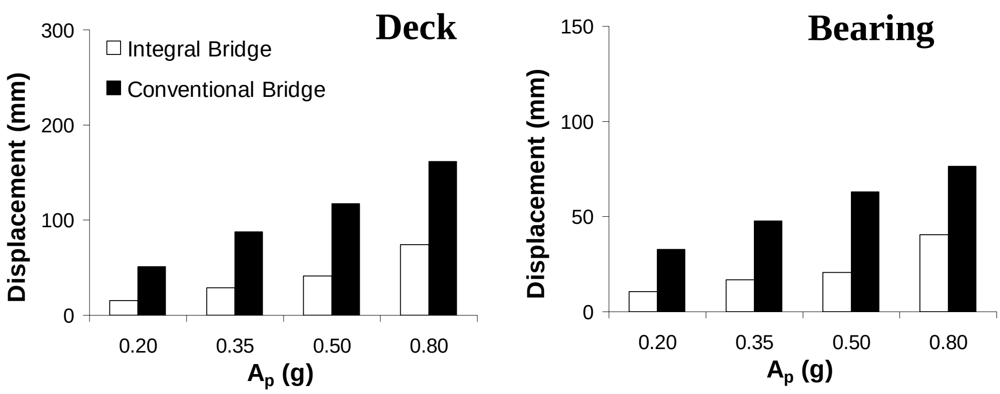

Figure 15.13. Deck and bearing displacements in longitudinal direction vs. peak ground acceleration for three span integral and conventional bridges

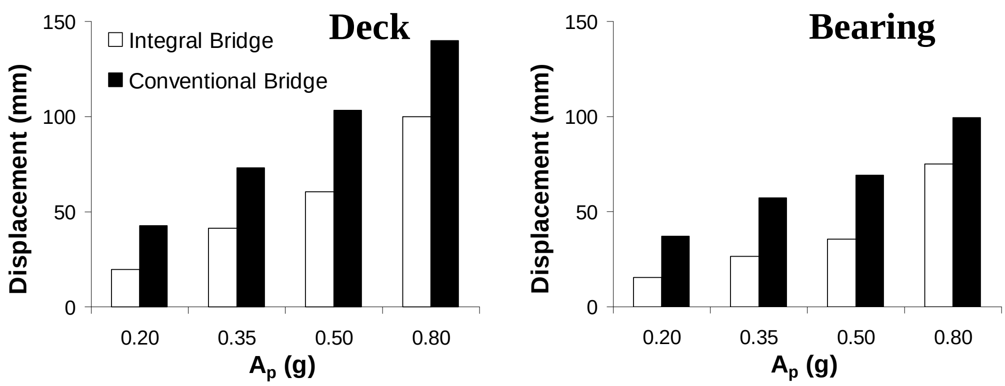

Figure 15.14. Deck and bearing displacements in transverse direction vs. peak ground acceleration for three span integral and conventional bridges

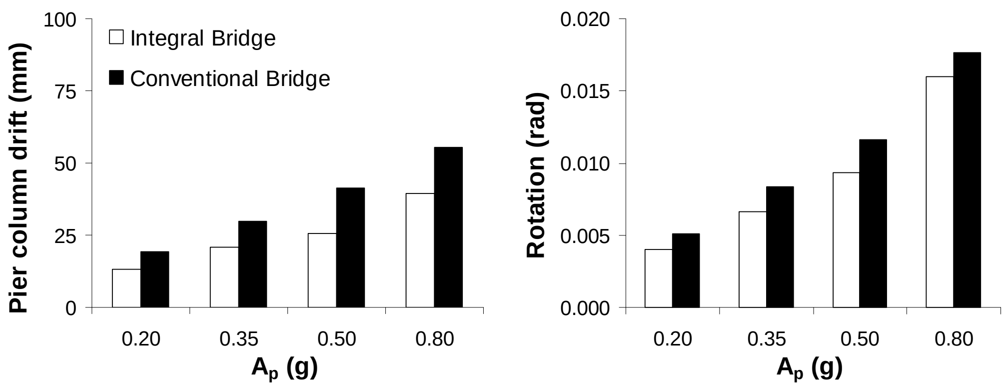

Figure 15.15. Pier column drifts and rotations in longitudinal direction vs. peak ground acceleration for three span integral and conventional bridges

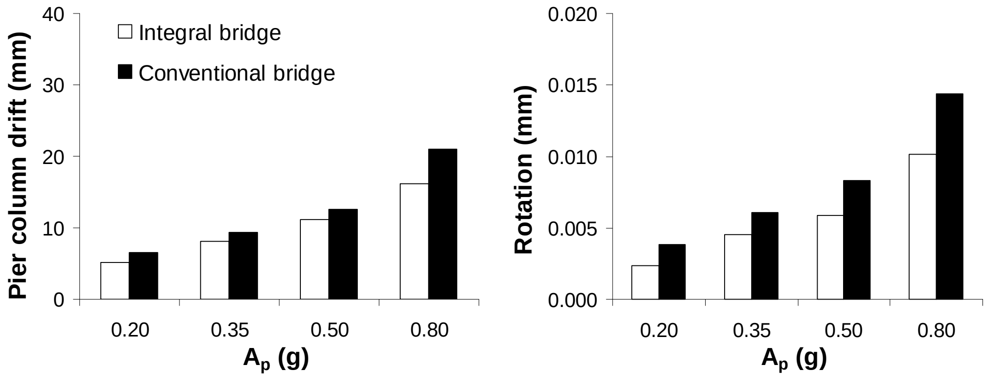

Figure 15.16. Pier column drifts and rotations in transverse direction vs. peak ground acceleration for three span integral and conventional bridges

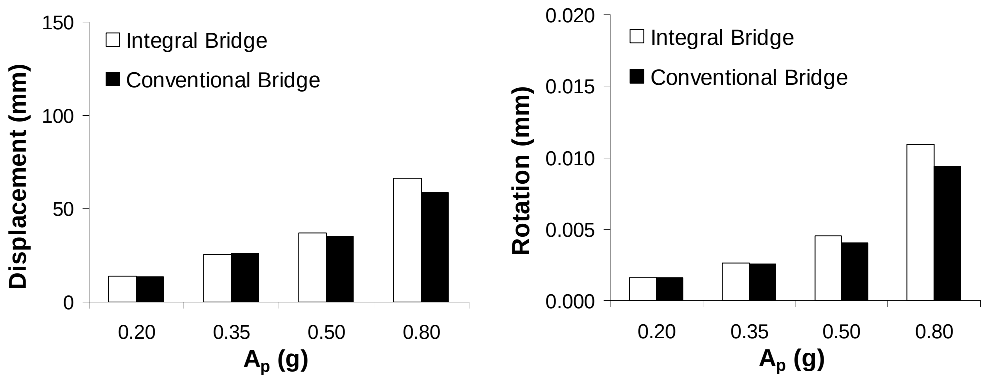

Figure 15.17. Steel H-piles displacements and rotations in longitudinal direction vs. peak ground acceleration for three span integral and conventional bridges

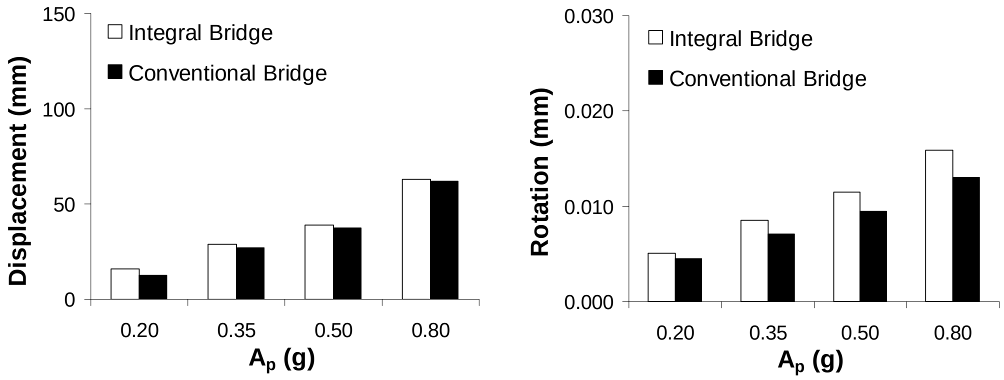

Figure 15.18. Steel H-piles displacements and rotations in transverse direction vs. peak ground acceleration for three span integral and conventional bridges

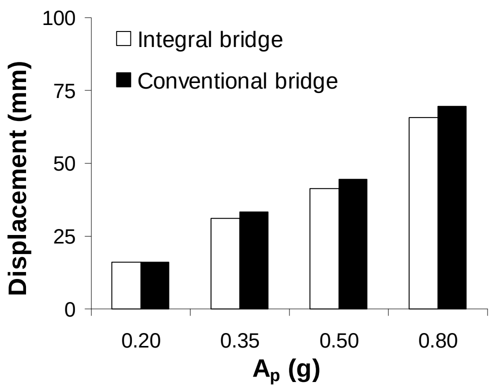

Figure 15.19. Reinforced concrete pile displacements and rotations in longitudinal direction vs. peak ground acceleration for two span integral and conventional bridges

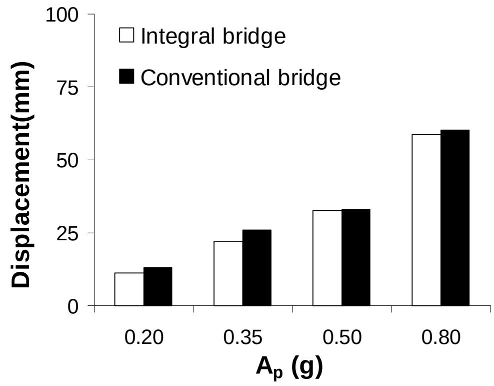

Figure 15.20. Reinforced concrete pile displacements and rotations in transverse direction vs. peak ground acceleration for two span integral and conventional bridges

CHAPTER 16

CONCLUSIONS

This thesis study is composed of two parts. In the first part of the thesis study, the performance of IBs under live load is studied. Live load distribution formulae are developed for the components of straight (no skew) IBs with presetressed concrete girders. The effect of abutment-superstructure continuity on live load distribution is also studied in comparison to conventional jointed bridges. Furthermore, the applicability of AASHTO live load distribution equations to IB components is investigated. In the second part of the thesis study, the seismic performance of IBs is evaluated in comparison to conventional jointed bridges. The effect of several structural, geometric and geotechnical parameters on the seismic performance of IBs is also investigated.

Followings are the conclusions deduced from the first part of this research study;

Live load analyses of IBs are performed for the girders and substructure components (piles and abutments). The analyses results revealed that the LLDFs obtained for the interior girder shear of IBs are generally in good agreement with those calculated using AASHTO LLDEs. Thus, AASHTO LLDEs for interior girder shear may be used to calculate the live load shear in the interior prestressed concrete girders of IBs. However, for the girder moment and exterior girder shear, the difference between the LLDFs obtained from finite element analyses of IBs and those calculated from AASHTO LLDEs may be as much as 87%. This difference is generally more pronounced for bridges with shorter spans (shorter than 30 m), larger girder size (larger than AASHTO Type IV girders), smaller girder spacing (smaller than 2.4 m), smaller slab thickness (smaller than 0.2 m) and larger bridge width. This large difference is mainly attributed to the effect of continuity at the abutment-deck joint in IBs. Consequently, the AASHTO LLDEs for the girder moment and exterior girder shear are not suited for IBs. It is suggested that modifications to the current AASHTO LRFD design specifications will make the calculation of LLDFs for IB girders more meaningful especially for IBs shorter than 30 m. Thus, using regression analysis techniques and the available analysis results, two sets of LLDEs are developed to estimate the live load girder moments and exterior girder shears of IBs. The first set of equations are developed in the form of correction factors, which are used to multiply the LLDEs present in AASHTO (2007) for slab-on-girder jointed bridges to accurately calculate the LLDFs for the girder moment and exterior girder shear of IBs. The second set of equations is developed to directly obtain the LLDFs for the girder moment and exterior girder shear of IBs independent of AASHTO (2007). Comparison of the LLDFs obtained from finite element analyses and those calculated using the developed equations revealed that the developed formulae yield a reasonably good estimate of the live the load moment and exterior girder shear for short to medium span IBs with no skew. In addition, further analyses of IBs under AASHTO live load revealed that the effects of substructure and soil properties on the distribution of live load effects among the girders of IBs are negligible. Therefore, the developed formulae are also valid for IBs with different foundation soil stiffness, abutment and pile properties. In addition, numerous finite element analyses are conducted to obtain the live load distribution factors for the abutments and piles of IBs as a function of various superstructure and substructure / soil properties. Then, using regression analysis techniques and the available analysis results, LLDEs are developed to estimate the live load moments and shears in the abutments and piles of IBs. Comparison of the live load distribution factors obtained from finite element analyses and those calculated using the developed equations revealed that the developed formulae yield a reasonably good estimate of live load moment and shear in short to medium span IB abutments and piles.

Followings are the conclusions deduced from the second part of this research study;

Nonlinear time history analyses conducted to assess the effect of modeling simplification on the seismic response of IBs revealed that nonlinear soil-pile and abutment-backfill interaction have remarkable effects on the seismic response of IBs under medium and large intensity earthquakes. In addition, the soil column model used to simulate the free field effects in the structural model is found to have significant effects on the seismic response of IBs. Therefore, for seismic analyses of IBs, the nonlinear soil-pile and abutment-backfill interactions as well as free-field effects must be considered in the structural models. Thus, for the seismic analyses of IBs, the most complicated structural model that includes complete soil-bridge interaction effects (Model 1) is used to accurately assess the seismic performance of IBs. Analyses of IBs using such complicated structural models revealed that cumulative fatigue damage in steel H-piles of IBs due to seismic displacement cycles is negligible. Thus, for the design of small and medium span IBs, low cycle fatigue effects due to seismic displacement cycles in the steel H piles at the abutments do not need to be considered. Further analyses conducted to investigate the seismic performance of IBs as a function of various structural and geotechnical parameters revealed that the foundation soil stiffness, abutment height and thickness have significant effects on the maximum deck, bearing, pier column and pile displacements of IBs under large intensity earthquakes. However, the backfill compaction level is found to have only negligible effects on the maximum displacement of the deck, bearing, pier columns and piles at the abutments. In addition, size and orientation of the steel H piles at the abutments are found to have significant effects on the abutment pile displacements, but negligible effects on the displacement of the deck, bearing, pier column and reinforced concrete piles underneath the pier. Moreover, the parametric study revealed that IBs with shorter and thinner abutments as well as large steel H piles oriented to bend about their strong axis exhibit better seismic performance especially under large intensity earthquakes.

Finally, comparison of the seismic performances of integral and conventional bridges reveals that single span integral bridges exhibit superior performance compared to that of conventional bridges. For multi span IBs, it is found that the deck displacements and pier column drifts and rotations are smaller nevertheless; abutment pile displacements and rotations are larger than those of conventional bridges. However, in the design of especially long IBs inelastic displacement and rotations in steel H piles are already expected under thermal movement. Therefore, seismically induced inelastic displacements and rotations in steel H-piles do not pose a problem as long as they do not lead to low cycle fatigue failure of steel H piles at the abutments. As earlier analyses revealed that low cycle fatigue is not of concern in steel H-piles at the abutments, the larger inelastic displacements and rotations in the steel H-piles of IBs are not indicative of an inferior performance compared to that of conventional bridges. Enlighten of these observations and explanations, it may be concluded that IBs have superior seismic performance compared to conventional bridges for the bridges under considerations.

REFERENCES

AASHTO. (2007) “Load and Resistance Factor Design (LRFD) Specifications” Washington, D.C.

Alfawakhiri, F. and Bruneau, M. (2000) “Flexibility of superstructures and supports in the seismic analysis of simple bridges” *Earthquake Engineering & Structural Dynamics*, 29:711–729,

Anandarajah, A., Zhang, J. and Ealy, C. (2005) “Calibration of dynamic analysis methods from field test data”. *Soil Dynamics and Earthquake Engineering*, 25(7-10):763-772,

Angelides, D.C. and Roesset, J.M. (1981) “Nonlinear lateral dynamic stiffness of pile” *Journal of the Geotechnical Engineering Division*, 107: 1443–1460.

API (2000) "Recommended practice for planning, designing and constructing fixed offshore platforms—Working stress design." 20th Edition, American Petroleum Institute, Washington, DC.

Barker, R.M. and Puckett J.A. (1997) “Design of Highway Bridges.” John Wiley and Sons, Inc.

Barr, P.J., Eberhard, M. O., and Stanton, F. (2001). “Live-load distribution factors in prestressed concrete girder bridges.” *Journal of Bridge Engineering*, ASCE 6(5), 298–306.

Bakth, B., and Moses. F. (1988). “Lateral Distribution Factors for Highway Bridges.” *Journal of Structural Engineering*, ASCE 114(8), 1785-1803

Basha B. M., Sivakumar Babu G.L (2009) “Computation of sliding displacements of bridge abutments by pseudo-dynamic method” *Soil Dynamics and Earthquake Engineering*, 29, 103–120.

Boulanger, R.W., Curras, C.J., Kutter, B.L., Wilson, D.W., Abghari, A. (1999) "Seismic soil-pile-structure interaction experiments and analyses." *Journal of Geotechnical and Geoenvironmental Engineering*, ASCE, 125(9), 750-759.

Brandenberg, S.J., Singh, P., Boulanger, R.W., Kutter, B.L. (2001) "Behavior of piles in laterally spreading ground during earthquakes" *Proc. Sixth Caltrans Seismic Research Workshop*, 2-106.

Brockenbrough, R.L. (1986) "Distribution factors for curved I-girder bridges" *Journal of Structural Engineering*, ASCE, 112(10), 2200-2215.

Buckle, I.G., Constantinou, M.C., Dicleli, M., Ghasemi, H., (2006) "Seismic Isolation of Highway Bridges" Special Publication MCEER-06-SP07, *Multidisciplinary Center for Extreme Events Research,* Buffalo, NY.

Burdette, E.G., Ingram, E.E., Tidwell, J.B., Goodpasture, D.W., Deatherage, J.H., Howard, S.C. (2004) "Behavior of Integral Abutments Supported by Steel H-Piles," *Transportation Research Board Meeting and published in the Transportation Research Record* Washington, D.C., USA.

Burke, M. P., Jr., (1988) "Bridge Deck Joints", *NCHRP Synthesis of Highway Practice*, No 141, *Transportation Research Board*, National Research Council, Washington, D.C., USA.

Burke, M. P., Jr., (1990a) "Integral Bridge Design is on The Rise", *AISC Modern Steel Construction*, 30 (4), 9-11.

Burke, M. P., Jr., (1990b) "Integral Bridges", *Transportation Research Record*, No 1275, Transportation Research Board, National Research Council, Washington, D.C., USA.

Burke, M. P., Jr., (1994) "Semi-Integral Bridges: Movements and Forces", Transportation Research Record, No 1460, Transportation Research Board, National Research Council, Washington, D.C., USA, 1-7.

Cai, S. C. (2005) "Discussion on AASHTO LRFD Load Distribution Factors for Slab-on-Girder Bridges" *Practice Periodical on Structural Design and Construction*, Vol. 10, No. 3.

Cai, Y.X., Gould, P.L., Desai, C.S. (2000) "Nonlinear analysis of 3D seismic interaction of soil–pile-structure system and application" *Engineering Structures*, 22(2),191–9.

California Dept. of Transportation (CALTRANS) (2006) "Seismic design criteria, ver. 1.4." *CALTRANS*, Division of Engineering Services, Office of Structure Design, Sacramento, California.

Chao, S.H. and Loh, C.H. (2007) "Inelastic response analysis of reinforced concrete structures using modified force analogy method" *Earthquake Engineering & Structural Dynamics* , 36(12), 1659 – 1683.

Chen Y, Aswad A. (1996) "Stretching span capability of prestressed concrete bridges under AASHTO LRFD." *Journal of Bridge Engineering*, ASCE 1(3), 112-120.

Coduto, D.P. (2001) "Foundation Design: Principles and Practices, 2nd ed. Upper Saddle River, NJ: Prentice Hall.

Cole, R. T., and Rollins, K. M. (2006) "Passive earth pressure mobilization during cyclic loading." *Journal of Geotechnical and Geoenvironmental Engineering*., 132(9), 1154–1164.

Cook R. D. (1995) Finite element modeling for stress analysis, New York, NY: John Wiley & Sons.

Clough, C. W., and Duncan, J. M. (1991) "Earth Pressures." Chapter 6, Foundation Engineering Manual, 2nd Ed.

Crouse, C.B., Hushmand, B., Martin, G.R. (1987) "Dynamic soil-structure interaction of a single span bridge" *Journal of Earthquake Engineering and Structural Dynamics*, 15: 711-729

Dehne, Y. and Hassiotis, S. (2003) "Seismic Analysis of Integral Abutment Bridge: Scotch Road I-95 Project." *Proceedings, 16th Annual ASCE Engineering Mechanics Conference*, July 16-18, University of Washington.

Dicleli, M. (2000). "Simplified Model for Computer-Aided Analysis of Integral Bridges", *Journal of Bridge Engineering*, ASCE Vol. 5, No.3.

Dicleli M. (2005) " Integral Abutment-Backfill Behavior on Sand Soil-Pushover Analysis Approach", *Journal of Bridge Engineering*, ASCE Vol. 10, No.3.

Dicleli M. and Albhaisi (2003) "Maximum Length of Integral Abutment Bridges Supported on Steel H-piles Driven in Sand", *Engineering Structures*, Elsevier Science, Vol. 25, No.12, pp. 1491-1504, 2003.

Dicleli M. and Albhaisi (2004) " Estimation of Length Limits for Integral Bridges Built on Clay", *Journal of Bridge Engineering*, Vol. 9, No.6.

Dicleli M. and Albhaisi (2005) “Analytical Formulation of Maximum Length Limits for Integral Bridges Built on Cohesive Soils”, *Canadian Journal of Civil Engineering*, Vol. 32, No.5, pp. 726-738, 2005.

Dicleli, M. (2007) “Supplemental Elastic Stiffness to Reduce Isolator Displacements for Seismic-Isolated Bridges in Near Fault Zones.” *Engineering Structures*, Elsevier Science, 29(5), 763-775.

Dicleli, M. and Erhan, S. (2008) “Effect of Soil and Substructure Properties on Live Load Distribution in Integral Abutment Bridges”, *Journal of Bridge Engineering*, ASCE, Volume 13, Issue 5, pp. 527-539.

Dicleli, M. and Erhan, S. (2010) “Effect of Superstructure-Abutment Continuity on Live Load Distribution in Integral Abutment Bridge Girders”, *Structural Engineering and Mechanics*, Volume. 34, Issue 5, pp. 635-662**.**

Dicleli M. and Mansour M. (2003) “Seismic Retrofitting of Highway Bridges in Illinois Using Friction Pendulum Seismic Isolation Bearings and Modeling Procedures”, *Engineering Structures*, 25(9), 1139-1156.

Dou, H. and Byrne, P.M. (1996) “Dynamic response of single piles and soil–pile interaction” *Canadian Geotechnical Journal*, 33(1), 80–96.

Dowell, R.K., Seible, F. and Wilson, E.L. , (1998) “Pivot hysteresis model for reinforced concrete members” *ACI Structural Journal* 95(5), 607-617

Duncan M. J. and Arsoy S. (2003) “ Effect of Bridge-Soil Interaction on Behavior of Piles Supporting Integral Bridges.” *Transportation Research Record 1849*, Paper No. 03-2633

Duncan, M. J., and Mokwa, R. L. (2001) “Passive earth pressure: Theories and tests.” *Journal of Geotechnical and Geoenvironmental Engineering*, 127(3), 248–257.

Dutta, S. C. and Das, P. K, (2002) “Inelastic seismic response of code-designed reinforced concrete asymmetric buildings with strength degradation” *Engineering Structures* 24(10), 1295-1314.

Eberhard, M. O. and Marsh, M. L. (1997) “Lateral Load Response of a Reinforced Concrete Bridge” *Journal of Structural Engineering*, 123(4), 451-460.

El-Gamal, M. and Siddharthan, R.V. (1998) "Stiffnesses of Abutments on Piles in Seismic Bridge Analyses," *Soils and Foundations*, 38(1), 77-87.

El Naggar, M.H. and Bentley, K.J. (2000) “Dynamic analysis for laterally loaded piles and dynamic p-y curves” *Canadian Geotechnical Journal*, 37(6), 1166-1183.

Evans, L. T. (1982). Simplified Analysis of Laterally Loaded Piles, Ph.D. Thesis, University of California, Berkeley, California, page 211.

Faraji, S., Ting, J.M., Crovo, D.S., Ernst, H., (2001). “Nonlinear analysis of integral bridges: finite element model.” *Journal of Geotechnical and Geoenvironmental Engineering,* ASCE 127(5): 454-462.

FHWA, (1986), Seismic Design of Highway Bridge Foundations – Volume II: Design Procedures and Guidelines, Publication No. FHWA-RD-94-052, Federal Highway Administration, US Department of Transportation, Washington, D. C.

Haliburton, T.A. (1971) ‘’Soil structure interaction: Numerical analysis of beams and beam columns.’’ Tech. Publication No.14, School of Civil Engineering, Oklohama State Univ., Stillwater, Okla.

Hays, C. O., Jr (1990). “Lateral Distribution Factors for Highway Bridges.” *Journal of Structural Engineering.*, ASCE 116(3), 868-871

Hays, C.O, Sessions, L.M., Berry, A.J. (1986) “Further Studies on Lateral Load Distribution Using a Finite Element Method” *Transportation Research Record* 1072, 6-14.

Hindi, R. and Dicleli, M. (2006) “Effect of Modifying Bearing Fixities on the Seismic Response of Short-to-Medium Length Bridges with Heavy Substructures”, *Earthquake Spectra*, EERI, 22(1), 65-84.

Huo, S. X., Wasserman, E. P., and Iqbal, A. R. (2005) “ Simplified Method for Calculating Lateral Distribution Factors for Live Load Shear” *Journal of Bridge Engineering* ASCE, Vol. 10, No.5.

Husain, I., and Bagnariol, D. (1996).” Integral abutment bridges.” Rep. No. SO-96-01, Struct. Ofc., *Ministry of Transportation of Ontario*, Toronto, Canada.

Ilki, A. and Kumbasar, N. “Hysteresis Model for Reinforced Concrete Members”, *Proc. ASCE 14th Engineering Mechanics Conference*, Austin, on CD, University of Texas, Austin (2000).

Ilki, A. and Kumbasar, N. “Hysteresis Model for Reinforced Concrete Members”, *Proc. ASCE 14th Engineering Mechanics Conference*, Austin, on CD, University of Texas, Austin (2000).

Imbsen, R.A. and Nutt, R.V. (1978) “Load distribution study on highway bridges using STRUDL finite element analysis capabilities” *Proceedings, Conference on Computing in Civil Engineering (ASCE),* New York, NY.

Imbsen, R. and Penzien, J. (1986) “Evaluation of energy absorption characteristics of highway bridges under seismic conditions”, Vol. I, UCB/EERC-84/17, Earthquake Engineering Research Center, University of California, Berkeley, CA.

Itani, A.M., Alex Krimotat A., Rubeiz G.C., (1999) “Seismic Modeling, Analysis, and Design of Modern Steel Bridges” *Mid-America Highway Conference* St. Louis, Missouri.

Jain, S. K., and Scott, R. F. (1989) "Seismic analysis of cantilever retaining walls." *Proc., of Struct. Mech. in Reactor Technol. (SMIRT),* Anaheim, Calif., 241-246.

Kato, B. (1989) “Rotation capacity of H-section members as determined by local buckling”, *Journal of Constructional Steel Research* , 13(2-3), 95–109.

Kotsoglou, A. and Pantazopoulou, S. (2007) “Bridge-embankment interaction under transverse ground excitation” *Earthquake engineering and structural dynamics* 36(12), 1719-1740.

Kawashima, K. and Penzien, J. (1976) “Correlative investigation on theoretical and experimental dynamic behavior of a model bridge structure”, [EERC76-26], Earthquake Engineering Research Center, University of California, Berkeley, USA.

Khodair Y. A. and Hassiotis H. (2005). “ Analysis of Soil-Pile Interaction in Integral Abutment.” *Computers and Geotechnics* 32 (2005) 201-209.

Lemnitzer, A., Eric R. Ahlberg, E.R., Nigbor, R.L., Shamsabadi, A., Wallace, J.W. and Jonathan P. Stewart, J.P. “Lateral performance of full-scale bridge abutment wall with granular backfill” *Journal of Geotechnical and Geoenvironmental Engineering,* 135(4), 506–514, (2009).

Mabsout, M.E., Tarhini, K.M., Frederick, G.R., Tayar, C. (1997) “Finite Element Analysis of Steel Girder Highway Bridges”, *Journal of Bridge Engineering (ASCE)*, 2(3), 83-87.

Maheshwari, B.K., Truman, K.Z., El Naggar, M.H., Gould P.L. (2004) “Three-dimensional nonlinear analysis for seismic soil–pile-structure interaction” *Soil Dynamics and Earthquake Engineering* 24: 343–356.

Maleki, S. (2002) “Deck modeling for seismic analysis of skewed slab-girder bridges.” *Engineering Structures*, 24(10): 1315–1326.

Mander, J. B., Priestley, M. J. N., and Park, R. (1988) "Observed stress-strain behavior of confined concrete." *Journal of Structural Engineering*, ASCE, 114(8), 1827-1849.

Maroney, B. H. (1995) “Large-scale abutment tests to determine stiffness and ultimate strength under seismic loading.” Ph.D. thesis, Univ. of California, Davis, Calif.

Matlock, H. , (1970) “Correlations for design of laterally loaded piles in soft clay” *Proc., 2nd Annu. Offshore Technol. Conf.,* Vol. 1, 577–594.

Memory. T.J., Thanbiratnam. D.P., Brameld, G.H. (1995). “Free vibration analysis of bridges” *Engineering Structures,* 17(10), 705–713.

Mourad, S., and Tabsh, W. S.(1999) “ Deck Slab Stresses in Integral Abutment Bridges” *Journal of Bridge Engineering* ASCE, Vol. 4, No.2.

Nogami, T., Otani, J., Konagai, K., and Chen, H.L. (1992) “Nonlinear Soil-Pile Interaction Model for Dynamic Lateral Motion.” *Journal of Geotechnical and Geoenvironmental Engineering*, 118(1), 89–106.

NCHRP (National cooperative Highway Research Program) (2000). “Comprehensive Specification for the Seismic Design of Bridges”. *Revised LRFD Design Specifications (Seismic Provisions), Third Draft of Specification and Commentary.*

Newmark, N. M. (1948) “Design of I-beam bridges”, *Journal of Structural Division*, 74(1), 305-330.

Nogami, T., Otani, J., Konagai, K., and Chen, H.L. (1992) “Nonlinear Soil-Pile Interaction Model for Dynamic Lateral Motion.” *Journal of Geotechnical and Geoenvironmental Engineering*, 118(1), 89–106.

Novak, M. and Aboul-Ella, F. (1978) "Impedence functions of piles in layered media", *J. Eng. Mech. Div., Proc* ASCE, 104, 643-661.

Patrick, M.D., Huo, X.S., Puckett, J.A., Jablin, M. and Mertz, D. (2006). "Sensitivity of live load distribution factors to vehicle spacing", *Journal of Bridge Engineering*, ASCE, 11(1), 131-134.

Ramachandran, J. (2005) "Analysis of pile foundations under seismic loading" CBE Institute Final Report.

Reese, L.C. (1997) "Analysis of laterally loaded piles in weak rock." *Journal of Geotechnical and Geoenvironmental Engineering*, ASCE, 123(11), 1010-1017.

Reese, L.C., Cox, W.R. and Koop, F.D. (1974) "Analysis of laterally loaded piles in sand." *Proceedings, VI Annual Offshore Technology Conference*, Houston, TX, II(OTC 2080), 473-485.

Reese, L.C., Cox, W.R. and Koop, F.D. (1975) "Field testing and analysis of laterally loaded piles in stiff clay." *Proceedings, VII Annual Offshore Technology Conference,* Houston, TX, II(OTC 2312), 672-690.

Reese, L.C. and Welch, R.C. (1975) "Lateral loading of deep foundations in stiff clay." *Journal of Geotechnical Engineering,* ASCE, 101(GT7), 633-649.

Romo, M.P. and Ovando-Shelley, E. (1999) "P–Y Curves for Piles under Seismic Lateral Loads" *Geotechnical and Geological Engineering*, 16(4), 251-272.

Ruangrassamee, A. and Kawashima, K. (2003) "Control of nonlinear bridge response with pounding effect by variable dampers." *Engineering Structures*, 25, 513-606.

Saadeghvaziri, M.A., Yazdani-Motlagh A.R., Rashidi, S. (2000) "Effects of soil–structure interaction on longitudinal seismic response of MSSS bridges, *Soil Dynamic and Earthquake Engineering*, 20(1–4), 231-242.

Saatcioglu, M. and Yalcin, C. (2003) "External Prestressing Concrete Columns for Improved Seismic Shear Resistance." *Journal of Structural Engineering*, ASCE, Vol. 129(8), 1057-1070.

Shamsabadi, A., Rollins K. M., Kapuskar, M. (2007) "Nonlinear Soil-Abutment-Bridge Structure Interaction for Seismic Performance-Based

Design” *Journal of Geotechnical and Geoenvironmental Engineering*, ASCE, 133(6), 707-720.

Shirato, M., Koseki, J. and Fukui, J. (2006) “ A new nonlinear hysteretic rule for winkler type soil-pile interaction spring that consider loading pattern dependency” *Soil and Foundation Japanese Geotechnical Society*, 46(2), 173-188.

Skempton, A. W. (1951), “The bearing capacity of clays”, *Building Research Congres, Division I*, Part 3, London, 180-189.

Soltani, A. A., Kukreti, A. R., (1992) . "Performance Evaluation of Integral abutment Bridges", *Transportation Research Record, No 1371*, Transportation Research Board, National Research Council, Washington, D.C., USA, 17-25.

Spyrakos, C. and Loannidis, G. (2003) “Seismic behavior of a post-tensioned integral bridge including soil-structure interaction (SSI).” *Soil Dynamics and Earthquake Engineering*, 23, 53-63.

Steiger, D. J., (1993) . "Jointless Bridges Provide Fuel For Controversy, *Roads and Bridges*, 31 (11), 48-54.

Takeda, T., Sozen, M.A., Nielsen, N.N. (1970) “Reinforced Concrete Response to Simulate Earthquake” *Journal of the Structural Division* ASCE, Vol. 96, No. ST12 2557-2573.

Tarhini, K. M. , Frederick R.G. (1992) “ Whell Load Distribution in I-Girder Highway Bridges”, *Journal of Structural Engineering*, Vol.118, No.5

Tseng, W. and Penzien, J. (1973) “Analytical investigations of the seismic response of long multiple-span highway bridges”, Earthquake Engineering Research Center, University of California, Berkeley, CA

Wang, S., Kutter, B. L., Chacko, J. M., Wilson, D. W., Boulanger, R. W., Abghari, A. (1998) ‘‘Nonlinear seismic soil-pile-structure interaction.’’ *Earthquake Spectra*, 14(2), 377–396,

Westergaard, H. M. (1930) “Computation of Stresses in Bridge Slabs due to Wheel Loads” *Public Roads*, 11 (1), 1-23.

Wilson, J. C. (1988) "Stiffness of non-skew monolithic bridge abutments for seismic analysis" *Earthquake Engineering and Structural Dynamics*, 16: 867–883.

Wilson, D. W., Boulanger, R. W., Kutter, B. L. (2000) "Seismic lateral resistance of liquefying sand." *Journal of Geotechnical & Geoenvironmental Eng*., 126(10): 898-906.

Wolde-Tinsae, A. M., Klinger, J. E., Mullangi, R., (1988a) . "Bridge Deck Joint Rehabilitation or Retrofitting - Final Report", Department of Civil Engineering, Maryland University, College Park, MD, USA.

Wolde-Tinsae, A. M., Klinger, J.E., White, E.J., (1988b). "Performance of Jointless Bridges", *ASCE Journal of Performance of Constructed Facilities,* 2 (2), 111-128.

Wu, G. and Finn, W.D.L. (1997) "Dynamic nonlinear analysis of pile foundations using finite element method in the time domain" *Canadian Geotechnical Journal*; 34: 44–52.

Veletsos, A.S. and Younan, A.H. (1993) "Dynamic modeling and response of soil-wall systems" *Journal of Geotechnical Engineering*, ASCE, Vol. 120, No. 12 2155-2179 R.A.

XTRACT v3.0.7 (2009) Cross-sectional X Structural Analysis of Components. Rancho Cordova CA. TRC/Imbsen Software Systems.

Yousif, Z. and Hindi, R. (2007) "AASHTO-LRFD Live Load Distribution for Beam-and-Slab Bridges: Limitations and Applicability" *Journal of Bridge Engineering*, ASCE 12(6), 765-773.

Zanardo, G., Hao, H., Modena, C. (2002) "Seismic response of multi-span simply supported bridges to a spatially varying earthquake ground motion" *Earthquake Engineering & Structural Dynamics* 31(6), 1325 – 1345.

Zokaie, T., Osterkamp, T.A., and Imbsen, R. A. (1991). " Distribution of Wheel Load Highway Bridges." *National Cooperative Highway Research Program Report 12-26/1*, Transportation Research Board, Washington, D.C.

Zokaie, T. (2000) "AASHTO-LRFD Live Load Distribution Specifications" *Journal of Bridge Engineering,* ASCE, Vol. 5, No.2.

CURRICULUM VITAE

Department of Engineering Sciences
Middle East Technical University
Ankara, 06531 Turkey

TEL: +90(312) 210-2396
FAX: +90(312) 210-4462
esemih@metu.edu.tr

EDUCATION

Ph.D. Engineering Sciences, Middle East Technical University

B.Sc. Civil engineering, Çukurova University

PUBLICATIONS

Journal Publications

- ***International Refered Journals (SCI & SCI Expanded index)***

1. Dicleli, M. and **Erhan, S.** "Effect of Soil and Substructure Properties on Live Load Distribution in Integral Abutment Bridges", *ASCE Journal of Bridge Engineering*, Volume 13, Issue 5, pp. 527-539, 2008.

2. Dicleli, M. and **Erhan, S**., "Effect of Soil-Bridge Interaction on the Magnitude of Internal Forces in Integral Abutment Bridge Components due to Live Load Effects", *Engineering Structures*, Elsevier Science, Volume 32, Issue 1, pp. 129-145, 2010

3. Dicleli, M. and **Erhan, S**., “Effect of Superstructure-Abutment Continuity on Live Load Distribution in Integral Abutment Bridge Girders”, *Structural Engineering and Mechanics*, Volume. 34, Issue 5, pp. 635-662 **,** 2010

4. Dicleli, M. and **Erhan, S**., “Live Load Distribution Formulae for Pre-stressed Concrete Integral Abutment Bridge Girders” *ASCE Journal of Bridge Engineering*, Volume 14, Issue 6, pp. 472-486, 2009.

5. **Erhan, S.** and Dicleli, M., “Investigation of the Applicability of AASHTO LRFD Live Load Distribution Equations for Integral Bridge Substructures”, *Advances in Structural Engineering*, Multi-Science, Volume 12, Issue 4, pp.559-578, 2009.

6. **Erhan, S.** and Dicleli, M., “Live Load Distribution Equations for Integral Bridge Substructures”, *Engineering Structures*, Elsevier Science, Volume 31, Issue 5, pp. 1520-1534, 2009.

7. Dicleli, M. and **Erhan, S.,** “Effect of Foundation Soil Stiffness on the Seismic Performance of Integral Bridges” Structural Engineering International (SEI) , Volume 21, Issue 2, pp. 162-168, 2011

- ***National Refered Journals***

8. **Erhan, S.** and Dicleli, M., "İntegral Köprülerde Hareketli Yük Dağılımına Yapı-Zemin Etkileşimi ve Uç Ayak-Tabliye Sürekliliğinin Etkileri", Turkish Chamber of Civil Engineers - Technical Journal (IMO Teknik Dergi), Volume 20, Issue 4, pp.4833-4850, 2009 (in Turkish).

9. **Erhan, S.** and Dicleli, M.," İntegral Köprülerde Dolgu ve Temel Zemininin Hareketli Yükler Altında Köprü Elemanlarında Oluşan İç Kuvvetlere Etkileri", Construction World (Yapı Dünyası), Issue 154, pp. 17-24, 2009 (in Turkish).

10. **Erhan, S.** and Dicleli, M., "İntegral Köprü Kirişleri İçin Hareketli Yük Dağılım Formülleri", Construction World (Yapı Dünyası), (in Turkish) (in press).

Conference Proceedings

1. Dicleli, M. and **Erhan S**., “Effect of soil-bridge interaction on the distribution of live load effects among IB components”, Proceedings of

the 3rd International Conference on Structural Engineering, Mechanics and Computation, Cape Town, South Africa, 10-12 September 2007.

2. **Erhan S**. and Dicleli M., “Effect of soil bridge interaction on the internal forces of IB components due to live load effects”, 1st Symposium on Bridges and Viaducts, Proceedings of the Association of Turkish Chambers of Engineers and Architects, Chamber of Civil Engineers, Antalya Branch, November 29-30, Antalya, Turkey, 2007.

3. **Erhan S**. and Dicleli M., “Effect of soil bridge interaction and abutment deck continuity on the live load distribution factors in IB components”, 1st Symposium on Bridges and Viaducts, Proceedings of the Association of Turkish Chambers of Engineers and Architects, Chamber of Civil Engineers, Antalya Branch, November 29-30, Antalya, Turkey, 2007.

4. Nayyeri Amiri, S., Dicleli M. and **Erhan, S**. “Optimization of the seismic isolation parameters for bridges”, 1st Symposium on Bridges and Viaducts, Proceedings of the Association of Turkish Chambers of Engineers and Architects, Chamber of Civil Engineers, Antalya Branch, November 29-30, Antalya, Turkey, 2007.

5. Dicleli, M. and **Erhan, S**., “Comparison of Live Load Distribution in Girders of Integral and Conventional Bridges”, Proceedings of the 10th International Conference on Application of Advanced Technologies in Transportation, Athens, Greece, 27-31 May 2008.

6. Dicleli, M. and **Erhan, S**., “Effect of Soil-Bridge Interaction and Continuity on Live Load Distribution in Integral Bridges”, Proceedings of the Fourth International Conference on Bridge Maintenance, Safety and Management, IABMAS'08, Seoul, Korea, July 13-17, 2008.

7. Dicleli, M. and **Erhan, S**., “Distribution of Live Load Effects in Integral Bridge Abutments and Piles”, Proceedings of the Fifth International Conference on Bridge Maintenance, Safety and Management, IABMAS'10, Philadelphia, Pennsylvania USA, July 11-15, 2010.

8. **Erhan, S** and Dicleli, M., “Effect of soil bridge interaction on the distribution of live load effects among IB components”, Proceedings of the Fifth International Conference on Bridge Maintenance, Safety and Management, IABMAS'10, Philadelphia, Pennsylvania USA, July 11-15, 2010.

9. **Erhan, S** and Dicleli, M., "Live Load Distribution in Integral Bridge Girders", Proceedings of the Fifth International Conference on Bridge Maintenance, Safety and Management, IABMAS'10, Philadelphia, Pennsylvania USA, July 11-15, 2010.

10. Dicleli, M. and **Erhan, S**., "Effect of Modeling Simplifications on Nonlinear Seismic Analysis of Integral Bridges Including Dynamic Soil-Structure Interaction", 34th IABSE Symposium, Venice, Italy, September 22-24, 2010

11. **Erhan, S** and Dicleli, M., "Seismic Performance Evaluation of Integral Bridges as a Function of Various Structural And Geotechnical Parameters" 14th European Conference on Earthquake Engineering, (14ECEE) Ohrid, Republic of Macedonia, August 30–September 3, 2010.

12. **Erhan, S** and Dicleli, M., "Effect of Dynamic Soil-Structure Interaction Modeling Assumptions on Seismic Analysis of Integral Bridges" 14th European Conference on Earthquake Engineering, (14ECEE) Ohrid, Republic of Macedonia, August 30–September 3, 2010.

13. Dicleli, M. and **Erhan, S**., "Low Cycle Fatigue Effects in Integral Bridge Piles Under Seismic Load Reversible" 14th European Conference on Earthquake Engineering, (14ECEE) Ohrid, Republic of Macedonia, August 30–September 3, 2010.

14. Dicleli, M. and **Erhan, S**., "Effect of Seismically Induced Cyclic Displacements on Low Cycle Fatigue Performance of Integral Bridge Piles" The 5th Civil Engineering Conference in the Asian Region and Australasian Structural Engineering Conference Sydney, Australia, August 8–12, 2010.

15. Dicleli, M. and **Erhan, S**., "Effect of Nonlinear Soil-Structure Interaction Modeling Simplifications on Seismic Analysis Results of Highway Bridges" The 5th Civil Engineering Conference in the Asian Region and Australasian Structural Engineering Conference Sydney, Australia, August 8–12, 2010.

PROJECTS

- The Scientific and Technological Research Council of Turkey (TUBITAK), Contract #: **106M169**, "Live Load Distribution in Integral Bridge Components", 2006-2008.

- FIRB Project, “Assessment and reduction of seismic risk to large infrastructural systems” Collaborators: University of Pavia and RELIUS of Italy and METU of Turkey, Involved in Task 5: Assessment and reduction of seismic risk to multi-span viaducts in road networks 2008-2011
- The Scientific and Technological Research Council of Turkey (TUBİTAK), Contract #: **108M313**, “Seismic Performance Evaluation of Integral Bridges”, 2009-2011.